Trinity College Dublin
Coláiste na Tríonóide, Baile Átha Cliath
The University of Dublin

Factors affecting the stability and performance of amorphous solid dispersions of poorly soluble active pharmaceutical ingredients

A thesis submitted for the degree of

Doctor of Philosophy

at the School of Pharmacy and Pharmaceutical Sciences

Trinity College Dublin, The University of Dublin

by

Emer Browne

B.Sc. (Pharm), M.Pharm., M.P.S.I.

under the supervision of

Professor Anne Marie Healy

B.Sc. (Pharm), Ph.D., M.P.S.I., F.T.C.D.

April 2020

Declaration

I declare that this thesis has not been submitted as an exercise for a degree at this or any other university. A small proportion of the work described in this thesis was carried out by others and this is duly acknowledged where relevant. I declare that all other work is entirely my own.

I agree to deposit this thesis in the University's open access institutional repository or allow the library to do so on my behalf, subject to Irish Copyright Legislation and Trinity College Library conditions of use and acknowledgement.

I consent to the examiners retaining a copy of the thesis beyond the examining period, should they so wish.

_____

Emer Browne

Summary

This thesis focuses on factors affecting the stability and performance of amorphous solid dispersions of poorly soluble active pharmaceutical ingredients (APIs).

Over the last twenty years, the poor solubility profile of pipeline drugs has limited their development as solid oral dosage forms. Formulating these APIs as amorphous solid dispersions is one strategy to overcome their poor aqueous solubility. The major limitation to amorphous solid dispersion development is the physical instability of the amorphous state. The objective of this thesis is to investigate factors affecting the physical and chemical stability of amorphous solid dispersions.

The work carried out in this thesis has demonstrated that the chirality of an API is a factor which should be considered when developing an amorphous solid dispersion, particularly when cellulose-based polymers are used, as chiral recognition may exist between the polymer and the API. This was demonstrated to be true for opposing enantiomers of ibuprofen and the cellulose polymer, HPMC, when cryo-milled together. The S-ibuprofen-HPMC system contained significantly less crystalline ibuprofen than the equivalent R-ibuprofen-HPMC system. However, this stereoselective effect was diminished when the amorphous solid dispersions were produced via spray drying. This is believed to be due to the superior molecular mixing facilitated by solubilising both components prior to spray drying, which enabled a greater extent of amorphisation for both enantiomeric systems. It was also discovered that when the R,S-ibuprofen is formulated as an amorphous solid dispersion with HPMC, a racemic switch (to the S enantiomer) can increase the amorphous ibuprofen content and increase ibuprofen's dissolution rate.

The choice of polymer in an amorphous solid dispersion formulation is acknowledged to influence amorphous solid dispersion stability and performance. However, a comprehensive evaluation of the effect that polymer physicochemical properties may have on amorphous solid dispersion stability and performance, which would aid polymer selection at an early stage of development, is lacking. The relationship between several physicochemical properties of poly-vinyl polymers, such as molecular weight and co-polymer substitution ratio, and ketoprofen amorphous solid dispersion stability and performance was determined. The relative humidity induced glass transition value was found to be useful to describe the effect that co-polymer substitution ratio has on moisture sorption and associated plasticisation. It was also discovered that it is the aqueous solubility of the polymer, rather than the complete amorphisation of ketoprofen in the dispersion, which is the critical factor determining the degree of ketoprofen supersaturation which is achievable.

The relationship between the route of amorphous solid dispersion generation and performance was also evaluated for two processes; electrospraying and spray drying. It was determined that solution conductivity had no impact on the morphology of the particles produced via spray drying, while solutions with lower conductivity, when processed via electrospraying, produced particles which displayed webbing. The drug loading, physical state and dissolution profile of the ketoprofen-PVP material was similar for both electrosprayed and spray dried material. However, the smaller particle size associated with the electrosprayed material resulted in poorer compressibility and higher surface moisture sorption rates compared to the equivalent spray dried material.

Factors affecting the chemical stability, specifically the photostability of spray dried amorphous solid dispersions of nifedipine were also investigated. It was discovered that the solvent composition of the solution which was spray dried was critical to the photostability of the amorphous solid dispersion, which is believed to be due to its effect on the surface enrichment of nifedipine.

Lastly, the potential of amorphous solid dispersions of nifedipine to be used in the treatment of autonomic dysreflexia, a hypertensive crisis, was explored. Soluplus and HPMC were determined to be unsuitable polymers for this purpose due to poor nifedipine release profiles attained from the solid dispersions produced, while PVP-based systems exhibited nifedipine release profiles which were similar to the nifedipine release profile obtained from a ruptured Adalat® capsule, which is the current standard of care. Clearly, the PVP-nifedipine amorphous solid dispersion formulations warrant further investigation for the treatment of this condition, as they may represent an improvement on the status quo.

Table of contents

Acknowledgements

Firstly, I would like to thank my supervisor Prof. Anne Marie Healy for giving me the opportunity to undertake a PhD at the School of Pharmacy and Pharmaceutical Sciences in Trinity College Dublin, which has been a lifelong ambition of mine. Her guidance and support, particularly in allowing me to direct the project towards areas of personal interest is greatly appreciated. I am also immensely grateful to Dr. Zelalem Worku for his guidance, wisdom and enthusiasm. I'd like to thank the SSPC and SFI for providing funding which enabled this research and allowed me to partake in conferences at home and abroad. I'd like to thank the collaborators who contributed to this work; Dr.'s Melba Simon, Roderick Jones, Justyna Knapik-Kowalczuk and Romina Charifou and Prof.'s Brian Glennon, and Ramesh Babu. A special mention to Ms. Sian Quinn for your help. I am indebted to all of your expertise and assistance.

Thank you to everyone I have worked alongside in the lab over the last four years; Ricardo, Alan, Kate, Svenja, Fiona, Claire, David, Karl, Dinesh, Kieran, Stefano, May, Loli, Lilian, Johannes, Erika, Mike, Valerio, Atif, Klaudia, Julija, Agnieszka, Hannah, Jinfan, Kate, Miriam, Gloria, Denise, Maria, Kit, Elena, Ondra and Caoimhe. Your friendship and company are greatly appreciated. A special thank you to my lab partner Jer, for never failing to motivate me with rebel music and Simpsons memes. A special mention is also due to Peter, whose troubleshooting I will be forever grateful for. Thank you for always making the time to help. Thank you to the technical and admin staff of the School of Pharmacy; Trevor, Brian, Conan, Pauline, Olga, Edelle, Joe, Ray, Rhona, Irene and Elizabeth.

Thank you to my friends and family for keeping me sane (just about!) over the last four years. Shane, Colin, Cliodhna, Kate, Lisa, Celine, Grace, Aoife, Rachel and Sarah Jane- thank you for your friendship. A special thank you to Claire for always supporting me and helping me to see the bigger picture. Thank you my Line-Up choir family whose music and friendship uplifted me every Wednesday. To my cousins and aunt; Gary, David, Megan, Deirbhile and Mary thanks for the support and encouragement. A special thank you to my brother Robert for always providing a listening ear and a plentiful supply of tea.

To my parents Michael and Michelle. Thank you for always supporting my education, in every way possible. Thank you for invoking a sense of curiosity about the world in me and thank you both for your unconditional support, love, patience and encouragement as I pursued the same.

Lastly, to my boyfriend James. Thank you for supporting me every step of the way through the last four years. Your reassurance, guidance and love has made completing this thesis a reality. You made every day better.

Publications and presentations

Publication associated with this thesis

- Browne, E., Charifou, R., Worku, Z.A., Babu, R.P., Healy, A.M. *Amorphous solid dispersions of ketoprofen and poly-vinyl polymers prepared via electrospraying and spray drying: A comparison of particle characteristics and performance*. International Journal of Pharmaceutics. **May 2019**. Vol 566 pgs173-184

Oral presentations associated with this thesis

- Browne. E, Worku, Z.A., Kumar, D., Simon, M., Glennon, B., Healy, A.M., *The effect of enantiomer composition on the stability of spray dried ibuprofen: HPMC composites.* Scientific Advisory Board Review of Synthesis and Solid State Pharmaceutical Centre. **June 2017**

Poster presentations associated with this thesis

- Browne. E, Worku, Z.A., Healy, A.M. *The impact of physicochemical properties of poly-vinyl polymers on the performance of ketoprofen amorphous solid dispersions.* AAPS Annual Meeting and Exhibition, Washington D.C, **November 2018.**
- Browne. E, Worku, Z.A., Kumar, D., Simon, M., Glennon, B., Healy, A.M. *Glass forming ability and stability differences of ibuprofen enantiomers and binary solid dispersions.* AAPS Annual Meeting and Exhibition, Denver, **November 2016.**

Abbreviations

AD	Autonomic dysreflexia
API	Active pharmaceutical ingredient
ASD	Amorphous solid dispersion
ATP	2-amino-1,1,3-triphenyl-1-propanol
ATR-FTIR	Attenuated total reflectance Fourier-transform infrared spectroscopy
BCS	Biopharmaceutics Classification System
BDS	Broadband dielectric spectroscopy
CCI	Carr's Compressibility Index
CM	Cryo-milling
DCS	Developability Classification System
DSC	Differential scanning calorimetry
DVS	Dynamic vapour sorption
E_a	Activation energy
ES	Electrospraying
FDA	Food and Drug Administration
GFA	Glass forming ability
GS	Glass stability
HN	Havrilak-Negami
HPC	Hydroxypropyl cellulose
HPLC	High performance liquid chromatography
HPMC	Hydroxypropylmethyl cellulose
HPMCAS	Hydroxypropylmethyl cellulose acetyl succinate
HPMCP	Hydroxypropylmethyl cellulose phthalate
HSP	Hansen Solubility Parameter
KETO	R,S-ketoprofen
KWW	Kohlrausch-Williams-Watts
MCC	Microcrystalline cellulose
mDSC	Modulated differential scanning calorimetry
MIPS	Moisture induced phase separation
MQ	Melt-quenched

NCE	New chemical entity
NIF	Nifedipine
NSAID	Non-steroidal anti-inflammatory drug
PAA	Polyacrylic acid
PAMPA	Parallel artificial membrane permeability assay
PEO	Polyethylene oxide
PM	Physical mixture
PTFE	Polytetrafluoroethylene
PVA	Polyvinyl acetate
PVAlc	Polyvinyl alcohol
PVAP	Polyvinyl acetate phthalate
PVP	Polyvinyl pyrrolidone
PVPVA	Polyvinyl pyrrolidone vinyl acetate
pXRD	Powder X-ray diffraction
R IBU	R-ibuprofen
R,S IBU	R,S-ibuprofen
RH	Relative humidity
RH_{Tg}	Relative humidity induced glass transition
S IBU	S-ibuprofen
SD	Spray drying
SEM	Scanning electron microscopy
SLAD	Solubility limited absorbable dose
Tg	Glass transition temperature
TGA	Thermogravimetric analysis
VFT	Vogel-Fulcher-Tammann
XPS	X-ray photon electron spectroscopy

Origin and scope

The poor solubility of new chemical entities (NCEs) has resulted in challenges in the pharmaceutical formulation sector [1], as solid oral dosage form development may not be feasible for these molecules.

A variety of formulation strategies exist to improve the aqueous solubility of active pharmaceutical ingredients (APIs), allowing for solid oral dosage form development. The generation of amorphous solid dispersions (ASDs) is one such strategy which has received increasing attention over the last twenty years [2]. The higher thermodynamic energy of the amorphous state, due to the absence of a crystal lattice, means that an amorphous API exhibits higher apparent solubility in aqueous media compared to its crystalline counterpart [3]. In theory, any API can be amorphised if the transition from the liquid state (solution or melt) to the solid state is sufficiently rapid [4]. In practical terms however, the amorphisation of an API or development of an amorphous form may be limited by its solid-state physical instability.

Efforts to correlate API physicochemical properties with amorphous stability have offered some insight into the interplay between the molecular weight, enthalpy of fusion and structural complexity of a molecule and its propensity towards reversion to the crystalline form [4]. The role that enantiomeric composition has on the amorphous stability of a chiral API has not been fully explored and is an area of research which may have significant implications in the context of "racemic switches" [5,6]. Furthermore, the idea that chiral recognition may exist between chiral APIs and the cellulose based polymers [7,8] which are commonly used in ASDs adds another factor to consider.

The role that polymer selection plays in the performance of an ASD is well known, but studies thus far have tended to focus on a solitary aspect of ASD performance, such as tendency towards moisture-induced phase transition [9], physical stability [10] or dissolution performance [11]. A holistic evaluation of the physicochemical properties of a range of polymers and their impact on the aforementioned ASD performance indicators is warranted to allow for rational ASD polymer selection.

The impact that manufacturing route has on the performance of an ASD is less well explored [12,13], which is surprising, as the micromeritic properties of powders, such as flow and density can clearly be influenced by their method of production. An area of intensive research at present in the ASD field is the application of electrohydrodynamic processes, such as electrospraying, to the production of ASDs [14–16]. A head-to-head comparison of ASD material produced via the relatively novel electrospraying method against material produced via the more traditional spray drying

method is necessary to evaluate the merits and/or disadvantages of both processes to guide manufacturing route selection.

While the physical instability of the amorphous form has understandably been a major area of research in the ASD field, the chemical instability of the amorphous form has been largely overlooked [17,18]. One aspect of the chemical stability of an API which is tested routinely, is its tendency to degrade due to the presence of photons - so called photodegradation. The influence that polymer selection has on the photostability of the amorphous form of an API is unexplored in the literature to date.

Lastly, while the growth of ASD formulations reaching the market is evident [2], the vast majority of these approvals have been for NCEs. ASD formulations may also be beneficial for the emergency administration of medicines which are already on the market, but which are unavailable in appropriate formulations, such as in the treatment of hypertensive crises.

Bearing the above limits to current understanding of ASDs in mind, the scope of this thesis is to:

- Investigate the difference, if any, in the glass forming ability and glass stability between a racemic compound and its single enantiomer counterpart using ibuprofen as a model API.
- Investigate if opposing enantiomers of ibuprofen demonstrate chiral recognition with regard to their ease of amorphisation and/or resistance to recrystallisation in the presence of cellulosic polymers.
- Investigate the impact that the physicochemical properties of polyvinyl polymers have on the stability and performance of ketoprofen amorphous solid dispersions.
- Compare the particle characteristics and performance of ketoprofen and poly-vinyl polymers ASDs prepared via spray drying and electrospraying.
- Investigate the influence that polymers have on the photostability of spray dried nifedipine ASDs.
- Develop an ASD formulation of a poorly soluble API for an unmet clinical need using nifedipine in the treatment of autonomic dysreflexia as a model scenario.

Chapter 1: Introduction

1.1 Bioavailability and properties of active pharmaceutical ingredients

1.1.1 Bioavailability

The bioavailability of an active pharmaceutical ingredient (API) has been defined by the Food and Drug Administration (FDA) as the rate and extent to which it is absorbed from a drug product and becomes available at the site of drug action [19]. In theory an API administered via intravenous injection has complete (100%) bioavailability. The bioavailability of the same API administered via an oral dosage form is dependent on many factors. Patient factors such as age [20], race [21], gastric contents [22] and concurrent drug use [23] may affect the bioavailability of an API . The choice of excipient(s) in the formulated medicine may also affect API bioavailability through mechanisms such as increasing the surface area of the API exposed to the dissolution media or by alteration of gastric transit time [22].

An API's bioavailability is also a function of its physicochemical properties, and is known to generally increase with a reducing number of rotatable bonds and reducing polar surface area [24].

1.1.2 Tools to predict the bioavailability of active pharmaceutical ingredients

Considering the multitude of factors which are known to affect the bioavailability of an API, as outlined above, a tool to predict the *in vivo* bioavailability from *in vitro* dissolution data would be very beneficial for the drug development sector. The most widely adopted tool for this purpose is termed the Biopharmaceutics Classification System (BCS) which was developed in the 1990s [25]. In this system, APIs are classified based on two parameters: solubility in water and intestinal permeability. APIs are deemed to have "high" solubility if the highest dose strength is soluble in 250 mL or less of water over the pH range 1-6.8 at 37 ^{o}C. APIs are deemed to have "high" permeability if the extent of absorption in humans is 85% or greater of the administered dose based on mass balance determination or relative to an intravenous dose [26]. The BCS categories are indicated below, in Figure 1.1. According to the BCS, Class 1 and Class 2 APIs formulated as immediate release preparations would be predicted to have a good *in vivo in vitro* correlation (IVIVC) as long as dissolution rate is slower than gastric emptying rate (for Class 1) or if *in vitro* dissolution rate is similar to *in vivo* dissolution rate (for Class 2). No IVIVC is expected for Class 3 and Class 4 compounds [25].

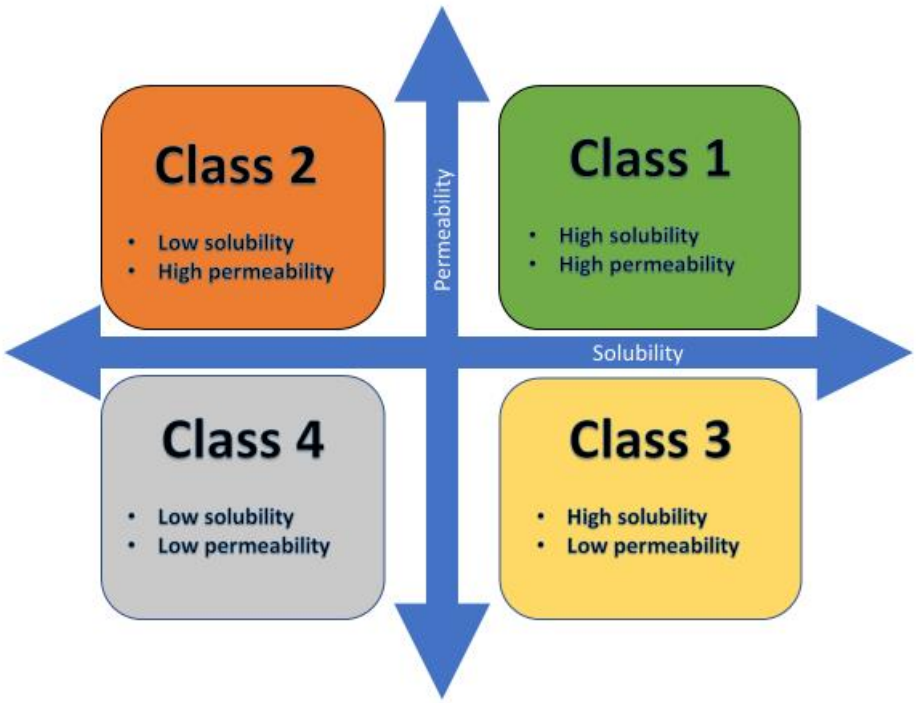

Figure 1.1: The Biopharmaceutics Classification System Categories

The BCS has been widely adopted by medical regulatory agencies to distinguish between generic products which require *in vivo* bioavailability testing for approval, and those for which *in vitro* dissolution equivalence to a reference product is sufficient - a condition known as a biowaiver [26].

Although the BCS is an extremely useful tool in drug development, it has received criticism for being overly conservative. In the case of weakly acidic drugs, such as ketoprofen (high permeability and pH dependent solubility), bioavailability is not dependent on solubility at gastric pH, as most of the compound's absorption occurs in the duodenum where the pH is >5 and ketoprofen is soluble [27]. As such, there is a strong argument for acidic compounds with high permeability to be considered for biowaivers as the extent of their oral absorption is not dependent on their solubility at gastric pH.

An alternative classification system, termed the developability classification system (DCS), was created by GlaxoSmithKline. One major difference between the BCS and the DCS is that in the latter system the solubility of the compound is determined in fasted small intestinal fluid rather than across the pH range of 1-6.8 as in the BCS [28]. Because of this, many non-steroidal anti-inflammatory drugs (NSAIDs) with pH dependent solubility, which are classified as Class 2 in the BCS are reclassified as Class 1 compounds in the DCS. Another major difference between the BCS and the DCS is the creation of 2 sub-classes in the DCS (2a and 2b), as shown in Figure 1.2. In Class 2a compounds, although concentration in the small intestine may exceed solubility limits, the high permeability of the compound ensures sink conditions are maintained *in vivo* through intestinal absorption. Thus, as long as the dissolution rate is sufficiently fast, bioavailability is high for these

compounds. For Class 2b compounds the high permeability of the compound cannot compensate sufficiently for the concentration of drug in the intestine and the compound's absorption is solubility limited. The boundary between Class 2a and Class 2b compounds is called the solubility limited absorbable dose (SLAD), which is determined as shown in Equation 1.1

$$SLAD = S_{si} \times V \times M_P \quad \textbf{Equation 1.1}$$

Where S_{si} is the solubility of the compound in the small intestine, V is the volume of fluid available (500 mL- note the increase from 250 mL in the BCS) and M_P is a permeability dependent multiplier.

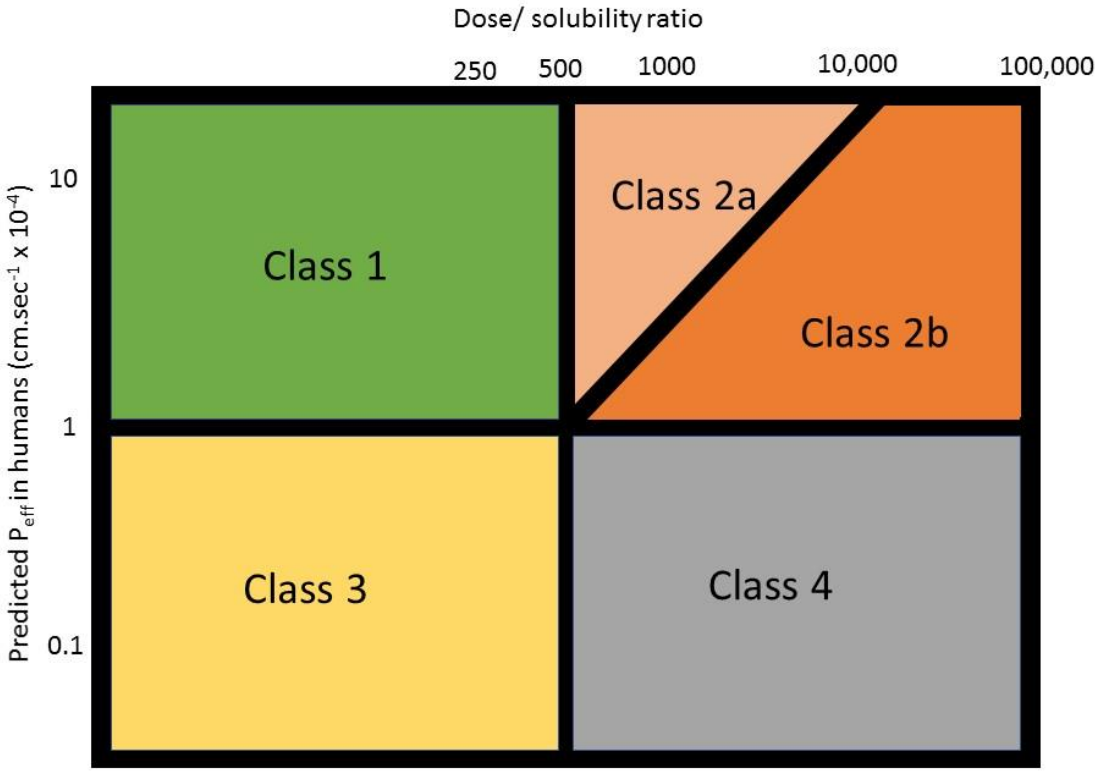

Figure 1.2: The Developability Classification System Categories

1.1.3 Properties of pipeline drugs

Although the emergence of high throughput screening and combinatorial chemistry in the pharmaceutical discovery sector in the early 1990s revolutionised lead molecule identification, it also contributed to a change in the physicochemical profile of new chemical entity (NCE) portfolios for many pharmaceutical companies [29,30]. As much as 90% of NCEs are poorly soluble in water, making them sub-optimal candidates for formulation into solid oral dosage forms [1,31] . Oral formulations are the most popular form of medicines administration for several reasons. From a patient's perspective, they are less invasive, more portable and painless to administer relative to

other formulations such as an injection. From a pharmaceutical company's perspective, manufacturing oral formulations generally means that aseptic processing and cold chain storage are not required and therefore the cost of manufacturing the medicine is minimized. As the expense of bringing a new molecule from inception to market is now estimated at $2.6 billion, the need for cost-savings is apparent [32]. There is therefore a pressing need for formulation scientists to develop methods to overcome the poor solubility profile of NCEs so that pharmaceutical companies can deliver new products to market, and ultimately to patients.

1.1.4 Solubility, supersaturation and dissolution

Solubility is a thermodynamic property of a molecule defined as the maximum amount of that molecule that will remain in solution in a given volume of solvent at a given temperature and pressure under equilibrium conditions [33]. A solution is supersaturated when the solute is dissolved at a concentration greater than the equilibrium solubility limit for that solute-solvent system. Supersaturation is a thermodynamically unstable state and eventually the solute in question will precipitate out of solution [34]. In the context of pharmaceutical development, it is the aqueous solubility of molecules that is of great importance. Just under 70% of NCEs have an aqueous solubility below 100 µg /mL, meaning they are considered practically insoluble in water [35].

The dissolution rate of an API refers to the rate at which the solid API enters solution. Dissolution is a kinetic phenomenon. The rate at which dissolution occurs ($\frac{dc}{dt}$) is proportional to the difference in the concentration of the drug in the solution at a given time (C_t) and the concentration of the saturated solution (C_s) in accordance with the Noyes-Whitney equation (Equation 1.2) [36], where K is a constant.

$$\frac{dc}{dt} = K(C_s - C_t) \qquad \textbf{Equation 1.2}$$

By applying Fick's second law of diffusion to the Noyes-Whitney equation Nernst and Brunner identified further factors affecting the dissolution rate of a substance which are described in Equation 1.3 [37]

$$\frac{dc}{dt} = \frac{DS(C_s - C_t)}{Vh} \qquad \textbf{Equation 1.3}$$

Where D is the diffusion coefficient, S is the surface area of the substance dissolving, V is the volume of the dissolution medium and h is the thickness of the diffusion boundary layer [38]. By examining this equation, it is apparent that the greater the difference between the concentration of the API in solution and the solubility limit of the API, the faster the dissolution rate will be.

Where the volume of the dissolution medium is very large, or where the API is being removed from the dissolution medium (such as would happen *in vivo* through intestinal absorption of the API), sink conditions may be present. Sink conditions refer to the situation where the concentration in solution is significantly less than the concentration of the saturated solution, commonly $C_t \leq \frac{C_s}{10}$ [39]. Under sink conditions the contribution of C_t to the dissolution rate becomes negligible and dissolution rate is proportional to the equilibrium saturated solubility (C_s) of the API.

From a thermodynamic perspective, the solubility of a solute in a solvent (S) can be expressed as a function of three separate processes described in Equation 1.4 [2].

$$S = f(Crystal\ Packing\ Energy + Cavitation\ Energy + Solvation\ Energy) \quad \textbf{Equation 1.4}$$

The crystal packing energy refers to the energy necessary to disrupt the crystal lattice (endoergic), the cavitation energy refers to the energy required to create a void in the solvent for the solute (endoergic) and the solvation energy refers to the release of energy due to favourable interactions being formed between solvent and solute (exoergic) [2]. In relative terms, the magnitude of the crystal packing energy tends to be larger than the other energetic processes and is the driving force which governs solubility and hence dissolution rate.

1.2 Formulation strategies to improve drug aqueous solubility and/or dissolution rate

In drug development, there is a desire for APIs to behave in a BCS Class 1 manner from a regulatory as well as a clinical perspective. The poor permeability of BCS Class 3 and Class 4 APIs may necessitate lead compound optimisation, while BCS Class 2 compounds may have BCS Class 1 properties conferred on them through suitable formulation strategies [40,41].

A non-exhaustive list of common formulation strategies used to improve API solubility for oral solid dosage forms is shown in Figure 1.3.

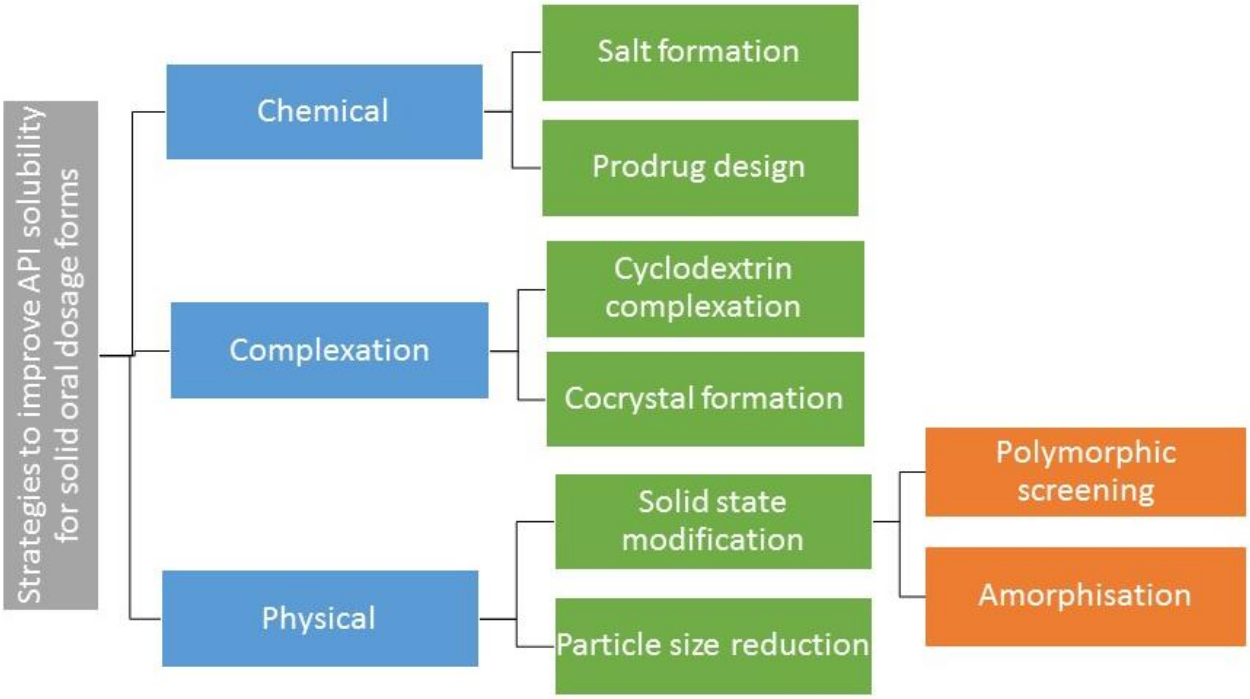

Figure 1.3: Common formulation strategies to improve API solubility for solid oral dosage forms

1.2.1 Chemical approaches

1.2.1.1 Salt formation

One commonly used strategy to improve API solubility is to create a salt of the compound. Salt formation is only possible where the API has an ionizable functional group such as a carboxylic acid or an amine. However, as almost two thirds of pharmaceutical compounds are considered to be weak electrolytes [42], salt formation should be considered during formulation development. Salt formation increases an API's dissolution rate by modifying the pH of the diffusion layer where the API is dissolving. The API-salt therefore acts as its own buffer. C_s is increased relative to the free acid or free base resulting in an increased dissolution rate in accordance with Equation 1.3 [43]. Salt screening is commonly carried out to determine which counterion will produce a pharmaceutical salt with acceptable stability, hygroscopicity, toxicity and solubility. Stable ionic bond formation between the acid and base may occur when the difference in their pKa values is greater than 3 [44]. The most commonly used anion and cation used in marketed pharmaceutical salts are hydrochloride and sodium ions respectively [43].

1.2.1.2 Prodrug formation

A prodrug is an inactive, chemically modified version of a parent drug, with improved physicochemical properties relative to the parent drug, which can undergo a rapid biotransformation to produce the parent drug *in vivo* [45]. Approximately 7% of marketed drugs in

2008 were prodrugs [46]. This percentage increased to 15% in 2015 [47]. The prodrug approach may be used to increase drug solubility through the addition of a polar functional group (such as a phosphate ester) to the parent molecule [48]. As the prodrug approach involves additional steps in the chemical synthesis of an API, it may not be favoured by pharmaceutical companies by the time formulation is considered.

1.2.2 Complexation approaches

1.2.2.1 Cocrystal formation

An alternative approach to salt formation, for APIs which do not possess an ionizable functional group, is the formation of a cocrystal. A cocrystal has been defined as a multicomponent assembly (consisting of an API and a coformer) held together by freely reversible non covalent bonds [49]. Solvates and hydrates may also be considered to fit this definition but the semantics of this is beyond the scope of this thesis. Cocrystal formation may confer a beneficial solubility profile to an API through two mechanisms: reduced crystal lattice energy and increased solvation [50]. Coformers commonly include molecules with carboxylic acid, alcohol and amide functional groups [51]. A difference in pKa values between the API and the coformer of less than 3 units [50], or a difference in Hansen Solubility Parameter values less than 7 units [52] are predictive of the propensity of two components to form a cocrystal. Common methods to produce cocrystals include hot melt extrusion, solvent evaporation and grinding.

1.2.2.2 Cyclodextrin complexation

Cyclodextrins are cyclic oligosaccharides with a hydrophilic surface and a hydrophobic cavity. They form inclusion complexes with low solubility API through non-covalent interactions [45]. While naturally occurring cyclodextrins have limited aqueous solubility, derivatives have been manufactured which exhibit high aqueous solubility such as hydroxypropyl-β-cyclodextrin. APIs which are suitable candidates for cyclodextrin complexation have molecular weights between 100 and 400 Daltons and should be relatively potent due to the high molecular weight of the cyclodextrin, otherwise the size of the dose administered may not be acceptable to the patient [53]. One disadvantage with the use of cyclodextrins is the potential for toxicological effects, particularly nephrotoxicity, although this risk is lower for oral formulations relative to parenteral formulations [54].

1.2.3 Physical approaches

1.2.3.1 Particle size reduction

As is clear from Equation 1.3, the dissolution rate of an API is proportional to surface area. As surface area is inversely related to particle size, when particle size is reduced, dissolution rate should increase. When particle size is reduced to the nanometre scale, the saturation solubility of the API is also increased. This is in accordance with the Knapp modified Ostwald-Freundlich equation (Equation 1.5) shown below.

$$\frac{RT}{V_m} ln \frac{S}{S_0} = \frac{2\gamma}{r} - \frac{q^2}{8\pi k r^4} \qquad \textbf{Equation 1.5}$$

Where R is the universal gas constant, T is the temperature, S is the solubility of particles of radius r, S_0 is the equilibrium solubility, V_m is the molar volume, γ is the surface tension, q is the electric charge and k is the permittivity of the medium in which the particles are dispersed [55].

Common methods to reduce particle size include milling, spray drying and anti-solvent precipitation. Particle size reduction is a universal approach that can be used to improve the dissolution rate and/or solubility of all APIs. However, when the particle size reduces to the nanometre scale, there is a thermodynamic driving force towards crystal growth caused by the high interfacial energy of the nanoparticles. In an effort to avoid this, many nanoparticulate formulations include "stabilisers" as excipients, such as surfactants and polymers [56]. Another factor which must be considered when using nanonisation as a formulation strategy is the potential for nanotoxicity. Particles below approximately 150 nm can be internalized by cells via pinocytosis, which may result in a greater potential for cellular toxicity than micron-sized particles [57].

1.2.3.2 Solid-state transformation

Another method of improving the solubility and/or dissolution rate of an API is to alter the solid-state form of the API. Pharmaceutical materials in the solid state can be classified as existing in the crystalline state or the amorphous state. A crystalline solid is characterised by the presence of three-dimensional long-range order. In contrast, in an amorphous solid this long-range order is absent, although there may be some degree of order present over short ranges [58]. The relative thermodynamic stability of a material in two different solid-state forms can be deduced by examining the difference in Gibbs free energy (ΔG), which is calculated using Equation 1.6.

$$\Delta G = \Delta H - T\Delta S \qquad \textbf{Equation 1.6}$$

Where ΔH is the enthalpy difference between the two forms, which is related to the structural energy differences, ΔS is the entropy difference between the two forms, which is related to the degree of disorder, and T is the temperature [59]. Where ΔG between two states is zero, they exist in equilibrium together. This is illustrated in Figure 1.4. Thermodynamic equilibrium exists between polymorphic form A and the liquid form at the melt temperature of form A (Tm A). The same is true for polymorphic form B and the liquid form at the melt temperature of form B (Tm B) and the amorphous and supercooled liquid form at the glass transition temperature (Tg).

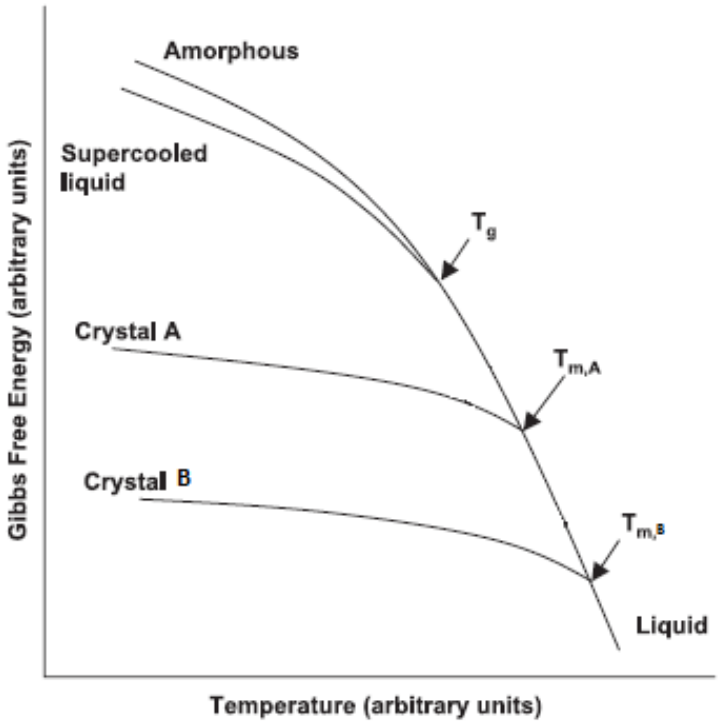

Figure 1.4: Gibbs free energy curves for a hypothetical compound. Adapted from Rodríguez-Spong et al.[59]

The amorphous state and high energy crystalline polymorphic states are likely to exhibit higher solubility compared to the thermodynamically stable crystalline state. An explanation for this is that these metastable states exist in a higher energy state relative to the thermodynamically stable polymorph, as shown in Figure 1.4. This energy is stored as potential energy in the solid form, which is released when added to a solvent, the so-called "spring" effect [2,60]. In the case of high energy polymorphic forms (e.g. polymorph A in Figure 1.4) the crystal packing energy term described in Equation 1.4 has a lower value than the thermodynamically stable polymorph B. Therefore, the solubility of polymorphic form A is higher than polymorphic form B as the energy barrier required to break the crystal lattice is lower. A general rule is that the solubility of a polymorphic form is inversely related to both its melting temperature and thermodynamic stability.

1.2.3.2.1 Polymorphic screening

Polymorphism has been defined as the ability of a substance to exist in different molecular arrangements and/ or different molecular conformations [59]. As part of NCE research and development it is prudent (as well as being a regulatory requirement), for companies to perform a screening study to identify all possible polymorphs of the API in the crystalline state. Conversion from one form to another may occur during pharmaceutical manufacturing, and the appearance of a previously unidentified polymorph during manufacture may have disastrous consequences, as was the case for the anti-retroviral, ritonavir [61]. Different polymorphic forms of the same API will have different solubilities, melting points, densities, hardness [62] and even chemical stability in some cases [63]. Control of processing parameters during manufacture is necessary to avoid accidental conversion of one polymorph to another. Generally speaking, the most stable polymorphic form i.e. the polymorph with the highest melting temperature, is desirable for pharmaceutical manufacturing [63]. Deliberate formulation of a metastable polymorph may be indicated with low aqueous solubility compounds in order to confer a clinical benefit to the patient e.g. faster onset of therapeutic effect. Although there are many examples of APIs with polymorphs of different solubilities, there are only a few examples where this has translated into a difference in bioavailability *in vivo* [64,65]. For example, the metastable form of chloramphenicol palmitate demonstrates faster absorption than the thermodynamically stable polymorph, but the same is not true not for mefenamic acid [66]. The anticipated solubility and hence bioavailability advantage of a thermodynamically unstable polymorphic state can be estimated from the free energy difference between the polymorphs. For mefenamic acid this difference is small (251 cal/mole), whereas for chloramphenicol palmitate this difference is large (774 cal/mole) [66]. It has been suggested that in order for a metastable polymorph to demonstrate superior bioavailability to the thermodynamically stable form, it should be at least 3.5 times more soluble than the stable form [67].

Methods to preferentially produce metastable polymorphic forms of an API tend to be methods which are rapid in nature such as melt-quenching or anti-solvent precipitation [68]. These rapid methods do not give the molecules sufficient time to orientate themselves into the most stable configuration. The main disadvantage with the development of a metastable polymorph is that, given enough time, the metastable polymorph will revert to the thermodynamically stable state.

1.2.3.2.2 Amorphisation

Amorphisation i.e. the prevention of the formation of a crystal lattice, or destruction of same, has grown in popularity as a method to improve the aqueous solubility of poorly soluble APIs over the last several decades. This is demonstrated in Figure 1.5 which shows a timeline of FDA approved medicines which contain an API in the amorphous state. Examining the therapeutic areas of marketed amorphous formulations, it is clear that many of the APIs are for areas of high clinical need e.g. anti-retrovirals, agents for the treatment of cystic-fibrosis and anti-neoplastic agents, which highlights the importance of this formulation approach.

In theory, any API can be amorphised if the transition from the liquid state (solution or melt) to the solid state is sufficiently rapid [4]. This means that amorphisation can be considered a universal approach, which could be applied to any molecule, as there is no requirement for ionizable functional groups or molecular weight restrictions, as there are for salt or cyclodextrin complex formation respectively.

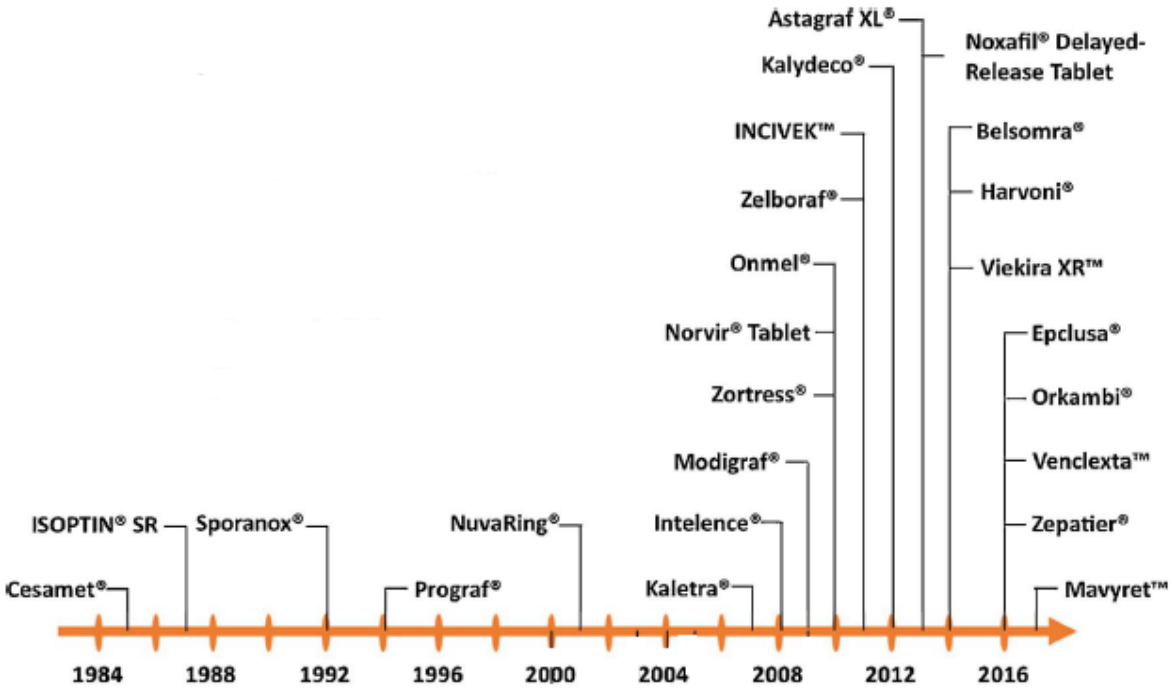

Figure 1.5: Timeline of FDA approval of medicines with APIs in the amorphous state. Adapted from Jermain et al. [2]

In reality, some molecules re-orientate themselves very rapidly to form the thermodynamically stable crystalline state and the amorphous state of the API cannot be created or maintained for a sufficient time for solubility enhancement to be realised. This issue of solid-state instability is the main disadvantage associated with amorphous formulations and approaches to minimise this will be expanded on in Section 1.3.

While the extent of the solubility advantage conferred by a metastable polymorphic form of an API can be relatively reliably estimated from thermodynamic properties, the same is not true for the amorphous state [69]. The absence of thermal events such as melting temperature and the associated heat of fusion, as well as the potential for rapid crystallisation during dissolution testing make such predictions difficult. Knowledge of the anticipated solubility advantage that the amorphous state poses would be beneficial to the formulator, as if this is not orders of magnitude greater than the crystalline form, it is unlikely to be a worthwhile approach. Hancock and Parks were the first scientists to address this issue, by relating the solubility ratio of the amorphous to the crystalline form at a given temperature ($\frac{\sigma_T^a}{\sigma_T^c}$) to the free energy difference between the two forms at that temperature ($\Delta G_T^{a,c}$), using Equation 1.7 [69].

$$\Delta G_T^{a,c} = -RTln(\frac{\sigma_T^a}{\sigma_T^c}) \qquad \textbf{Equation 1.7}$$

The free energy difference between the two forms can be calculated using Equation 1.8

$$\Delta G_T^{a,c} = \left[\Delta H_f^c - \left(C_p^a - C_p^c\right)\left(T_f^c - T\right)\right] - T\left[\frac{\Delta H_f^c}{T_f^c} - \left(C_p^a - C_p^c\right)\left(ln\left(\frac{T_f^c}{T}\right)\right)\right] \qquad \textbf{Equation 1.8}$$

Where ΔH_f^c is the enthalpy of fusion, C_p^a and C_p^c are the specific heat capacities at constant pressure for the crystalline and amorphous forms respectively, and T_f^c is the melting temperature. The theoretical amorphous solubility advantage for a range of APIs calculated using this method ranged from 12-fold for iopanoic acid to 1652-fold for glibenclamide [69]. However, the experimentally determined solubility advantage was much lower than this, ranging from 1.1-fold for hydrochlorothiazide to 24-fold for glucose. The cause of this discrepancy stems from the fact that amorphous form dissolution is a non-equilibrium process. While Equation 1.8 gives an indication of the driving force for the initial rapid dissolution rate, the propensity for dissolution mediated crystallisation prevents amorphous formulations from reaching their theoretical solubility advantage.

Despite this non-concordance with expected solubility advantage, amorphous formulations have shown their benefit over other formulation strategies. Amorphous formulations were demonstrated to improve the solubility of the poorly soluble APIs etoposide and progesterone, while also increasing their permeability across a membrane [70,71]. This was in contrast to with other formulation strategies such as cyclodextrin complexation, which although improved solubility, reduced permeability. This was explained by consideration that permeability is directly related to the APIs partition coefficient between the membrane and aqueous phases. As aqueous phase equilibrium solubility increases, the partition coefficient decreases, decreasing the observed

permeability. In the case of an amorphous formulation, it is the apparent (i.e. non-equilibrium) solubility which is increased through supersaturation rather than the equilibrium solubility. This means that the partition coefficient (and hence permeability) should not be affected by the increase in apparent solubility.

1.3 Factors affecting the stability of amorphous solid dispersions

As highlighted in Section 1.2.3.2.2 the thermodynamic instability of the amorphous form of an API is the major disadvantage or risk when using amorphisation as a tool to improve the aqueous solubility of an API. The most popular method to mitigate this risk is to disperse the amorphous API in a carrier (often a polymer) which prevents crystallisation of the API.

The term "solid dispersion" was initially defined in 1971 as "the dispersion of one or more active ingredients in an inert solid carrier or matrix at solid state prepared by the melting (fusion), solvent, or melting-solvent method" [72]. This broad definition encompasses situations where the solid dispersion is a eutectic mixture, solid solution, glass solution or glass suspension, depending on the solid form of the API, the solid form of the carrier(s), the number of phases and their miscibility in the solid state as clarified in Table 1.1.

Table 1.1: Classification of solid dispersions. Adapted from Laitinen et al. [73]

Physical state of API	Number of phases	
	One phase	Two phases
Crystalline	Solid solution	Eutectic mixture
Amorphous	Glass solution	Glass suspension

As the popularity of amorphisation of APIs has grown since 1971, the term "solid dispersion" has become interchangeable with the term "amorphous solid dispersion" or ASD. ASDs refer to glass solutions as detailed in Table 1.1, i.e. where both the API and the carrier are present in the amorphous form and mixed at the molecular level to form a monophasic system [74]. Amorphous solid solutions can be further classified into those which have a matrix which is polymer based, mesoporous silica based, or small molecule based (so called co-amorphous systems). Mesoporous silica amorphous solid dispersions consist of an API in the amorphous form adsorbed onto the surface of silica, which has pores with a diameter of between 2 nm and 50 nm [75]. This pore size is often smaller than the crystal nucleus of the API, preventing crystallisation [76]. Drug loading is often limited to 20-30% w/w and the loading process often involves the use of organic solvents.

Co-amorphous systems involve combining the API with an amorphous coformer (either another API or a low molecular weight excipient; commonly an amino acid [77,78]). The main advantage of co-

amorphous solid dispersions is that the drug loading which can be achieved may be higher than the equivalent polymeric solid dispersion. Co-amorphous formulations have also found use in fixed dose combination therapy i.e. where two or more APIs are administered in the same tablet. However, the therapeutically relevant ratio/doses of two APIs may not be the ratios at which co-stabilisation occurs, if at all.

While mesoporous silica and co-amorphisation are certainly growing trends in the field of amorphous solid dispersions, the vast majority of research to date has focused on polymeric amorphous solid dispersions. Polymers can stabilise an ASD in the solid state by reducing molecular mobility, and/or can prevent crystallisation from a supersaturated solution. A supersaturated solution is thermodynamically unstable, and the API will precipitate from solution, if given enough time. This precipitation may occur rapidly when ASDs are added to aqueous media. During the dissolution of an amorphous solid, crystallisation can occur via two distinct, but non-exclusive mechanisms; matrix crystallisation and/or solution crystallisation [79]. With matrix crystallisation, the amorphous solid is the source of crystal nucleation and growth in the media, meaning that the achievable degree of supersaturation will be minimised. With solution crystallisation, crystal nucleation and growth originates in the supersaturated solution, and limits the amount of time the supersaturated solution is maintained [80].

For a clinical benefit to be conferred by administration of an ASD, the supersaturated solution must be maintained for a sufficient time for absorption to occur. To achieve this, crystal nucleation and growth must be inhibited. Polymers can be used for this purpose and thus provide a “parachute”, slowing down the reversion of a supersaturated solution to a saturated solution, allowing time for absorption to occur [60]. The cellulosic polymer, HPMC, has proven to be particularly effective as a precipitation inhibiting polymer [81,82].

Although the role of polymers in maintaining solution supersaturation is critical to the successful development of an ASD formulation, the focus of this thesis is on the factors affecting the stability of ASDs in the solid-state. A graph showing factors which are known to influence the physical stability of polymeric ASDs (which shall be referred to as ASDs henceforth) is shown in Figure 1.6. Broadly speaking, these can be classified as API, polymer, formulation, manufacturing and environmental factors.

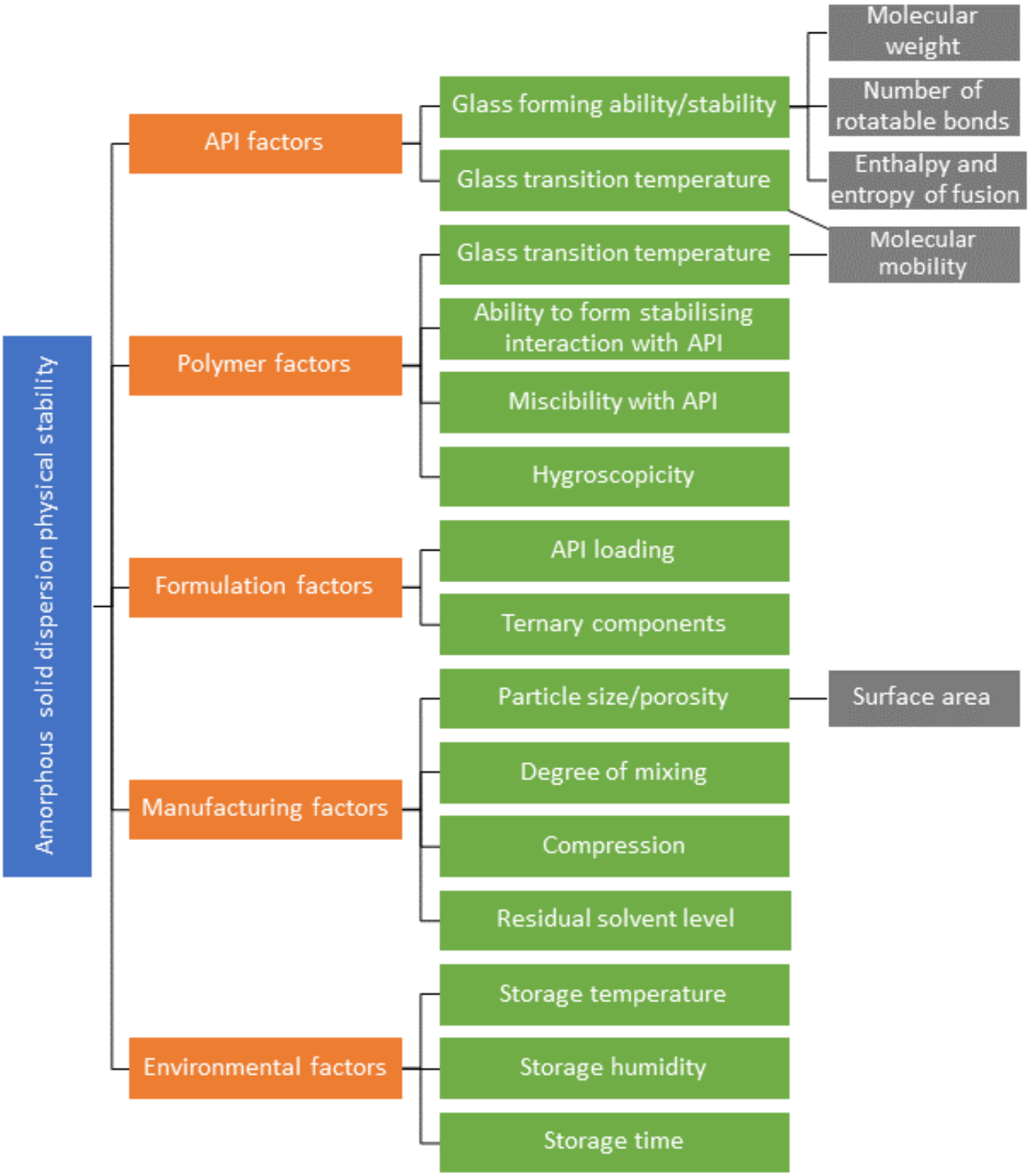

Figure 1.6: Factors known to affect ASD physical stability

1.3.1 API factors affecting ASD physical stability

1.3.1.1 Glass forming ability and stability

As mentioned previously, in theory, any crystalline API can be transformed into the amorphous state from the molten liquid state if cooled sufficiently quickly, so as to avoid the formation of crystal nuclei. The glass forming ability (GFA) of an API has been defined as the ease with which a glass/amorphous form is formed from a liquid on cooling [4]. The minimum cooling rate for this to occur is called the critical cooling rate, which is often regarded as an inverse measure of GFA. The critical cooling rate is determined using a time-temperature-transformation plot. In practice, the critical cooling rate for some APIs may be so high as to be unachievable by current technology. The glass stability (GS) of an API may be regarded as its resistance to recrystallisation when reheated from the amorphous state, above the glass transition temperature, into the supercooled liquid state. GFA and GS are often related, i.e. the ease at which an amorphous form is created is a predictor of how long it is likely to remain in the amorphous form, although this is not always the case [4].

While the GFA and GS are clearly critical to the feasibility of developing an ASD of an API, there is very little understanding in the scientific community of why some APIs are easier to amorphise than others. An excellent study carried out by the Taylor group attempted to correlate the physicochemical features of an API with its GFA and GS using a library of 51 APIs. Using a DSC method, where the crystalline API was heated above its melting temperature and then cooled to -75 ^{o}C before being reheated, they classified APIs into three categories. Those for which crystallisation was detected during the cooling cycle were termed Class 1, those where crystallisation was detected during the reheating cycle were termed Class 2 and those for which no crystallisation was observed in either cycle were termed Class 3 [4]. They discovered that APIs which crystallised during cooling (i.e. Class 1 compounds) were likely to have lower molecular weight, fewer rotatable bonds and higher enthalpy and entropy of fusion relative to the APIs with good GFA/GS (i.e. Class 3 compounds). All of these observations are logical. APIs with high molecular weight and a large amount of rotatable bonds will require more time to orientate themselves into a position where nucleation and crystal growth can occur. Similarly, lower entropy and enthalpy of fusion implies a lower enthalpy and entropy difference between the amorphous and crystalline states for a compound with equal differences in heat capacity between the amorphous and crystalline form as a function of temperature [4]. This means that the larger the Gibbs free energy difference between the amorphous and the crystalline form, the more spontaneous the reversion to the crystalline form will be. Other studies have echoed these findings, observing that molecular weight and free energy difference are critical to an API's glass forming ability and stability [83, 84].

The above studies classified GFA and GS using a DSC method where the API was heated above the melt temperature and then cooled to below the glass transition temperature. This amorphisation method can be considered to be a miniaturised version of hot melt extrusion, a method commonly used to manufacture ASDs. The other commonly used ASD preparation method is spray drying, a solvent evaporation-based method. Spin-coating has been used as a miniaturised version of spray drying for screening studies previously [85]. The Taylor group attempted to amorphise the same panel of 51 APIs using a spin-coating method to determine if the same relationship between API physicochemical properties and ease of amorphisation was observed. In nearly 70% of the APIs examined, the crystallisation tendency classification was the same, regardless of the route of amorphisation [86]. These studies highlight that it is the inherent physicochemical properties of the API rather than the method of manufacture which is the greatest predictor of amorphous state formation/ stabilisation of the API. If the API does not easily form the amorphous state, the formulator will face an uphill battle formulating an ASD.

1.3.1.2 Glass transition temperature

A defining feature of an amorphous material is the presence of a glass transition temperature. The glass transition temperature is a phenomenon that can be understood when the enthalpy or molar volume of a substance versus temperature is plotted. These parameters increase linearly up until a point where there is a discontinuity in the relationship between temperature and enthalpy/ volume as shown in Figure 1.7. This point is known as the glass transition temperature of a substance [87]. At temperatures below the glass transition temperature, the molecular mobility and relaxation processes of the API are much slower than above the glass transition temperature [74].

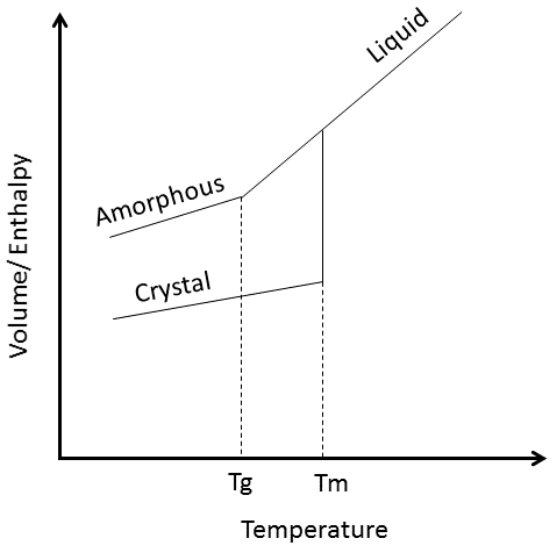

Figure 1.7: Relationship between amorphous and crystalline forms and temperature/enthalpy. Tg = glass transition temperature, Tm = melting temperature. Adapted from Hancock et al. [3]

At the glass transition temperature, the API molecules can rotate relatively freely and α-relaxation (also called global relaxation) can occur. This type of relaxation involves the co-operative movement of several molecules of the API. Below the glass transition temperature, API molecules are less free to rotate and co-operative relaxation cannot occur. Secondary relaxation processes (often termed β and γ relaxation), may occur at temperatures below the glass transition temperature. These secondary relaxation processes involve the local motions of the molecule which may include intramolecular re-orientation [88].

The relationship between the speed of these molecular relaxation processes and the stability of an amorphous solid is poorly understood. A longstanding rule-of-thumb originated in 1995 when Hancock et al. found that the molecular mobility of three amorphous materials (PVP, indomethacin and sucrose) was so low at temperatures 50 °C below their respective glass transition temperatures, that they may be considered "kinetically frozen". This temperature is also known as the Kauzmann temperature [3]. They concluded that at this temperature (Tg-50 °C) the molecular motions "slowed to a point where they are insignificant over the normal lifetime of a pharmaceutical product" [89]. Due to their findings, common consensus was that amorphous materials should be stored at a temperature at least 50 °C below their glass transition temperature to ensure physical state stability. Ensuring physical state stability for pharmaceutical compounds may necessitate cold chain storage, as the glass transition temperature is generally approximately two-thirds of the melting-temperature (in degrees Kelvin) [90,91].

A more recent study examined the relationship between molecular mobility and the amorphous state stability of nine pharmaceutical compounds. They discovered that the physical stability

correlated well with the temperature at which secondary β relaxation occurs. If the storage temperature was less than the temperature at which β relaxation occurred, no crystallisation was observed. Conversely, if the storage temperature was greater than the temperature at which β relaxation occurred, crystallisation was observed. The authors concluded that it is the β relaxation temperature which is the critical temperature below which physical state stability can be assured [92]. Although interesting, there is clearly a need to test this theory on a larger panel of APIs to validate these findings.

The glass transition temperature (i.e. molecular mobility) of an API can therefore be considered a critical factor in the solid- state stability of an ASD.

1.3.2 Polymer factors affecting ASD physical stability

1.3.2.1 Glass transition temperature

One of the main attractions of using a polymer to stabilise an ASD, is that many polymers have high glass transition temperatures, meaning they can be used as an anti-plasticiser in a binary mixture of a polymer and an API. This means that the glass transition temperature of the binary mixture of API and polymer, mixed at the molecular level, is raised relative to the glass transition temperature of the API and lowered relative to the glass transition temperature of the polymer. Several different mathematical models describe the relationship between the glass transition temperature of the binary system ($T_g mix$) and the glass transition temperatures of the API and polymer (T_{g1} and T_{g2}) respectively. These models include the Fox, Couchman-Karasz and Kwei equations [93]. However, the most popular model is the Gordon-Taylor equation, shown in Equation 1.9 [94].

$$T_g mix = \frac{(W_1 T_{g1} + K W_2 T_{g2})}{(W_1 + K W_2)} \qquad \textbf{Equation 1.9}$$

W_1 and W_2 are the weight fractions of the API and the polymer respectively and K is a constant which can be calculated from Equation 1.10, where ρ is the true density of the material.

$$K = \frac{T_{g1}\,\rho_1}{T_{g2}\rho_2} \qquad \textbf{Equation 1.10}$$

It is therefore unsurprising that the commonly used polymers in ASD preparation tend to have relatively high glass transition temperatures. Examples include HPMC, HPMCAS and PVP, which all have Tgs > 100 °C.

The molecular weight of the polymer influences its Tg. The higher the molecular weight of a particular polymer, the higher the Tg, as more thermal energy is required to cause an α relaxation (glass transition) due to an increase in the viscosity of the polymer. Increasing the molecular weight

of PVP used in ASDs of piroxicam increased the ability of the polymer to supress crystal growth in the ASD [95]. However, increasing the molecular weight of the polymer may result in retardation of dissolution rate due to the increase in viscosity of the boundary layer in aqueous media [96].

1.3.2.2 Interaction with API

The ability of a polymer to form a stabilising interaction with the API should also be considered when formulating a polymeric ASD. This can reduce the molecular mobility of the ASD and prevent crystallisation. For example, PVP is capable of hydrogen bond formation with nifedipine and probucol, which results in ASDs which are physically stable in the solid state relative to the equivalent systems created with polymers with weaker or no hydrogen bonding propensity [10,97]. The ability of a polymer to hydrogen bond with an API may also prevent crystallisation during the dissolution of an ASD, as has been demonstrated for the dietary flavonoid quercetin [98]. For APIs and polymers with ionizable functional groups, the potential for salt formation should also be considered. Salt formation between Eudragit E and indomethacin, ibuprofen and naproxen has previously been described [99,100].

The potential for intermolecular interaction can be evaluated by examining the chemical structures of the API and the polymer for potential hydrogen bond donor and acceptor functional groups. Intermolecular interaction between the ASD and the polymer can be demonstrated experimentally through spectroscopic techniques such as ATR-FTIR. The presence of any intermolecular interaction is also commonly inferred from DSC data. One of the assumptions underlying the glass transition temperature prediction from the Gordon Taylor equation is that there are no strong intermolecular interactions between the two components [94]. If intermolecular interactions between the API and the polymer are present in the ASD, and stronger than any intramolecular interaction experienced by either component, a positive deviation from the Gordon-Taylor predicted value is generally observed [93].

1.3.2.3 Miscibility with API

As defined previously, solubility is a thermodynamic property of an API at a given temperature and pressure with a specified solvent under equilibrium conditions. This definition can be extended to encompass an ASD, whereby the crystalline API is considered as a solute and the amorphous polymer, above its own Tg (i.e. supercooled liquid), is considered to be a solvent. However, as solubility measurements should be determined for systems in a state of equilibrium, and an ASD represents a non-equilibrium state [93], experimental determination of an API's solubility in a given polymer is difficult, if not impossible to calculate. Because of this, API solubility in a polymer is often determined under non-equilibrium conditions, and solubility at ambient temperature is determined

by extrapolation [101]. The crystalline API-polymer solubility limit at a specified temperature can then be estimated.

The "miscibility" of an API and a polymer is generally understood to refer to the solubility of an amorphous (rather than crystalline) API in an amorphous polymer [101,102]. The degree of miscibility between the polymer and the API is a critical factor to consider in the creation of an ASD, as it determines the maximum drug loading which can be obtained at a specified temperature in a stable ASD. This limit is known as the amorphous API-polymer miscibility limit. The more miscible an API and a polymer are, the greater the amount of amorphous API which can be incorporated into the polymeric matrix before the polymer becomes saturated with respect to the amorphous API, and crystallisation of the API begins. If a drug and polymer are immiscible, or miscible only at very low API concentrations, the development of an oral formulation of an ASD may require very large polymer concentrations which may require a very large tablet mass.

Several methods of predicting the miscibility between an API and polymers exist. Perhaps the most well-known is the melting point depression method. In this method, a mixture of crystalline API and amorphous polymer are heated in a DSC pan, and the onset temperature of the melting point of the API is recorded. If the melting point of the mixture is depressed relative to the melting point of the pure API, a degree of miscibility between the components is present, as its chemical potential is reduced. Conversely, if the melting point remains unchanged there is no miscibility present [102]. By application of Flory-Huggins theory, the melting point depression can be used to determine the interaction parameter (χ) between drug and polymer [103,104]. A negative interaction parameter indicates that mixing between the components is energetically favoured and the two components should be miscible with each other [105]. In order for this methodology to be applied, the API should not decompose at its melting temperature and the melting temperature of the API should be at least 20 °C higher than the glass transition of the polymer [106]. This method will not work in situations where the API has a melting point below or very near the glass transition of the polymer.

Alternative methods to predict API-polymer miscibility include measuring the solubility of the drug in a monomeric liquid analogue of the polymer or the use of Hansen Solubility Parameters. The Hansen Solubility Parameter (δ) approach involves examining the molecular structure of the two components and ascribing values to each of them based on dispersive forces (δ_d) , potential for interaction between polar groups (δ_p) and hydrogen bonds (δ_h) using tables created by Van Krevelen [107] . The equation for determining the Hansen Solubility Parameter (HSP) of a substance is shown in Equation 1.11.

$$\delta^2 = \delta_d^2 + \delta_p^2 + \delta_h^2 \qquad \textbf{Equation 1.11}$$

If an API and a polymer have HSP values which differ by less than 7 units they are likely to be miscible, while if this difference is greater than 10 units they are likely to be immiscible [52]. Clearly, there is a grey area whereby if the difference in HSP values is between 7 and 10, there is no predictive power in this model. Another disadvantage with this model is that, as it is calculated based on the monomeric unit, polymers with randomly occurring substituents e.g. HPMC, will only have estimated HSP values.

The homogeneity of an ASD can be inferred by the presence of a single glass transition temperature. This homogeneity may be considered as evidence that there is miscibility between the polymer and the API at the examined ratio. There has been some criticism of this technique however, as the sensitivity of a DSC in detecting a phase separated system is approximately 30 nm i.e. the API-region or polymer-region must be at least this size in order for two glass transitions (and immiscibility) to be detected [108]. Solid-state NMR can determine regions of phase separation from regions as small as 5 nm, but not as many facilities have the equipment or expertise for this type of analysis as have DSC, for example [109].

1.3.2.4 Hygroscopicity

The hygroscopicity of a polymer will also influence the physical stability of an ASD. Water is a very strong plasticiser with a Tg of approximately -137 ^{o} C [3]. Therefore, only a small amount of water, mixed at the molecular level with the polymer, may plasticise the system to a significant degree, depressing the glass transition temperature of the polymer in accordance with the Gordon-Taylor equation. If this water is not removed during the preparation of the ASD, it will also depress the glass transition temperature of the ASD, reducing its physical stability at ambient temperatures.

The hygroscopicity of the polymer will also govern the amount of water sorbed by the ASD at conditions of high humidity. As well as the plasticising effect, the addition of water to the system may mean that water molecules displace the API in the ASD by forming hydrogen bonds with the polymer. This can lead to phase separation, whereby instead of a homogenous, molecularly mixed system, with a single glass transition temperature, a drug-rich region and a polymer-rich region are created. The presence of this biphasic system is often detectable due to the presence of two distinct glass transition temperatures. Where water causes this phase separation by the aforementioned mechanisms, the process is termed moisture induced phase separation (MIPS). MIPS has been demonstrated in PVP-felodipine, PVP-ibuprofen and PVPVA-felodipine ASDs [110,111]. Phase separation may result in an ASD which is initially maintained in the amorphous state, but may be a process which precedes API crystallisation, as was observed for a PVP-felodipine ASD stored at high relative humidity [110].

The propensity of a polymer to sorb moisture can be experimentally determined using thermogravimetric analysis (TGA) or dynamic vapour sorption (DVS) analysis. DVS is particularly useful as it can be used to determine the relative humidity induced glass transition i.e. the relative humidity at which sufficient water has been adsorbed by the polymer for the glass transition to occur at the temperature of the analysis [112].

1.3.3 Formulation factors affecting ASD stability

1.3.3.1 API loading

As explained in Section 1.3.2.3, the degree of miscibility between polymer and API determines the amount of API which can be thermodynamically stabilised in the ASD. This limit should determine the ratio of API to polymer used in the formulation. This can best be understood visually, as shown in Figure 1.8. Zones 1 and 3 describe thermodynamically stable ASDs and supersaturated ASDs respectively. There is no thermodynamic driving force for recrystallisation in Zone 1 ASDs, while there is for Zone 3 ASDs [101]. Ideally ASD formulation design should aim for Zone 1 classification. However, this may mean that drug loading is too low for a viable formulation to be developed.

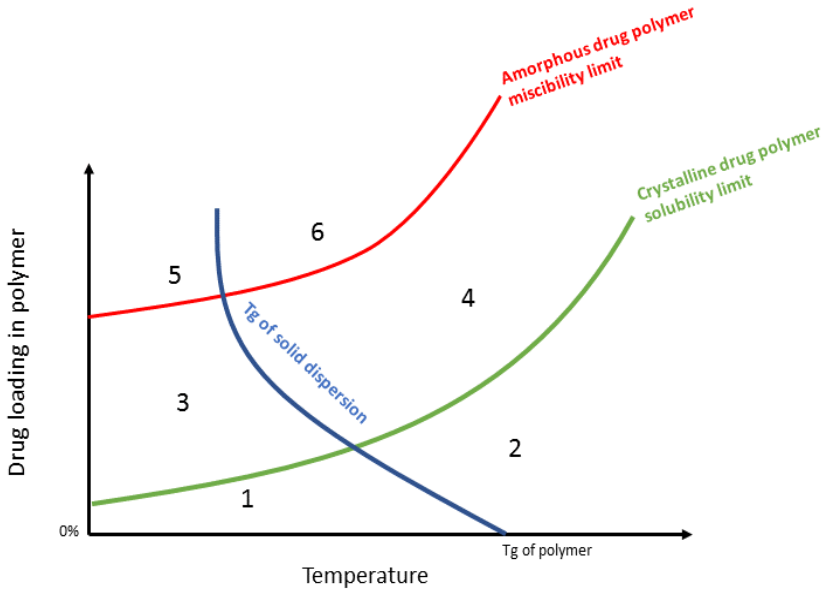

Figure 1.8: Hypothetical phase diagram of ASDs adapted from Qian et al [101]. Zone 1- thermodynamically stable glass, Zone 2- thermodynamically stable liquid, Zone 3- supersaturated glass, Zone 4- supersaturated liquid, Zone 5 – supersaturated immiscible glass, Zone 6- supersaturated immiscible liquid

In this instance, a Zone 3 ASD formulation should be considered. Zone 3 ASDs may be stabilised through kinetic processes i.e. by reducing the molecular mobility of the system through favourable interaction with the polymer, as described in Section 1.3.2.2. A remarkable case study of a thermodynamically metastable (Zone 3) ASD (nifedipine-PVP-Eudragit RS), which remained

amorphous after 25 years of storage, was explained by kinetic stabilisation [113] . Conversely, phase separation was observed for a supersaturated ASD (Zone 3) of griseofulvin and PVP, which was attributed to a lack of kinetic stabilisation [114].

1.3.3.2 Ternary components

As the physical stability of ASDs is the major limitation to their development in commercial products, formulators have explored the use of other excipients in ASD formulations to optimise stability. One of the most common approaches is the use of a second polymer to create a ternary ASD [115–119]. The logic behind the use of a second polymer is that the drug loading achievable may be increased relative to a binary system. One of the polymers might be chosen because of its very high Tg, i.e. stabilisation through kinetic mechanisms, while the other might be chosen because of its ability to solubilise the API or inhibit its crystallisation from a supersaturated state i.e. stabilisation through thermodynamic mechanisms. A judicious combination of polymers should ensure ASD stability in the solid-state during storage, as well as inhibition of crystallisation from a supersaturated solution during dissolution. The advantage of ternary ASDs over binary ASDs, in terms of solid state stability and supersaturation maintenance during dissolution, has been demonstrated for an ASD of indomethacin using PVP and Eudragit synergistically [117].

Other excipients which may be considered in ASD formulations include surfactants and fillers. Ternary ASDs containing surfactants such as sodium dodecyl sulphate have demonstrated increased dissolution rates relative to binary systems, as they increase API solubility through solubilisation as well as amorphisation [120]. This solubilisation effect could not be attributed to the formation of micelles, as surfactant concentrations in the dissolved ternary formulations were below their respective critical micelle concentrations [120]. The improved dissolution profile conferred by the inclusion of surfactants in ternary ASDs may, instead, be explained by the improved drug wettability and reduced interfacial tension between drug particles and the dissolution medium caused by the presence of the surfactant [120]. However, it has been theorised that surfactants in ASDs may induce nucleation by decreasing the viscosity of the system, reducing the kinetic barrier to recrystallisation or alternatively may inhibit nucleation by acting as an impurity at the interface of clusters of APIs [121].

Fillers such as MCC, mannitol and lactose which are blended with the ASD prior to tabletting, are commonly used to improve the wettability and compression properties of ASDs [122]. The effect of these additives on the physical stability of ASDs was investigated by Leane et al. They found that tabletted ASDs which used mannitol as a filler exhibited the poorest amorphous state stability of the API ibipinabant upon storage, while MCC stabilised the amorphous API the most effectively [123].

This observation was explained by consideration that mannitol is more crystalline in nature than MCC, therefore it provides a surface onto which the amorphous API can crystallise.

These studies demonstrate that although excipients are often considered inert components of a formulation, they can play an active role in stabilisation and performance of an ASD.

1.3.4 Manufacturing related factors affecting ASD physical stability

1.3.4.1 Particle size/porosity

The manufacturing process chosen to produce an ASD can also affect the stability and performance of the system, as this will determine the particle size and or/ porosity of the ASD particles. As crystallisation is known to be orders of magnitude faster from the surface of a material relative to the bulk of the material [124,125], the higher the surface area of ASD particles, the more prone to crystallisation they may be. This has been demonstrated experimentally for an ASD of a BCS Class 2 compound (referred to as compound X in the study) and PVPVA prepared via spray drying and hot melt extrusion. The spray dried ASD exhibited poorer physical stability after 2 months compared to its hot melt extruded equivalent, which was attributed to differences in surface area [12].

1.3.4.2 Degree of polymer-API mixing achieved

Different methods of manufacturing ASDs can allow different degrees of mixing between the polymer and API during the amorphisation process. It has been demonstrated previously that a higher drug loading can be achieved for ASDs prepared by spray drying relative to milling [126]. This was explained by consideration that, during spray drying, the polymer and API are freer to interact as they are already molecularly dispersed in a solution, while during milling the crystal lattice of the API must be mechanically destroyed before the API and polymer can be mixed at a molecular level. A similar finding was observed for a formulation containing ramipril and hydrochlorothiazide prepared with either PVPVA or Soluplus by hot melt extrusion or spray drying. While ramipril was successfully amorphised via both processes, hydrochlorothiazide was only completely amorphised via spray drying. The hydrochlorothiazide material processed via hot melt extrusion remained partially crystalline and continued to crystallise on storage [13].

1.3.4.3 Compression

ASD formulations are commonly processed via direct compression into tablets. ASD systems which are metastable (i.e. in Zones 3 and 5, Figure 1.8), such as naproxen 30% w/w in PVP, were found to be susceptible to compression induced demixing when compaction pressures above 367 MPa were used [127] . This resulted in phase separation which was observed as two distinct glass transitions. In contrast, a compressed ASD of naproxen and PVPVA showed improved physical state stability

relative to the uncompressed powder due to increased drug-polymer interaction, as evidenced through FTIR spectra [128].

As solubility is a thermodynamic limit described for a given solute-solvent system at a specified temperature and pressure, it is understandable that when pressure is applied to a system, such as through direct compression, the stability of a system may change. Although this seems obvious, compression induced demixing is a phenomenon that has not been explored extensively in the literature to date.

1.3.4.4 Residual solvent level

Although solvent mediated mechanisms of ASD preparation, such as spray drying, may enable a greater degree of mixing between the polymer and the API as outlined above, removal of any residual solvent to an acceptable level must be carried out to maintain ASD physical stability as well as ensure compliance with regulatory requirements. Ensuring that residual solvent levels are at an acceptable standard may require a secondary drying step such as tray drying or fluid bed drying [129].

1.3.5 Environmental factors affecting ASD physical stability

1.3.5.1 Storage temperature

The temperature at which an ASD is stored is a critical factor in its stability. Interestingly, reducing the storage temperature of an ASD can have oppossing effects on the thermodynamic and kinetic stabilising forces acting on the ASD [73]. As temperature reduces, an ASD which is at its API's thermodynamic solubility limit may become supersaturated and prone to recrystallisation. It is also known that the Flory-Huggins interaction parameter, one of the tools used to predict drug-polymer miscibility, is temperature dependent. A study examining the relationship between temperature and interaction parameter for felodipine ASDs found that as temperature increased, the Flory-Huggins interaction parameter reduced in value, indicating an increased driving force for mixing [130].

From a kinetic perspective, reducing the storage temperature slows down molecular mobility, reducing the risk of crystallisation. Generally speaking, kinetic factors would be expected to dominate during storage at elevated temperatures i.e. high storage temperatures would be anticipated to result in increased crystallisation of an API relative to ambient conditions. By using a variable temperature FTIR, Marsac et al. showed that the hydrogen-bonding strength between felodipine and PVP decreased when temperature was increased, in line with this assumption [110].

1.3.5.2 Storage humidity

Due to their higher volume, amorphous materials are more prone to sorption of atmospheric moisture relative to their crystalline counterparts [112,131]. As well as the inherent increased hygroscopicity of the amorphous state, many of the polymers selected for ASD development tend to be hygroscopic. As water is a strong plasticiser as previously described, the sorption of water can dramatically increase the molecular mobility of an ASD, leading to API crystallisation. Indeed, there is a strong argument that most ASDs should be treated as ternary systems, as the presence of water is ubiquitous. When sorbed moisture was accounted for in the predicted glass transition temperature values using the Gordon Taylor equation for an ASD of PVP and ketoconazole, the predicted values matched well with the experimental values [132]. If the presence of water had been disregarded, the experimental values would have deviated negatively from those predicted from the binary Gordon Taylor equation. Any inferences regarding the intermolecular interaction between ketoconazole and PVP based on these findings would have been flawed.

1.3.5.3 Storage time

As described previously, ASDs can be stabilised thermodynamically and kinetically. Often ASDs will be stabilised via a combination of both mechanisms and the relationship between these forces is often complex and intertwined. The kinetic component of ASD stabilisation is commonly described in terms of a characteristic relaxation time, taken as a measure of the molecular mobility of an ASD [133,134135]. The longer the relaxation time, the more stable the ASD is, as the ASD will take longer to "relax" or revert to the ordered crystalline form. Given enough time, all ASDs will eventually revert to a phase separated system with the API in a crystalline state. Formulators must ensure that this does not happen in a pharmaceutically relevant time frame.

1.4 Chemical stability of the amorphous state

Factors affecting the physical stability of APIs in the amorphous state and in ASDs have been well explored in the literature as described in Section 1.3. Logically, as the amorphous form of an API exists in a higher free energy state than its crystalline counterpart, as shown in Figure 1.4, one may expect the amorphous form of an API to exhibit reduced chemical stability relative to the crystalline state. Research on amorphous state chemical stability is sparse relative to amorphous state physical stability, and much of it dates from the 1970s, but this assumption of amorphous state chemical instability has been demonstrated to be true in several studies as described in two review articles [3,136].

The amorphous state has a greater tendency to sorb moisture than the crystalline state [3] and the presence of water can plasticise the amorphous API, resulting in increased molecular mobility and

reduced physical stability as outlined in Section 1.3.2.4. The presence of water may also contribute to chemical instability, as chemical reactions requiring water, such as hydrolysis, may be able to proceed.

The rate of solid-state hydrolytic degradation of the cephalosporin antibiotic, cephoxitin sodium, is known to be dependent on the water content of the sample [137]. It is not surprising therefore, that the amorphous form of this antibiotic showed reduced chemical stability relative to the crystalline form. What is surprising however, is that this observation persisted even when the amorphous and crystalline forms had the same water content (0.5% w/w) [137]. The superior chemical stability of the crystalline state over the amorphous state (with equivalent moisture content) has also been described for two salt forms of an antibiotic in the same drug class as cephoxitin; cephamandole sodium and cephamandole nafate [18]. The same author also found that for cephalothin sodium, the crystalline content of the solid form correlated well with its chemical stability [17].

Another example of amorphous state chemical instability has been described for insulin. When insulin is converted to the amorphous state via lyophilisation, it decomposes due to water sorption, and a cyclic anhydride intermediate is formed [138].

Lastly, another study examined the chemical decomposition of indomethacin at temperatures very close to the melting temperature of the crystalline form, and found that the amorphous form decomposed faster, and via a different kinetic model to crystalline indomethacin [139].

A detailed mechanistic explanation for amorphous state chemical instability has not been deduced for any of the above examples. One theory is that, in the amorphous state, molecules are more free to re-orientate themselves than they would be in a rigid crystal lattice, allowing for a greater degree of interaction with other molecules involved in the chemical degradation reaction [3,18,136]. Clearly, this is an area of research which needs further investigation. It is apparent that formulation scientists should assess the often-overlooked chemical stability of the amorphous state of an API, if an ASD formulation is being considered.

1.5 Summary

In summary, the deliberate creation of an amorphous state of an API is a technique to overcome the poor aqueous solubility of pipeline NCEs. The growth in popularity of this approach is apparent. A remarkable example of the successful application of an ASD formulation has been demonstrated for the anti-neoplastic agent vemurafenib. Preliminary clinical trials with crystalline vemurafenib showed no tumour regression, even with doses as high as 1.6 g [2]. This lack of efficacy was attributed to poor oral bioavailability of the API and the clinical trial was halted. The decision was made to re-formulate the API as an ASD. When the clinical trial resumed using the new formulation, the bioavailability of the API was dramatically improved [140], and tumour regression was observed in a majority of patients [2]. The ASD formulation was subsequently approved by the FDA under the trade name Zelboraf ®.

If ASD success stories such as this are to be replicated, the amorphous form's inherent physical instability must be overcome via stabilisation over a pharmaceutically relevant timeframe. Understanding the many factors which affect this stabilisation are thus of the utmost importance, and a contribution to the same is the basis of this thesis.

Chapter 2: Materials and Methods

2.1 Materials

A list of the materials used in this thesis are detailed in Table 2.1 below

Table 2.1 Material and supplier list for materials used

Material	Supplier
(R)-(-)-ibuprofen (98% purity) **(R IBU)**	Fluorochem Ltd. (U.K.)
(R)-(-)-ibuprofen (98% purity)[#] **(R IBU)**	School of Chemical and Bioprocess Engineering, UCD (Ireland)
(R,S)-(±)-ibuprofen (99% purity) **(R,S IBU)**	Kemprotec Ltd. (U.K.)
(R,S)-(±)-ketoprofen (98% purity) **(KETO)**	Sigma Aldrich (Ireland)
(S)-(+)-ibuprofen (98% purity) **(S IBU)**	Kemprotec Ltd. (U.K.)
Acetonitrile (HPLC grade)	Fisher Scientific (Ireland)
Adalat® 10mg soft capsule	Bayer (U.K.)
Ethanol (96% v/v)	Corcoran Chemicals (Ireland)
Hydrochloric acid (37% w/v)	Sigma Aldrich (Ireland)
Hydroxypropyl cellulose (L-HPC) **(HPC)** Mw 100,000 g/mol	ShinEtsu (Japan)
Hydroxypropyl methyl cellulose (Pharmacoat 606) (**HPMC)** Mw 35,600 g/mol	ShinEtsu (Japan)
Hydroxypropyl methyl cellulose acetyl succinate (Aqoat LF) **(HPMCAS)** Mw 140,000 g/mol	ShinEtsu (Japan)
Hydroxypropyl methyl cellulose phthalate (HP-55) **(HPMCP)** Mw 45,600 g/mol	ShinEtsu (Japan)
Liquid nitrogen	BOC (Ireland)
Magnesium stearate	Sigma Aldrich (Ireland)
Methanol (HPLC grade)	Fisher Scientific (Ireland)
Microcrystalline cellulose (Avicel PH 102)	FMC Biopolymer (Belgium)
Microcrystalline cellulose spheres (Vivapur-500 µm diameter)	JRS Pharma (Germany)
Monosodium phosphate	Sigma Aldrich (Ireland)
Nifedipine (98% purity)	Fluorochem Ltd. (U.K.)
Nifedipine (micronized) (98% purity)	ICFTI (Italy)
Nifedipine Impurity A CRS (100% purity)	European Pharmacopoeia (France)
Nifedipine Impurity B CRS (100% purity)	European Pharmacopoeia (France)
Phosphorous pentoxide	Acros Organics (Belgium)
Polyvinyl acetate **(PVAcetate)** Mw 100,000 g/mol	Acros Organics (Belgium)
Polyvinyl acetate phthalate **(PVAP)** Mw 47,000-61,000 g/mol [141]	Colorcon (U.S.A.)
Polyvinyl alcohol **(PVAlcohol**) Mw 15,000 g/mol	MP Biomedicals (U.S.A.)
Polyvinyl pyrrolidone K17 **(PVP 17)** Mw 7,000-11,000 g/mol	BASF (Germany)
Polyvinyl pyrrolidone K30 **(PVP 30)**	BASF (Germany)

Mw 54,000-55,000 g/mol	
Polyvinyl pyrrolidone K90 **(PVP 90)** Mw 1,000,000-1,500,000 g/mol	BASF (Germany)
Polyvinyl pyrrolidone vinyl acetate 3:7 E335 **(VP:VA 3:7)** Mw 28,000 g/mol [106]	Ashland (U.S.A.)
Polyvinyl pyrrolidone vinyl acetate 6:4 **(Kollidon VA 64)** Mw 45,000-70,000 g/mol	BASF (Germany)
Polyvinyl pyrrolidone vinyl acetate 7:3 E735 **(VP:VA 7:3)** Mw 56,700 g/mol [106]	Ashland (U.S.A.)
Sodium chloride	Sigma Aldrich (Ireland)
Sodium hydroxide	Sigma Aldrich (Ireland)
Polyvinyl caprolactam polyvinyl acetate polyethylene glycol **(Soluplus)** Mw 118,000 g/mol	BASF (Germany)
Water (HPLC grade)	Elix 3 connected to Synergy UV system (U.K.)

[#] The methodology for the crystallisation and isolation of R-(-)-ibuprofen (98% purity) used by personnel at the School of Chemical and Bioprocess Engineering, UCD, Ireland is described in Section 2.2.1.6

2.2 Methods

2.2.1 Unit operations

2.2.1.1 Spray drying (SD)

All spray drying was carried out using a B-290 Mini Spray Dryer (Büchi, Switzerland) equipped with a high efficiency cyclone configured in the open mode. For all systems, a solution feed rate of *ca.* 9-10 mL/min, a drying air flow of *ca.* 35 m^3/hr and an atomisation air flow of *ca.* 667 normlitres/hr at standard temperature and pressure were used. Specific inlet and outlet temperatures for each spray dried system described in this thesis are outlined below.

2.2.1.1.1 Preparation of ibuprofen-HPMC samples via SD

A 1% w/v solution of varying mass ratios of one of R,S-ibuprofen, S-ibuprofen or R-ibuprofen (Fluorochem Ltd., U.K.) and HPMC were prepared by dissolving these components in a 50:50 v/v ethanol: water mixture under constant stirring. The resulting solutions were spray dried using an inlet temperature of 105 °C. The outlet temperature fluctuated between 49 °C and 56 °C. The production yield from this process ranged from 7.5% to 52%.

2.2.1.1.2 Preparation of solid samples of polymeric solutions via SD

As the source material for VP:VA 7:3 and VP:VA 3:7 were supplied as 50% w/w ethanolic solutions it was necessary to process these solutions via spray drying to obtain a fine powder. The solutions as supplied were diluted with ethanol to a 2% w/v solution and spray dried using an inlet temperature of 78 °C. The outlet temperature fluctuated between 45 °C and 48 °C. The typical batch size processed was 250 mL. The production yield for this process was approximately 70%.

2.2.1.1.3 Preparation of ketoprofen-polymer samples via SD

The polymer (PVP30 or Kollidon VA 64 with molecular weights of 54,000-55,000 g/mol or 45,000-70,000 g/mol respectively) was dissolved in ethanol and the total solute concentration was fixed at 5% w/v. Ketoprofen content was 0%, 10% or 20% w/w total solute. Solutions were spray dried using an inlet temperature of 80 °C. The outlet temperature fluctuated between 44 °C and 56 °C. The typical batch size processed was 100 mL. The production yield for this process varied between 58 % and 74%.

2.2.1.1.4 Preparation of nifedipine-polymer samples via SD

The polymer (HPMC, PVP or Soluplus) and nifedipine (Fluorochem Ltd., U.K.) were dissolved in ethanol (PVP and Soluplus systems) or ethanol and water (70:30 v/v ratio for all systems and 50:50 v/v ratio for HPMC-nifedipine). Total solute content concentration was fixed at 2% w/v and nifedipine concentration was either 0%, 15% or 30% w/w of total solute concentration. Solutions were spray dried using an inlet temperature of 105 ^{o}C for solutions containing ethanol and water or an inlet temperature of 78 ^{o}C for solutions containing ethanol only. The outlet temperature fluctuated between 49 ^{o}C and 55 ^{o}C. The typical batch size processed was 200 mL. The production yield for this process ranged from 35% to 55%. The nifedipine-containing solutions were protected from light by covering the spray dryer glass in aluminium foil. The powders produced via spray drying were stored in amber jars immediately after manufacture.

2.2.1.2 Cryo-milling (CM)

All cryo-milling was carried out using a Cryogenic Mixer Mill CryoMill (Retsch, Germany) attached to an auto filling liquid nitrogen dewar (Retsch, Germany). A stainless steel cryo-mill chamber of 25 mL capacity filled with three stainless steel balls of 12 mm diameter were used for all cryo-milling carried out in this thesis. An automatic precooling step was applied before any milling was commenced. This consisted of the mill operating at a frequency of 5 Hz while liquid nitrogen circulated around the stainless-steel chamber until cryotemperature was reached, which was automatically detected via a sensor. The material was milled for three cycles, where each cycle consisted of a grinding step at a frequency of 30 Hz for 5 minutes followed by an intermediate cooling step at a frequency of 5 Hz for 2 minutes. Cryotemperature was maintained throughout milling via liquid nitrogen circulating around the milling chamber.

Specific methods used for each cryo-milled system described in this thesis are outlined below.

2.2.1.2.1 Chiral recognition screening of ibuprofen-cellulose polymer systems via CM

250 mg of ibuprofen (R,S-ibuprofen, S-ibuprofen or R-ibuprofen (Fluorochem Ltd., U.K.) and 250 mg of the cellulose polymer (HPC, HPMC, HPMCAS or HPMCP) were placed in the cryo-mill chamber and milled as described above.

HPMCP was too fibrous to mix well in a physical mixture and so was cryo-milled (as outlined above) prior to testing.

2.2.1.2.2 Generation of ketoprofen-polymer solid dispersions via CM

As PVAlcohol and PVAcetate were supplied as large grains/ beads (approx.. 3mm and 5mm in length respectively) it was necessary to process these using a cryo-mill prior to physically mixing these with

ketoprofen. 1 g of these materials as supplied were placed in the cryo-mill chamber and milled as described above.

Physical mixtures of ketoprofen and polymer in a 20:80 w/w ratio were melt-quenched in an aluminium weighing boat by placing on a PC-400D hot plate (Corning, USA) at 120 °C for 10 minutes before being quenched in liquid nitrogen and then cryo-milled to obtain a powder. Cryo-milling was necessary as some of the system formed glassy films upon melt quenching which would not have been suitable for dissolution and stability testing. 500 mg of the melt-quenched material was placed in the cryo-mill chamber and milled as outlined above.

2.2.1.3 Electrospraying (ES)

Solutions were electrosprayed using a Nanon-01A Electrospinner (Mecc Co. Ltd, Japan) using a 25G needle (0.26 mm nominal inner diameter) as a nozzle. The collector consisted of metal stage platform approximately 20 cm x 20cm in dimension, which was covered in aluminium prior to electrospraying. The distance between nozzle tip and collector was fixed at 30 cm, the flow rate was 1 mL/h and the potential difference applied was 15 kV. Electrospraying was carried out under ambient conditions of approximately 20 °C and 40% RH. The polymer (PVP30 or Kollidon VA 64 with molecular weights of 54,000-55,000 g/mol or 45,000-70,000 g/mol respectively) was dissolved in ethanol and the total solute concentration was fixed at 5% w/v. Ketoprofen content was 0%, 10% or 20% w/w total solute. The typical feed solution batch size was 10 mL. The solution containing PVP and 20% w/w ketoprofen was chosen for further studies so a larger batch (~35 mL) was processed for this purpose. The production yield for the electrospraying process outlined above was approximately 72%.

2.2.1.4 Tabletting

2.2.1.4.1 Tabletting, tablet hardness, tensile strength and ejection force measurements of polymer-ketoprofen systems

Solid dispersions were mixed with MCC in a 50:50 w/w ratio in an agate pestle and mortar. 200 mg of this mixture was tabletted using an NP-RD10 single punch tablet press (Natoli, U.S.A) with an 8 mm diameter flat-faced die. The compaction pressure applied was 6 kN and the tablet was held at this pressure for 60 seconds. Tablets were removed from the die using the bottom punch and the force required to eject the tablet was recorded. Immediately after manufacture, the tablet thickness was recorded using a micrometre (AnyiMeasuring, China) and the tablet was subjected to radial hardness testing using a handheld tablet hardness tester (Electrolab, India). The tensile strength of the tablets was calculated using Equation 2.1.

$$\sigma = \frac{2F}{\pi DH} \qquad \textbf{Equation 2.1}$$

Where σ is the tensile strength (MPa), F is the radial hardness (N), D is the tablet diameter (mm) and H is the tablet thickness (mm).

Control measurements were also recorded for each polymer-ketoprofen system by physically mixing crystalline ketoprofen, the polymer of choice and MCC in a 10:40:50 w/w ratio in an agate pestle and mortar. For each solid dispersion and their crystalline ketoprofen controls, a minimum of 3 tablets were manufactured and tested.

2.2.1.4.2 Tabletting of amorphous solid dispersions of nifedipine

Spray dried amorphous solid dispersions of nifedipine, containing nifedipine and polymer in a 15:85 w/w ratio, were mixed with 500 µm MCC spheres in a 50:50 w/w ratio in an agate pestle and mortar. 134 mg of this mixture (equivalent to 10mg nifedipine) was tabletted using an NP-RD10 single punch tablet press (Natoli, U.S.A) and an 8 mm diameter flat-faced die. The compaction pressure applied was 1 kN and the tablet was held at this pressure for 60 seconds. Pitting of the tablets was prevented by brushing the die with magnesium stearate.

2.2.1.5 Production of physical mixtures

Physical mixtures of polymers and crystalline APIs (used as controls in many studies in this thesis) were prepared by gentle mixing of specified polymer: API mass ratios with an agate pestle and mortar. For the photostability studies in Chapter 6 physical mixtures were prepared by mixing the polymer-only powders produced by spray drying (as described in Section 2.2.1.1.4) with micronized nifedipine (ICFTI, Italy) in an agate pestle and mortar in an 85:15 w/w ratio.

2.2.1.6 Crystallisation and isolation of R-ibuprofen

(R)-(-)-ibuprofen (98% purity) was isolated by dissolving 1 mole of racemic ibuprofen with 0.5 mole L-lysine monohydrate to create the R-ibuprofen-S-lysinate salt. The salt was removed from the solution by filtration and recrystallized twice to improve purity. Free (R)-(-)-ibuprofen was isolated from the lysine salt through the addition of concentrated hydrochloric acid. This work was carried out by staff and students in the School of Chemical and Bioprocess Engineering, UCD, Ireland.

2.2.2 Characterisation of ketoprofen-polymer solutions for electrospraying and spray drying

The polymer (PVP or PVPVA64) was dissolved in ethanol and the total solute concentration was fixed at 5% w/v. Ketoprofen content was 0%, 10% or 20% w/w total solute. The conductivities of the solutions were measured using an EL30 Benchtop Conductivity Meter (Mettler Toledo™, U.S.A).

The dynamic viscosities of the solutions were measured using an SV-10 Vibro Viscometer (A&D, Japan). The surface tensions of the solutions were measured using a 701 Force Tensiometer (Sigma, Sweden). All measurements were carried out at a solution temperature of 25 ^{o}C and were conducted in triplicate. The solution properties were tested for statistically significant differences ($p<0.05$) using an unpaired two-tailed student t-test (GraphPad, U.S.A)

2.2.3 Solid state characterisation

2.2.3.1 Powder X-ray diffraction (pXRD)

Samples were analysed using a Miniflex II X-ray diffractometer (Rigaku, Germany) with Ni-filtered Cu Kα radiation (1.54 Å). The tube voltage and tube current used were 30 kV and 25 mA respectively. The samples were analysed on a silicon zero-background sample holder in the reflection mode. Diffraction patterns were collected for 2θ ranging from 5^{o} to 40^{o} at a step scan rate of 0.05^{o} per second.

2.2.3.2 Attenuated Total Reflectance Fourier-Transform Infrared Spectroscopy (ATR-FTIR)

Samples were analysed using a Spectrum 1 FT-IR Spectrometer (Perkin Elmer, U.S.A) equipped with a Universal Attenuated Total Reflectance and diamond/ZnSe crystal accessory. Each spectrum was scanned in the range of 650-4000 cm-1 with a resolution of 1 cm^{-1}. The data was normalised by dividing the absorbance values in each spectra by the maximum absorbance value recorded for that spectra.

For the ibuprofen-cellulose systems whose spectra showed a shoulder in the carbonyl region, the relative intensity of the absorbance of the shoulder to the main peak was determined.

2.2.3.3 Thermogravimetric analysis (TGA)

Ketoprofen-PVP ASDs prepared via SD and ES were analysed using a Q50 TGA (TA Instruments, U.K.). Samples (weighing between 1 and 3 mg) were loaded into standard aluminium pans with a capacity of 20 µL and heated from room temperature to 150 ^{o}C at a heating rate of 10 ^{o}C/min, using nitrogen as a purge gas. The mass loss in this temperature range was determined. Analysis was performed in duplicate.

The same procedure was used to determine the moisture/ residual solvent levels of spray dried nifedipine-polymer ASDs in Chapter 6.a. Analysis was performed in triplicate.

2.2.3.4 Differential scanning calorimetry (DSC)/ Modulated differential scanning calorimetry (mDSC)

All (m)DSC work carried out in this thesis was performed using a TA Q200 DSC (TA Instruments, U.K.) equipped with an RCS-90 refrigerated cooling system (TA Instruments, U.K.) and purged with nitrogen gas at a flow rate of 50 mL/min. The temperature was calibrated with indium and tin and further validated with indium. The enthalpy and the specific heat capacity were calibrated and verified using indium and sapphire, respectively. Standard aluminium pans with a capacity of 20 µL and 3 pinholes were used in all experiments except where otherwise stated. Universal Analysis software (TA Instruments, U.K) was used to analyse data. Methodologies specific to different systems which were examined using DSC are detailed below.

2.2.3.4.1 Thermal analysis of ibuprofen-cellulose polymer samples by mDSC

Samples of the ibuprofen-cellulose polymer systems (2-8mg) were weighed out in standard aluminium pans and cooled to -60 °C and then heated to 120 °C using a ramping speed of 5 °C/min while the temperature was modulated by 0.80 °C every 60 seconds. The melting endotherm, where present, was determined from the total heat flow signal. The proportion of ibuprofen in the ibuprofen-cellulose polymer systems which remained crystalline after cryo-milling was determined by dividing its melting endotherm by the melting endotherm of an unprocessed physical mixture of the cellulose polymer-ibuprofen (enantiomer or racemic compound) at the same weight ratio and multiplying by 100 to obtain a percentage.

The glass transition temperature of the systems, where present, was determined from the reversing heat flow.

2.2.3.4.2 Determination of glass transition temperature of polymers and ketoprofen by mDSC

Samples of the polymers (2-8mg) used in Chapter 4 were weighed out and placed in standard aluminium pans which were then heated from 15 °C to 200 °C using a ramping speed of 5 °C/min while the temperature was modulated by 0.80 °C every 60 seconds. The glass transition onset temperature was determined from the reversing heat flow signal.

The glass transition temperature of ketoprofen as received was determined by heating a sample in a pan from 5 °C to 110 °C and holding it at this temperature for 2 minutes to allow crystalline ketoprofen to melt. The pan was then cooled at 10 °C/min to -30 °C to form ketoprofen in the amorphous state. The pan was then reheated at 5°C/ min to 110 °C while the temperature was modulated by 0.80 °C every 60 seconds and the glass transition onset temperature was taken from the reversing heat flow signal in the second heating cycle. These analyses were carried out in triplicate for each system.

2.2.3.4.3 Determination of glass transition temperature of polymer-ketoprofen systems by mDSC

The glass transition onset temperatures of polymer-ketoprofen systems used in Chapter 4 were determined by creating melt-quenched systems *in situ* in the DSC. Samples were first mixed in an agate pestle and mortar (80:20 w/w polymer: ketoprofen) and accurately weighed into standard aluminium pans (2-6mg). No pin holes were placed in the lids. The pan was then heated at 10 °C/min to 120 °C and held isothermally at this temperature for 10 minutes to allow molten ketoprofen to diffuse through the polymer. The pan was then cooled at 10 °C/min to -30 °C and reheated at 5 °C/min while the temperature was modulated by 0.53 ° C every 40 seconds. Pans were re-weighed after analysis. The glass transition onset temperature was determined from the reversing heat flow signal in the second heating cycle. This was carried out in triplicate for each system.

2.2.3.4.4 Prediction of glass transition temperature of polymer-ketoprofen systems

The predicted glass transition temperature was calculated using the Gordon-Taylor equation (Equation 2.2).

$$T_g mix = \frac{(W_1 T_{g1} + K W_2 T_{g2})}{(W_1 + K W_2)} \qquad \textbf{Equation 2.2}$$

Where $T_g mix$ is the glass transition temperature of the mixed system, T_{g1} and W_1 are the glass transition onset temperature and weight fraction of the first component respectively, and T_{g2} and W_2 are the glass transition onset temperature and weight fraction of the second component respectively. K is a constant which can be calculated from Equation 2.3

$$K = \frac{T_{g1}\,\rho_1}{T_{g2}\rho_2} \qquad \textbf{Equation 2.3}$$

Where ρ is the true density of the material.

2.2.3.4.5 Determination of glass transition temperature of polymer-ketoprofen SD and ES systems by mDSC

Pans were first heated to 180 °C to remove residual moisture before being cooled to -40 °C. The temperature was then modulated by 0.53 °C every 40 seconds and the pan was reheated at 5 °C/min to 200 °C. The glass transition temperature was taken from the second heating run.

2.2.3.4.6 Determination of glass transition temperature of polymer-nifedipine systems by mDSC

Pans were equilibrated at 10 °C before being heated at 5 °C/min to 190 °C while the temperature was modulated by 0.80 °C every 60 seconds.

2.2.3.4.7 Non-isothermal crystallisation studies of R,S-ibuprofen and S-ibuprofen

R,S-ibuprofen and S-ibuprofen were heated at 10 °C/min to 10 °C above their respective melting temperatures and held isothermally for 3 minutes. The melt was then cooled at 10 °C/min to -70 °C and held isothermally for 3 minutes before being re-heated at 10 °C/min to 10 °C above the respective melting temperature. This procedure was repeated using cooling rates of 5, 2 and 1 °C/min and secondary heating rates of 5 and 2 °C/min.

2.2.3.4.8 Enthalpy recovery studies of R,S-ibuprofen, S-ibuprofen and R-ibuprofen

R-ibuprofen (UCD, Ireland) was used in this study. Samples were placed in hermetically sealed pans with a capacity of 40 µL . Pans were heated at 10 °C/min to 100 °C and held isothermally for 2 minutes before being cooled at 10 °C/min to –77 °C and held isothermally for 2 minutes. This heat-cool cycle was repeated a second time to ensure that the sample was completely amorphous. The sample was then heated from –77 °C to –66 °C or -56°C at 10 °C/min and held isothermally for 10, 60, 180, 360 or 720 minutes. Finally, the sample was held at –60 °C and then the temperature was modulated by 0.32 °C every 60 seconds and heated at 2 °C/min to –20 °C. Enthalpy recovery was calculated from the total heat flow using Universal Analysis software (TA Instrument, UK). Enthalpy recovery was plotted using the Kohlrausch-William-Watts (KWW) stretched exponential function [142] (Equation 2.4) to determine the characteristic relaxation time (τ) of the material.

$$\Delta H_{relax} = \Delta H_{\infty}\left[1 - exp\left\{-(t/\tau^{KWW})^{\beta}\right\}\right] \qquad \textbf{Equation 2.4}$$

ΔH_{relax} and ΔH_{∞} are the enthalpy relaxation and the maximum enthalpy recovery at a given temperature. The other parameters t, τ^{KWW} and β are the ageing time, enthalpy relaxation time and the non-exponential parameter respectively [142,143]. ΔH_{∞} was calculated using Equation 2.5

$$\Delta H_{\infty} = \Delta C_p\left(T_g - T\right) \quad \textbf{Equation 2.5}$$

Where, ΔC_p is the change in the heat capacity at the glass transition temperature and T is the ageing temperature. ΔC_p was calculated as the average change in heat capacity for each material at the glass transition of the unaged sample.

2.2.3.5 Specific surface area analysis

Specific surface area was measured using a Gemini VI analyser (Micromeritics, U.S.A.). Prior to analysis, samples were degassed under nitrogen gas, using a SmartPrep degasser (Micromeritics, U.S.A.) at 40 °C overnight, to remove residual moisture. The amounts of nitrogen gas adsorbed at the relative pressures of 0.05, 0.10, 0.15, 0.20, 0.25 and 0.30 were determined and the BET multipoint surface area was calculated. Each experiment was carried out in triplicate for the

ketoprofen-polymer studies (Chapter 5) and in duplicate for the nifedipine-polymer studies (Chapter 6).

2.2.3.6 Density and compressibility analysis

2.2.3.6.1 Determination of true density by helium pycnometry

The density of samples was determined using an Accupyc II 1340 Pycnometer (Micromeritics, U.S.A). The samples were weighed prior to analysis and were placed in a sample cup of 1 cm^3 capacity where they were purged with dry helium (99.995% purity) at a pressure of 19.2 psig using an equilibration rate of 0.0050 psig/ min. Samples were analysed in duplicate and each analysis consisted of five consecutive measurements. Results are presented as the average of ten values.

2.2.3.6.2 Determination of bulk and tapped densities

Samples of select solid dispersion systems studied were gravity fed into a 1 mL glass syringe with graduations of 0.02 mL and the mass and volume of the sample were recorded. The bulk density (ρ_b) was calculated by dividing the mass by the volume. The syringe was tapped against a flat surface 100 times and the new volume that the sample occupied in the syringe was recorded. The tapped density (ρ_t) was calculated by diving the mass by the new volume value [144].

2.2.3.6.3 Carr's Compressibility Index determination

The Carr's Compressibility Index (CCI) was calculated using Equation 2.6

$$Carr's\ Compressability\ Index = 100\frac{(\rho_b - \rho_t)}{\rho_b} \qquad \textbf{Equation 2.6}$$

2.2.3.7 Dynamic vapour sorption (DVS)

Dynamic vapour sorption studies carried out in this thesis were conducted using a DVS Advantage-1 automated gravimetric vapour sorption analyser (Surface Measurement Systems, U.K.).

2.2.3.7.1 Determination of relative humidity induced glass transition by DVS

The relative humidity induced glass transitions (RH_{Tg}) for melt-quenched cryo-milled ketoprofen-polymer samples were determined at 25 °C (± 0.1 ° C). Between 6 and 14 mg of powder were dried to a constant mass (dm/dt <0.002mg/min) at 0% RH in the sample basket in the DVS. After drying, the powder was exposed to a 10% RH increase per hour from 0% RH to 90% RH. From this data a curve of mass versus time was generated. The initial linear portion of this curve was taken to be the surface adsorption of water, and the second linear portion of this curve was taken to be a combination of surface and bulk sorption of water by the powder. The intercept of these two lines

was determined and the time at which RH_{Tg} occurred was determined. The relative humidity at which RH_{Tg} occurred was then determined by plotting time versus RH. A sample plot is shown in Figure 2.1. The amount of water sorbed by the powder at the RH_{Tg} as a percentage of starting sample mass, was also determined. Analysis was carried out in triplicate for each system and although determination of the RH_{Tg} values required manual fitting of portions of the data, the results were deemed to be sufficiently reproducible.

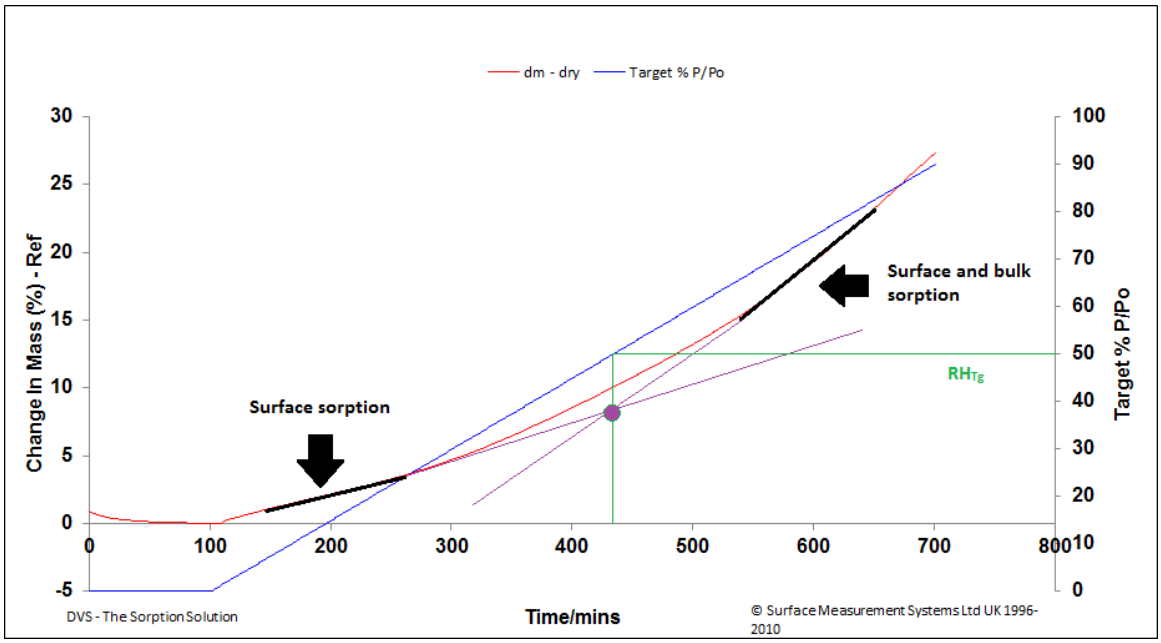

Figure 2.1: Sample plot of RH_{Tg} determination for melt-quenched cryo-milled PVP30KETO system

2.2.3.7.2 Moisture diffusion studies and surface adsorption rate determination

Moisture sorption profiles of electrosprayed and spray dried PVP containing 20% w/w ketoprofen were determined at 25 ° C (± 0.1 ° C). Between 6 and 14 mg of powder were dried to a constant mass (dm/dt <0.002 mg/min) at 0% RH in the sample basket in the DVS. After drying, the powder was exposed to 20% RH until equilibrium mass was reached (defined as dm/dt <0.002 mg/min). After reaching equilibrium mass at 20% RH the powder was then dried at 0% RH until equilibrium mass was reached again, and the process was repeated at 40%, 60% and 80% RH.

The diffusion coefficient (*D)* of water molecules into the powder was determined using a modified Fick's equation shown in Equation 2.7 using the in-built software (DVS Advantage-1 Control Software Ver 1.2.1.2)

$$\frac{M_t}{M_{inf}} = \frac{6}{r_p}\left(\frac{Dt}{\pi}\right)^{0.5} - \frac{3Dt}{r_p^2} \; for \; \frac{M_t}{M_{inf}} < 0.8 \quad \textbf{Equation 2.7}$$

Where $\frac{M_t}{M_{inf}}$ is the ratio of the mass at a given time t (M_t) and the mass at equilibrium (M_{inf}), r_p is the particle radius (determined from the SEM analysis results in Section 5.2.2.2 Particle size analysis) and *t* is the diffusion time [145–147]. A sample diffusion analysis plot is shown in Figure 2.2. The diffusion coefficients of the powders prepared via both spray drying and electrospraying were analysed for statistical significance using an unpaired two tailed student t-test using Prism software (GraphPad, U.S.A).

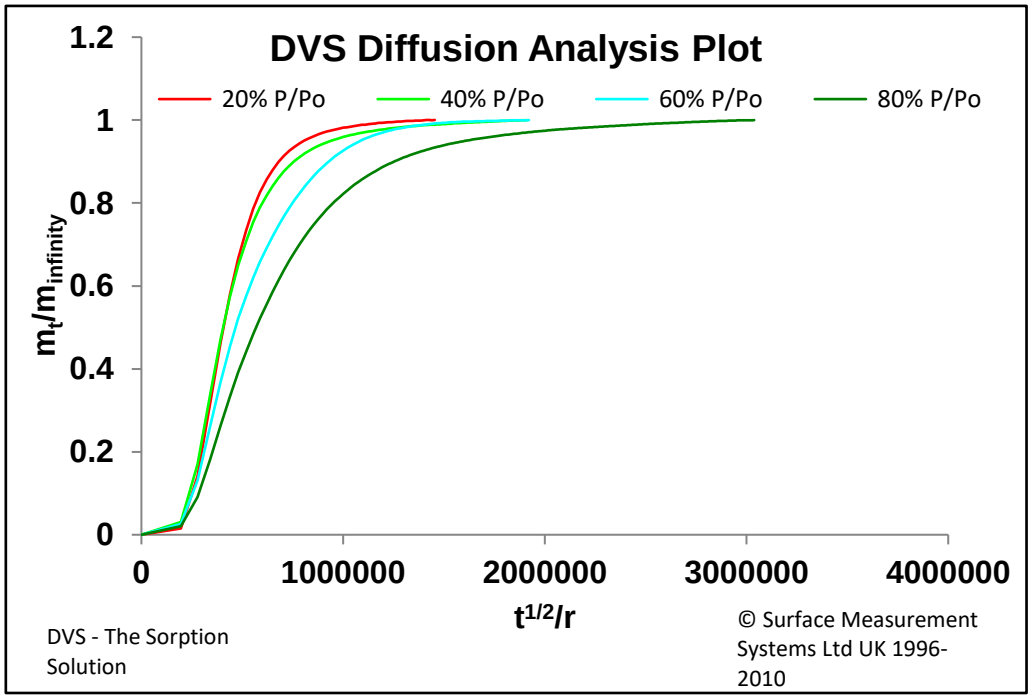

Figure 2.2: Sample diffusion analysis plot for electrosprayed PVP 20% w/w ketoprofen at 20%, 40% 60% and 80% RH.

The rate of moisture uptake on the surface of the powders was determined by analysing the initial increase of mass at each relative humidity stage. By normalising the percentage mass increase to the starting mass of the sample, a curve of mass increase versus time was generated. The linear portion of this curve was plotted and the rate of mass increase (taken to be the surface adsorption of moisture onto the powder) was determined for both spray dried and electrosprayed samples. The surface adsorption of the powders prepared via both processes were analysed for statistical significance using an unpaired two tailed student t-test using Prism software (GraphPad, U.S.A).

2.2.3.8 Scanning electron microscopy (SEM)

Images of select samples were captured using a Supra Variable Pressure Field Emission Scanning Electron Microscope (Zeiss, Germany) equipped with a secondary electron detector at 2 kV. Samples were mounted onto aluminium pin stubs and sputter-coated with gold-palladium under vacuum using a 208HR Sputter Coater (Ted Pella, U.S.A) prior to analysis.

2.2.3.9 Particle size analysis

2.2.3.9.1 SEM image-based particle size analysis

Images of particles produced by both spray drying and electrospraying in Chapter 5 were captured using SEM as outlined above. Each stub was divided into quadrants and representative images from each quadrant were analysed using Image J (N.I.H., U.S.A.) to determine the average particle diameter using the projected area diameter. Where agglomerates were present, each individual sphere was counted as a separate particle. A minimum of 168 particles were analysed for each sample. The average diameters for each set of particles prepared by electrospraying and spray drying were analysed for statistical significance using a two tailed Mann-Whitney test using Prism software (GraphPad, U.S.A.).

2.2.3.9.2 Laser diffraction-based particle size analysis

The particle size distributions of nifedipine-polymer system were determined using a Malvern Mastersizer 3000 (Malvern Instruments, U.K.). Particles were dispersed using an Aero S dry powder disperser (Malvern Instruments, U.K.) using a micro-volume tray under 2 bars of pressure. An obscuration value of 0.5-3% was obtained under a vibration feed rate of approximately 30%. Mastersizer 3000 software (Version 3.63) was used for the analysis of particle size. Each sample was analysed in triplicate.

2.2.3.10 Broadband dielectric spectroscopy (BDS)

Dielectric spectroscopy studies of R,S-ibuprofen and S-ibuprofen samples were carried out in the Silesian Centre for Education and Interdisciplinary Research, Chorzow, Poland. Dielectric spectroscopy studies were carried out using an Alpha dielectric spectrometer (NovoControl, Germany), in the frequency range from 10^{-1} Hz to 10^{6} Hz, at temperatures from 153 K to 323 K with steps of 5 K. The temperature was controlled by a Quattro temperature controller (NovoControl, Germany) with temperature accuracy greater than ± 0.1 K. The samples were physically mixed for 2 minutes before being placed on a parallel-plate cell made of stainless steel with a diameter of 10 mm and a 0.1 mm gap using Teflon spacers. Samples were heated to 373 K and held at this temperature for 30 minutes to ensure complete melting of the ibuprofen and to dry the sample before analysis was commenced at 153 K. The data was fitted and analysed by Dr. Justyna Knapik-Kowalczuk (University of Silesia, Poland) using WinFit software (NovoControl, Germany). The α, β and ɣ-relaxation times of the samples were determined using the Havrilak-Negami (HN) function (Equation 2.8)

$$\varepsilon^*_{HN}(\omega) = \varepsilon'(\omega) - i\varepsilon''(\omega) = \varepsilon_\infty + \frac{\Delta\varepsilon}{[1+(i\omega\tau_{HN})^a]^b} \qquad \textbf{Equation 2.8}$$

Where $\varepsilon^*_{HN}(\omega)$ is the Havrilak Negami permittivity over the frequency range ω , ε' and ε'' are the real and imaginary parts of complex dielectric permittivity, ε_∞ is the high frequency limit permittivity, $\Delta\varepsilon$ is the dielectric strength and τ_{HN} is the Havrilak-Negami relaxation time. Symmetric and asymmetric broadening of the relaxation peak are represented by parameters *a* and *b* respectively [148].

The calculated fitting parameters were then used to calculate τ_α using Equation 2.9 [148,149]

$$\tau_\alpha = \tau_{HN}\left[sin\left(\frac{\pi a}{2+2b}\right)\right]^{-1/a}\left[sin\left(\frac{\pi ab}{2+2b}\right)\right]^{1/a} \qquad \textbf{Equation 2.9}$$

To parametrize the τ_α(T) dependence the Vogel-Fulcher-Tammann (VFT) equation [150,151] (Equation 2.10) was used for the alpha relaxation process where τ_∞, T_0 and D are fitting parameters.

$$\tau_\alpha(T) = \tau_\infty \exp\left(\frac{DT_o}{T-T_0}\right) \qquad \textbf{Equation 2.10}$$

T_o is called the Vogel temperature which is 50-70K below the glass transition temperature. To parameterise the $\tau_{\beta,\gamma}$ (T) dependencies in the glassy state, the Arrhenius equation was used (Equation 2.11) where E_a is the activation energy for the process and R is the gas constant in kJ K^{-1} mol^{-1}.

$$\tau_{\beta/\gamma}(T) = \tau_\infty \exp\left(\frac{E_a}{RT}\right) \qquad \textbf{Equation 2.11}$$

The fragility was calculated using the dynamic fragility or "steepness index", m_P. This has been defined as follows [152]

$$m_P = \frac{d\ log\tau_\alpha}{d(\frac{Tg}{T})} = \frac{D(T_0/T_g)}{\left(1-(T_0/T_g)\right)^2 \ln(10)} \qquad \textbf{Equation 2.12}$$

2.2.3.11 Physical stability studies of ketoprofen-polymer samples

150 mg of freshly prepared samples of melt-quenched cryo-milled ketoprofen were measured into amber glass vials and placed in a vacuum sealed storage box containing either phosphorous pentoxide (0% RH) or a saturated sodium chloride solution (75% RH) [153] . These storage containers were placed in an oven (Gallenkamp, U.K.) and maintained at 25 °C. Temperature and humidity were monitored using a logger (Sensirion, Switzerland). Samples were taken after 1, 2, 4, 8 and 12 weeks of storage for analysis by DSC and pXRD.

2.2.3.12 Photostability testing of nifedipine samples

The spray dried powders containing 15% w/w nifedipine and their equivalent physical mixtures were placed in a photostability chamber which was constructed from a plastic container, covered in aluminium foil, with two light sources placed at the top of the container. The light sources consisted of two fluorescent tube light holders (Beamz, The Netherlands), powered by alternating current. One light holder contained a 15 W coolwhite lightbulb, while the other contained a 15 W U.V. lightbulb (Sylvania, U.S.A). Approximately 50mg of the powder being tested was spread thinly on a glass slide of dimensions 76 mm x 26 mm (Hirschmann Laborgerate, Germany) which was placed 10 cm from the light sources in the photostability chamber. Care was taken not to compress the powder in any way so as to allow as much of the nifedipine powder as possible to be exposed to light. The light intensity inside the photostability chamber was quantified using an RS PRO ILM13324 lux meter (Radionics, Ireland). The light intensity in the photostability chamber was determined to be 3000 lux.

2.2.3.13 Ibuprofen spherulite growth studies

2.2.3.13.1 Preparation of ibuprofen–HPMC mixtures for spherulite studies by rotary evaporation

Ibuprofen and HPMC were dissolved in an 80:20 v/v ethanol: deionised water mixture to create a 1% w/v solution. R-ibuprofen (UCD, Ireland) was used in this study. The solvent was removed by rotary evaporation using a Rotavapor R-205 (Büchi, Switzerland). The heating bath was maintained at 60 °C, the round bottom flask was rotated at 200 rpm and the vacuum was set to 175 mbar for 10 minutes before being reduced to 72 mbar for a further 10 minutes to ensure complete solvent evaporation. The resulting samples were gently ground in an agate mortar and pestle for 5 minutes.

2.2.3.13.2 Measurement of ibuprofen spherulite growth rate

Approximately 2-4 mg of ibuprofen or ibuprofen-HPMC mixtures prepared as described above (Section 2.2.3.13.1) were added to a glass slide which was then placed onto an LTS420 hot stage (Linkam, U.K.) of a BX53 polarised light optical microscope (Olympus, U.K.). The hot stage temperature was calibrated using indium and tin. The powder was heated to 100 °C using a heating rate of 10 °C/min per minute and held isothermally for 30 seconds before being cooled at 10 °C/min to a specific temperature (25/30/35/40 °C) to create a supercooled liquid state of ibuprofen. A second slide was added on top of the supercooled liquid to induce crystallisation, following a method described by another group [154]. The sample was held at this temperature for 10 minutes, while an image of the sample was captured every 2 seconds. The growth rate of the crystalline spherulite was determined by plotting the radius of the spherulite over time. Radial measurements of the spherulites were determined using Image J software (N.I.H., U.S.A.).

2.2.4 Dissolution testing

2.2.4.1 Dissolution testing of spray dried ibuprofen-HPMC samples

Spray dried IBU: HPMC 60:40 w/w samples were tested under sink conditions using an AT7 Dissolution Apparatus (Sotax, Switzerland) with paddle attachment using 500 mL of phosphate buffer pH 6.8 equilibrated for an hour at 37 (± 1) °C. 42 mg of a freshly prepared spray dried sample (equivalent to 25.2 mg of ibuprofen) was added to the dissolution vessel. The paddle was rotated at 50 rpm and 5 mL of the test solution was removed at regular intervals for 90 minutes and replaced with the same volume of warmed dissolution medium. The samples were filtered using a 0.45 µm polytetrafluoroethylene (PTFE) filter (Fisher Scientific, U.S.A) prior to HPLC analysis. Dissolution profiles were compared using the statistical analysis software DDSolver (Y. Zhang, China Pharmaceutical University, Nanjing, China) using difference factor (f_1) and similarity factor (f_2) analyses [155].

2.2.4.2 Dissolution testing of spray dried and electrosprayed ketoprofen-PVP samples

Samples were tested under sink conditions using a CE7 flow through cell apparatus (Sotax, Switzerland). A quantity of the amorphous dispersion containing 3 mg of ketoprofen was placed on top of 500 mg of glass beads in a dry cell of 12 mm diameter. A 4 mm ruby bead was placed at the bottom of the cell to ensure laminar flow of the medium. The water bath was maintained at 37(± 1) °C. The dissolution medium was 0.1 M hydrochloric acid (pH 1.2) and the volume used was 100 mL. The dissolution medium was recirculated through the cell in a closed loop system using a flow

rate of 8 mL/min. At sampling time points, 1 mL of the medium was filtered using a 0.45 µm PTFE filter (VWR, U.S.A) and diluted using appropriate volumes of methanol prior to HPLC analysis. After each sample was taken it was immediately replaced with an equal volume of pre-heated medium. Each experiment was carried out in triplicate.

2.2.4.3 Dissolution testing of nifedipine-polymer tablets and Adalat® capsules

2.2.4.3.1 Paddle method using aqueous dissolution medium

Aqueous medium (dilute hydrochloric acid pH 1.2) was degassed immediately prior to use by heating to 41 °C before filtering through a 0.45 µm PES membrane filter (Supor PALL Corporation, U.S.A.), as recommended by the British Pharmacopoeia [156]. This was performed to avoid the formation of bubbles which may adhere to the dissolving surface of the tablet, affecting its dissolution performance. Dissolution was carried out in an AT7 dissolution paddle apparatus (Sotax, Switzerland) using 900 mL of the degassed dilute hydrochloric acid heated to 37 (± 1) ^{o}C. The paddle speed was set to 50 rpm and a 2 mL sample of the solution was withdrawn at 1, 2, 5, 10, 15, 30, 60, 90 and 120 minutes after the tablet/capsule was added to the vessel. The samples were filtered using 0.45 µm PTFE syringe filters (VWR, U.S.A.). The sample volume was immediately replaced using pre-warmed medium. All consumables which came into contact with the sample were pre-heated prior to use.

Amorphous solid dispersion tablets were added to the vessel directly. To recreate the 'bite and swallow' technique a blade was used to make a horizontal incision through the middle of the capsule, and the capsule was added to the dissolution bath. Any nifedipine solution which escaped from the capsule during this process (i.e. onto blade/ gloves) was rinsed into the vessel with dissolution medium from the vessel. Both capsules and tablets were observed to sink to the bottom of the dissolution vessel and therefore no sinkers were required. This experiment was carried out in triplicate for each formulation studied. Due to the photolabile nature of nifedipine, the dissolution apparatus was covered in aluminium foil for the duration of the experiment.

Solid fractions of the formulations which remained after two hours were extracted from the dissolution medium and allowed to dry over night at ambient temperatures prior to a repeat pXRD analysis.

2.2.4.3.2 Paddle method using biphasic dissolution media

A second paddle dissolution experiment was carried out for the two best performing ASD formulations (PVP17NIF and PVP30NIF) as well for the Adalat® capsule. This was also carried out in the Sotax AT7 dissolution bath. This method involved using a biphasic medium i.e. 450mL of an

aqueous layer (dilute hydrochloric acid pH 1.2) and 150mL of 1-octanol and was adapted from a method reported in the literature [157]. The capsule/ tablet was added to the degassed aqueous layer before the addition of 1-octanol on top of the aqueous layer. This was done to avoid contamination of the octanol layer with nifedipine while adding the capsule/tablet to the medium. The capsule was split open as described in Section 2.2.3.3.1 prior to adding to the dissolution vessel. Both phases of the dissolution medium were maintained at 37 (± 1) ^{o}C throughout the experiment. The paddle was centred in the aqueous phase and set to a rotation speed of 100 rpm. At each time point (1, 2, 5, 10, 15, 30, 60, 90 and 120 minutes after the paddle was turned on), 2 mL was withdrawn from both the aqueous and octanol phases. The aqueous phase was filtered using a 0.45 µm PTFE syringe filter (VWR, U.S.A.) and diluted to an appropriate concentration using HPLC grade methanol prior to analysis. The octanol sample was also diluted using HPLC grade methanol prior to analysis. The sample volumes were immediately replaced using pre-warmed media (aqueous and octanol phase). All consumables which came into contact with the samples were pre-heated prior to use.

2.2.5 Solubility testing

2.2.5.1 Determination of crystalline ketoprofen equilibrium solubility at pH 1.2

An excess of ketoprofen was added to a glass amber vial with a capacity of 10 mL containing 5 mL of 0.1 M hydrochloric acid (pH 1.2). These vials were sealed and crimped and placed in a reciprocal shaking water bath (ThermoFisher Scientific, U.S.A) maintained at 37 (± 1) ^{o}C and shaken at 50 cpm. After 24 hours 1 mL of the solution was filtered using a 0.45 µm PTFE filter (Fisherbrand, U.S.A) and diluted to an appropriate concentration in methanol before being analysed using HPLC. All consumables which came into contact with the undiluted ketoprofen suspension were pre-heated prior to use. This was carried out for three separate vials.

2.2.5.2 Determination of ketoprofen-polymer solid dispersion dynamic solubility at pH 1.2

100 mg of each polymer-ketoprofen system was added to 20 mL dilute hydrochloric acid (pH 1.2) in a jacketed beaker with a capacity of 60mL containing maintained at 37 (±1) oC via a water bath (Lauda, Germany). The suspension was stirred continuously by magnetic stirring at 1000 rpm with a 12 mm long magnet for 2 hours. At various time points, 1mL of the liquid was filtered through a 0.45 µm PTFE filter (Fisherbrand, U.S.A.), and diluted with methanol. Ketoprofen concentration was determined using HPLC. All consumables which came into contact with the undiluted ketoprofen suspension were pre-heated prior to use. Each system was tested in triplicate.

2.2.5.3 Determination of crystalline nifedipine equilibrium solubility at pH 1.2

An excess of crystalline nifedipine was added to a glass amber vial with a capacity of 10 mL containing 5 mL of 0.1 M hydrochloric acid (pH 1.2). These vials were sealed and crimped and placed in a reciprocal shaking water bath (ThermoFisher Scientific, U.S.A) maintained at 37(± 1) °C and shaken at 50 cpm. After 24 hours 1 mL of the solution was filtered using a 0.45 µm PTFE filter (Fisherbrand, U.S.A.) and diluted to an appropriate concentration in methanol before being analysed using HPLC. All consumables which came into contact with the undiluted nifedipine suspension were pre-heated prior to use. This analysis was carried out for three separate vials.

2.2.6 High performance liquid chromatography (HPLC)

2.2.6.1 Ibuprofen HPLC analysis

Ibuprofen concentration in the dissolution medium was determined using an Alliance HPLC with 2695 Separations Module system and 2996 Photodiode array detector (Waters, Ireland) which was used at a wavelength of 222 nm. The mobile phase consisted of acetonitrile and phosphate buffer pH 7.5 in a 45 to 55 (v/v) ratio. The phosphate buffer was prepared by adjusting the pH of a 50 mM potassium dihydrogen phosphate solution with 1 M sodium hydroxide. The column used was a Spherisorb® ODS2 C18 column (250 mm x 4.6 mm, particle size 5 µm; Waters, Ireland). Isocratic elution was used with a column temperature of 25 °C, 1 mL/min flow rate and 10 µL injection volume. Three samples were analysed at each time point and this experiment was performed in duplicate. Calibration curves for R,S-ibuprofen and S-ibuprofen were constructed by measuring the peak area for six concentrations in triplicate in the 50-500 µg/mL range. Sample HPLC traces and calibration curves are shown in the Appendix.

2.2.6.2 Ketoprofen HPLC analysis and drug loading determination

Ketoprofen concentration in aqueous media was determined using an Alliance HPLC with 2695 Separations Module system and 2996 photodiode array detector (Waters, Ireland) which was used at wavelength 259 nm. The mobile phase consisted of acetonitrile and phosphate buffer pH 3 in a 45 to 55 (v/v) ratio. The phosphate buffer was prepared by adjusting the pH of a 20 mM solution of monosodium phosphate with 1 M sodium hydroxide. The column used was an ODS C18(2) column (150 mm x 4.6 mm, particle size 5 µm; Phenomenex, France). Isocratic elution was used with a column temperature of 25 °C, 20 µL injection volume and a flow rate of 1 mL/min. A six-point calibration curve was created spanning 0.5 µg/mL to 500 µg/mL. Sample calibration curves and HPLC traces are shown in the Appendix.

Ketoprofen loading of the spray dried and electrosprayed PVP polymers with a theoretical drug loading of 20% w/w was analysed by dissolving samples in methanol and quantifying ketoprofen

concentration using the HPLC method outlined above. Drug loading was determined using the following equation

$$Drug\ loading = \frac{Actual\ drug\ concentration}{Theoretical\ drug\ concentration} \times 100 \quad \textbf{Equation 2.13}$$

2.2.6.3 Nifedipine HPLC analysis

2.2.6.3.1 Nifedipine photostability testing and aqueous dissolution medium HPLC method

Nifedipine and its related photodegradants (Impurity A and B) were quantified in the spray dried powders and equivalent physical mixtures before, during and after photostability testing using a HPLC method modified from the British Pharmacopoeia [158]. An Alliance HPLC with 2695 Separations Module system and 2996 photodiode array detector (Waters, Ireland) were used at a wavelength of 235 nm. The mobile phase consisted of acetonitrile, methanol and deionised water in a 9:36:55 (v/v/v) ratio. The column used was an ODS C18(2) column (150 mm x 4.6 mm, particle size 5 µm; Phenomenex, France). Isocratic elution was used with a column temperature of 25 ^{o}C, 20 µL injection volume and a flow rate of 2 mL/min (adapted from the 1mL/min flow rate prescribed in the British Pharmacopoeia). Calibration curves (r^2>0.99) for nifedipine and related impurities were created using a minimum of six concentrations spanning from 2.5 µg/mL to 500 µg/mL for nifedipine and 3 µg/mL to 245 µg/mL for the impurities. Calibration was repeated approximately fortnightly during HPLC analysis. Impurity A, B and nifedipine had elution times of 10, 13 and 18 minutes respectively. The three peaks (where observed) complied with the system suitability test, as specified in the British Pharmacopoeia, as resolution between peaks was greater than 1.5. Sample calibration curves and HPLC traces are shown in the Appendix.

2.2.6.3.2 Nifedipine biphasic dissolution medium HPLC method

In order to reduce the HPLC running time (which was approximately 30 minutes per sample using the method above) , an alternative nifedipine HPLC method described in the literature was used [159]. This method used the same HPLC module system, column, PDA and wavelength as described above. The mobile phase consisted of methanol and deionised water in a 2:1 (v/v) ratio. Isocratic elution was used with a column temperature of 25 ^{o}C, 20 µL injection volume and a flow rate of 0.7 mL/min. The elution time of nifedipine using this method was 7 minutes. A calibration curve for nifedipine spanning 1 µg/mL to 50 µg/mL was created for this method. Sample calibration curves and HPLC traces are shown in the Appendix. Photodegradant impurities were not detected using this method. As previous dissolution tests showed no photodegradation of nifedipine, due to the protective measures taken, this was deemed acceptable.

Chapter 3: The impact of chirality on ASD stability and performance

3.1 Introduction

3.1.1 The impact of API chirality on glass forming ability and stability

As outlined in Chapter 1 Section 1.3, there are many factors which may influence the physical stability of ASDs. Chief amongst these are API and polymer characteristics. API characteristics which affect the physical stability of the amorphous state include molecular weight, number of rotatable bonds, and structural complexity, as well as thermodynamic properties, such as the free energy difference between the crystalline and amorphous state of the drug [4]. The role that enantiomeric composition plays in the glass forming ability and glass stability of chiral APIs has not been fully elucidated to date.

Chirality is ubiquitous in science as amino acids, many chemical reagents and approximately 60% of marketed APIs exhibit this "handedness" [160]. Any molecule with a stereogenic centre, such as an asymmetric carbon, exhibits chirality and therefore can exist in different enantiomeric states. Enantiomers are stereoisomers which are non-superimposable images of each other that may be distinguished by their specific optical rotation [161]. Enantiomers are termed "R" or "S" depending on the position of substituents around the chiral centre, in accordance with Cahn-Ingold-Prelog rules [162]. An example of a chiral API is thalidomide, shown in Figure 3.1.

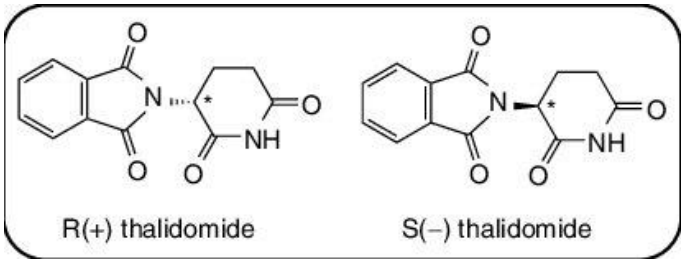

Figure 3.1: Enantiomers of thalidomide [163].

Opposing enantiomers of the same API may have different therapeutic and toxicological profiles. This is the case for thalidomide, warfarin, thyroxine and non-steroidal anti-inflammatory drugs such as ibuprofen [164–166]. An increasing number of APIs reaching the market are formulated as single enantiomers (44% of all APIs on the market between the years 1991 and 2002) [160], in part due to regulatory requirements, which necessitate toxicological evaluation of both enantiomeric forms [167]. This trend towards single enantiomer API development also stems from commercial concerns. Existing patents on racemic APIs may be extended by replacing the racemic mixture with the active enantiomer, a strategy known as a "racemic switch" [168,169] . Between 1994 and 2011, the FDA approved 15 of these racemic switches, the first of which was for ibuprofen [170]. Ibuprofen is an interesting example of a chiral molecule as it was originally marketed as a racemic mixture, although the pharmacological activity resides in the S-enantiomer, as is the case for many NSAIDs [171].

Interestingly, when ibuprofen is administered as a racemic mixture, the R enantiomer undergoes unidirectional chiral inversion *in vivo* to form the active S-enantiomer.

Racemic APIs can exist in the solid state as racemic compounds, conglomerates or solid solutions (also known as pseudo racemates) [172]. The differences between these categories, in terms of their phase diagrams, are shown in Figure 3.2. In a racemic compound, each enantiomer has a stronger affinity for its opposing enantiomer than for itself. Therefore, the unit cell of a racemic compound consists of a 50:50 ratio of each enantiomer, combined to form a single type of crystal lattice [173]. Racemic compounds are the most common solid-state presentation of chiral APIs. Ibuprofen is an example of a marketed API which is a racemic compound [174].

Conversely, racemic conglomerates account for only 10-20% of chiral molecules [172,175]. In racemic conglomerates, each enantiomer has a stronger affinity for itself than for its opposing enantiomer. This means that the two enantiomers crystallise separately to form R crystal lattices and S crystal lattices [173]. A racemic conglomerate therefore consists of two phases (R crystals and S crystals) which are physically mixed in a 50:50 ratio [174]. Racemic solid solutions (or pseudo racemates) occur less frequently than either racemic compounds or conglomerates. In racemic solid solutions, there is little difference in the attractive forces between enantiomers of opposite rotation and the same rotation. As such, both enantiomers compete for the same positions in the crystal structure and a racemic solid solution results [173].

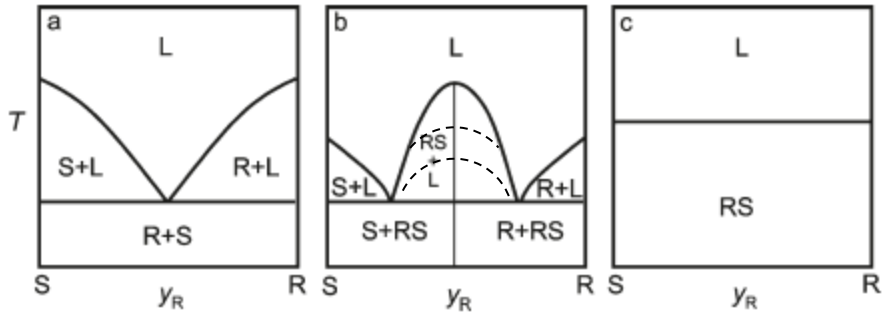

Figure 3.2: Phase diagrams of enantiomeric mixtures forming a) a racemic conglomerate b) a racemic compound c) a racemic solid solution. R, S, RS, and L represent solid R-enantiomer phase, solid S-enantiomer phase, solid racemic compound RS, and liquid phase L respectively. y_R represents the fraction of R enantiomer present and T represents temperature. Boundaries between regions represent melting point temperatures. Adapted from Srisanga et al. [172]

As shown in Figure 3.2, racemic compounds and conglomerates show different patterns in the relationship between enantiomeric composition and melting point temperature. For racemic conglomerates, the 50:50 R,S mixture has a lower melting point temperature than either the pure R or pure S enantiomer (Figure 3.2a). For racemic compounds, the 50:50 R,S mixture may have a melting point which is higher, lower or equal to the melting point than either enantiomer alone [173](Figure 3.2b) but the presence of two eutectic composition allows for distinction between racemic compounds and conglomerates via construction of binary phase diagrams .

Interestingly, while different enantiomeric compositions of the same molecule demonstrate different melting points, the glass transition temperature of a chiral substance is constant, regardless of enantiomeric composition. This has been demonstrated previously for limonene [176], diprophylline [177], 5-ethyl-5-methylhydantoin [6] and ibuprofen [178].

As described in Chapter 1 Section 1.3, compounds with high enthalpies of fusion tend to be poor glass formers and poorly stable in the glassy state [4]. As racemic compounds may have higher melting points (and associated higher enthalpies of fusion) than their single enantiomer counterparts,[179] they may be assumed to be more stable in the crystalline state than their single enantiomer counterparts [180]. It would therefore be anticipated that for a racemic compound fulfilling this requirement, the single enantiomer form may be more stable in the glassy state or more easily form the glassy state than the equivalent racemic mixture as the thermodynamic driving force for crystallisation to occur is smaller. Conversely, in the case of chiral molecules which crystallise as racemic conglomerates, the racemic mixture would be predicted to be more stable in the glassy state or more easily form the glassy state than the equivalent single enantiomer form.

The assumption that racemic compounds have superior thermodynamic stability relative to their single enantiomer forms is an extension of Wallach's rule, which states that racemic compounds

are denser in the crystalline state than their single enantiomer counterparts [181]. The validity of this assumption has been questioned however [182], as the use of melting point data to determine the relative stabilities of racemic mixtures and their pure enantiomer counterparts may be flawed. At the melting point of a compound, molecules are in thermodynamic equilibrium between the solid and liquid states. In the case of a racemic compound, the melting point is the point at which equilibrium is reached between a racemic liquid and a racemic solid, while for the pure enantiomer the melting point represents the temperature at which equilibrium between a pure enantiomer solid and pure enantiomer liquid is reached. Therefore, melting point comparisons of racemic mixtures and pure enantiomers should be interpreted with caution, as they do not represent points of equilibria with the same liquid, but rather with different liquids [182]. This is in contrast to polymorphic forms, where melting temperatures represent points of equilibria with the same liquid, allowing for direct ranking of thermodynamic stability. However, Wallach's rule has been tested experimentally, and in 65% of cases a racemic mixture does crystallise into a denser crystal than its single enantiomer counterpart [175]. This implies that the driving force for crystallisation from the amorphous state would be stronger for the racemic mixture compared to the single enantiomer form. As most racemic mixtures are racemic compounds, this agrees with the assumptions outlined above.

The influence that the difference in thermodynamic stability between racemic and single enantiomer crystals has on their glass forming ability and glass stability has not been investigated thoroughly to date. Using the chiral molecule 5-ethyl-5-methylhydantoin, as a model API, Atawa et al have explored this question [6]. R,S-5-ethyl-5-methylhydantoin has a melting point and enthalpy of fusion of 140 ^{o}C and 18 kJ/mol respectively while R-5-ethyl-5-methylhydantoin and S-5-ethyl-5-methylhydantoin have melting points and enthalpies of fusion of 173 ^{o}C and 21 kJ/mol respectively and is classified as a racemic conglomerate [6]. 5-ethyl-5-methylhydantoin (regardless of enantiomeric composition) is a poor glass former, according to the classification system described by Baird et al. [4], making it suitable for probing enantiomer influence on crystallisation tendency. Atawa found that the glass forming ability and glass stability of 5-ethyl-5-methylhydantoin increased with counter enantiomer content [6]. Therefore, the racemic conglomerate formed a more stable glass than the pure enantiomer counterpart, which agreed with the predictions outlined above.

The glass forming ability and glass stability of two racemic compounds and their single enantiomer counterparts has also been investigated. Adrjanowicz et al. found that the $T_{1/2}$ of crystallisation from a melt was 4 hours for R,S-ketoprofen and 10 hours for S-ketoprofen [183]. Viel at al. however, found very little difference in the glass forming ability, glass stability and molecular mobility of R,S-diprophylline and S-diprophylline [5,177]. The difference in melting temperature between R,S-

ketoprofen and S-ketoprofen is more significant than in the case of R,S-diprophylline and S-diprophylline (94 °C/ 75 °C versus 166 °C/160 °C respectively), which may explain the contradictory observations. Interestingly, while Adrjanowicz et al. found that R,S- ketoprofen crystallised more rapidly from its molten form than S-ketoprofen did from its melt at ambient pressure, the reverse was true at elevated pressures; an observation which was not fully explained [183]. Further research is clearly needed to expand the limited understanding of the factors affecting the glass forming ability and glass stability of chiral molecules.

The first section of this work will be to investigate the relationship between enantiomeric composition and glass forming ability and glass stability for the racemic compound, ibuprofen.

3.1.2 The impact of chiral recognition between API and polymer on ASD stability

While the influence of enantiomeric composition on the glass forming ability and glass stability of chiral APIs is clearly an area of research which needs further work, the potential for chiral recognition between a chiral API and polymer, and its potential impact on ASD physical stability, has received very limited attention in the literature.

Chiral recognition refers to the situation where there is a specific, reversible interaction between two chiral molecules based on three points of contact, the interaction being different for the different diastereomeric pairings [184]. Chiral recognition was first identified in pharmacology, where stereochemical differences in the activities of APIs were attributed to the differential binding of enantiomers to a common site on an enzyme or receptor surface [185]. For chiral recognition to occur, the receptor/enzyme must contain three non-equivalent binding sites, and one enantiomer must be able to interact with all three sites (via attractive or repulsive forces)[186], while the other enantiomer may only interact with one or two sites [185]. This concept is illustrated for receptor sites on protein surfaces in Figure 3.3 below.

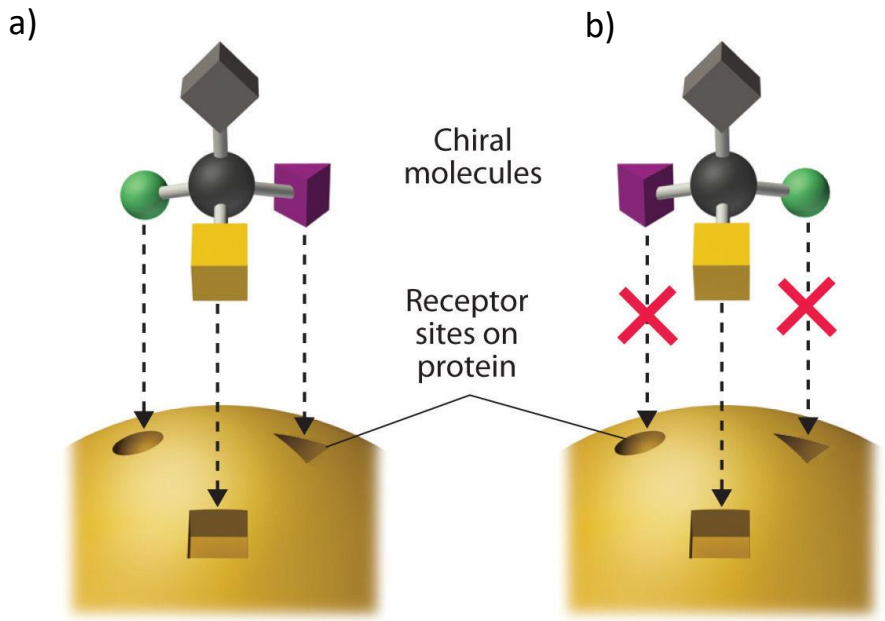

Figure 3.3: Illustration of the three-points of interaction model for chiral recognition between proteins and enantiomers. In scenario a) three enantiomer substituents interact with three receptor sites, while in scenario b) only one substituent can interact with one receptor site. Adapted from saylordotorg.github.io [187]

The "three-points-of-interaction" explanation remains the predominant explanation when chiral recognition phenomena are observed, as is the case in many branches of pharmaceutical science including pharmacology, medicinal chemistry and chromatography [188].

The potential for chiral recognition between a chiral API and an "inert" excipient when formulating a medicine appears to be an area of pharmaceutical research which holds much promise, although research to date is limited. Chiral recognition has been observed between enantiomers of chiral molecules and β-cyclodextrins during complex formation, but predicting which enantiomer will interact more strongly with β-cyclodextrin remains a challenge [189]. As in the case of β-cyclodextrin, all cellulose based polymers commonly used in ASD formulations (HPC, HPMC, HPMCAS and HPMCP) have structures which are based on the dextrorotatory (+) glucose monomer [85]. Therefore, intuitively, chiral recognition should exist between such polymers and opposing enantiomers of a chiral API where the "three-points-of-interaction" criteria is fulfilled for one enantiomer but not the other.

Previous work in this area has examined the ability of the chiral polymers HPMC, HPMCP and HPMCAS to inhibit the crystallisation of two model chiral compounds (nitrendipine and 2-amino-1,1,3-triphenyl-1-propanol) to differing extents [7,8]. Miyazaki et al. demonstrated that R-nitrendipine had slower nucleation and crystal growth rates than S-nitrendipine when formulated via melt-quenching into an ASD with either HPMC or HPMCP [8]. Sato and Taylor's work demonstrated that the crystal growth rate of 2-amino-1,1,3-triphenyl-1-propanol (ATP) from its molten state, in the

presence of 5% w/w HPMCAS, differed depending on which ATP enantiomer was being studied and the degree of functional group substitution present in HPMCAS [7]. Two other chiral polymers used in this study demonstrated either no inhibitory effect on the crystallisation rate of ATP, regardless of ATP enantiomer type (in the case of polyhydroxy butyrate), or no difference in the degree of crystallisation inhibition between ATP enantiomers (as was the case with HPMCP). The authors postulated that the absence of chiral recognition in these cases could be explained by a lack of interacting functional groups between the API and the chiral polymer, as is the case with polyhydroxy butyrate, or due to steric hinderance by the phthalate moiety in the case of HPMCP. The literature to date, although sparse, does seem to indicate that the presence (or absence) of drug-polymer intermolecular interactions dictates whether chiral recognition is observed in an ASD.

It is unclear whether chiral recognition, if present, is influenced by the method of ASD production, as both papers highlighted above used melt-quenched ASDs for analysis. As the degree of mixing between polymer and API is influenced by ASD preparation method, chiral recognition, if present, may be influenced by the route of ASD preparation, as solvent based methods (e.g. spray drying) may allow a greater degree of interaction than milling, for example [126].

In the context of a growing trend towards single enantiomer API approval, coupled with the poor-aqueous solubility profile of most APIs, understanding the molecular basis of chiral recognition in ASDs could provide further insight into the rational formulation of physically stable ASDs. The aim of this section of work is to examine which cellulosic polymers successfully amorphise the chiral API ibuprofen, or its enantiomers, and whether chiral recognition is observed in this series of ASDs. A secondary objective is to examine whether the route of ASD preparation has an influence on the degree of chiral recognition which is observed.

3.2 Results

3.2.1 The impact of ibuprofen chirality on its glass forming ability and glass stability

3.2.1.1 Non-isothermal crystallisation studies

The purpose of this work was to identify which, if any, of the easily calculated thermal parameters outlined in Baird et al. [4] are predictive of the glass forming ability (GFA) or glass stability (GS) of R,S-ibuprofen (R,S IBU) and S-ibuprofen (S IBU), and whether a difference in any of these properties is apparent between the racemate and single enantiomers.

R,S IBU has been identified as a good glass former and it also recognised as being stable in the glassy state [4]. The GFA of S IBU has not been described in the literature, however, with regard to the GS of S IBU there is some evidence to suggest that it may be even more resistant to crystallisation in the glassy state than R,S IBU [190]. This was theorised to be due to minor differences in molecular dynamics in the amorphous state, particularly at temperatures close to the glass transition temperature. This mirrors the assumptions outlined previously about the relative GS of racemic compounds and their single enantiomer counterparts (Section 3.1.1).

The thermal properties of R,S IBU and S IBU which contribute to GFA and GS, along with GFA and GS predictor parameters, which were determined as outlined in Chapter 2 Section 2.2.3.4.7, are shown in Table 3.1.

Table 3.1: Thermal properties, GFA and GS predictors of R,S IBU and S IBU determined by DSC with a heat/cool/heat cycle (conducted at a rate of 10/10/10 °C/min) ± standard deviation. Values in italics are those predicting a glass that forms more readily or is more stable in the glassy state relative to the comparator in the adjacent column.

Thermal properties	R,S IBU	S IBU	
T_m (°C)	74.36 ± 0.13	50.99 ± 0.18	
$T_{g\ (onset)}$ (°C)	-46.13 ± 0.12	-46.39 ± 0.03	
$T_{g\ (midpoint)}$ (°C)	-43.72 ± 0.12	-43.92 ± 0.04	
$T_{cryst\ onset\ heat}$ (°C)	37.40 [a]	33.87 [a]	
GFA predictors	**R,S IBU**	**S IBU**	**P-value**
ΔH_{fus} (J/g)	119.07 ± 2.15	*86.72 ± 0.35*	<0.0001
ΔS_{fus} (J/g/°C)	*1.60 ± 0.03*	1.70 ± 0.01	0.0067
T_{rg}	0.65 ± 0.00	*0.70* ± 0.00	<0.0001
$T_{cryst\ onset\ heat}$ - $T_{g\ (onset)}$ (°C)	*83.53 ± 0.07*	80.26 ± 0.03	<0.0001
GS predictor	**R,S IBU**	**S IBU**	**P-value**
T_{red}	0.69 ± 0.00	*0.82* ± 0.00	<0.0001

[a] *Value is taken from a heat, cool, heat cycle (conducted at a rate of 10/2/10 °C/min).*

Ibuprofen, regardless of enantiomeric composition has a glass transition at approximately -46 °C, while the melt temperature of R,S IBU is 74 °C and that of S IBU is 51 °C. The heat of fusion, ΔH_{fus}, is related to GFA as the higher the value, the more energy is required to break the intermolecular bonds of the crystal lattice, and the more stable the compound is in the crystalline state. Poor glass formers are likely to have higher specific heat of fusion values, as there is a stronger thermodynamic driving force for crystallisation to occur [4]. S IBU has a lower ΔH_{fus} than R,S IBU (86.72 ± 0.35 J/g versus 119.07 ± 2.15 J/g) and would therefore be predicted to be a better glass former. The entropy of fusion ΔS_{fus} (where $\Delta S_{fus} = \Delta H_{fus}/T_{melt\ onset}$) is also inversely related to GFA [4].The entropy of fusion was determined to be higher for S IBU than for R,S IBU (1.70 ± 0.01 J/g/ °C and 1.60 ± 0.01 J/g/ °C). This implies that R,S IBU should more easily form a glass than S IBU from an entropic perspective.

The reduced glass transition temperature (T_{rg}) is another parameter which describes the GFA of substances and is calculated using Equation 3.1.

$$T_{rg} = \frac{T_{g(onset)}}{T_{melt(onset)}} \qquad \textbf{Equation 3.1}$$

$T_{g\ (onset)}$ is the onset temperature of the glass transition in degrees Kelvin and $T_{melt(onset)}$ is the onset temperature of the melt in degrees Kelvin. The T_{rg} of a substance is related to its GFA due the

effect of viscosity [191]. Assuming viscosity is constant at $T_{g(onset)}$, a larger T_{rg} value indicates higher viscosity (and hence lower molecular mobility) between $T_{g(onset)}$ and T_{melt}. A rule of thumb has developed that a T_{rg} > 0.67 signifies a substance which can only crystallise slowly over a narrow temperature range while being cooled, and hence is more likely to be a good glass former [192,193]. As the T_{rg} of S IBU is slightly higher than that of R,S IBU (0.70 versus 0.65) and is > 0.67, S IBU is predicted, from the T_{rg}, to more readily form a glass than R,S IBU.

Another GFA parameter can be calculated using Equation 3.2

$$T_{cryst.\ onset\ heat} - T_{g\ onset} \quad \textbf{Equation 3.2}$$

$T_{cryst.\ onset\ heat}$ is the temperature at which the onset of crystallisation is detected during heating [4]. The larger the difference between this temperature and the glass transition temperature the more likely it is that the liquid will form a glass [4]. As the difference between the glass transition temperature and the temperature of crystallisation for R,S IBU is slightly higher than for S IBU (83.53 ± 0.07 °C versus 80.26 ± 0.03 °C), this parameter indicates that R,S IBU is in fact more likely to form a glass.

A commonly used thermal predictor of GS is termed the reduced temperature T_{red} which is calculated using the formula in Equation 3.3. This equation allows for comparisons of crystallisation tendencies of different materials as it represents a normalised measure of how far above the glass transition temperature a material must be before spontaneous crystallisation is observed [194].

$$T_{red} = \frac{T_{cryst.\ onset\ heat} - T_{g\ midpoint}}{T_{melt} - T_{g\ midpoint}} \qquad \textbf{Equation 3.3}$$

Higher T_{red} values are associated with slower crystallisation rates [194]. The T_{red} for R,S IBU is 0.69 and for S IBU is 0.82. Therefore, on the basis of this parameter, S IBU is predicted to be the more stable glass, a prediction which agrees with a previous study comparing the molecular dynamics of R,S IBU and S IBU [190].

Thus, the various GFA parameters outlined by Baird et al.[4], and detailed here for IBU in Table 3.1, appear to contradict each other in terms of predicting whether R,S IBU or S IBU more readily form a glass. As the glass transition temperature for R,S IBU and S IBU are identical and both are good glass formers, the calculated parameters may have limited predictive power, as any difference in GFA may not be of a magnitude which is observable using standard thermal analysis.

To determine whether the GFA parameters calculated in Table 3.1 have any predictive power, samples of R,S IBU and S IBU were melted and cooled to below the glass transition in a DSC at varying rates as outlined in Chapter 2 Section 2.2.3.4.7. GS was assessed by reheating at varying

rates. Recrystallization during either the cooling or re-heating cycle was recorded. The results for each of three replicates are shown in Table 3.2.

Table 3.2: Crystallization tendencies of R,S IBU and S IBU in a DSC with varying cooling and re-heating rates

Cooling/Reheating rate (°C/min)	10/10	5/10	2/10	1/10	5/5	2/2
R,S IBU	***	***	**Δ	*Δ#	ΔΔ*	ΔΔΔ
S IBU	**Δ	ΔΔΔ	**Δ	##*	Δ#*	#**

**the sample remained amorphous upon cooling and reheating; Δ the sample partially recrystallised upon reheating and # the sample partially recrystallised in the cooling cycle*

Regarding the GFA of the samples, it was not possible to detect a critical cooling rate (R_{crit}) which is commonly used to describe the ease with which a glass can be formed. This is because R_{crit} determination requires cold crystallisation at several cooling rates and as seen in Table 3.2, cold crystallisation only occurred using a cooling rate of 1 °C/min for R,S IBU.

However, some summary observations are noted. S IBU underwent cold crystallisation using cooling rates of 5, 2 and 1 °C/min, while R,S IBU only underwent cold crystallisation using a 1 °C/min cooling rate. This appears to indicate that R,S IBU has better GFA than S IBU as a very slow cooling rate was required for cold crystallisation to occur.

Regarding GS, it is interesting to note that one S IBU replicate partially recrystallised during the reheating cycle when a 10 °C/min cooling and re-heating rate was used which was not observed with R,S IBU. In fact, when a 5 °C/min cooling rate (with 10 °C/min re-heating rate) was used S IBU crystallised upon reheating in all replicates while R,S IBU did not recrystallise in any of the replicates with the same thermal profile. This suggests that S IBU has a greater crystallisation tendency than R,S IBU which contradicts the prediction given by (T_{red}).

The discrepancy between predictions and experimental observations may be due to a difference in impurity profiles, as crystallisation rates are dramatically influenced by even low levels of impurities, as has been demonstrated for diprophylline and its major impurity theophylline [177]. Although the R,S IBU and S IBU used in this experiment were of reagent grade, R,S IBU had a labelled purity of 99% and S IBU had a labelled purity of 98%. Although determination of the impurity profiles of the ibuprofens which were used is beyond the scope of this thesis, their impurities and their relative abundancies may have contributed to the non-isothermal crystallisation which was observed. In the case of diprophylline, the presence of theophylline reduced the overall diprophylline crystallisation rate but favoured the formation of primary crystals of diprophylline [177]. As impurity levels play a complex role in the crystallisation of materials, and this factor was not

addressed in the non-isothermal crystallisation studies, any observed differences in the GFA and GS of R,S IBU and S IBU from this study should be interpreted with caution.

3.2.1.2 Enthalpy recovery studies

The thermodynamic instability of the amorphous state means that during storage, also known as physical ageing, the disordered state undergoes a "relaxation" process to an equilibrium state. This often involves complex molecular dynamics (Section 1.3.1.2) which are generally determined using broadband dielectric spectroscopy. The time dependence of these relaxation mechanisms is characteristic of the stability of the amorphous state, with stable glasses exhibiting prolonged relaxation times. Differential scanning calorimetry can be used to determine the enthalpy recovery at the glass transition, which is considered a substitute measure of relaxation (Figure 3.3) [195], by integrating the endothermic peak at the glass transition, as shown in Figure 3.4.

The aim of this experiment is to determine if there is any apparent difference in the extent of enthalpy recovery between R,S IBU and S IBU using DSC methods, as outlined in Chapter 2 Section 2.2.3.4.8. The enthalpy recovery of R IBU (UCD, Ireland) was also measured, as it should be identical to S IBU.

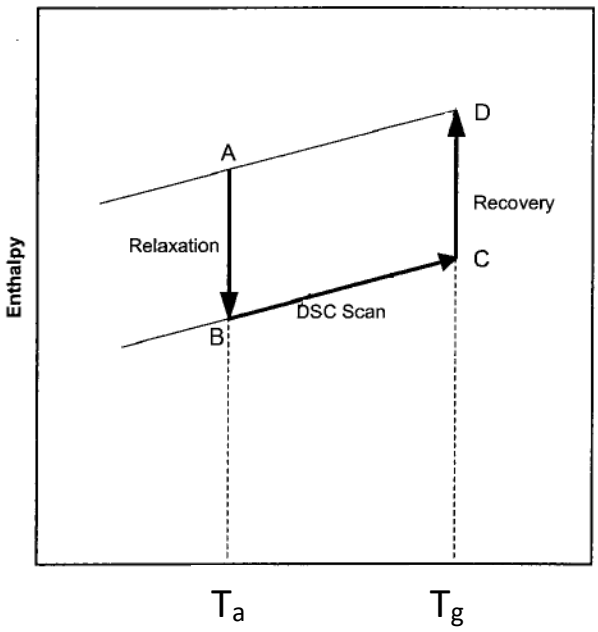

Figure 3.3: Illustration of the enthalpy relaxation and recovery relationship as revealed by DSC. T_a is the annealing temperature. A and B refer to the unaged and aged amorphous sample respectively. As the amorphous sample is heated in the DSC scan, sample B becomes sample C. At the Tg enthalpy recovery is recorded as the sample transitions to state D. Adapted from Kawakami and Ida [195].

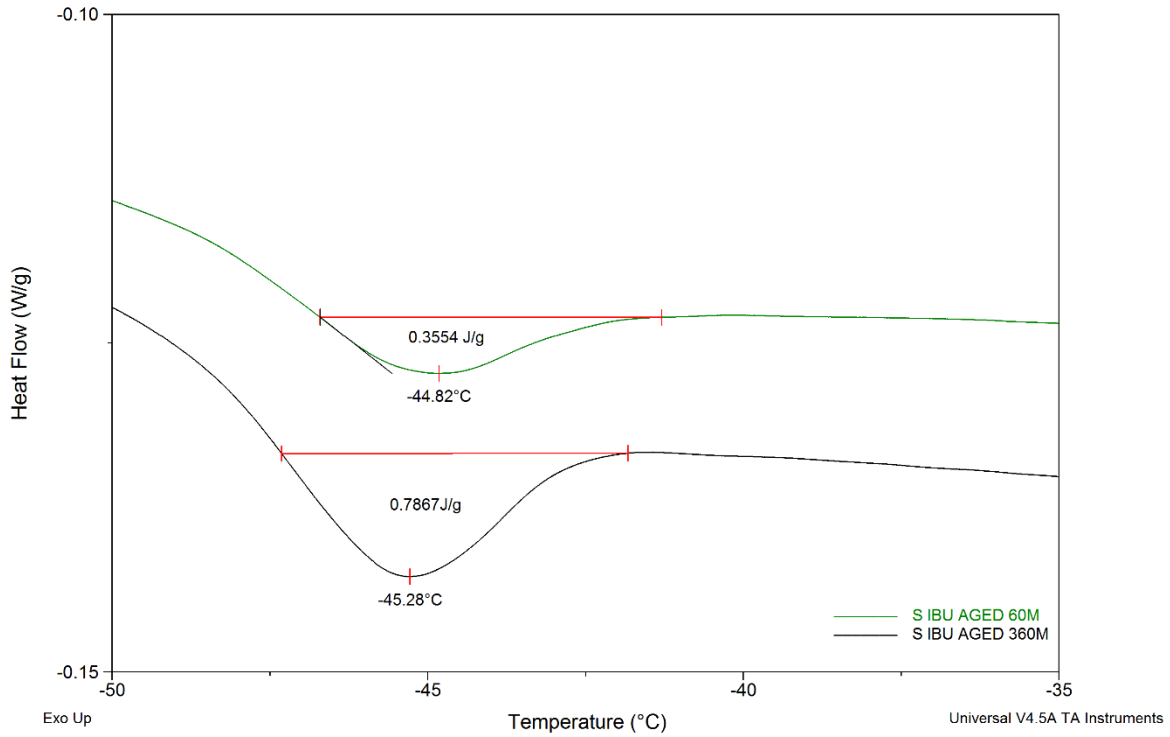

Figure 3.4: DSC thermograph of S-ibuprofen aged at -66 °C for 1 hour and 6 hours showing integration of the endothermic peak at the Tg, as a measure of enthalpy recovery.

3.2.1.2.1 Enthalpy recovery as a function of ageing time

A linear regression analysis of enthalpy recovery versus ageing time dependency at the ageing temperature of -66 °C was performed for the three ibuprofen samples. The extent of enthalpy recovery for each ibuprofen sample was plotted against ageing time from the linear portion of the recovery curve for ageing times between 0 and 360 minutes (Figure 3.5). Data was normalised by dividing each enthalpy recovery value by the average enthalpy recovery for an unaged sample. The slopes were tested for statistically significant differences using an F-test, the results of which are shown in Table 3.3. The extent of enthalpy recovery increased with increasing ageing time for R,S

IBU, R IBU and S IBU. This is not surprising, as it means that when ibuprofen was given more time in the amorphous state, it relaxed to a greater extent.

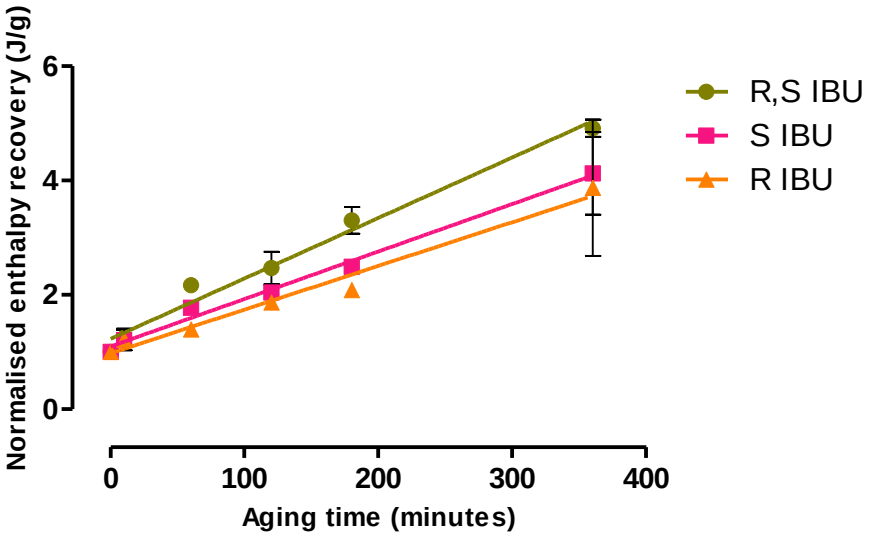

Figure 3.5: Normalised ibuprofen enthalpy recovery as a function of ageing time at -66 °C for R,S IBU, S IBU and R IBU

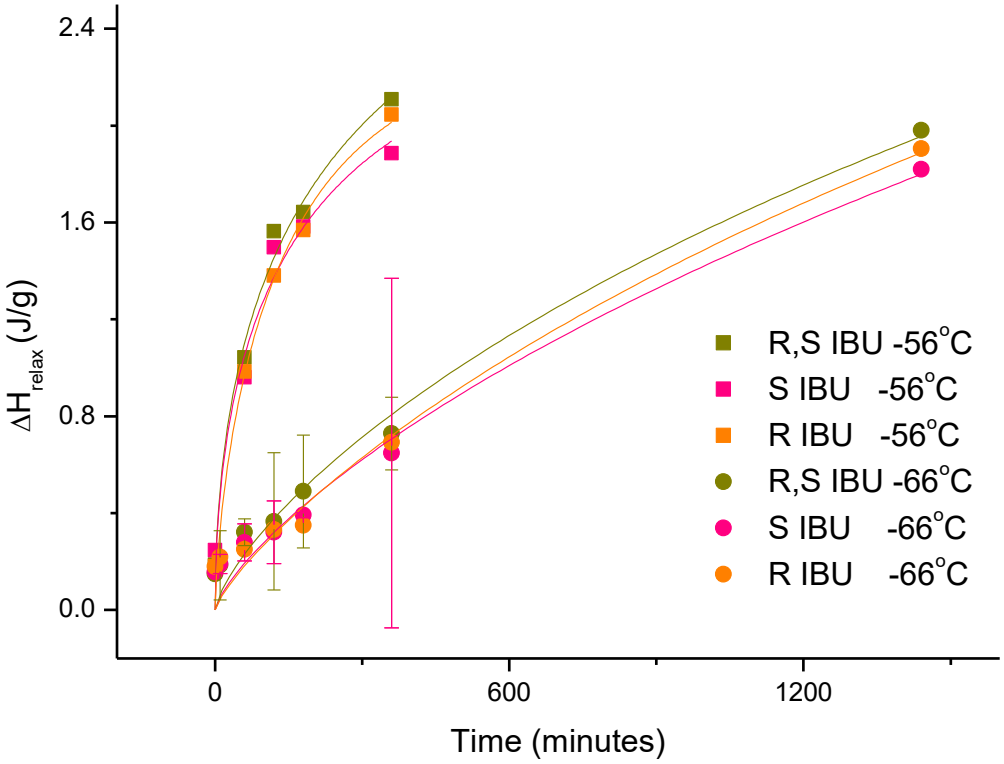

Figure 3.6: Enthalpy recovery as a function of ageing time and temperature for R,S IBU, S IBU and R IBU. Solid lines represent the best fit to the Kohlrausch-Williams-Watts equation.

Table 3.3: Linear regression of normalised ibuprofen enthalpy recovery as a function of ageing time at -66°C

Normalised ibuprofen enthalpy recovery when aged at -66°C			
Ibuprofen enantiomer	**Equation of the line**	**R^2 value**	**Slope ± S.D**
R,S IBU	y = 0.011x+1.229	0.97	0.011 ± 0.001
S IBU	y = 0.008x+1.096	0.95	0.008 ± 0.001
R IBU	y = 0.008x+0.978	0.86	0.008 ± 0.001
F-test of slopes	**F-value**	**p-value**	**Statistically significant**
R,S IBU vs S IBU	7.655	0.01	Yes
R,S IBU vs R IBU	6.881	0.02	Yes
S IBU vs R IBU	0.343	0.57	No

As shown in Figure 3.5 and Table 3.3, when the samples were aged at -66 °C R,S IBU's enthalpy recovery over varying ageing times was statistically significantly different to that of both R IBU and S IBU. The difference in enthalpy relaxation between the two opposing enantiomers over time was not significant. This suggests that glassy R,S IBU undergoes faster relaxation towards an equilibrium state than S IBU or R IBU, which agrees with the theoretical stabilities of racemic ibuprofen and its single enantiomer counterparts in the amorphous state, as outlined in Section 3.1.1.

This observation of faster enthalpic relaxation over time for R,S IBU relative to S IBU appears to contradict observations from the crystallisation study, where R,S IBU appeared to have superior GFA and GS compared to S IBU (Section 3.2.1.1). However, it must be considered that in the non-isothermal crystallisation studies, crystallisation occurred in the super-cooled liquid state, while in the enthalpy recovery study the samples have relaxed in the glassy state i.e. below the glass transition.

In order to determine the characteristic relaxation time (τ) of the materials, the enthalpy relaxation data was fitted to the Kohlrausch-Williams-Watts equation (Equation 2.4) [142] as described in Chapter 2 Section 2.2.3.4.8, and is graphed in Figure 3.6.

$$\Delta H_{relax} = \Delta H_{\infty}\left[1 - exp\left\{-(t/\tau^{KWW})^{\beta}\right\}\right] \qquad \textbf{Equation 2.4}$$

ΔH_{relax} and ΔH_{∞} are the enthalpy relaxation and the maximum enthalpy recovery at a given temperature. The other parameters t, τ^{KWW} and β are the ageing time, enthalpy relaxation time and the non-exponential parameter respectively [142,143]. ΔH_{∞} can be calculated using Equation 2.5

$$\Delta H_{\infty} = \Delta C_p\left(T_g - T\right) \quad \textbf{Equation 2.5}$$

Where ΔC_p is the change in the heat capacity at the glass transition temperature and T is the ageing temperature. ΔC_p was calculated as the average change in heat capacity for each material at the glass transition of the unaged sample. Results are shown in Table 3.4 and 3.5.

Table 3.4: Determination of ΔH_∞ for R,S IBU, S IBU and R IBU aged at -66 °C and -56 °C

	Aged at -66°C				Aged at -56°C			
	ΔC_p (J/g.C°)	Tg (K)	T (K)	ΔH_∞	ΔC_p (J/g.C°)	Tg (K)	T (K)	ΔH_∞
R,S IBU	0.3263	224.46	207.15	5.6482	0.4462	224.49	217.15	3.2751
S IBU	0.3607	224.12	207.15	6.1211	0.3457	224.68	217.15	2.6031
R IBU	0.2930	224.39	207.15	5.0513	0.3246	224.51	217.15	2.3891

Table 3.5: Fitted parameter values using the Kohlrausch-Williams-Watts equation for R,S IBU, S IBU and R IBU aged at -66 °C and -56 °C. Standard error in parentheses.

	Aged at -66°C		Aged at -56°	
	β	τ^{KWW}(minutes)	β	τ^{KWW}(minutes)
R,S IBU	0.73 ± 0.06	4641 ± 768	0.52 ± 0.09	333.53 ± 58.4
S IBU	0.75 ± 0.08	5858 ± 1193	0.54 ± 0.15	210.79 ± 40.98
R IBU	0.80 ± 0.09	3706 ± 657	0.71 ± 0.12	150.89 ± 14.88

As seen in Figure 3.6 the ΔH_{relax} for all three ibuprofen samples increased when the ageing temperature increased from -66°C to -56°C, while relaxation times (τ^{KWW}) decreased, indicating higher molecular mobility. The relaxation times which were calculated (Table 3.5) have significant error values associated with them, and therefore it is not possible to conclude whether there are any differences in the molecular mobilities of the samples.

The β value indicates the extent to which the data deviates from a true exponential function, where 1 is a true exponential function. Values should be within ± 0.1 of each other to allow for meaningful comparison [196]. In this work, the error associated with the τ^{KWW} value may stem from the deviation of β from 1, as well as the fact that samples were aged in duplicate for samples aged for 0-360 minutes at -66 °C, while only single runs were performed for samples aged for 1440 minutes at -66 °C and all ageing times at -56 °C. The relaxation time of R,S IBU at -66°C calculated in this study of 4641 minutes differs substantially from a value of 1416 minutes reported in another study, however the β value is not reported in this other study, making direct comparison difficult [197].

3.2.1.2.2 Enthalpy recovery as a function of ageing temperature

The activation energy (E_a) required for relaxation in the glassy state may be considered to correspond to the molecular mobility and hence GS, as has been demonstrated with amorphous trehalose [198]. The E_a can be determined by examining the temperature dependency of the enthalpy relaxation time at -56 °C and -66 °C using an Arrhenius plot as shown in Figure 3.7. The slope of the line represents the E_a for enthalpy relaxation. Higher E_a values are associated with more stable glasses as they represent a higher energy barrier between the amorphous and crystalline state [198].

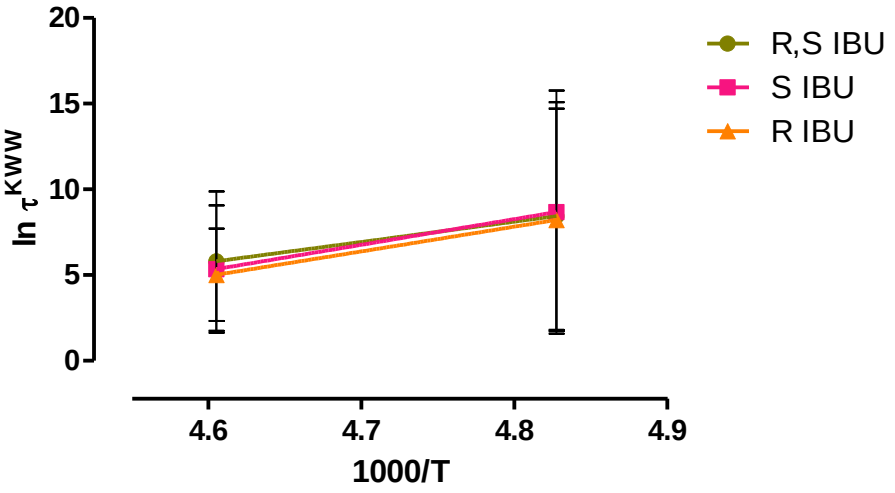

Figure 3.7: Arrhenius plot of τ^{KWW} for R,S IBU, S IBU and R IBU aged at -56 °C and -66 °C

Table 3.6 Values used for amorphous state relaxation activation energy determination for R,S IBU, S IBU and R IBU

	1000/T	R,S IBU	S IBU	R IBU
		ln τ^{KWW} (mins)	ln τ^{KWW}(mins)	ln τ^{KWW}(mins)
Aged at -66 °C	4.827	8.44 ± 6.64	8.68 ± 7.08	8.22 ± 6.49
Aged at -56 °C	4.605	5.81 ± 4.07	5.35 ± 3.71	5.01 ± 2.70
Activation energy (kJ/mol)		11.84	14.96	14.40

The slopes (i.e. E_as) of R,S IBU, S IBU and R IBU in Figure 3.7 are 11.84, 14.96 and 14.40, respectively. As only two ageing temperatures were used, the calculated E_as had no error values associated with them, but the lnτ^{KWW} values used to fit these lines have significant error values associated with them as shown in Table 3.6. Therefore, it is not possible to make any definitive conclusion from this data.

Unfortunately, it was not possible to measure τ^{KWW} at a temperature lower than -66°C as the DSC cooler could not maintain this temperature for the required time. Similarly, attempts to age glassy

ibuprofen at a temperature higher than -56°C were unsuccessful, as the aging temperature was too close to the glass transition temperature and an accurate enthalpy recovery value could not be determined.

The DSC studies (non-isothermal crystallisation and enthalpy recovery studies) outlined above, demonstrate contradictory findings, as supercooled liquid R,S IBU appears to be more resistant to crystallisation during cooling and heating in a DSC pan, yet simultaneously appears to demonstrate faster relaxation in the amorphous state compared to S IBU. The significant error associated with the values determined for these experiments, such as shown in Table 3.6, means that, while interesting, the level of certainty around these findings is poor.

3.2.1.3 Broadband dielectric spectroscopy (BDS)

The relaxation processes governing amorphous R,S IBU have been well described by separate groups. There are multiple processes (often overlapping) which govern the molecular mobility of R,S IBU and S IBU in the amorphous state, namely α, β, γ and D(Debye) processes [149,190,199]

The purpose of this experiment was to compare the molecular mobility of R,S IBU and S IBU using dielectric spectroscopy, as outlined in Chapter 2 Section 2.2.3.10. Graphs showing the dielectric loss for both compounds are shown in Figure 3.8.

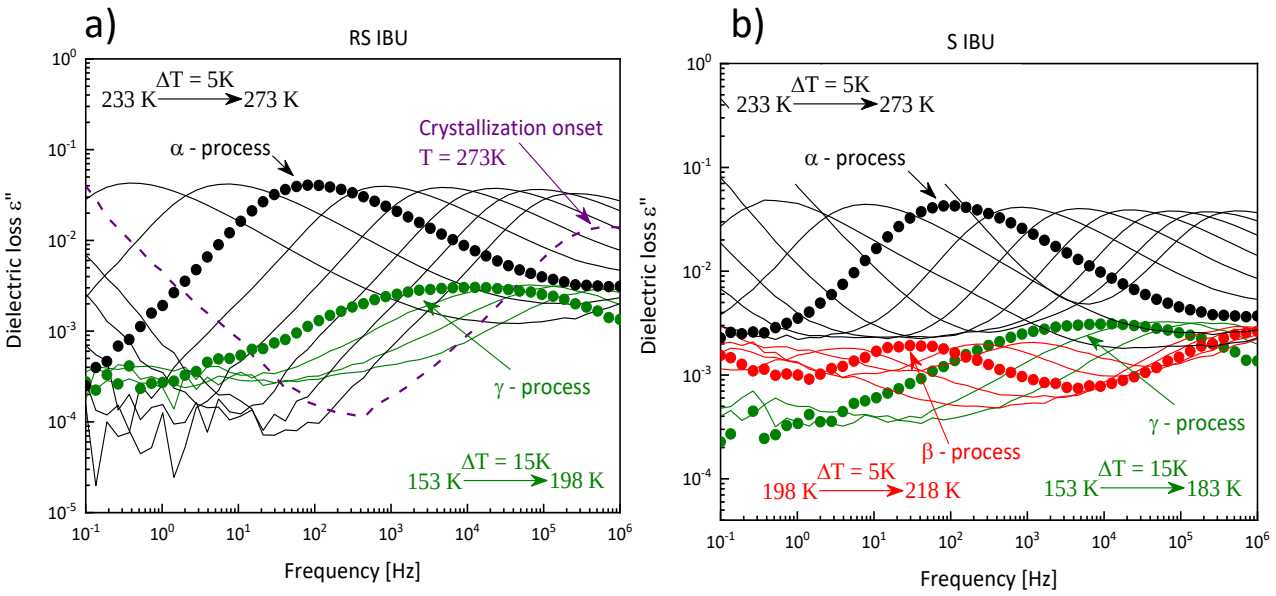

Figure 3.8: Dielectric loss spectra of a) R,S IBU and b) S IBU. Black lines represent the α process, red and green lines represent the β process and ɣ process respectively, and the violet line represents the onset of crystallisation.

The α-process moves to higher frequencies with increasing temperatures, with no change in peak intensity in the case of S IBU. In the case of R,S IBU, there is a sharp decrease in the intensity of the dielectric loss peak at 273 K, which corresponds to the onset of crystallisation of the polymorphic

form of R,S IBU (form II) [154,200]. The growth of form II R,S IBU results from prolonged exposure to temperatures below the glass transition temperature, as was the case in the BDS method used here. The presence of form II of R,S IBU has been documented using DSC, pXRD and hot-stage microscopy. Although a secondary method was not used to confirm the presence of form II R,S IBU, the onset of crystallisation during BDS is most likely due to crystallisation of this polymorph.

At temperatures below the glass transition, the secondary relaxation called the γ- process, is visible in both samples between 153 K and 183 K. In the S IBU sample a further secondary process (termed the β-process) is observed between 198 K and 218 K. This is not apparent in R,S IBU. These secondary relaxation processes result from local molecular motions as opposed to the α-process which reflects reorientation of the entire molecule [201]. Therefore, according to the analysis carried out here, there may be some minor differences in the local molecular motions between R,S IBU and S IBU.

From the analysis of the spectra collected above the glass transition, the α relaxation times of the samples were determined using the Havrilak-Negami (HN) function as described in Chapter 2 Section 2.2.3.10. However, before determining these characteristic relaxation times, the $\tau_\alpha(T)$ dependence had to be parameterised using the Vogel-Fulcher-Tammann (VFT) equation [150,151] as described in Chapter 2 Section 2.2.3.10. The parameters given by the VFT equation are shown in Table 3.7**.** These values are similar to those reported by Bras et al. [149] and Adrjanowicz et al.[199] for R,S IBU and by Shin et al. for S IBU [190]

Table 3.7: α-relaxation parameter estimates for R,S IBU and S IBU using VFT equation

	$\log_{10}\tau_\infty$ (seconds)	D	T_0 (K)
R,S IBU	-14.2 ± 0.5	8.1 ± 0.8	185 ± 2
S IBU	-13.7 ± 0.5	7.5 ± 0.9	187 ± 3

By extrapolating the VFT fit to τ_α = 100 seconds ($\log_{10}\tau_\alpha = 2$), which is the characteristic relaxation time at the glass transition [201] , the glass transition temperature of R,S IBU and S IBU was estimated to be 226 K from the relaxation map (Figure 3.9). This is within 1 K of the glass transition temperature as measured by DSC.

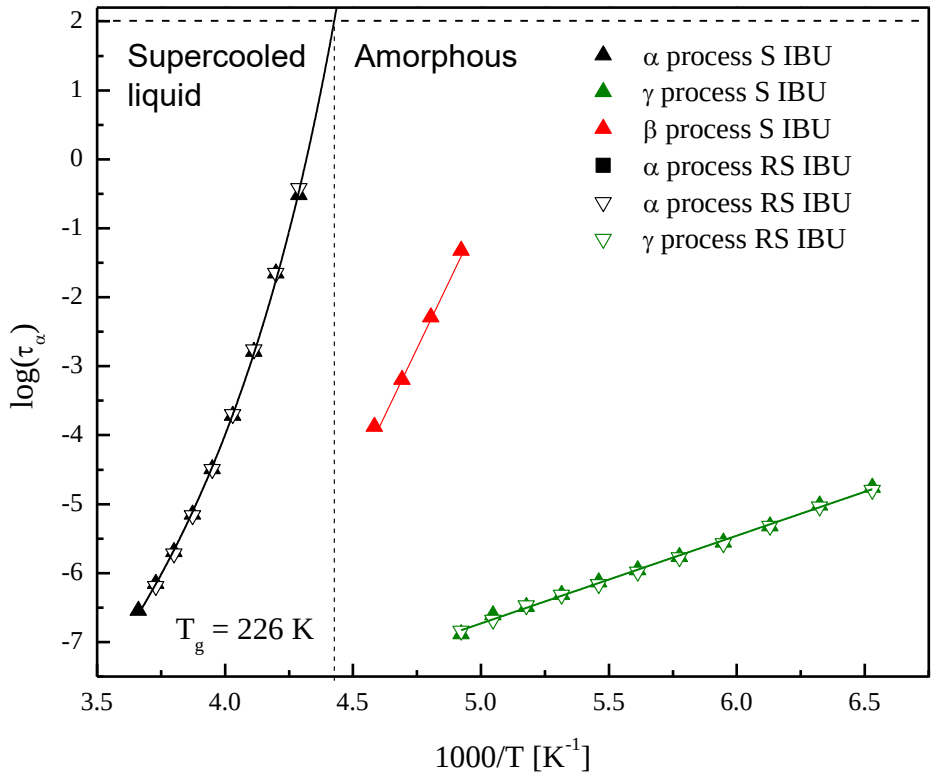

Figure 3.9: Relaxation map of R,S IBU and S IBU

In order to parameterize $\tau_{\beta,\gamma}$(T) dependencies in the glassy state the Arrhenius equation was used as described in Chapter 2 Section 2.2.3.10. The calculated activation energies are shown in Table 3.8.

Table 3.8: Secondary relaxation parameters for R,S-ibuprofen and S-ibuprofen

Secondary process	E_a(kJ mol^{-1})
R,S IBU (ɣ)	24.1 ± 0.3
S IBU (ɣ)	24.4 ± 0.4
S IBU (β)	145.6 ± 5.8

The E_a for the γ-process in amorphous R,S IBU corresponds well to what has been described in the literature [149,199]. Both of these cited studies also describe a β-process for R,S IBU which had an activation energy of approximately 50 kJ mol^{-1} associated with it. This was not observed in the current study, which may be due to the crystallisation which was observed in this sample, which has not been recorded previously in the literature.

A previous study examining the secondary relaxation process(es) of amorphous S IBU, found a single secondary relaxation process, which they termed the β relaxation, which had an E_a of 39.2 kJ/mol associated with it [190]. In the present study, two secondary relaxation processes are described for S IBU, the γ-process (which was quasi-identical to the R,S IBU sample) and a β-process which

was not observed in the R,S IBU sample. Upon further examination of the S IBU β-process, the activation energy of 145.6 kJ mol^{-1} is much higher than what would be anticipated for a secondary relaxation process and may in fact be the α-process of an impurity/ degradation product.

Supercooled liquids can be classified into two categories "strong" and "fragile" using the M_p parameter [202], as described in Chapter 2 Section 2.2.3.10. The higher the value of the steepness index the more fragile the system is. It has been postulated that fragility i.e. the measure of deviation of $\tau_\alpha(T)$ from Arrhenius behaviour, may be an inverse measure of physical stability of amorphous APIs. The higher the value of M_p, the more unstable the system is likely to be in the supercooled liquid state. The M_p for S IBU was calculated as 91, this is significantly higher than the fragility values which have been previously reported for S IBU which ranged from 73 to 76 [178,190]. The M_p value determined for R,S IBU in this work was 90, which is similar to literature values which ranged from 87 to 93 [149,199]. Based on these values both samples can be classified as fragile glass formers, meaning they would both be anticipated to be poorly stable in the glassy state, although the opposite has been observed experimentally [4].

It is clear from the studies described in Section 3.2.1 that determining the relative amorphous stabilities of racemic compounds and their single enantiomer counterparts is challenging and complex. A summary of the observations made in this section is given in Table 3.9. Non-isothermal crystallisation studies appeared to contradict the assumption that S IBU should be more resistant to crystallisation in the supercooled liquid state than R,S IBU. Quantification of the extent of enthalpy recovery experienced by R,S IBU and S IBU in the amorphous state was difficult using DSC and a more detailed picture of the relaxation processes was captured via BDS.

Table 3.9: Summary of amorphous stability predictors determined for R,S IBU and S IBU in Section 3.2.1

	R,S IBU	S IBU
Non-isothermal crystallisation		
GFA	Superior	Inferior
GS	Superior	Inferior
Enthalpy recovery		
Enthalpy recovery over time	Possibly faster	Possibly slower
Activation energy for recovery	Possibly lower	Possibly higher
Broadband dielectric spectroscopy		
Crystallisation	Polymorphic crystallisation	No crystallisation
Relaxation processes	α and γ processes	α, β and γ processes
α process relaxation time	$\log_{10}(\tau_\infty)$ = -14.2 ± 0.5	$\log_{10}(\tau_\infty)$ = -13.7 ± 0.5
β process activation energy	Not observed	145.6 ± 5.8 kJ/ mol
γ process activation energy	24.1 ± 0.3 kJ/ mol	24.4 ± 0.4 kJ/ mol
Fragility	90	91

3.2.2 The impact of chiral recognition between API and polymer on ASD stability and performance

3.2.2.1 Chiral recognition between ibuprofen and cellulose polymers: screening using cryo-milling (CM)

A chiral recognition screening study of ibuprofen and cellulose polymers was carried out as outlined in Chapter 2 Section 2.2.1.2.1. Briefly, ibuprofen (R,S IBU, S IBU or R IBU) and a cellulose polymer (HPC, HPMC, HPMCAS or HPMCP) were cryo-milled at a 50:50 w/w ratio and the resulting powder was tested for amorphisation using DSC and pXRD.

3.2.2.1.1 Thermal analysis

Representative DSC scans for the cellulose polymers cryo-milled with R,S IBU, S IBU or R IBU are shown in Figures 3.10, 3.11 and 3.12 respectively, and thermal parameters determined from these scans are shown in Table 3.10

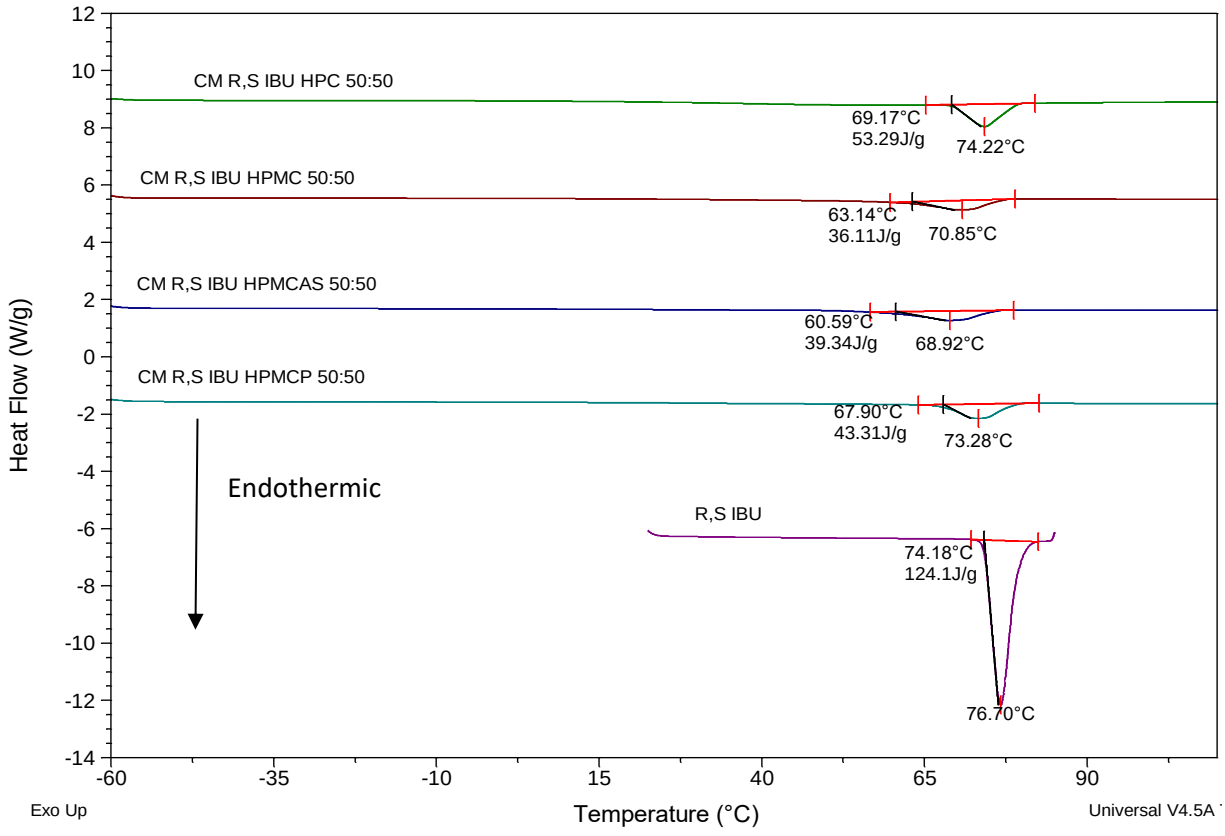

Figure 3.10: Representative DSC scans of R,S-ibuprofen/ cellulose polymer systems post cryo-milling, with a pure R,S-ibuprofen scan as a reference (purple line)

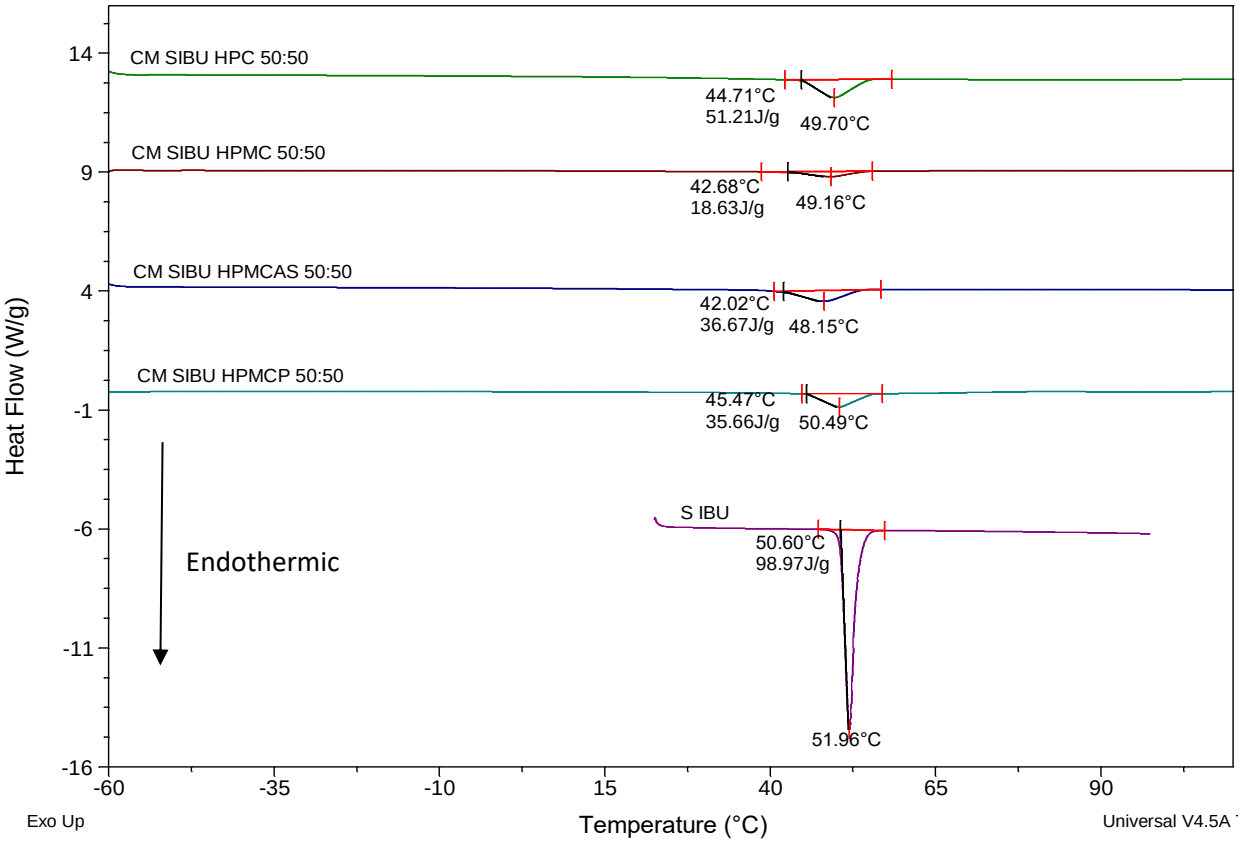

Figure 3.11: Representative DSC scans of S-ibuprofen/ cellulose polymer systems post cryo-milling, with a pure S-ibuprofen scan as a reference (purple line)

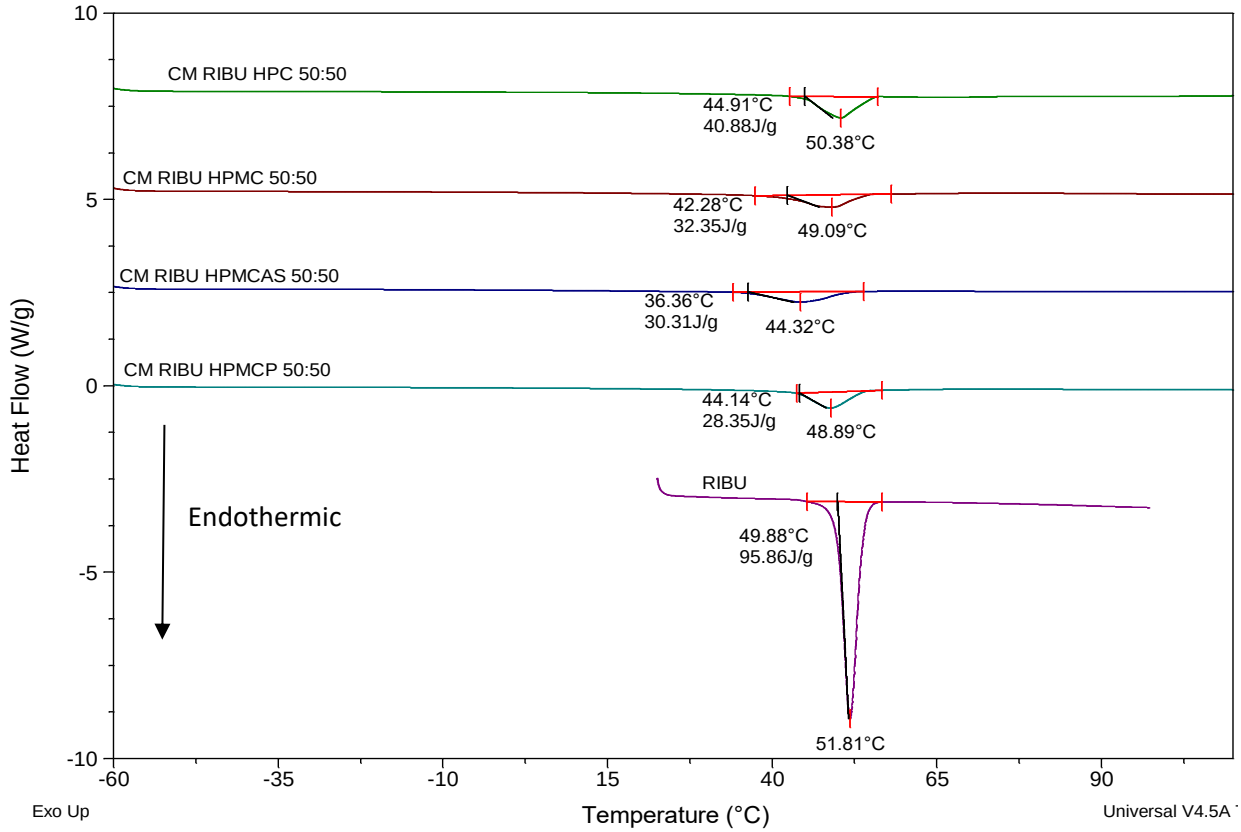

Figure 3.12: Representative DSC scans of R-ibuprofen/ cellulose polymer systems post cryo-milling, with a pure R-ibuprofen scan as a reference (purple line)

Table 3.10: Onset melting temperatures (Tm) and enthalpies of fusion (ΔH_f) for physical mixtures (PM) and cryo-milled samples (CM) of cellulose polymers: ibuprofen systems 50:50 w/w. Values are mean values ± standard deviation.

	HPC			HPMC			HPMCAS			HPMCP		
	R,S IBU	S IBU	R IBU	R,S IBU	S IBU	R IBU	R,S IBU	S IBU	R IBU	R,S IBU	S IBU	R IBU
PM Tm (°C)	70.06 ± 0.20	47.59 ± 0.15	45.43 ± 0.52	68.83 ± 0.32	46.37 ± 0.63	45.47 ± 0.38	67.62 ± 0.11	47.44 ± 0.05	44.76 ± 0.26	69.67 ± 0.15	46.61 ± 0.34	45.48 ± 0.58
CM Tm (°C)	69.26 ± 0.12	45.57 ± 0.71	45.62 ± 0.19	61.94 ± 1.48	42.20 ± 0.42	41.50 ± 0.45	59.50 ± 0.59	42.39 ± 1.01	35.31 ± 0.62	67.66 ± 0.70	46.13 ± 0.78	43.43 ± 0.29
PM ΔH_f (J/g)	59.25 ± 1.77	43.79 ± 0.41	47.36 ± 5.45	52.13 ± 2.11	40.50 ± 0.75	47.63 ± 2.69	58.78 ± 7.63	38.14 ± 2.05	41.79 ± 7.66	57.80 ± 0.86	34.61 ± 4.94	48.86 ± 1.20
CM ΔH_f (J/g)	53.90 ± 0.64	47.29 ± 4.22	43.96 ± 1.97	44.11 ± 5.03	20.98 ± 1.59	35.93 ± 4.09	49.38 ± 3.05	36.96 ± 6.00	32.76 ± 3.09	48.07 ± 5.69	31.36 ± 6.23	37.57 ± 0.43
CM % crystalline	90.97 ± 1.08	108.00 ± 9.63	92.82 ± 4.17	84.63 ± 10.15	51.81 ± 3.59	75.86 ± 8.65	84.01 ± 5.19	96.89 ± 15.76	78.38 ± 7.42	83.16 ± 9.85	90.61 ± 17.99	76.89 ± 0.89

It is clear from the DSC scans shown in Figures 3.10-3.12 that none of the cryo-milled ibuprofen-cellulose systems were completely amorphous as evidenced by the presence of a melting endotherm in all samples, which corresponded to the melting endotherm of crystalline R,S IBU, S IBU or R IBU. Interestingly, no glass transition temperatures were detected for any of the cryo-milled samples, even though an overall reduction in the amount of ibuprofen present in the crystalline form was apparent for many systems (Table 3.10).

However, it is apparent that two of the cellulose polymers (HPMC and HPMCAS) have depressed the melting points of all ibuprofen material (regardless of enantiomeric composition) more than the other two cellulose polymers (HPC and HPMCP) which were tested. This is represented graphically in Figure 3.13.

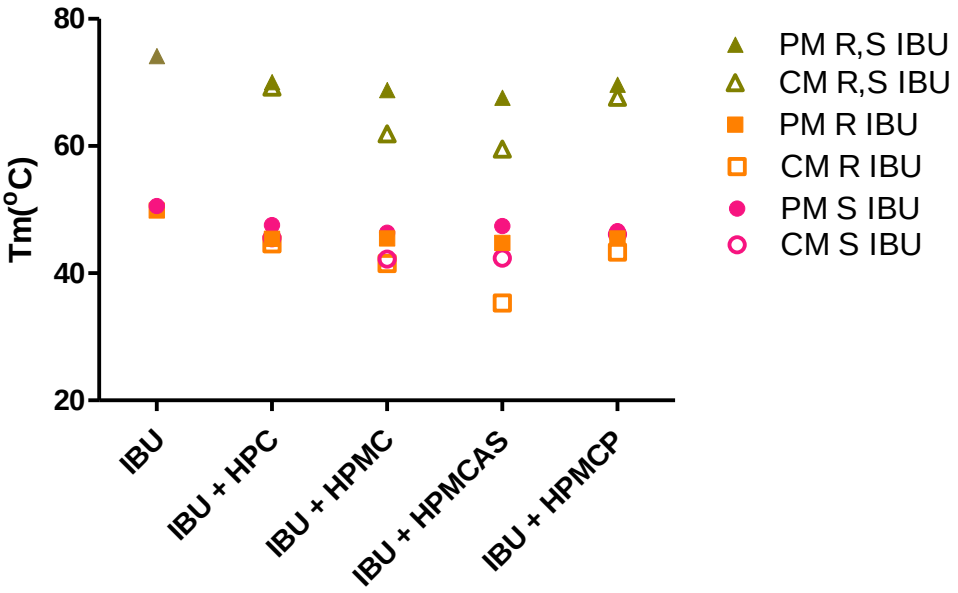

Figure 3.13: Melting point depression of cryo-milled ibuprofen-cellulose samples at a 50:50 w/w ratio compared to their equivalent physical mixtures. PMs are physical mixtures of ibuprofen and polymer and CMs are cryo-milled mixtures of ibuprofen and polymer.

The melting point of a crystal represents the temperature at which the chemical potential of the crystal is equal to the chemical potential of the melt [106]. When an amorphous polymer is mixed at the molecular level with a crystalline substance, if miscible, the chemical potential of the crystalline material is reduced, resulting in the melting point occurring at lower temperatures than the pure crystalline substance [102].

For the systems studied in Figure 3.13 it is clear that HPMCP and HPC are poorly miscible with all three enantiomeric forms of ibuprofen, as evidenced by low/ negligible melting point depression in the cryo-milled samples relative to the equivalent physical mixtures. By contrast, the cryo-milled HPMC and HPMCAS systems exhibit melting points which are depressed relative to the physical

mixtures in both enantiomeric forms and the racemate of ibuprofen. This is interesting, as it appears that the miscibility of cellulose polymers to and ibuprofen is similar across all three enantiomeric compositions of ibuprofen, except for HPMCAS. The R IBU-HPMCAS cryo-milled system demonstrated a melting point which was significantly lower than the S IBU-HPMCAS cryo-milled system (35.31 ± 0.62 °C versus 42.39 ± 1.01 °C, Table 3.10) which may indicate differences in miscibility between HPMCAS and R IBU and S IBU.

The amount of crystalline material still present in the cryo-milled samples was estimated using DSC, as described in Chapter 2 Section 2.2.3.4.1, and results are graphed in Figure 3.14 and listed in Table 3.10.

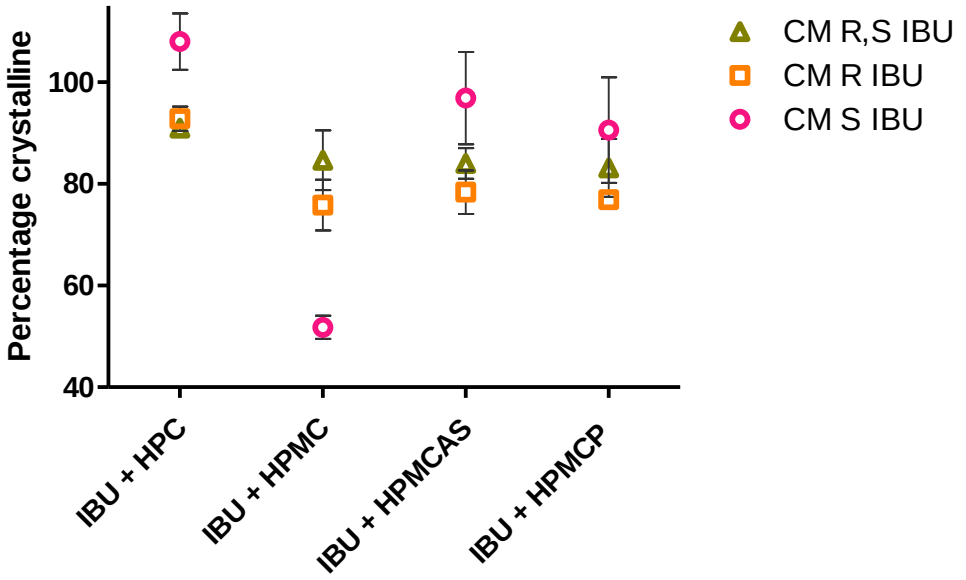

Figure 3.14: Estimates of the proportion of ibuprofen present in the crystalline state post cryo-milling with cellulose polymers at a 50:50 w/w ratio, relative to an equivalent physical mixture. CMs are cryo-milled mixtures of ibuprofen and polymer.

Examining Figure 3.14, it is clear that the systems containing HPC appear to contain the greatest amount of crystalline ibuprofen after cryo-milling, regardless of the enantiomeric composition of ibuprofen. The quantity of R,S IBU which remains crystalline when cryo-milled with HPMC, HPMCAS and HPMCP is approximately 84% in all cases. Similarly, the quantity of R IBU which remains crystalline when cryo-milled with HPMC, HPMCAS and HPMCP is approximately 76% in all cases. By contrast, the proportion of S IBU which remained crystalline in the cryo-milled systems appears to differ depending on the type of cellulose polymer which was used. The proportion of S IBU which remained crystalline after cryo-milling with HPMC, HPMCAS and HPMCP was estimated as 52%, 97% and 91% respectively. These results point towards a stereospecific facilitation of amorphisation and/or suppression of recrystallisation as a result of interaction between ibuprofen and cellulose polymers, which is particularly prominent between S IBU and HPMC.

3.2.2.1.2 pXRD analysis

The pXRD patterns for HPC, HPMC, HPMCAS and HPMCP ibuprofen systems 50% w/w before and after cryo-milling are shown in Figures 3.15-3.18. Bragg peaks are evident in all physical mixtures and in all cryo-milled samples, indicating that crystalline ibuprofen is present in all samples, which agrees with findings from the thermal analysis in Section 3.2.2.1.1.

In the pXRD patterns of R,S IBU-cellulose polymer systems, the intensity of the Bragg peak located at 22.40 degrees 2θ appears to reduce in intensity for all cryo-milled samples (pattern b in Figures 3.15-3.18) relative to their physical mixture counterparts (pattern a in Figures 3.15-3.18), which indicates some degree of amorphisation of ibuprofen has taken place. Similarly, in the pXRD patterns of S IBU and R IBU cellulose polymer systems, the intensity of the Bragg peak located at 7.50 degrees 2θ reduces in intensity for all cryo-milled samples (patterns d and f in Figures 3.15-3.18) relative to their physical mixture counterparts (patterns c and e in Figures 3.15-3.18).

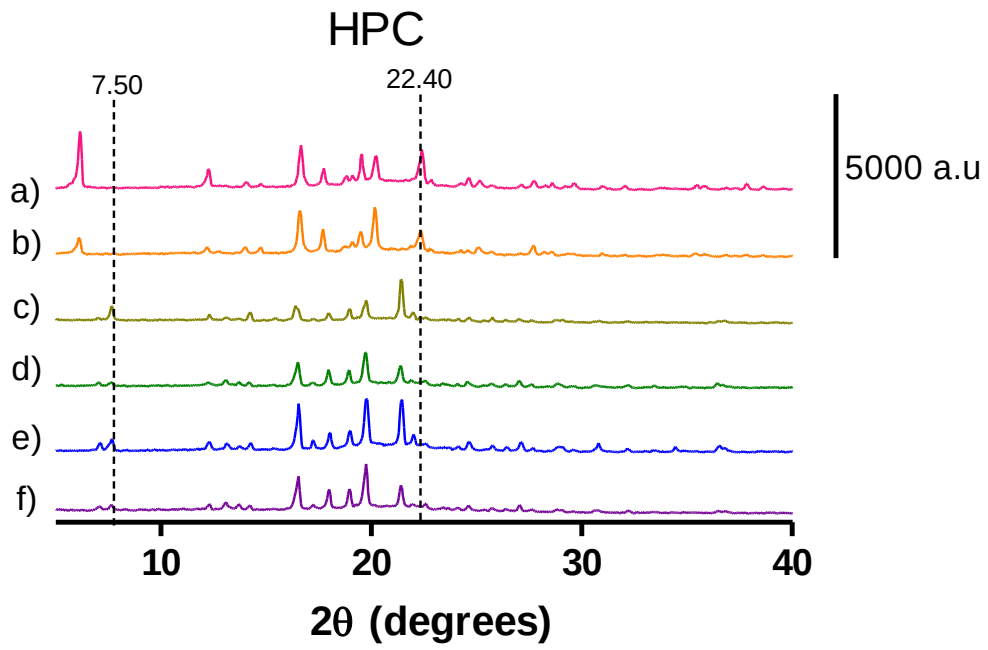

Figure 3.15: pXRD patterns of physical mixtures (PM) and cryo-milled samples (CM) of HPC and ibuprofen in a 50:50 w/w ratio. a) PM R,S IBU b) CM R,S IBU c) PM S IBU d) CM S IBU e) PM R IBU f) CM R IBU

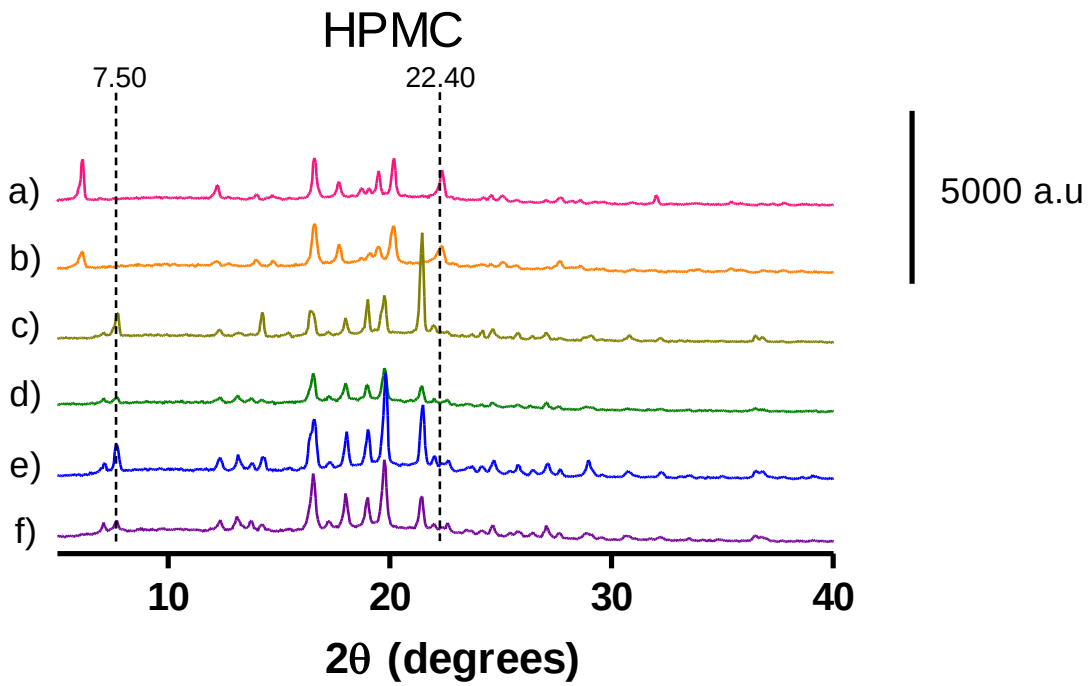

Figure 3.16: pXRD patterns of physical mixtures (PM) and cryo-milled samples (CM) of HPMC and ibuprofen in a 50:50 w/w ratio. a) PM R,S IBU b) CM R,S IBU c) PM S IBU d) CM S IBU e) PM R IBU f) CM R IBU

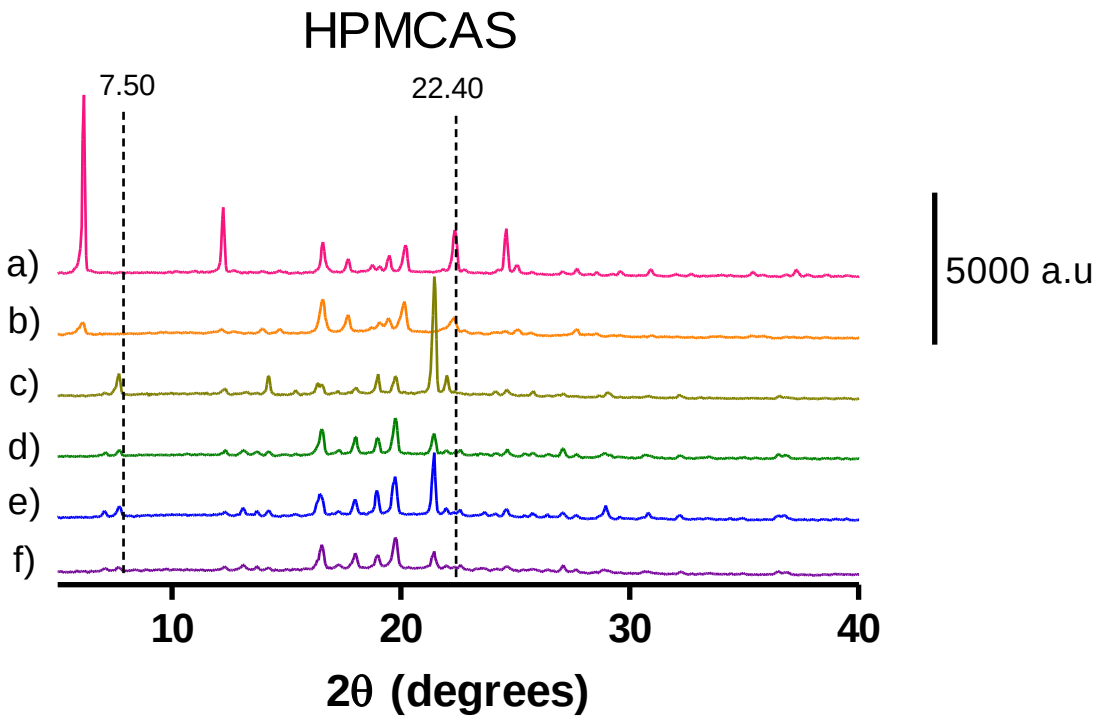

Figure 3.17: pXRD patterns of physical mixtures (PM) and cryo-milled samples (CM) of HPMCAS and ibuprofen in a 50:50 w/w ratio. a) PM R,S IBU b) CM R,S IBU c) PM S IBU d) CM S IBU e) PM R IBU f) CM R IBU

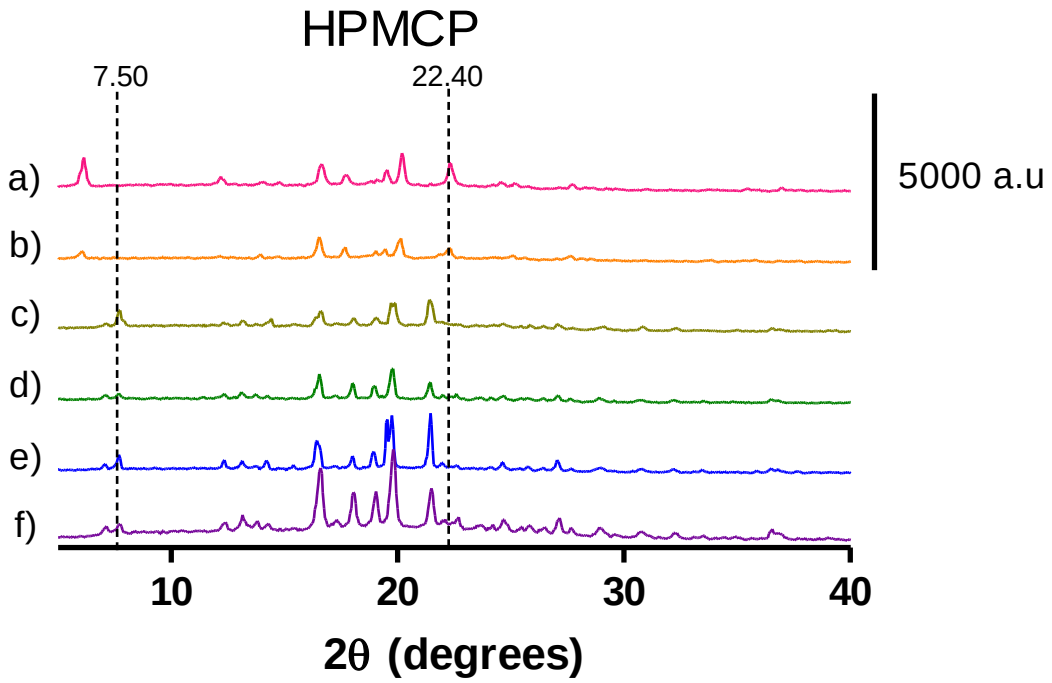

Figure 3.18: pXRD patterns of physical mixtures (PM) and cryo-milled samples (CM) of HPMCP and ibuprofen in a 50:50 w/w ratio. a) PM R,S IBU b) CM R,S IBU c) PM S IBU d) CM S IBU e) PM R IBU f) CM R IBU

Interestingly, comparing the patterns of CM SIBU HPMC and CM R IBU HPMC (Figure 3.16 d and f respectively), the S IBU sample appears to have Bragg peaks which have reduced intensity relative to the R IBU sample. This corresponds well to the thermal analysis which showed that after cryo-milling the crystalline ibuprofen content of the S IBU-HPMC sample was approximately 52% of the total ibuprofen content, while the same value for the R IBU HPMC sample was approximately 76%.

As the HPMCAS systems also appear to show chiral recognition in terms of the differential ability to facilitate amorphisation and supress crystallisation from a metastable ASD, it was anticipated that a difference in the intensity of the CM pXRD patterns would also be apparent between S and R IBU systems for this polymer, as it was for the HPMC systems, but this is not the case (Figure 3.17 d and f). The reason for this is unclear.

3.2.2.1.3 ATR-FTIR analysis of CM samples

In order to probe the intermolecular interactions between the cellulose based polymers and different enantiomeric compositions of ibuprofen, ATR-FTIR spectra of the cryo-milled samples were normalised and analysed as described in Chapter 2 Section 2.2.3.2. The regions of the spectra which were of interest were the OH region and the carbonyl region. Unbonded OH groups show an absorption peak at approximately 3520 cm^{-1}, while OH groups which are hydrogen bonded show a signal between 3300-2500 cm^{-1} [149]. R,S IBU shows a carbonyl peak at 1717 cm^{-1}, while S IBU shows a carbonyl peak at 1705 cm^{-1}. These peaks are attributed to the carbonyl (C=O) of the carboxylic acid group of IBU. The carboxylic acid groups in IBU form dimers [203] via two hydrogen bonds which are symmetric or asymmetric for crystalline R,S IBU and S IBU, respectively. The two asymmetric, non-identical hydrogen bonds in crystalline S-ibuprofen have bond lengths of 2.6228 and 2.6588 Å whereas the bond length of the symmetric intermolecular hydrogen bond is 2.6265 Å for crystalline R,S-ibuprofen [203]. The slight shift to lower wavenumber for the C=O peak in S IBU compared to R,S IBU can be attributed to the longer bond length (2.6588 Å) of its dimer form.

The spectra for the ibuprofen-cellulose polymer cryo-milled samples are shown in Figures 3.19-3.22, and the normalised absorbance values for the peaks of interest are shown in Table 3.11.

As shown in Figure 3.19, a solitary peak is present in the carbonyl region (1705-1717 cm^{-1}) for all cryo-milled HPC systems, regardless of ibuprofen enantiomeric composition. The hydrogen bonded OH group also shows a peak at approximately 2954 cm^{-1}. The normalised absorbance of these peaks for all HPC-ibuprofen samples was similar for R, S IBU, S IBU and R IBU (1, 0.997 and 0.986 respectively) (Table 3.11).

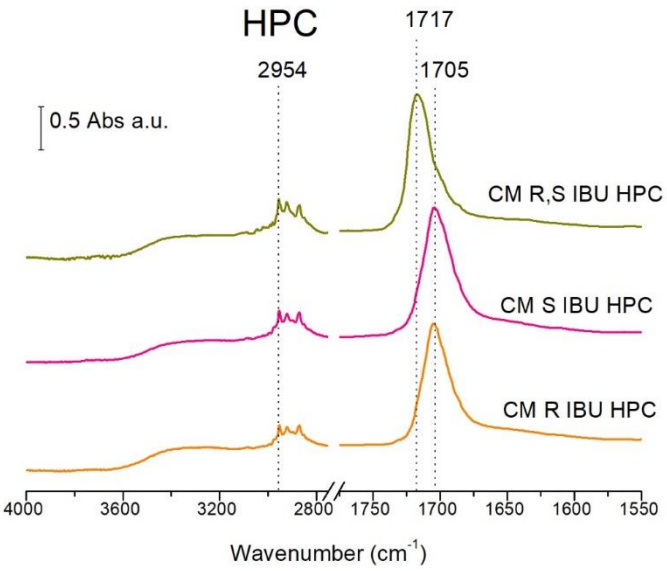

Figure 3.19: ATR-FTIR spectra of cryo-milled samples (CM) of HPC and ibuprofen in a 50:50 w/w ratio

In Figure 3.20, the presence of a shoulder in the carbonyl peaks of cryo-milled HPMC S IBU and R IBU is apparent. This shoulder is lacking in the equivalent R,S IBU HPMC spectra. The presence of these shoulders indicates that the population of carbonyl groups in S IBU and R IBU consists of two distinct groups; hydrogen bonded carbonyls which are present in crystalline dimers at 1705 cm^{-1} and non-hydrogen bonded carbonyls present in the monomeric amorphous form of ibuprofen, which appears as a shoulder at 1734 cm^{-1} [204,205]. By assessing the ratio of these two components, the relative abundance of monomeric ibuprofen compared to dimeric ibuprofen can be deduced. Although thermal analysis showed that cryo-milled S IBU HPMC was less crystalline than R IBU HPMC, spectral analysis shows that the ratio of monomeric carbonyl groups and dimeric carbonyl groups is similar for both systems (0.442 and 0.463 respectively). The same is true for the intensity of the non-hydrogen bonded OH region (0.027 and 0.026 for S IBU HPMC and R IBU HPMC respectively at 3700 cm^{-1}) and the hydrogen bonded OH region (0.279 and 0.263 for S IBU HPMC and R IBU HPMC respectively at 2954 cm^{-1}).

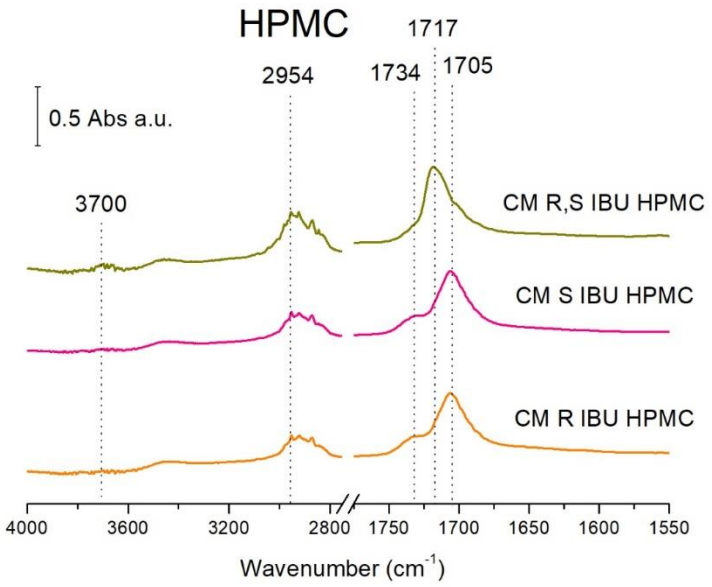

Figure 3.20: ATR-FTIR spectra of cryo-milled samples (CM) of HPMC and ibuprofen in a 50:50 w/w ratio

In Figure 3.21, the presence of a shoulder in the carbonyl peaks of all three cryo-milled ibuprofen-HPCMAS systems is evident, indicating that amorphous monomeric ibuprofen is also present in all three systems. However, in this instance the ratios of monomeric shoulder to dimeric peak is different for all three systems (0.558, 0.796 and 0.691 for R,S IBU, S IBU and R IBU HPMCAS systems respectively).

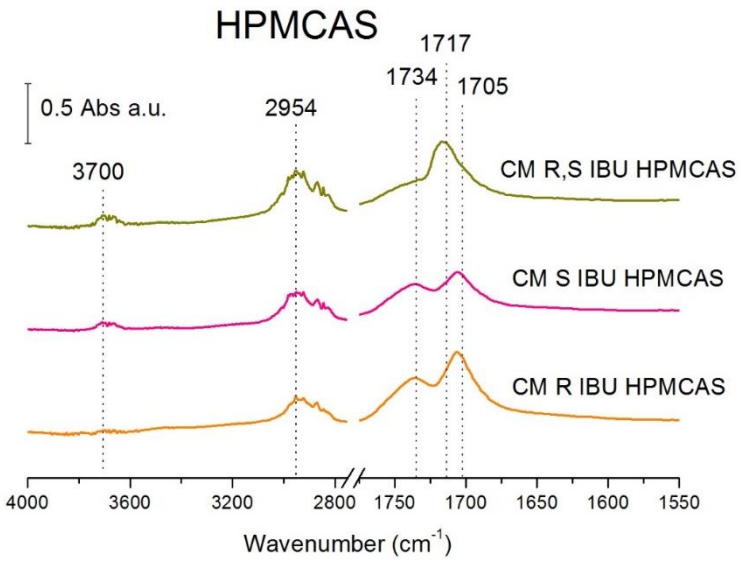

Figure 3.21: ATR- FTIR spectra of cryo-milled samples (CM) of HPMCAS and ibuprofen in a 50:50 w/w ratio

In Figure 3.22 only S IBU HPMCP and R IBU HPMCP show a shoulder in the carbonyl region, indicating the presence of amorphous monomeric ibuprofen, while R,S-ibuprofen HPMCP does not. The carbonyl shoulder to peak ratio was quite different between S IBU and R IBU HPMCP systems (0.590 and 0.434 respectively). This is surprising, as the thermal analysis showed that HPMCP did not demonstrate a differential ability to cause amorphisation of either enantiomer of ibuprofen.

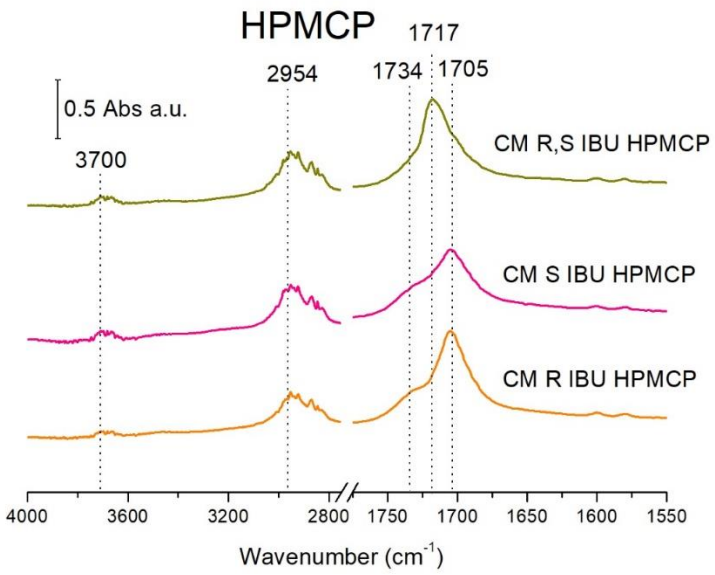

Figure 3.22: ATR-FTIR spectra of cryo-milled samples (CM) of HPMCP and ibuprofen in a 50:50 w/w ratio

Table 3.11: Normalised absorbance from ATR-FTIR spectra of cryo-milled ibuprofen-cellulose samples at a 50:50 w/w ratio. (P) refers to a main peak while (S) refers to a shoulder.(S)/(P) refers to the ratio of the shoulder absorbance to main peak absorbance

Polymer	Wavenumber (cm^{-1})	R,S IBU	S IBU	R IBU	S IBU/R IBU
HPC	1717 (P)	1			
	1705 (P)		0.997	0.986	1.011
	2954	0.364	0.335	0.307	1.091
HPMC	1717 (P)	0.578			
	1734 (S)		0.248	0.252	0.984
	1705 (P)		0.561	0.544	1.031
	(S)/(P)		0.442	0.463	0.954
	3700	0.050	0.027	0.026	1.038
	2954	0.336	0.279	0.263	1.060
HPMCAS	1734 (S)	0.288			
	1717 (P)	0.516			
	(S)/(P)	0.558			
	1734 (S)		0.304	0.407	0.747
	1705 (P)		0.382	0.589	0.649
	(S)/(P)		0.796	0.691	1.150
	3700	0.075	0.052	0.033	1.576
	2954	0.346	0.252	0.275	0.916
HPMCP	1717 (P)	0.671			
	1734 (S)		0.315	0.313	1.006
	1705 (P)		0.533	0.722	0.738
	(S)/(P)		0.590	0.434	1.363
	3700	0.062	0.065	0.049	1.327
	2954	0.347	0.327	0.309	1.058

The ATR-FTIR analysis of the cryo-milled IBU-cellulose systems demonstrated that HPMCAS and HPMCP exhibited differing ratios of amorphous-to-crystalline IBU based on carbonyl peak assessment. No evidence of hydrogen bonding between the carbonyl of ibuprofen and any of the polymers was observed, as evidenced by the lack of a shift in the wavenumber of the carbonyl for any of the systems studied.

This screening study has demonstrated that HPC and HPMCP are poor choices of polymers for ASD manufacture of IBU (both R,S IBU and S IBU or R IBU) via cryo-milling. HPMCAS and HPMC were more successful in this regard and demonstrated some differences in either their miscibility or extent of suppression of crystallisation of IBU depending on whether R IBU or S IBU was being used. The stereoselective stabilisation that HPMC and HPMCAS have on amorphous IBU is unlikely to be explained via hydrogen bonding but may be due to other interactions and/or differences in miscibility.

All polymers tested have the same basic glucose sub-unit but different substituents and different relative abundancies of these substituents. The percentages of each substituent (as a % of the polymer Mw) in the four polymers used, are listed in Table 3.12. This difference may explain their differing abilities to amorphise IBU via cryo-milling. Although the degree of substitution in the cellulose polymer is controlled, their arrangement relative to each other may vary along the polymer chain. This means that the "three-points-of-interaction" which is required for chiral recognition, may vary along the polymer chain. This may explain the complex picture that this screening study has demonstrated in the ability of cellulose polymers to differentially suppress the crystallisation of different enantiomers of amorphous IBU. In the chromatography sector, the ability of chiral stationary phases to resolve enantiomers is greatly influenced by the type and position of the substituent groups [206]. It is recognised that enantioselectivity is influenced greatly by substituents with ester groups [207], such as the succinoyl functional group. This may explain the observation that HPMCAS showed some degree of enantioselectivity for IBU in the amorphous state.

Table 3.12: Substituent percentages of HPC, HPMC, HPMCP and HPMCAS

Substituent % (of Mw)	Hydroxypropyl	Acetyl	Succinoyl	Methoxy	Phthalyl
HPC	8.1	0	0	0	0
HPMC	9.1	0	0	28.7	0
HPMCAS	7.0	7.9	14.7	22.3	0
HPMCP	6.1	0	0	19.5	33

3.2.2.2 Spherulite growth studies

3.2.2.2.1 Ibuprofen spherulite growth as a function of temperature

Given the demonstrated ability of HPMC to facilitate amorphisation of IBU enantiomers on cryo-milling to different extents, the potential differential ability of HPMC to suppress crystallisation of different enantiomers of IBU was assessed by examining the growth rate of ibuprofen spherulites over time using hot stage microscopy, as outlined in Chapter 2 Section 2.2.3.13. Firstly, a suitable temperature for spherulite growth rate was identified by plotting the radius of the spherulite over time for R,S IBU at 25 °C, 30 °C, 35 °C and 40 °C. These values are shown in Table 3.13. In each case, the spherulite growth rate was linear over all time points studied (R^2 values > 0.99), which has also been observed in a similar study with felodipine [208]. Growth rates increased with increasing temperature; this relationship was well captured by linear regression with an R^2 value > 0.95 as shown in Figure 3.23b.

Table 3.13: Radial growth rates of R,S IBU spherulites at various temperatures

Temperature	Radial growth rate (µm/s)
25° C	1.23
30° C	2.89
35° C	3.43
40° C	4.38

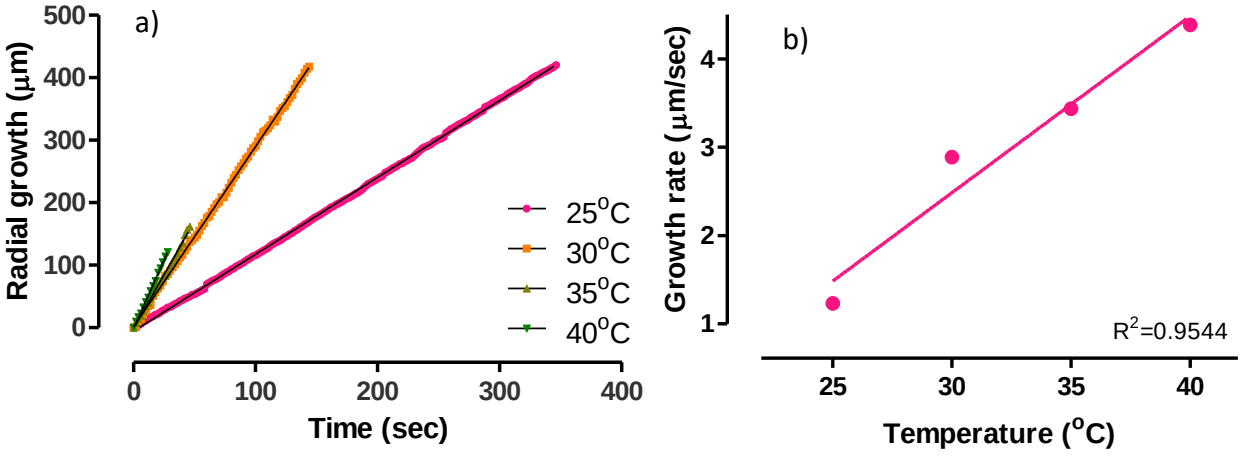

Figure 3.23: a) Radial growth and b) radial growth rate of R,S IBU spherulites at various temperatures

3.2.2.2.2 Ibuprofen spherulite growth as a function of polymer composition

The growth rates of R,S IBU spherulites in the presence of various HPMC concentrations (5%, 10% and 20% w/w) were determined at 30 °C. Results are presented in Table 3.14 and Figure 3.24. Growth rate was found to be inversely related to HPMC concentration which is logical as HPMC is known to inhibit ibuprofen crystalline growth rate [209]. This finding is also in agreement with a similar study which tested felodipine spherulite growth as a function of concentration of a variety of different polymers (HPMCAS, PVPVA and PVP), although in the cited study the growth rate-polymer concentration relationship was described by a log-linear relationship [208]. This effect is thought to be due to specific interactions between polymer and API and/or the anti-plasticization effect of the polymer [204].

Table 3.14: Radial growth rate of R,S IBU spherulites at 30°C with varying HPMC concentrations. Results are presented as an average of three spherulites ± standard deviation

HPMC concentration (%w/w)	Radial growth rate (µm/s)
0	2.97 ± 0.56
5	1.97 ± 0.12
10	1.56 ± 0.30
20	0.44 ± 0.03

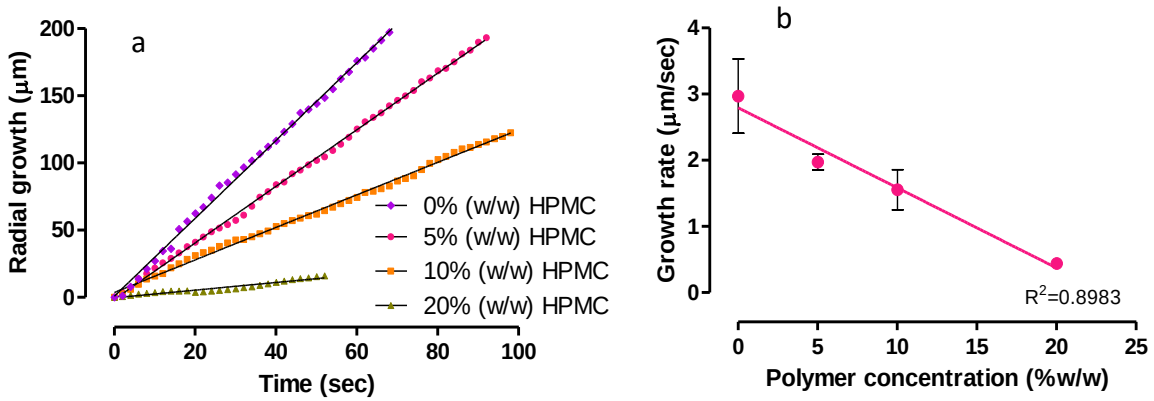

Figure 3.24: a)Radial growth and b) radial growth rate of R,S IBU spherulites at 30 °C in the presence of varying HPMC concentrations

3.2.2.2.3 Ibuprofen spherulite growth as a function of enantiomer composition

The radial growth rates of ibuprofen spherulites (R,S IBU, S IBU and R IBU) were determined at 30 °C in the absence of any polymer as well as in the presence of 5% (w/w) HPMC. Sample spherulites are shown in Figure 3.25 and radial growth rates are presented in Table 3.15 and Figure 3.26.

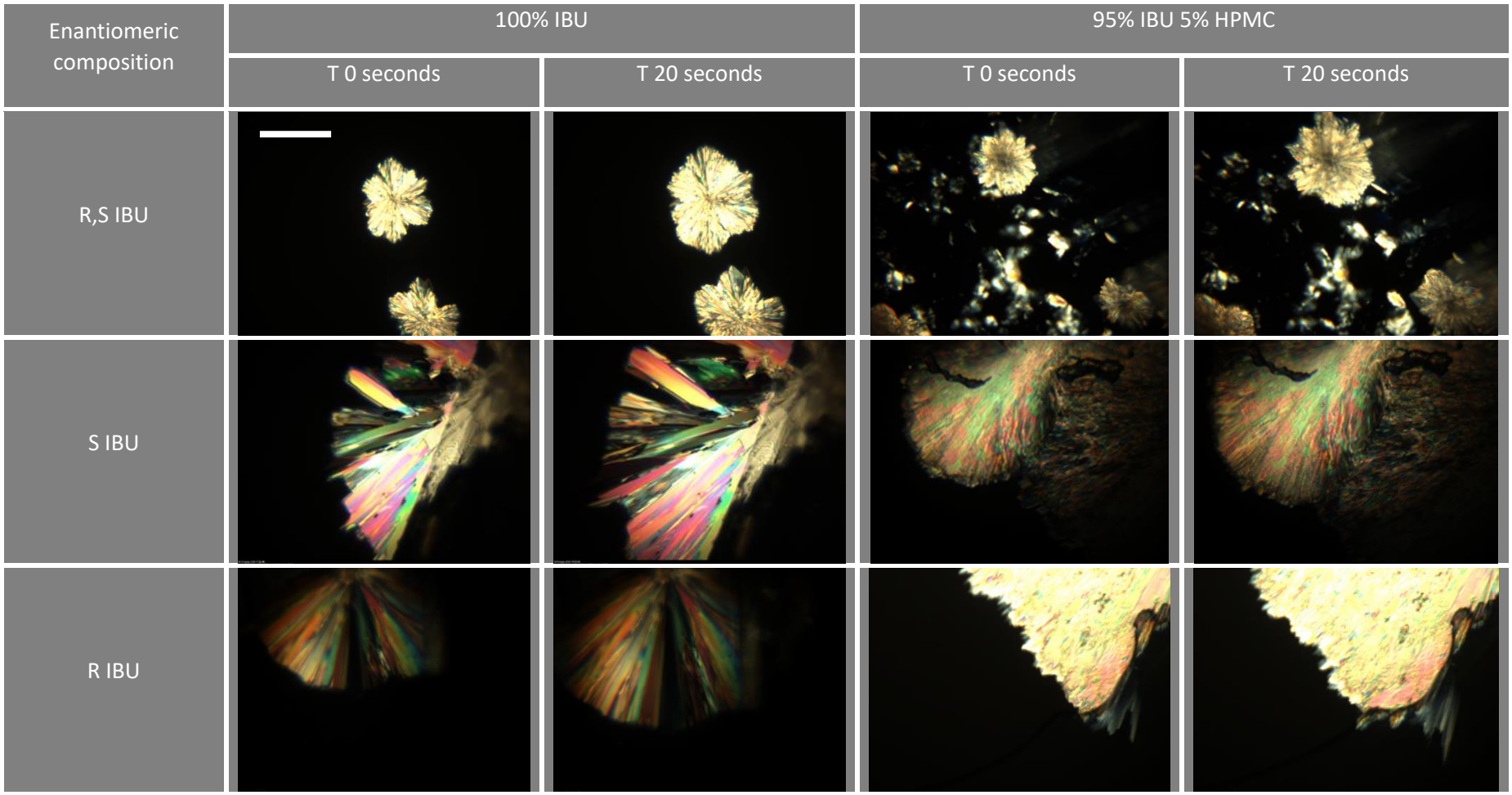

Figure 3.25: Sample spherulites used to determine the radial growth rate of IBU in the presence and absence of 5% w/w HPMC at 30 °C. The white scale bar in the upper left image represent 220 µm and is valid for all images

Table 3.15: Radial growth rates ± standard deviation of R,S IBU, S IBU and R IBU spherulites at 30°C in the presence and absence of 5% w/w HPMC

Enantiomeric composition	Radial growth rate (µm/s)	
	HPMC concentration (0% w/ w)	HPMC concentration (5% w/w)
R,S IBU	2.97 ± 0.560	1.97 ± 0.12
S IBU	10.04 ± 0.87	4.93 ± 0.62
R IBU	9.40 ± 0.34	7.76 ± 0.62
S IBU vs R IBU p-value	0.298	0.005

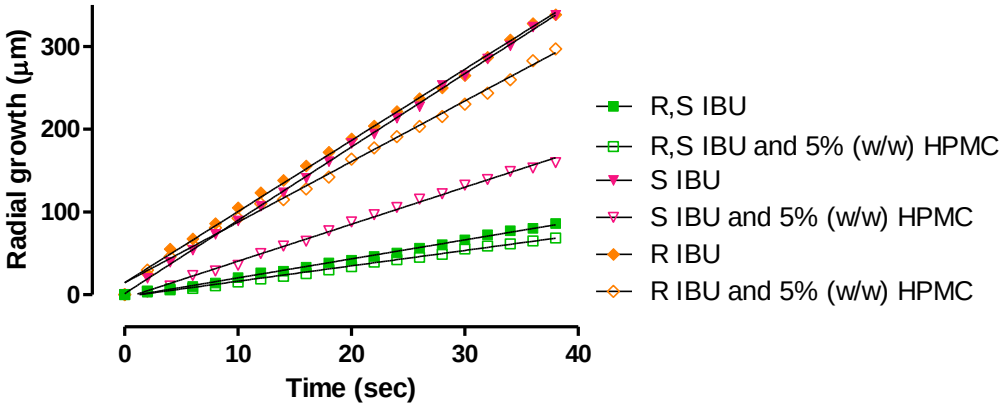

Figure 3.26: Radial growth of R,S IBU, S IBU and R IBU spherulites at 30°C in the presence and absence of 5% w/w HPMC

As seen in Figure 3.26 and Table 3.15, R IBU and S IBU spherulites, without the presence of HPMC did not have statistically significant differences in their spherulite radial growth rates (p = 0.298). This is unsurprising as both enantiomers share the same thermal properties as outlined in Section 3.2.1, therefore they have the same thermodynamic driving force towards crystallisation. The growth rate of the R,S IBU spherulites, in the absence of HPMC was much slower (2.97 µm/s) than for S IBU or R IBU (10.04 µm/s and 9.40 µm/s respectively). The reason for the slower spherulite growth rates for R,S IBU compared to single enantiomer IBU at 30 °C probably stems from different crystallisation rate-temperature relationships. This is evidenced by the different temperatures of crystallisation onset for S IBU (33.87 °C) and R, S IBU (37.40 °C) (Table 3.1)

In the presence of 5% (w/w) HPMC, the radial growth rate of all IBU spherulites was reduced. The magnitude of this reduction for S IBU was much higher than for R IBU. The S IBU spherulite growth rate in the presence of 5% w/w HPMC was statistically significantly lower than for R IBU spherulites

in the presence of 5% w/w HPMC (p=0.005). This provides further evidence of chiral discrimination by a cellulose polymer.

3.2.2.3 Effect of manufacturing method on chiral recognition

When the term chiral recognition is used in the literature, it generally refers to situations where at least one of the interacting molecules is in solution, as is the case in stereospecific pharmacological effects and chiral chromatography [210]. Solubilisation allows the chiral molecule a greater degree of rotational freedom and a greater chance to interact with a chiral stationary phase for example, than if it were present in the solid state.

The screening study carried out in Section 3.2.2.1 used cryo-milling to screen a series of cellulose-ibuprofen systems for chiral recognition. Production of an ASD via milling requires mechanical destruction of the crystalline API's lattice before the API and polymer can be mixed at a molecular level to allow for ASD generation [126]. Production of an ASD from a solution however, allows for molecules to interact and form stabilising interactions prior to ASD formation. In order to examine the effect that the route of amorphisation has on the ability of potentially discriminating systems to interact, a system which showed some degree of chiral recognition from the screening study (ibuprofen: HPMC 50:50 w/w), was also produced via spray drying as outlined in Chapter 2 Section 2.2.1.1.1.

3.2.2.3.1 Thermal analysis

Representative DSC scans (showing the total heat flow) for the spray dried ibuprofen HPMC systems, along with their cryo-milled and physical mixture counterparts are shown in Figure 3.27. In Figure 3.28, the glass transition of the spray dried systems is shown in the reversing heat flow signal, while the absence of a glass transition is shown for the equivalent cryo-milled sample.

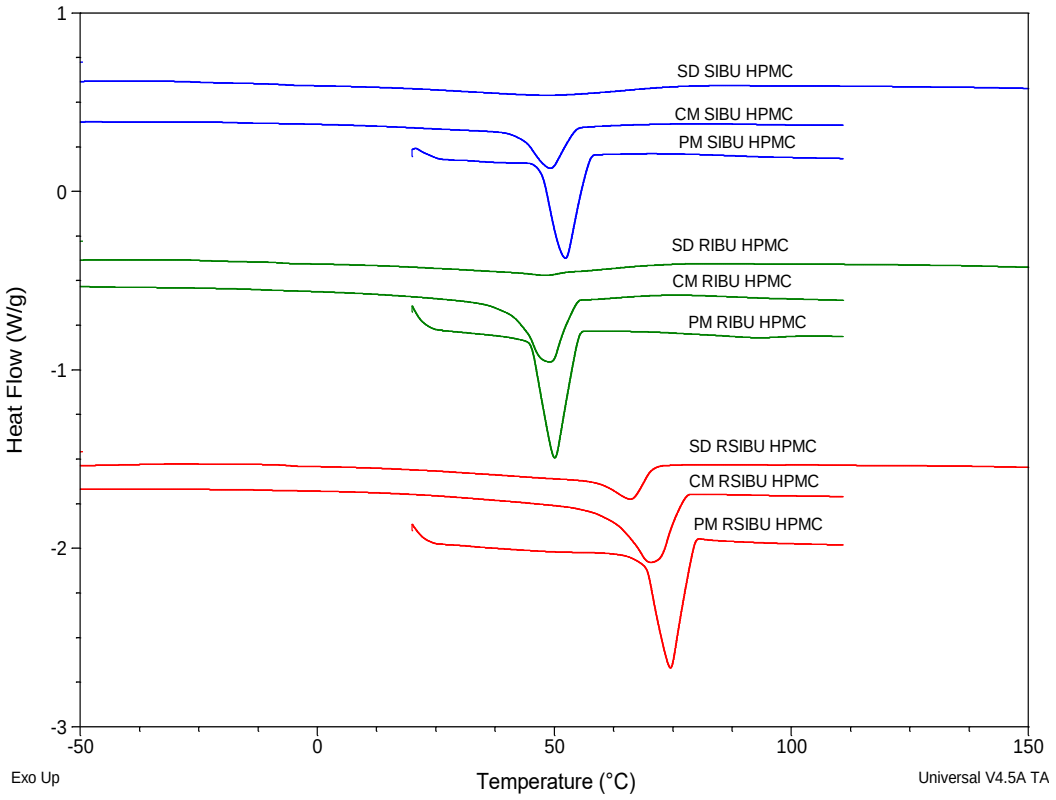

Figure 3.27: Total heat flow DSC scans of ibuprofen-HPMC 50:50 w/w systems. SD=spray dried CM=cryo-milled PM=physical mixture

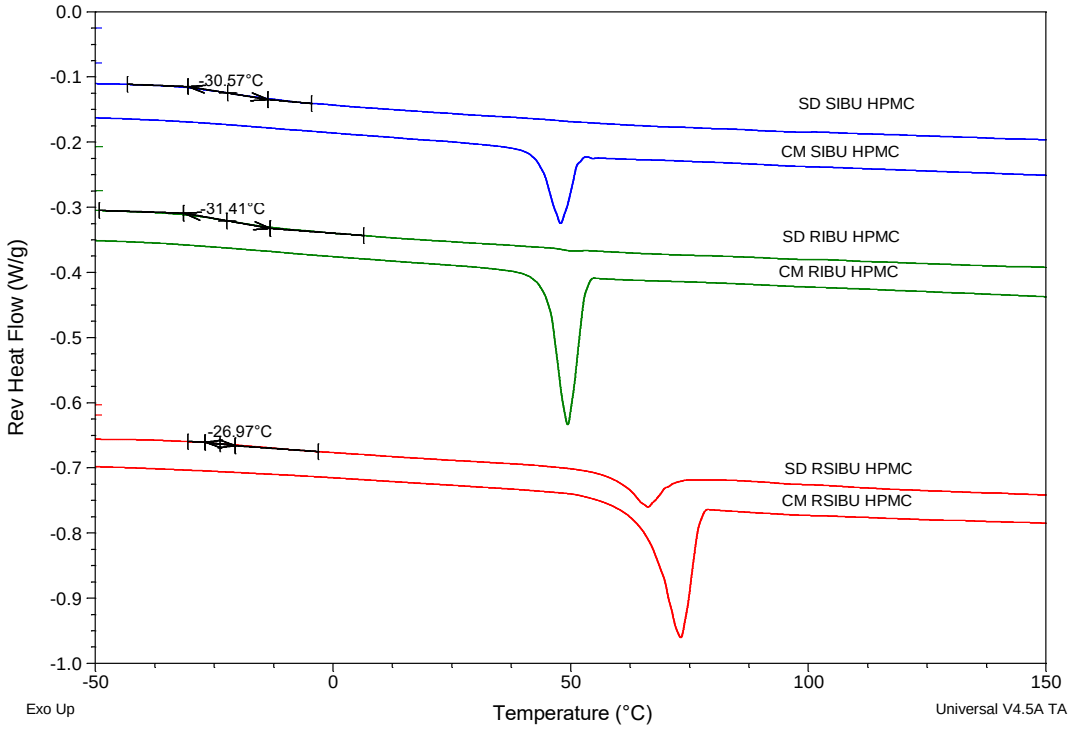

Figure 3.28: Reversing heat flow DSC scans of ibuprofen-HPMC 50:50 w/w systems. SD=spray dried CM=cryo-milled PM=physical mixture

From Figure 3.27 it is apparent that the spray dried systems have less crystalline ibuprofen material present as evidenced by the absence of a melting endotherm (as is the case with SD S IBU HPMC and SD R IBU HPMC samples graphed) or a much smaller melting endotherm than the equivalent cryo-milled melting endotherm (as is the case in SD R,S IBU HPMC). All three replicates of the SD RS IBU HPMC showed a melting endotherm, while two of three replicates of the SD R IBU HPMC show a melting endotherm and only one in three of the SD S IBU HPMC exhibited a melting endotherm. The onset melting temperature of these endotherms and the specific heat of fusion associated with them are compared to the equivalent cryo-milled samples in Figure 3.29. The extent of melting point depression for the spray dried systems is similar to the cryo-milled systems for both R,S IBU-HPMC and R IBU-HPMC but is markedly different for the S IBU-HPMC system as shown in Figure 3.29 (a). However as only one of the three spray dried S IBU HPMC samples showed an endotherm corresponding to the melt endotherm of crystalline ibuprofen, the Tm value for SD S IBU HPMC is based on one sample, but is an interesting observation nonetheless. Regarding the amount of crystalline ibuprofen present in the spray dried samples, all spray dried samples contained less crystalline ibuprofen than their equivalent cryo-milled sample. While a difference in the amount of crystalline ibuprofen between S IBU HPMC and R IBU HPMC is apparent for the cryo-milled samples, the same is not true for the spray dried samples, with both showing negligible crystalline ibuprofen. This shows that while spray drying led to a greater amount of ibuprofen amorphisation than cryo-milling, it also resulted in an attenuation of the stereoselective facilitation of amorphisation effect.

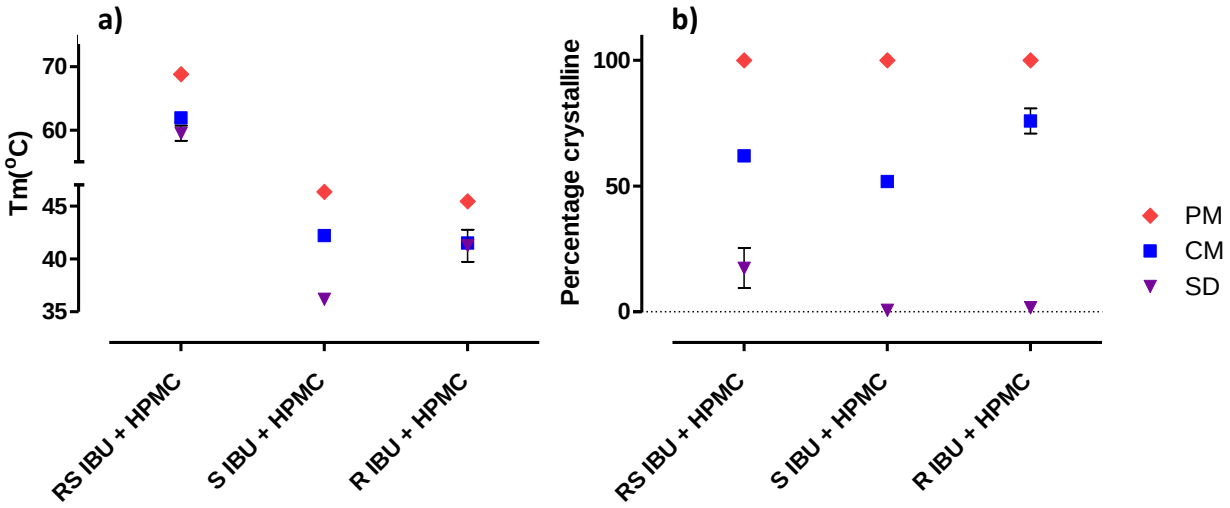

Figure 3.29: a) Onset melting temperature b) Percentage crystalline ibuprofen for ibuprofen-HPMC 50:50 w/w systems. PM= physical mixtures CM=cryo-milled SD=spray dried

In Figure 3.28, the reversing heat flow signal shows the glass transition temperature of the spray dried ibuprofen-HPMC samples. No glass transition temperature is discernible for the cryo-milled samples. The glass transition temperature onset, midpoint and offset values for the spray dried systems are shown in Figure 3.30.

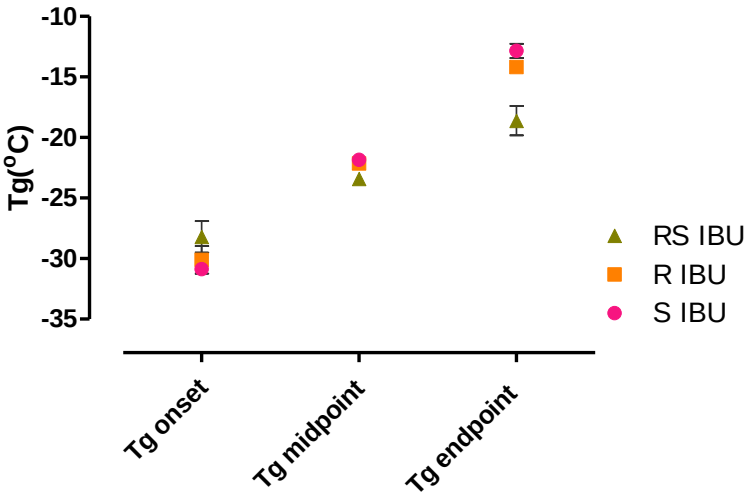

Figure 3.30: Glass transition onset, midpoint and offset values for spray dried IBU HPMC 50:50 w/w samples.

The glass transition onset temperature and midpoint temperature are similar for all three spray dried ibuprofen-HPMC samples, while the glass transition offset temperature is lower for R,S IBU-HPMC than the S IBU-HPMC or R IBU-HPMC. The specific heat capacity associated with the glass transition temperature for spray dried R,S IBU HPMC was 0.137 ± 0.101 J/g °C, while for spray dried S IBU HPMC and R IBU HPMC it was 0.274 ± 0.029 J/g °C and 0.266 ± 0.042 J/g °C respectively. The lower specific heat capacity associated with the glass transition of the R,S IBU HPMC system implies lower amorphous ibuprofen content [211], which is a logical observation as the R,S IBU HPMC sample showed higher crystalline ibuprofen content compared to the single enantiomer IBU-HPMC samples (Figure 3.29 b).

3.2.2.3.2 pXRD analysis

The powder X-ray diffraction patterns of the spray dried IBU-HPMC samples compared to the cryo-milled and physical mixture sample equivalent samples are shown in Figure 3.31 below.

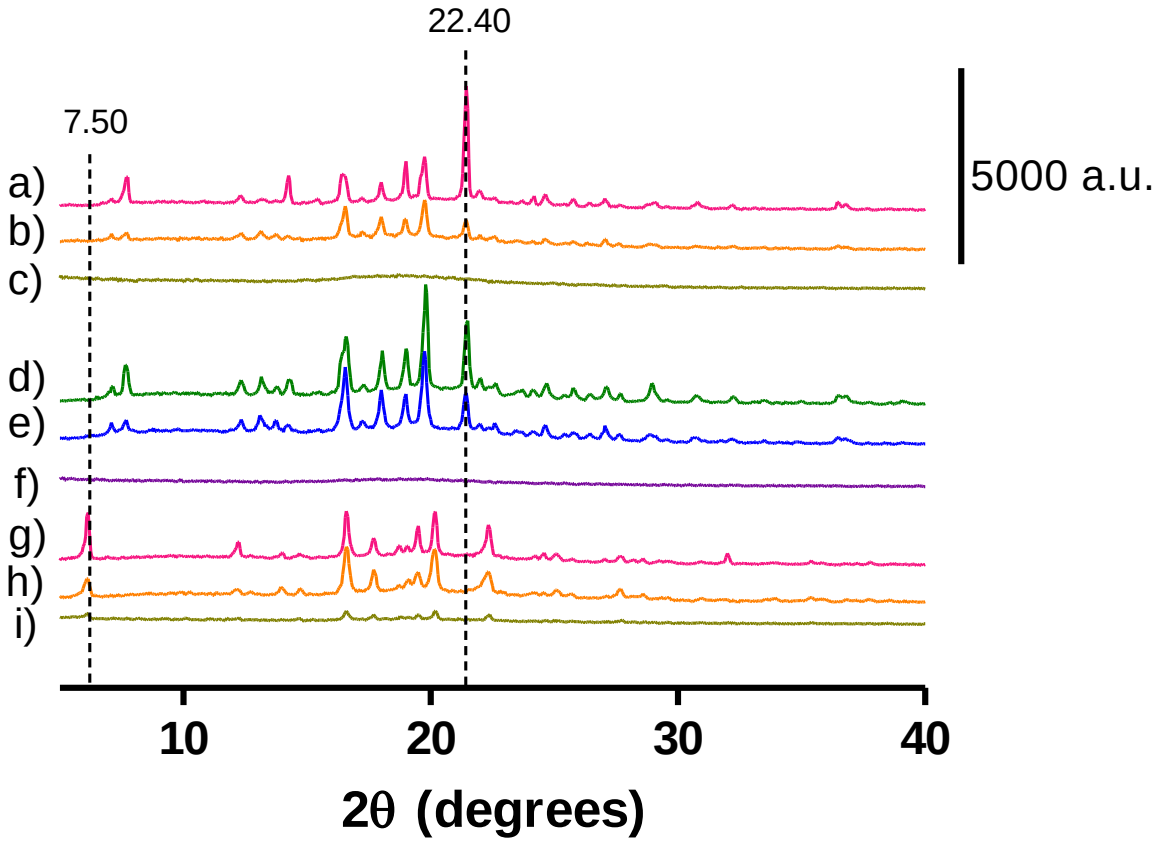

Figure 3.31: pXRD pattern of spray dried, cryo-milled and physical mixtures of ibuprofen and HPMC in a 50:50 w/w ratio. a) PM S IBU HPMC b) CM S IBU HPMC c) SD S IBU HPMC d) PM R IBU HPMC e) CM R IBU HPMC f) SD R IBU HPMC g) PM R,S IBU HPMC h) CM R,S IBU HPMC i) SD R,S IBU HPMC

The spray dried R IBU HPMC and S IBU HPMC samples are devoid of Bragg peaks, while in the equivalent R,S IBU HPMC sample some small Bragg peaks are visible, although they are diminished relative to the equivalent cryo-milled sample, which agrees with the thermal analysis shown in Section 3.2.2.3.1.

3.2.2.3.3 ATR-FTIR analysis

The normalised aborbance of the spray dried IBU HPMC samples are graphed in Figure 3.32, along with their equivalent cryo-milled samples. The intensity of the absorbance for each system in the carbonyl and OH region is listed in Table 3.16. There are clear differences in the carbonyl region of samples prepared via spray drying compared to those prepared via cryo-milling. The intensity of the shoulder of the carbonyl peak relative to the intensity of the main peak is higher in the spray dried samples compared to the cryo-milled samples. There is also a difference in the shoulder-to-peak intensity of the carbonyl region for spray dried S IBU HPMC and sray dried R IBU HPMC. This ratio is 0.469 for spray dried S IBU HPMC and 0.913 for R IBU HPMC. This means that monomeric ibuprofen is relatively more abundant in the spray dried R IBU HPMC sample than in the spray dried S IBU HPMC. This is in contrast to the cryo-milled sample where there the shoulder-to-peak ratios were more similar (0.442 and 0.463 for S IBU HPMC and R IBU HPMC respectively).

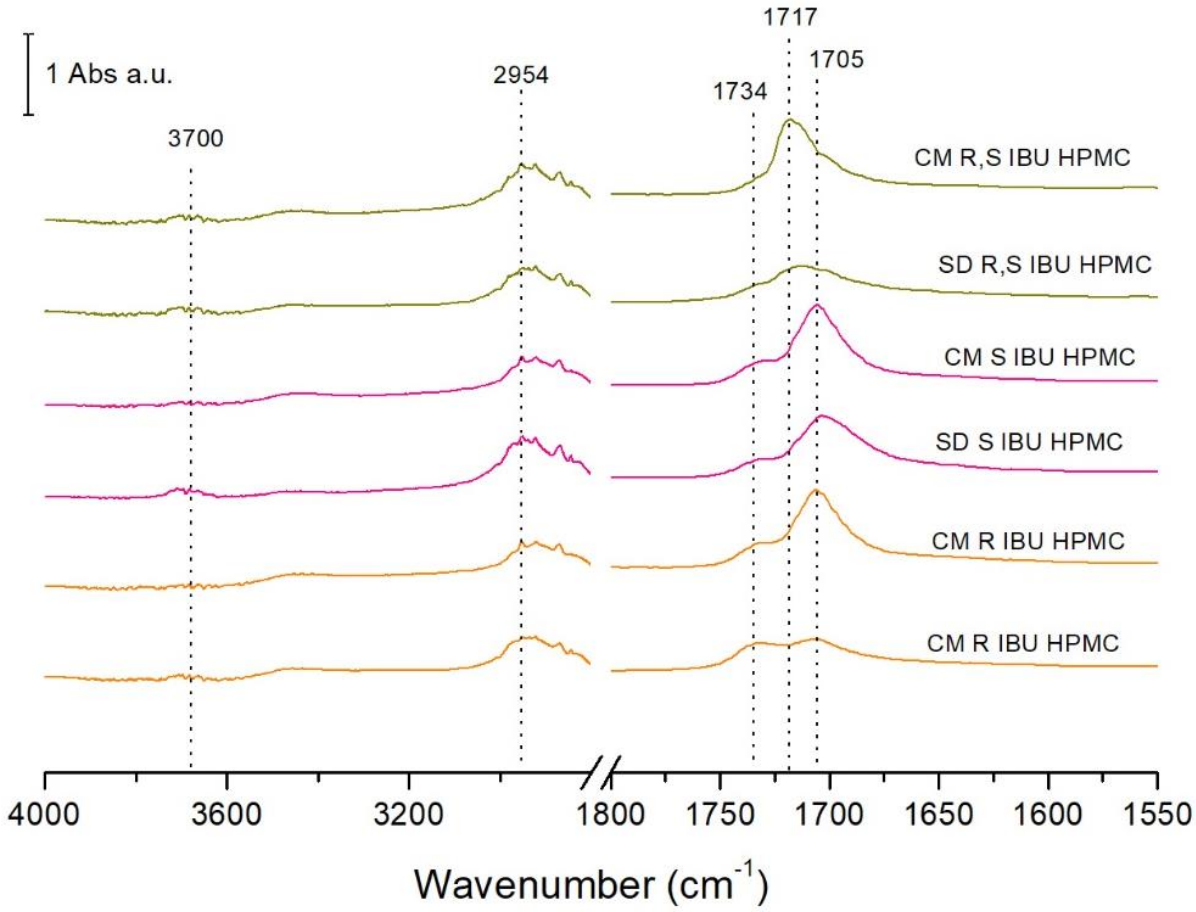

Figure 3.32: ATR-FTIR spectra of spray dried (SD) and cryo-milled samples (CM) of HPMC and ibuprofen in a 50:50 w/w ratio

Table 3.16: Normalised absorbance from ATR-FTIR spectra of cryo-milled (CM) and spray dried (SD) ibuprofen-HPMC samples at a 50:50 w/w ratio. (P) refers to a main peak while (S) refers to a shoulder.(S)/(P) refers to the ratio of the shoulder absorbance to main peak absorbance

Polymer	Wavenumber (cm^{-1})	R,S	S	R	S/R
CM	1717 (P)	0.578			
	1734 (S)		0.248	0.252	0.984
	1705 (P)		0.561	0.544	1.031
	(S)/(P)		0.442	0.463	0.954
	3700	0.050	0.027	0.026	1.038
	2954	0.336	0.279	0.263	1.060
SD	1717 (P)	0.268			
	1734 (S)	0.176	0.212	0.209	1.014
	1705 (P)		0.452	0.229	1.973
	(S)/(P)	0.657	0.469	0.913	0.514
	3700	0.047	0.049	0.032	1.531
	2954	0.265	0.342	0.238	1.437

3.2.2.4 Effect of ibuprofen loading and a racemic switch on spray dried IBU-HPMC stability and performance

As spray drying allowed a greater degree of IBU amorphisation than cryo-milling as outlined in Section 3.2.2.3, it was decided to use this route of amorphisation to probe the impact that the IBU:HPMC ratio had on amorphous stability. For this purpose, different weight ratios of R,S IBU or S IBU and HPMC were spray dried as outlined in Chapter 2 Section 2.2.1.1.1. R IBU was not studied in this section of the analysis as it is not used clinically [212], and the focus of this section was to examine the effect that a racemic switch may have on an ASD's performance.

3.2.2.4.1 pXRD analysis

The powder X-ray diffraction patterns of R,S IBU-HPMC and S IBU-HPMC at varying w/w compositions immediately after production are shown in Figure 3.33 below.

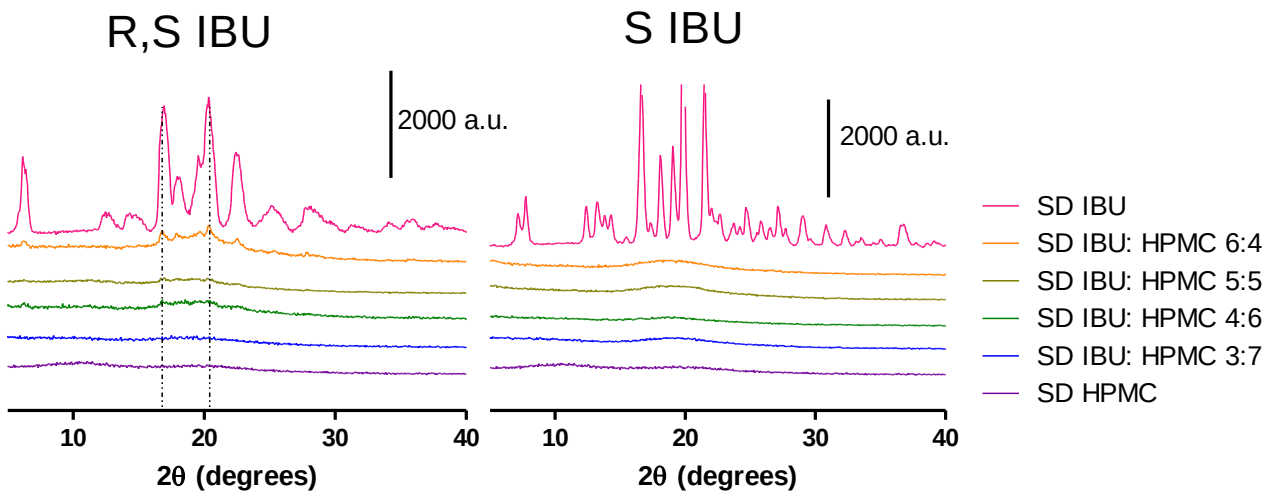

Figure 3.33: pXRD patterns of spray dried IBU and HPMC at various weight ratios

Interestingly, the spray dried S IBU-HPMC systems were completely X-ray amorphous at all ibuprofen loadings studied (30%, 40% 50% and 60% w/w). In contrast the spray dried R,S IBU-HPMC was completely X-ray amorphous for a 30% w/w ibuprofen loading, but Bragg peaks, of low intensity, were visible in the pXRD patterns for systems containing 40%, 50% and 60% R,S IBU w/w. The amorphous stability of the S IBU-HPMC 60% w/w IBU was noted to be poor, as Bragg peaks were observed to appear after just 24 hours of storage at 30 °C, as shown in Figure 3.34 below.

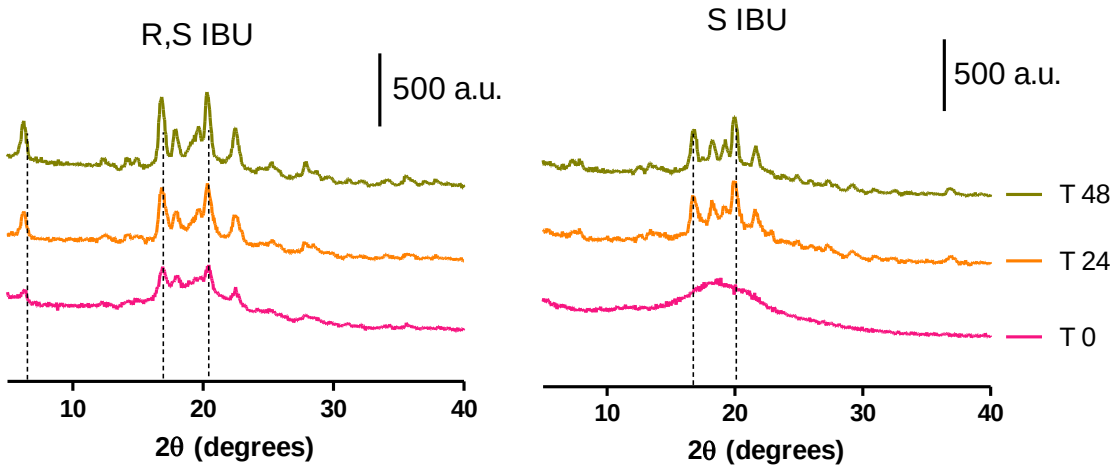

Figure 3.34 pXRD patterns of spray dried R,S IBU-HPMC and S IBU-HPMC with 60% w/w IBU immediately after production (T 0), after 24 hours (T 24) and after 48 hours (T 48).

This demonstrates that the S IBU-HPMC 60% w/w IBU system is metastable in the amorphous state, and the amorphous S IBU crystallises quite rapidly from the matrix. With the time sensitivity of the spray dried material in mind, all experiments were conducted with time matched samples i.e. SD R,S IBU-HPMC and SD S IBU-HPMC samples which were prepared within hours of each other.

3.2.2.4.2 Thermal Analysis

3.2.2.4.2.1 Glass transition temperature and specific heat capacity

The thermal properties of the raw materials (R,S IBU, S IBU and HPMC) as well as the spray dried IBU-HPMC systems as measured by reversing heat flow signal using mDSC as described in Chapter 2 Section 2.2.3.4.1 are shown in Figures 3.35 and 3.36.

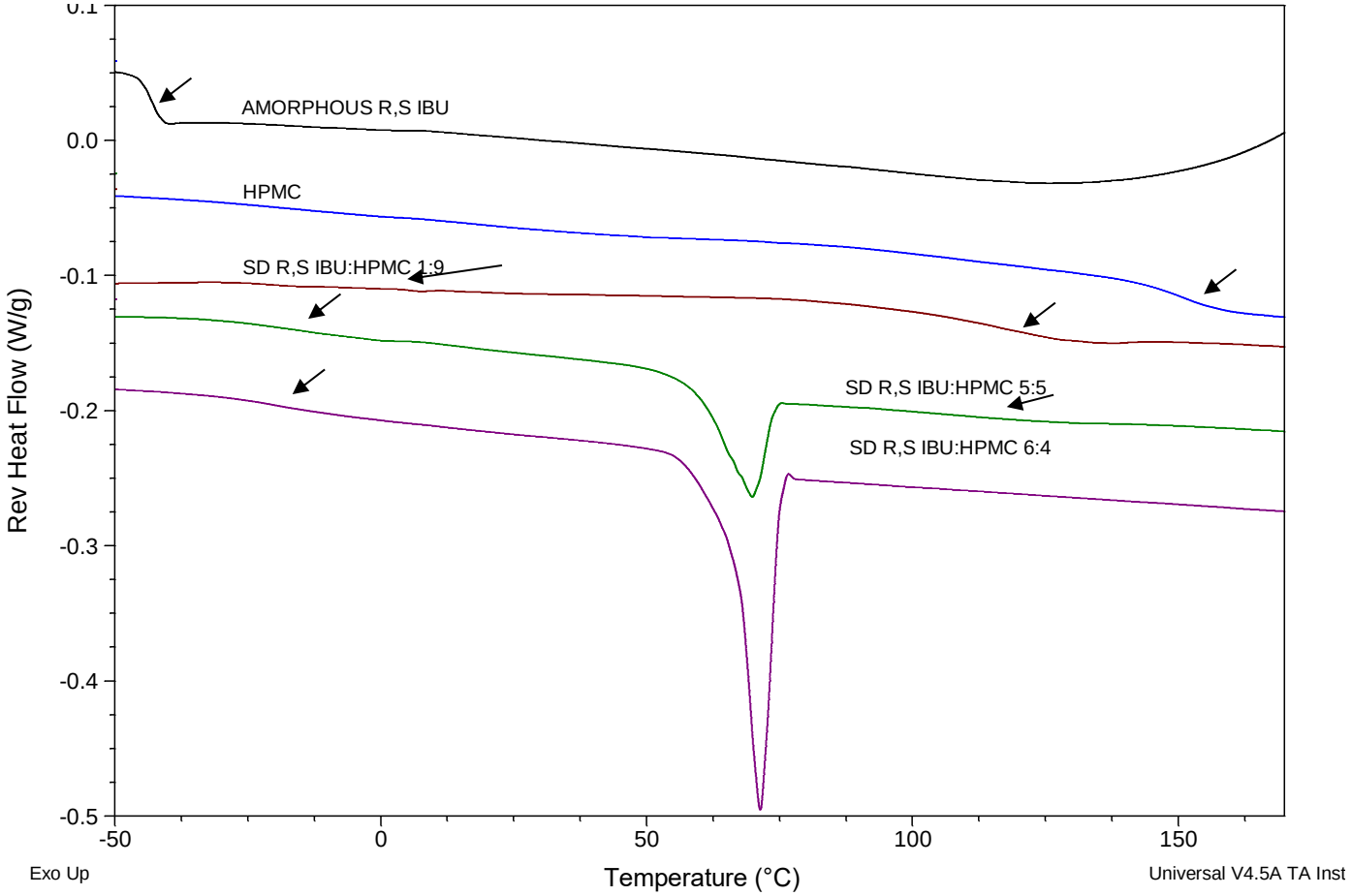

Figure 3.35: Reversing heat flow scans of R,S IBU, HPMC and spray dried R,S IBU-HPMC systems. Glass transitions are highlighted with an arrow

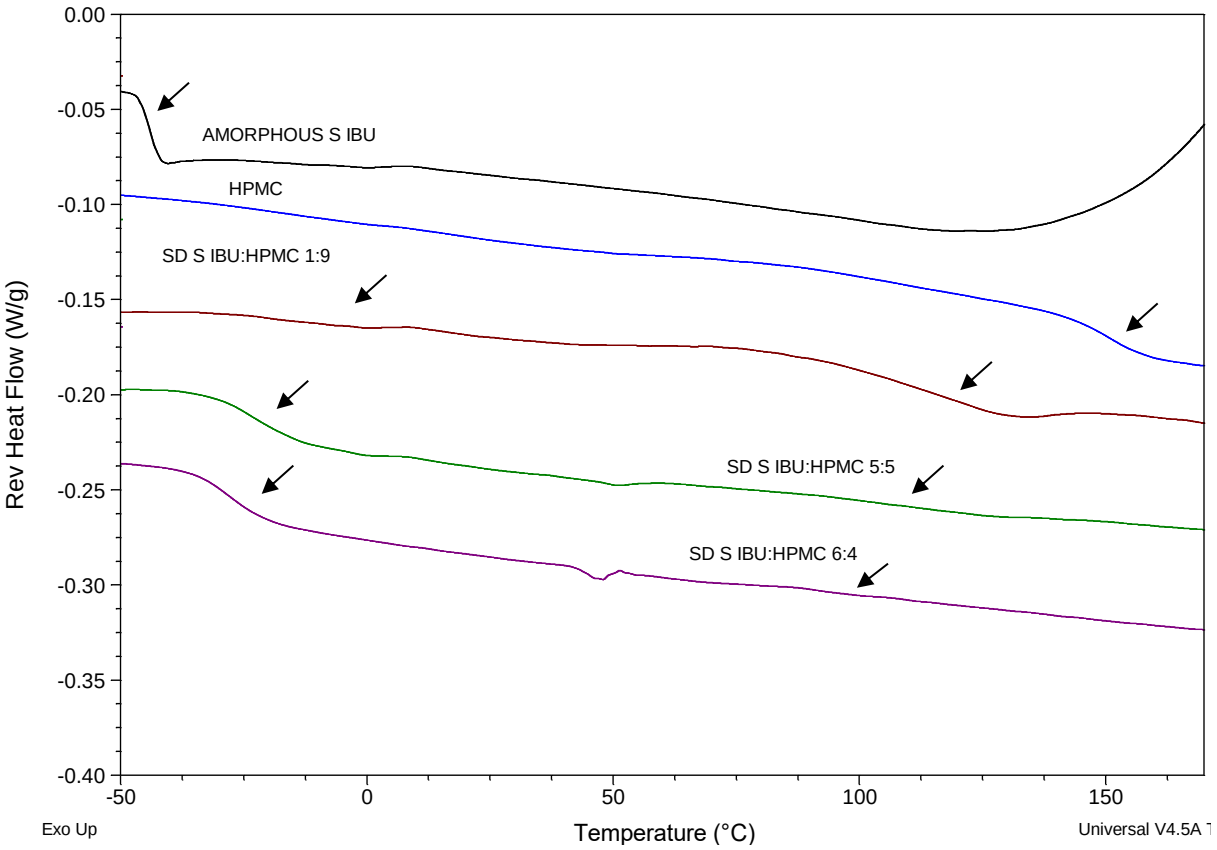

Figure 3.36: Reversing heat flow scans of S IBU, HPMC and spray dried R,S IBU-HPMC systems. Glass transitions are highlighted with an arrow.

Amorphous R,S IBU and S IBU show a single glass transition with an onset temperature of -45.63 ± 0.48 °C and -45.96 ± 0.45 °C, respectively, as well as the absence of any endothermic melting peaks. Both R,S IBU and S IBU begin to degrade at approximately 120 °C. This explains the exothermic event which begins in both of their mDSC traces at around this temperature. The glass transition temperature of HPMC is apparent at 142.46 ± 0.45 °C.

The spray dried IBU: HPMC systems with 10% ibuprofen w/w, show two distinct glass transitions, with glass transitions at approximately -24°C and 100°C for drug-rich and polymer-rich zones, respectively. The spray dried R,S IBU-HPMC 60% w/w system contains only one detectable glass transition in the amorphous HPMC rich region while the equivalent S IBU system contains two detectable glass transitions. The presence of two distinct glass transitions signifies that the system under observation is not molecularly homogenous. This heterogeneity has been previously described for amorphous ibuprofen with the structurally similar polymer, ethyl cellulose [205]. The difference in amorphous homogeneity between the R,S IBU HPMC systems and the S IBU HPMC systems may not be related to a true difference in molecular mixing but rather a difference in the crystalline ibuprofen content of the samples. As the S IBU HPMC samples have higher amorphous IBU content, both amorphous regions are apparent. As the R,S IBU HPMC system with an ibuprofen content of 60% w/w has lower amorphous ibuprofen content, only one glass transition temperature

is apparent. The glass transition onset temperature, inflection temperature, offset temperature, width and specific heat capacity for these spray dried binary systems were determined for both the ibuprofen rich region and the HPMC rich region and are presented in Table 3.17 and Figures 3.37.

Table 3.17 Ibuprofen-rich and HPMC-rich glass transition parameters for spray dried R,S IBU and S IBU HPMC composites. Results are the average of three values. Standard deviation in parentheses

Ibuprofen-rich glass transition parameters										
IBU % (w/w)	Tg onset (°C)		Tg mid (°C)		Tg offset (°C)		Tg width (°C)		ΔCp (J/g.°C)	
	R,S	S	R,S	S	R,S	S	R,S	S	R,S	S
10	-23.89 (0.80)	-22.45 (0.73)	-20.35 (0.24)	-15.87 (4.07)	-13.40 (6.37)	-7.02 (2.06)	10.49 (6.96)	15.43 (2.50)	0.02 (0.01)	0.03 (0.02)
50	-23.96 (1.83)	-30.52 (0.79)	-14.48 (0.42)	-24.20 (0.21)	-6.07 (4.67)	-14.55 (1.73)	17.89 (6.40)	15.97 (1.69)	0.16 (0.01)	0.35 (0.04)
60	-27.19 (0.22)	34.17 (0.25)	19.69 (0.47)	-27.86 (0.01)	-12.39 (0.55)	-21.91 (0.43)	14.80 (0.33)	12.26 (0.68)	0.13 (0.02)	0.35 (0.02)
100	-45.63 (0.45)	-45.97 (0.45)	-43.35 (0.55)	-43.53 (0.29)	-41.26 (0.63)	-41.82 (0.67)	4.37 (0.45)	4.15 (0.61)	0.39 (0.03)	0.41 (0.01)
HPMC-rich glass transition parameters										
IBU % (w/w)	Tg onset (°C)		Tg inflection (°C)		Tg offset (°C)		Tg width (°C)		ΔCp(J/g.°C)	
	R,S	S	R,S	S	R,S	S	R,S	S	R,S	S
0	142.46 (0.45)		151.18 (0.20)		157.14 (1.79)		14.68 (1.35)		0.246 (0.06)	
10	97.29 (6.01)	92.55 (1.29)	118.03 (1.73)	109.47 (6.53)	131.55 (1.25)	128.45 (1.84)	32.26 (7.14)	35.91 (1.10)	0.26 (0.11)	0.39 (0.02)
50	98.68 (4.05)	87.81 (0.61)	104.59 (3.91)	101.71 (3.45)	117.15 (7.81)	113.21 (2.14)	18.48 (11.85)	25.39 (2.12)	0.096 (0.04)	0.14 (0.02)
60	n/a	*92.36 (6.72)	n/a	*95.52 (4.67)	n/a	*102.6 (8.14)	n/a	*10.29 (1.42)	n/a	*0.02 (0.01)

* Analysis in duplicate

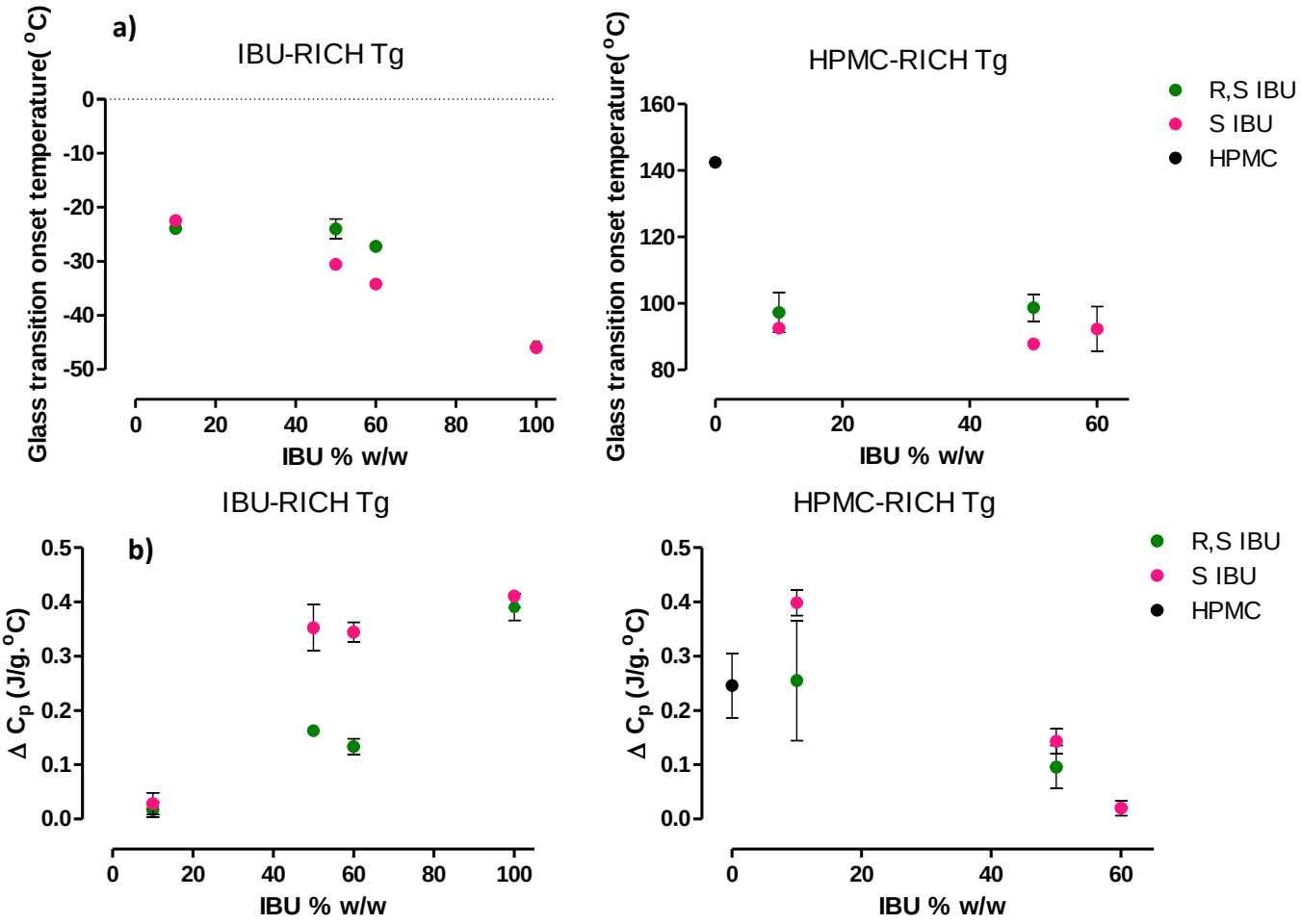

Figure 3.37: a) Glass transition onset temperatures and b) specific heat capacity change at the glass transition for IBU-rich and HPMC-rich glass transition for R,S IBU and S IBU HPMC systems

As seen in Figure 3.37 the glass transition onset and the change in specific heat capacity for R,S IBU and S IBU are identical. Spray dried IBU-HPMC systems with an IBU loading > 50% w/w showed differences in the glass transition onset temperature and change in specific heat capacity at the glass transition for both IBU-rich amorphous regions and HPMC-amorphous regions.

The IBU-rich glass transition onset temperature of spray dried R,S IBU: HPMC 50:50 w/w was -23.96 ± 1.83 °C, while the equivalent S IBU composition had a value of -30.52 ± 0.79 °C. Similarly, the IBU-rich glass transition onset temperature of spray dried R,S IBU: HPMC 60:40 w/w was -27.19 ± 0.22 °C, while the equivalent S IBU value was -34.17 ± 0.25°C. It is interesting to note that the R,S IBU HPMC systems have IBU-rich glass transition temperatures approximately 7 °C higher than S IBU at both 50% and 60% w/w IBU content. Systems with higher glass transition temperatures are generally considered to be more stable in the amorphous state as at any given temperature they exhibit lower molecular mobility and hence a reduced crystallisation tendency [213]. In this study, however the S IBU HPMC spray dried systems have higher amorphous content than their R,S IBU counterparts as evidenced by pXRD diffractograms and DSC scans. This may be explained by considering that the ambient conditions under which these samples were stored exceeded the IBU-

rich glass transition region by approximately 50 °C, meaning that the IBU-rich clusters in the spray dried powder were in the super-cooled liquid state. As shown in Section 3.2.2.2.3, S IBU's crystallisation rate from the super-cooled liquid state was significantly more retarded than that of R,S IBU's in the presence of only 5% w/w HPMC, however the absolute growth rate of S IBU spherulites remained higher than for R,S IBU at 30 °C. Measuring spherulite growth rate at polymer concentrations >20% w/w was not feasible, but it is clear that increasing polymer concentration reduces growth rate (Figure 3.24).

It can be deduced from the spray dried systems that when IBU content increased to 50 % w/w the chiral discrimination effect of the polymer on crystalline growth dominated over the inherent growth rates of the R,S IBU and S IBU resulting in a larger amount of crystalline IBU in the R,S IBU systems. As there is more crystalline IBU material in the spray dried R,S IBU: HPMC samples, there is less super-cooled ibuprofen in the IBU-rich glass transition region for the R,S IBU sample compared to the S IBU sample meaning that the R,S IBU samples have a higher glass transition temperature, in accordance with the Gordon-Taylor equation.

The HPMC-rich glass transition region of all IBU-HPMC systems have glass transition onset temperatures lower than that of pure HPMC, indicating that there is a mixture of amorphous ibuprofen and HPMC present in this region.

The width of the IBU-rich glass transition of spray dried R,S IBU: HPMC 50:50 w/w spanned 17.89 ± 6.40 °C, while the width of the equivalent S IBU glass transition spanned 15.97 ± 1.67 °C. When IBU content increased to 60% w/w, the glass transition width reduced to 14.80 ± 0.32 °C and 12.26 ± 0.67 °C for the spray dried R,S IBU and S IBU HPMC systems respectively. This observation is interesting as glass transition "broadness" is inversely associated with the degree of drug-polymer mixing and local homogeneity [128,214] as well as the strength of the intermolecular interactions at play in the system [215]. The R,S IBU-HPMC spray dried systems have a wider IBU-rich glass transition region (approximately 3 °C) than the equivalent S IBU-HPMC systems. This may indicate that the IBU-rich glass transitions of the R,S IBU-HPMC systems are more heterogenous than the S IBU-HPMC systems. This may be explained by consideration that the R,S IBU-HPMC systems can be considered as a tri-component system (HPMC, S IBU and R IBU molecules) while the S IBU-HPMC systems are binary systems. The IBU-rich glass transition region width decreases when the ibuprofen content increases from 50% to 60% w/w for both R,S IBU and S IBU HPMC systems (by approximately 2 °C in both cases). This reduction in amorphous heterogeneity in the drug rich glass transition region may be explained by considering that in both of the 60% w/w samples there is an increased quantity of crystalline IBU relative to the 50% w/w IBU systems. As there is more crystalline IBU, logically there is less amorphous IBU in the IBU-rich glass transition region, reducing the amorphous phase heterogeneity.

The width of the glass transition temperature for pure HPMC spanned 14.68 ± 1.35 °C. With the addition of 10% w/w ibuprofen, the polymer rich glass transition region width increased to 34.26 °C ± 7.14 °C for R,S IBU HPMC and 35.91 ± 1.10 °C for S IBU HPMC, indicating an increase in amorphous heterogeneity. The IBU HPMC systems which contained 50 % w/w IBU had narrower glass transition width (18.47 ± 11.85 °C and 25.39 ± 2.12 °C for R,S IBU HPMC and S IBU HPMC respectively). It is interesting to note that in the IBU-rich glass transition region R,S IBU HPMC has a wider glass transition than S IBU while in the HPMC-rich region this observation appears to be reversed, as outlined in Table 3.17, however these values have significant error associated with them.

The change in specific heat capacity (ΔCp) in the IBU-rich glass transition region differed between the R,S IBU-HPMC and S IBU-HPMC systems when the IBU content was > 50% w/w. There is a clear relationship between the magnitude of the change in the heat capacity at the IBU-rich glass transition region and the percentage of ibuprofen in the system. This is logical as it is reported in the literature that larger changes in heat capacity are correlated with increased amorphous content [3,211,216] . When IBU content in the spray dried systems was 10% w/w both R,S IBU-HPMC and S IBU-HPMC were completely amorphous (with the major amorphous component being in the HPMC-rich region) and hence the very small ΔCp in the IBU-rich region is not significantly different between the two formulations. As IBU content increases to 50% and 60% w/w the spray dried S IBU-HPMC systems have a higher ΔCp at the IBU-rich glass transition region relative to their corresponding R,S IBU systems as they have higher levels of amorphous IBU.

The ΔCp values in the HPMC-rich glass transition region differed between the R,S IBU-HPMC and S IBU-HPMC systems even when the ibuprofen content was as low as 10% w/w. The ΔCp of the HPMC-rich glass transition region decreases as IBU loading increases. This is because as IBU loading increases, the IBU-rich region becomes the predominant amorphous zone and the amorphous content of the HPMC-rich region reduces.

3.2.2.4.2.2 Amorphous stability

The IBU-rich glass transition onset temperature, change in specific heat capacity at the glass transition and percentage crystallinity of the spray dried R,S IBU-HPMC 60% IBU w/w system and S IBU-HPMC 60% IBU w/w system stored at 20 °C are presented in Figure 3.38.

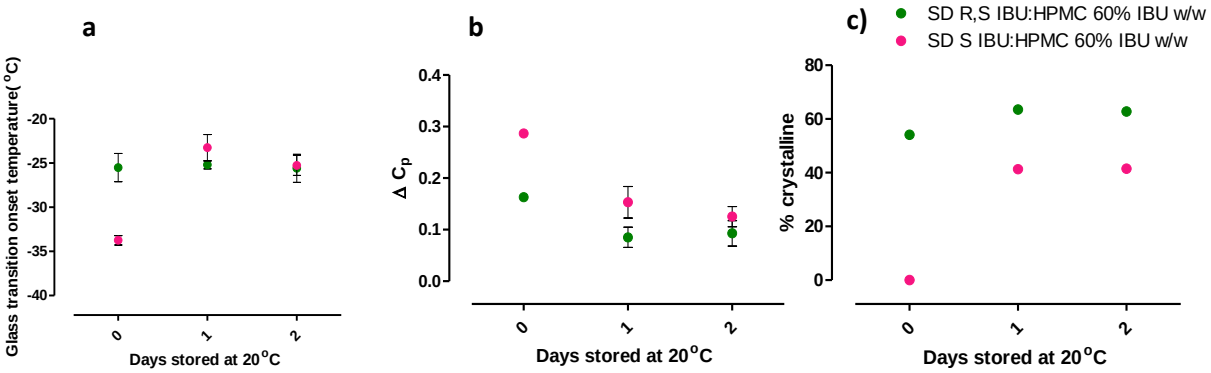

Figure 3.38: a) Glass transition onset temperature b) Change in specific heat capacity c) percentage of IBU which is crystalline in spray dried IBU HPMC 60% IBU w/w stored at 20 °C

As seen in Figure 3.38 a) the initial difference in the IBU-rich glass transition onset temperatures of the spray dried R,S IBU and the S IBU HPMC is negated after only 2 days of storage at 20 °C.

As seen in Figure 3.38 b), the ΔCp of both systems reduce after 2 days which can be attributed to time dependent crystallisation of ibuprofen. The ΔCp of the S IBU system is higher than the equivalent R,S IBU system, indicating higher amorphous content, but the magnitude of the difference in ΔCp between the systems reduces over two days.

As seen in Figure 3.38 c) there is a higher amount of crystalline ibuprofen in the spray dried R,S IBU than in the S IBU HPMC system. Although S IBU HPMC crystallises within a day, the amount of crystalline ibuprofen in the S IBU HPMC system remains lower at all time points studied than the equivalent R,S IBU HPMC system. This study was continued up to 34 days and at this time point, R,S IBU HPMC was determined to contain 67.89 ± 1.61 % of its total IBU content in the crystalline form, while S IBU HPMC contained 56.81 ± 0.39 % of its total IBU content in the crystalline form.

3.2.2.4.3 Dissolution testing

The in-vitro dissolution performance of spray dried IBU: HPMC 60% w/w IBU was determined as described in Chapter 2 Section 2.2.3.1. A difference factor (f_1) and similarity factor (f_2) analysis was performed on these profiles using DDSolver. Results are shown in Figure 3.39.

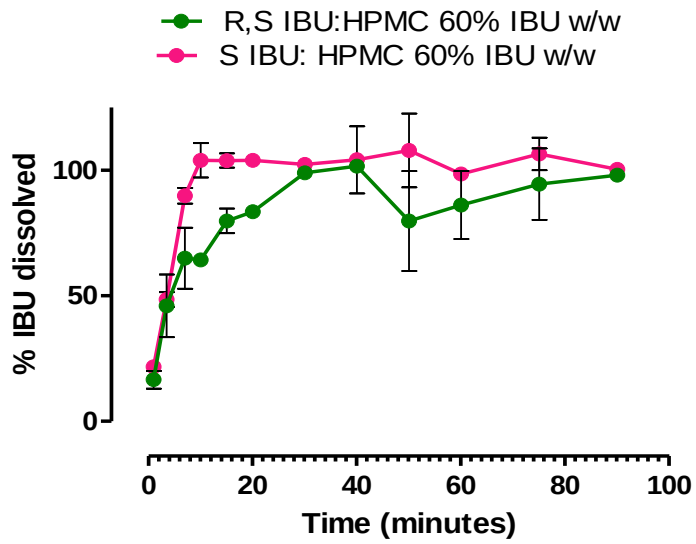

Figure 3.39: Dissolution rate profile of spray dried IBU HPMC systems

As can be seen in Figure 3.39 the mean time to complete dissolution for R,S IBU HPMC is 30 minutes, while for S IBU HPMC is only 5 minutes. The difference factor was 19.64 and the similarity factor was 36.01. An f_1 value less than 15 indicates that the difference between two dissolution profiles is not significant while a similarity result above 50 means that the profiles are considered similar [217,218]. This difference in dissolution performance can be accounted for by considering that the two samples contained different ratios of crystalline to amorphous ibuprofen. The more amorphous sample (S IBU HPMC) demonstrated a faster dissolution profile, as would be anticipated [74].

3.3 Conclusions

This work has demonstrated that a variety of easily calculated glass forming ability and glass stability parameters are of limited utility in determining whether R,S IBU or S IBU is more stable in the amorphous state during non-isothermal crystallisation. This is likely because the glass transition temperature is identical in both substances. Non-isothermal crystallisation studies appeared to show that S IBU is more likely to undergo cold crystallisation at slow cooling rates and more likely to crystallise from the supercooled liquid state than R,S IBU. DSC was found to be of limited utility when determining the molecular mobility properties of amorphous IBU, while BDS showed that their molecular mobility is similar. It is likely therefore, that any differences in glass stability or glass forming ability stems from the thermodynamic differences between R,S IBU and S IBU as their kinetic differences are relatively minor.

The ability of cellulose polymers to differentially supress the crystallisation and/or facilitation of amorphisation of different IBU enantiomers appears to be related to the structure of substituent groups on the cellulose ring and is greatly influenced by the route of amorphisation.

This work has demonstrated that racemic switches, particularly of an ASD formulation, should consider the possibility that cellulose based polymers can interact with a chiral API. In this case, a racemic switch from an R,S IBU-HPMC system to an S IBU-HPMC system affected the solid-state properties of the material such as crystalline content, amorphous stability and ultimately dissolution performance.

Chapter 4: The role of polymer choice on ASD performance and stability

4.1 Introduction

The rational choice of a polymer for an ASD is critical to the ASD's physical stability and performance. The dissolution rate, propensity to supersaturate and processability of an ASD are influenced by the choice of polymer. Physicochemical properties of polymers which may be considered during formulation development include; glass transition temperature, aqueous solubility, molecular weight, hygroscopicity and potential for stabilisation via intermolecular interactions between the polymer and the API.

The role of the molecular weight of the polymer in preventing the recrystallisation of an API in an ASD is an important factor to consider. For a given polymer, as the molecular weight increases, the glass transition temperature of the polymer increases. This increase in glass transition temperature of the polymer will likely lead to an increase in the glass transition of the ASD, which may increase the stability of the ASD during storage. This has been borne out in the literature to varying degrees. Increasing PVP molecular weight was shown to reduce nucleation and crystal growth of piroxicam [95], while in a separate study it was shown to have little effect on the ability of amorphous indomethacin to crystallize from an ASD [219]. The molecular weight of the polymer also plays a critical role in the solubility and dissolution rate of the API in an ASD in aqueous media. Selecting a polymer of high molecular weight may retard drug dissolution rate from the ASD due to an increase in the viscosity of the diffusion layer [96]. This may be desirable or not depending on the target drug release profile. In the case of ketoprofen, immediate release ASDs have been formulated through selection of low molecular weight HPC [220]. In the same study the authors found that the lower molecular weight HPC resulted in an ASD which had less elastic recovery and higher plasticity than the equivalent higher molecular weight HPC formulation. This meant that the lower molecular weight HPC formulation was more suitable for processing by direct compression.

While the influence of polymer molecular weight is clearly significant in ASD formulation development, it has been shown to have virtually no effect on the solubility of the API in the polymer [221]. Conversely, the ratio of co-polymer substituents was found to have a significant influence on celecoxib solubility in PVPVA systems [222]. As the proportion of vinyl-pyrrolidone to vinyl-acetate increased, the solubility of indomethacin in the polymer increased. Co-polymer substitution ratio also affects polymer hygroscopicity. The tendency of an ASD to sorb moisture is critical to its propensity to undergo moisture induced phase separation (MIPS) [9], which may precede drug crystallization. The PVPVA co-polymer (which is typically present in commercial ASD preparations as a 6:4 VP:VA ratio) is less hygroscopic than PVP, and has been demonstrated to sorb less moisture than PVP when formulated as an ASD [9]. This is likely due to the complete insolubility of vinyl acetate in water [141]. This means that water is less likely to be sorbed due to repulsive effects.

While the vinyl acetate functional group may be useful in terms of protection of the ASD from moisture during storage, it may limit the dissolution rate of the amorphous drug in aqueous media. The ability to identify the optimal ratio of VP:VA where dissolution rate is high while moisture sorption is low is therefore important.

The prudent choice of a stabilising polymer should also consider the propensity of a polymer to form intermolecular interactions with the API. The formation of intermolecular interactions in an ASD can reduce the molecular mobility of the API and prevent crystallization. This has been borne out experimentally in ASDs composed of amorphous nifedipine and either PVP, HPMCAS or polyacrylic acid (PAA) [10]. Of the three polymers, PVP was found to have the strongest hydrogen bonding with nifedipine which resulted in a 65-fold increase in relaxation time and the highest resistance to nifedipine recrystallizing. In an older study, PVP was found to hydrogen bond to probucol allowing ASD formation, while polyethylene oxide (PEO) and PAA did not, resulting in probucol being present in a polymorphic crystalline state [97]. Interestingly, hydrogen bonding between polymer and drug may be disrupted during the direct compression process leading to phase separation [127], particularly for metastable formulations. Worku et al. described phase separation of the hydrogen bonded naproxen-PVP ASDs upon compression while no such phase separation was observed for equivalent naproxen-PVPVA ASDs where less hydrogen bonding is present [127,128].

Bearing all the above factors in mind, the aim of this chapter is to examine the influence of physicochemical properties of a range of polyvinyl-based polymers on the stability and performance of ketoprofen in ASDs. Polyvinyl alcohol, polyvinyl pyrrolidone (of differing molecular weights), polyvinyl pyrrolidone vinyl acetate in a 7:3 VP:VA ratio and a 3:7 VP:VA ratio, polyvinyl acetate and polyvinyl acetate phthalate were used to probe these effects. The molecular structures of ketoprofen and these polymers are shown in Figure 4.1.

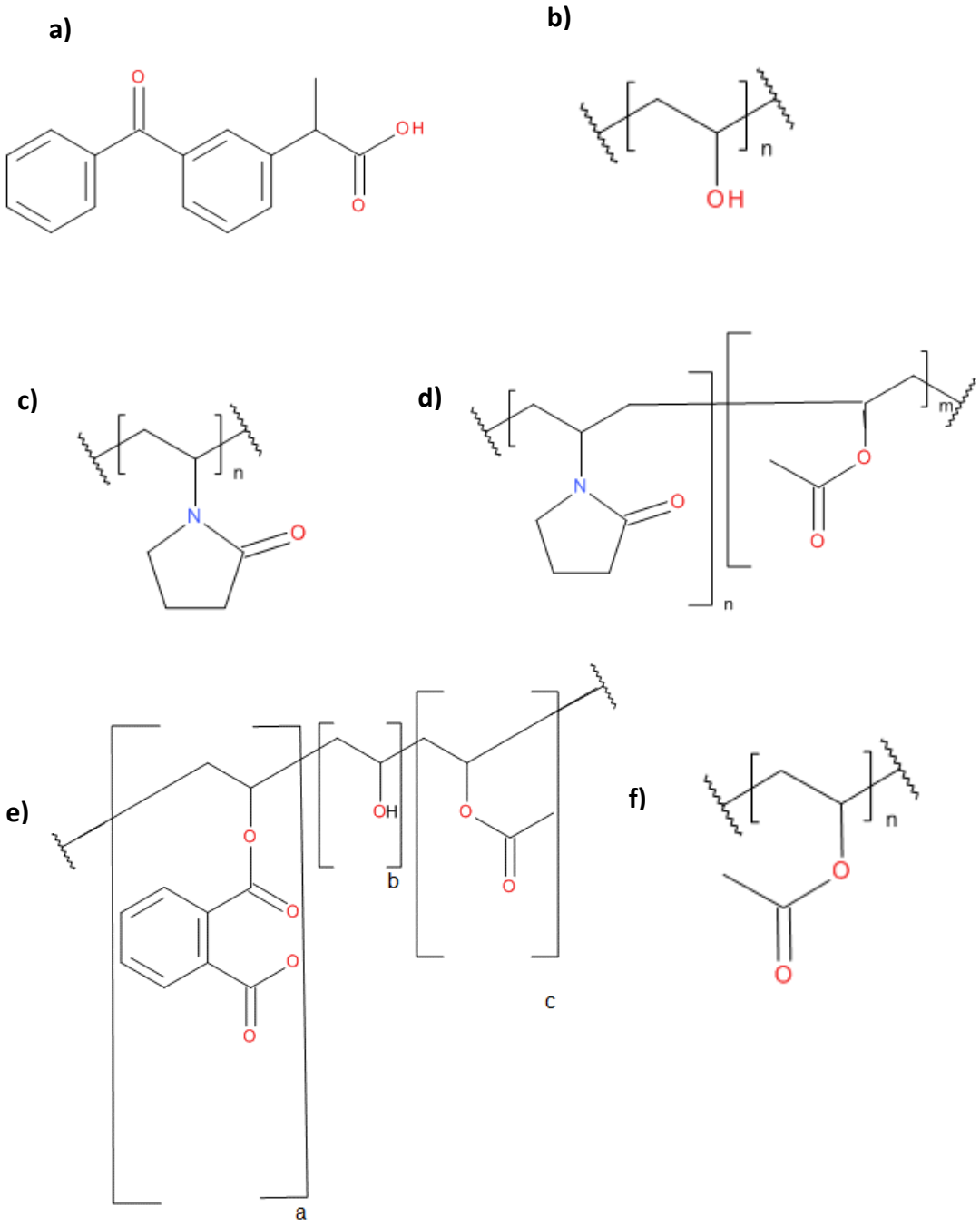

Figure 4.1: Molecular structures of a) ketoprofen b) polyvinyl alcohol c) polyvinyl pyrrolidone d) polyvinyl pyrrolidone vinyl acetate e) polyvinyl acetate phthalate f) polyvinyl acetate

4.2 Results

4.2.1 Characterisation of raw materials

4.2.1.1 Thermal properties

The glass transition onset temperatures for the polymers studied in this chapter determined using mDSC as described in Chapter 2 Section 2.2.3.4.2, are shown in Figure 4.2 and summarised in Table 4.1 along with the glass transition onset temperature of ketoprofen which was melt-quenched *in situ* in the DSC.

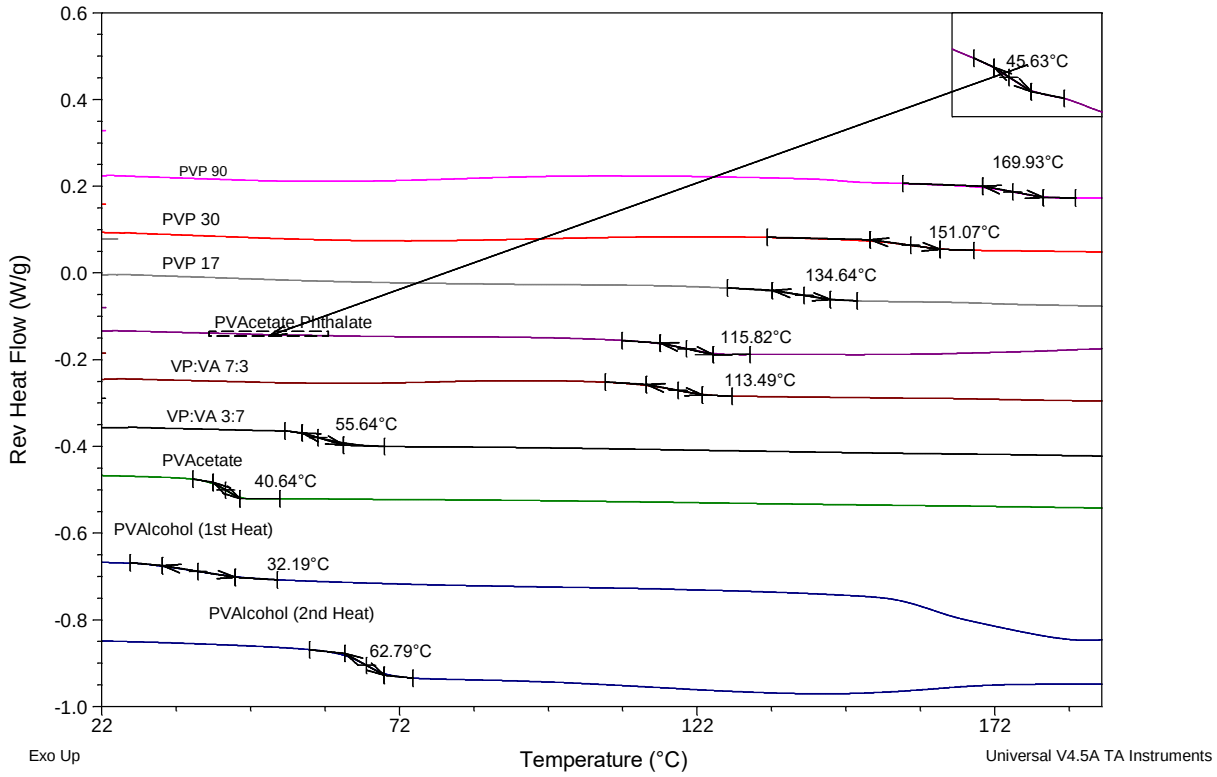

Figure 4.2: mDSC scans showing glass transitions of polymers. Inlay shows first glass transition of PVAP.

Table 4.1: Thermal event values with standard deviation of raw materials.

Polymer	Tg	Tm (onset)
PVP 90	172.0 ± 1.2 °C	
PVP 30	153.6 ± 2.1 °C	
PVP 17	135.6 ± 0.3 °C	
PVPVA 7:3	114.2 ± 1.1 °C	
PVPVA 3:7	57.9 ± 4.3 °C	
PVAcetate	38.6 ± 1.4 °C	
PVAP	46.3 ± 0.7 °C/ 116.0 ± 0.6 °C	
PVAlcohol 1st heating run	41.1 ± 3.9 °C	155.0 ± 0.1 °C
PVAlcohol 2nd heating run	64.5 ± 1.15 °C	
Ketoprofen	-5.9 ± 0.2 °C	92.3 ± 0.4 °C

As seen in Figure 4.2 the polymer with the highest glass transition temperature is PVP90, followed by PVP30 and PVP17. The glass transition temperature increases with increasing molecular weight, as would be expected from the literature [223]. The glass transition temperature also appears to reduce with increasing vinyl acetate substitution. This is logical, as we can see that the glass transition onset temperature of polyvinyl acetate is 38.6 °C, so as the substitution ratio of the vinyl acetate moiety increases, the glass transition temperature of the polymer approaches the glass transition temperature of polyvinyl acetate.

Interestingly polyvinyl acetate phthalate displays two glass transition temperatures. The first smaller glass transition temperature is at 46 °C (shown in inlay), while the second glass transition temperature, which has a larger heat capacity associated with it, is shown at 116 °C. This is interesting as one paper reports only a single Tg for PVAP [224]. Examining this work further, the authors only examined the range between -30°C and 50°C so therefore the higher glass transition would not have been apparent. The higher Tg has been reported by another group [225] and appears to be the predominant Tg. As there is a vinyl acetate moiety in the PVAP structure, this lower Tg may be due to the presence of some polyvinyl acetate impurity.

Polyvinyl alcohol is the only polymer which is partially crystalline, therefore the glass transition was determined for both the partially crystalline and the fully amorphous system. A fully amorphous system was created by heating, cooling and then re-heating the polymer as shown in Figure 4.3. On

the first heating cycle a small endotherm is apparent at 41 °C in the total heat flow axis. This has been attributed by other authors to the glass transition of the amorphous region of semi-crystalline PVAlcohol [226,227]. This glass transition is followed by a broad endotherm associated with the release of bound water with a peak at around 80 °C as well as a broad melting endotherm centred at 192 °C [227]. On the second heating run this endotherm is not apparent and the glass transition is higher, at 62 °C. This shift in Tg must be due to the incorporation of the previously crystalline portion of polyvinyl alcohol into the amorphous region.

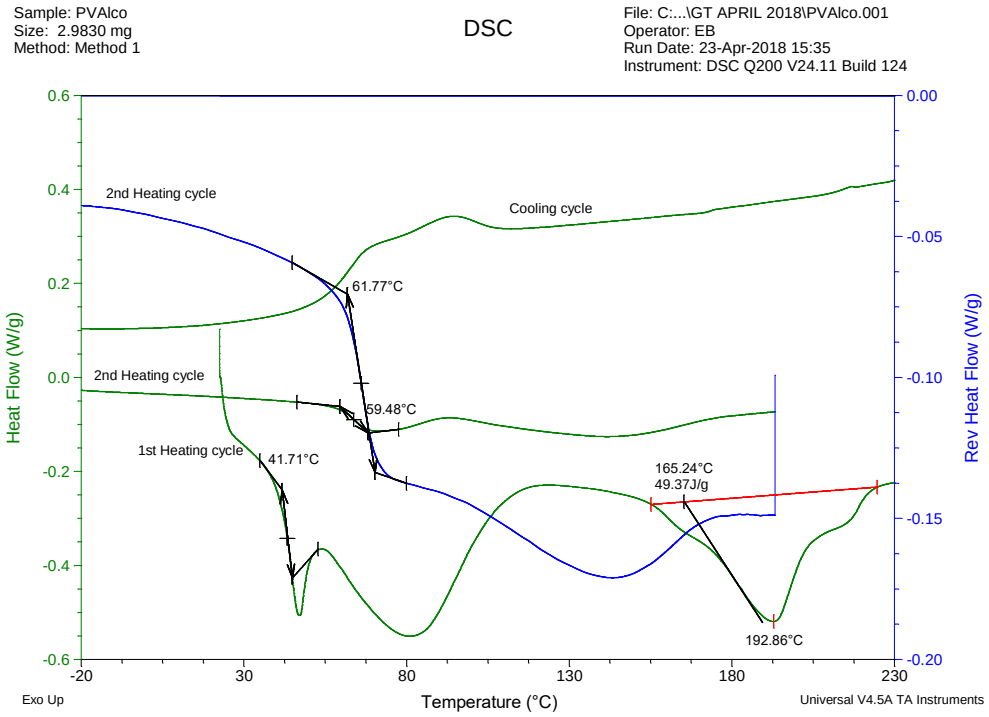

Figure 4.3: Differential scanning calorimetry scans showing glass transitions/melt endotherm of PVAlcohol.

A heat-cool-heat profile of ketoprofen is shown in Figure 4.4. Crystalline ketoprofen has a melt onset at 91 °C and no cold crystallisation occurs in the cooling cycle as ketoprofen is a good glass former [4]. The glass transition onset temperature of ketoprofen is -6 °C, as seen in the second heating run. Ketoprofen remains amorphous upon reheating as evidenced by the lack of an endotherm in the second heating cycle.

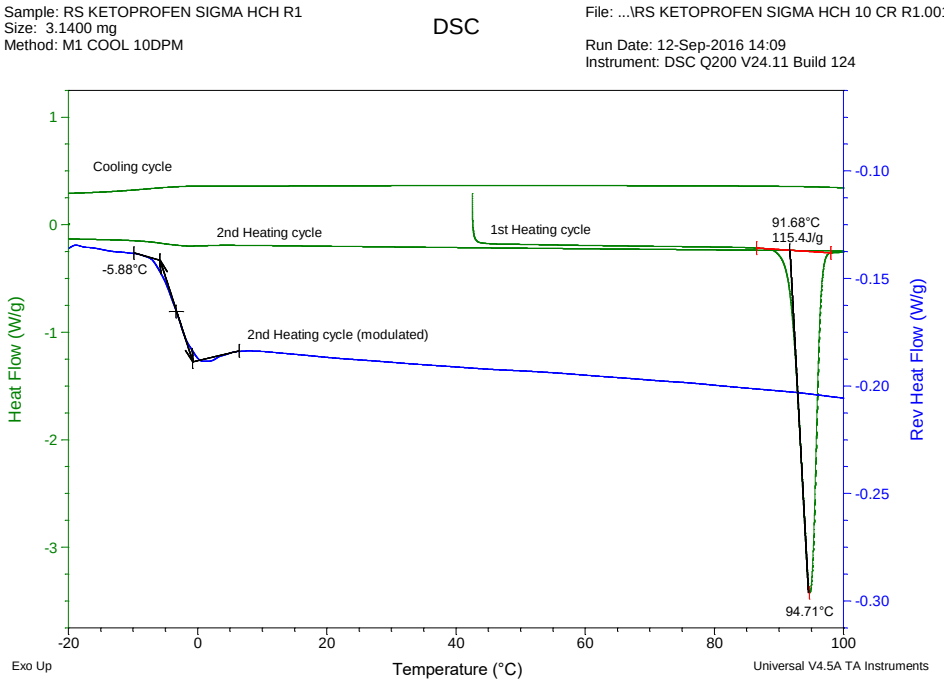

Figure 4.4: mDSC calorimetry scans showing melt endotherm and glass transition of ketoprofen

4.2.1.2 pXRD analysis

The pXRD patterns of the polymers are shown in Figure 4.5. As can be seen, all polymers except for PVAlcohol are amorphous, as indicated by the absence of Bragg peaks. As PVAlcohol is semi-crystalline, a Bragg peak is apparent at 20° 2θ, which corresponds to the literature [228].

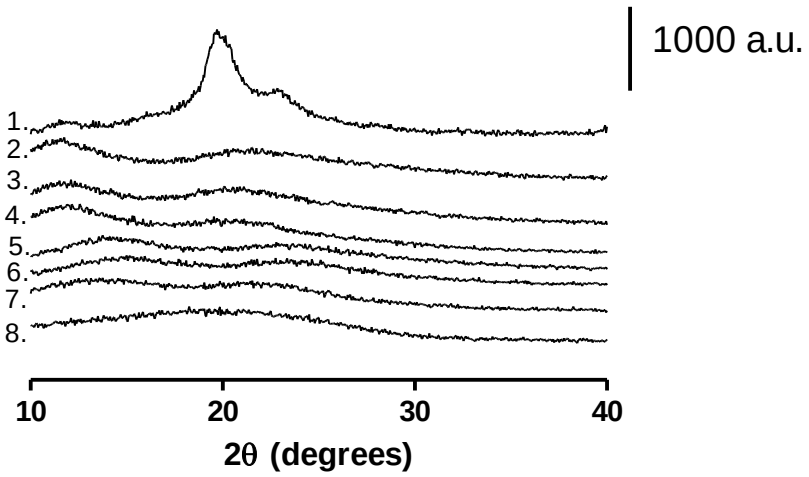

Figure 4.5: pXRD patterns of the polymers used. 1. PVAlcohol 2. PVP90 3. PVP30 4. PVP17 5. VP:VA 7:3 6. VP:VA 3:7 7. PVAcetate 8. PVAP

4.2.2 Polymer-ketoprofen system characterisation

4.2.2.1 Thermal properties

The DSC thermograms for polymer-ketoprofen systems with 20% w/w ketoprofen loading (henceforth termed POLYMERKETO e.g. PVPKETO), which were prepared as described in Chapter 2 Section 2.2.3.4.3, are shown in Figure 4.6 below. Ketoprofen is present in the amorphous state in all DSC samples, as evidenced by the absence of a melt endotherm at 91 ^{o}C in the second heating cycle. While glass transitions are evident for all three PVPKETO systems in the 50-80 ^{o}C region, there also appears to be small secondary glass transitions present (indicated by arrows in Figure 4.6) in all PVPKETO systems at higher temperatures (>120 ^{o}C). This may be due to slow ketoprofen diffusion through the polymer matrix resulting in heterogenous systems, whereby there is a ketoprofen/PVP phase and a separate PVP phase. This is supported by the fact that the secondary glass transitions occur at the same temperatures as the polymer only glass transition temperatures listed in Table 4.1. By contrast the higher vinyl-acetate containing systems have sharp, clear glass transitions with narrower glass transitions indicating that homogenous systems were achieved within the 10 minutes annealing time allowed for in the DSC method. This glass transition narrowing effect appears to be more evident in systems with higher vinyl acetate content. The PVAPKETO system appears to have one very broad glass transition which is probably a result of the two distinct amorphous regions, as highlighted in Figure 4.2, mixing with amorphous ketoprofen to form one very broad glass transition. The PVAlcoholKETO system shows a glass transition onset at approximately 30 ^{o}C before the crystalline portion of PVAlcohol starts melting at 150 ^{o}C.

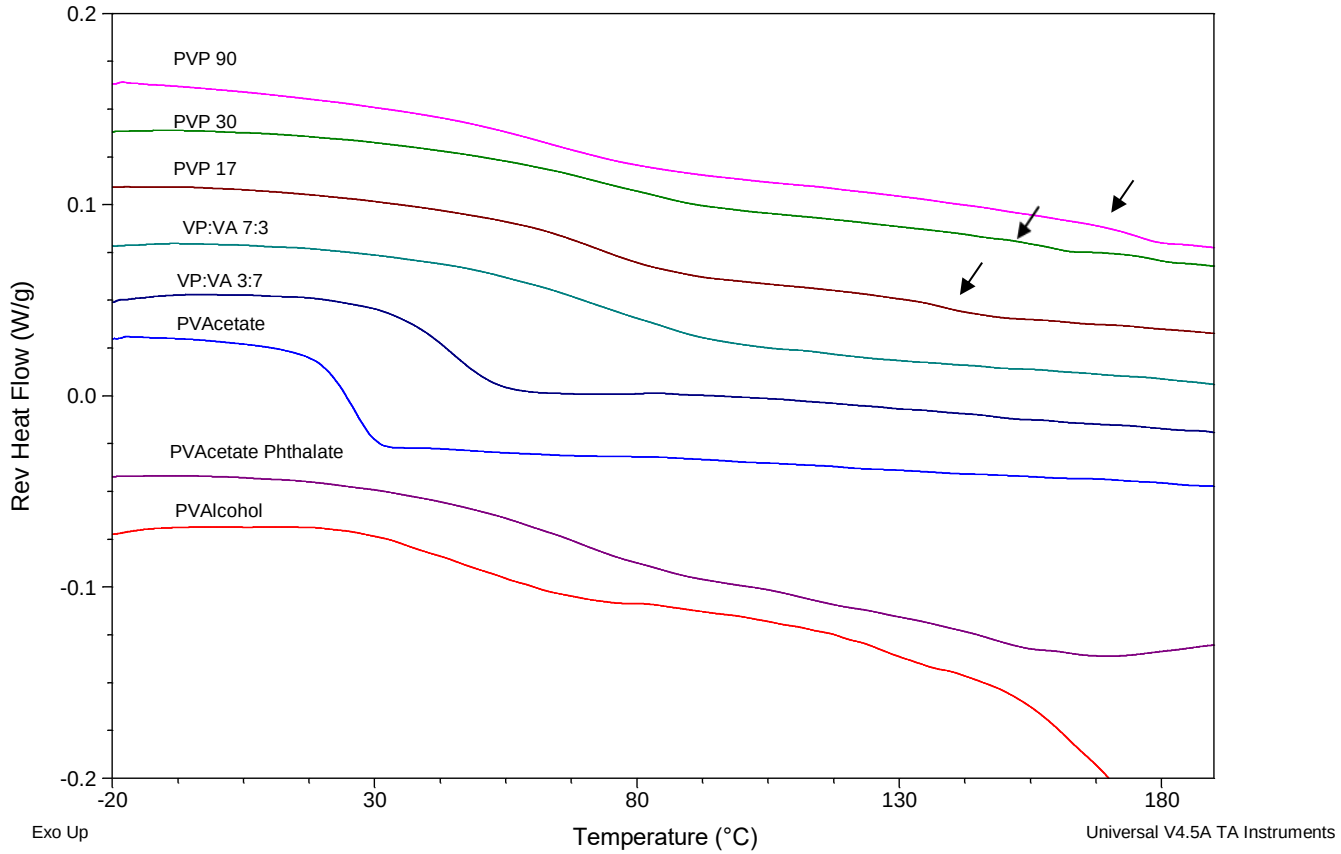

Figure 4.6: mDSC scans showing glass transitions of POLYMERKETO systems with 20% w/w ketoprofen. Arrows point to the secondary polymer-rich glass transitions

The predominant glass transition onset temperatures from Figure 4.6 were compared to values predicted by the Gordon-Taylor equation (using true density values determined by helium pycnometry as detailed in Chapter 2 Section 2.2.3.6.1 and shown in Table 4.2). As the glass transition of ketoprofen is below room temperature it is not possible to determine the true density of amorphous ketoprofen using traditional pycnometry. It is known that the density of amorphous compounds is lower than that of their crystalline counterparts [3]. The amorphous density of small molecules used in pharmaceutical formulations, such as indomethacin and sucrose, have been experimentally determined by a variety of research groups. The difference between the crystalline density and the amorphous density varied between 1.5% and 10.1%[3,229,230]. In a previous study where pure API amorphous density measurement was not possible, the amorphous density was assumed to be 5% less than the crystalline density [132] therefore, in this study the same assumption has been made resulting in an assumed amorphous ketoprofen density of 1.19 g/cm^3.

Table 4.2: True density values of ketoprofen and studied polymers. Values are presented as an average ± standard deviation. *Value determined by reducing the crystalline density by 5%

Material	True density (g/cm^3)
Crystalline ketoprofen	1.25 ± 0.01
Amorphous ketoprofen*	1.19 ± 0.01
PVP 17	1.20 ± 0.00
PVP 30	1.20 ± 0.00
PVP 90	1.24 ± 0.00
VP:VA 7:3	1.21 ± 0.00
VP:VA 3:7	1.23 ± 0.00
PVAcetate	1.22 ± 0.00
PVAlcohol	1.31 ± 0.00
PVAP	1.38 ± 0.02

Table 4.3: Gordon Taylor predicted glass transition onset temperatures and experimental glass transition onset and offset temperatures and glass transition temperature widths for POLYMERKETO systems with 20% w/w ketoprofen. Values are presented as an average ± standard deviation

Material	Gordon Taylor predicted Tg onset (°C)	Experimental Tg onset (°C)	Deviation from Gordon Taylor Tg onset (°C)	Experimental Tg offset (°C)	Experimental Tg width (°C)
PVP 17 KETO	94.35	63.28 ± 0.95	-31.08	80.48 ± 1.87	17.20 ± 1.97
PVP 30 KETO	106.67	61.66 ± 3.78	-45.02	88.58 ± 1.32	26.91 ± 2.47
PVP 90 KETO	117.50	49.44 ± 1.59	-68.06	74.85 ± 6.24	25.41 ± 5.56
VP:VA 7:3 KETO	80.16	58.25 ± 4.83	-21.92	88.95 ± 2.17	30.70 ± 3.32
VP:VA 3:7 KETO	40.68	36.01 ± 2.52	-4.67	54.68 ± 1.36	18.67 ± 2.23
PVAcetate KETO	29.35	21.61 ± 1.97	-7.74	31.63 ± 1.79	10.02 ± 0.53
PVAlcohol KETO	29.90	27.47 ± 1.96	-2.44	65.94 ± 8.25	38.47 ± 9.22
PVAP KETO	79.67	51.39 ± 1.26	-28.28	79.79 ± 5.40	28.41 ± 6.47

The deviation between experimental and predicted glass transition onset temperature of the POLYMERKETO systems are detailed in Table 4.3 and graphed in Figure 4.7. For many of the systems studied there is significant deviation between these values. The experimental values were lower than expected for the PVP-containing systems. PVPKETO systems of high molecular weight deviated the most from predicted values in terms of an absolute deviation, up to 68 ^{o} C in the case of the PVP90KETO system. This may be partially explained by considering that the viscosity of the high Mw polymers may limit the diffusion of ketoprofen through the system, resulting in secondary polymer-rich glass transition temperatures as seen in Figure 4.6. Systems containing vinyl acetate deviated the least from the predicted values. Initially this difference in Gordon-Taylor deviations between vinyl acetate-rich and vinyl pyrrolidone-rich systems was thought to be due to variation of water content in the mixtures, as water is known to be a potent plasticiser [3].

However, by re-weighing the pans after the first heating cycle of the DSC measurement it was confirmed that sorbed water had evaporated despite the absence of pin-holes in the DSC lid. The mass percentage of water loss during the first heating cycle was the same as the mass percentage loss during a thermogravimetric analysis. Therefore, the systems present in the second heating cycle, where the glass transition was measured, were binary systems of drug and polymer.

The fact that vinyl acetate rich systems had glass transition temperature values closer to Gordon-Taylor predicted values than vinyl pyrrolidone rich systems is somewhat surprising as the vinyl acetate functional group is thought to be a poorer hydrogen bond acceptor than vinyl pyrrolidone [231]. Generally, hydrogen bonding between the drug and polymer would be expected to produce a positive deviation from the Gordon-Taylor equation [10,232]. However, in specific instances where one of the components is able to self-associate (e.g. dimer formation) through hydrogen bonding while the other component can only act as a hydrogen bond donor or acceptor, the creation of an ASD involving hydrogen bond formation between the two components may lead to a net reduction in the total strength of hydrogen bonds present in the system [233]. As ketoprofen is known to self-associate to dimers through hydrogen bond formation via the carboxylic acid group [234], it may be that the negative deviation from the Gordon-Taylor equation is a result of the new hydrogen bonds formed between ketoprofen and PVP being weaker than the hydrogen bonds between amorphous dimers of ketoprofen. The vinyl acetate systems experience a less negative deviation from Gordon-Taylor predicted glass transition values as they are less likely to hydrogen bond with ketoprofen and thus the strong dimer hydrogen bonds are retained. Evidence substantiating this theory is found in work carried out with the structurally similar drug indomethacin and PVP/PVPVA. By using solid-state NMR the authors determined that ASDs formed with PVP had fewer indomethacin dimers present than ASDs formed with PVPVA [231].

The PVAPKETO system's glass transition onset temperature also negatively deviated from the value predicted by the Gordon-Taylor equation, which is likely due to its very broad glass transition (28 ^{o}C), which, in turn, is due to the presence of a small poly vinyl acetate rich domain, as seen in the inlay in Figure 4.2. As the polymer itself had two glass transitions, when the ASD was created the addition of ketoprofen provided further heterogeneity to the system resulting in a very broad glass transition. As shown in Figure 4.7 the experimental glass transition offset temperature of PVAPKETO was very similar to the Gordon Taylor predicted onset temperature.

The PVAlcohol system glass transition temperature was very similar to the value predicted by the Gordon-Taylor equation which is indicative of ideal mixing and the absence of any strong attractive or repulsive forces between the drug and polymer.

This experiment has shown that one limitation with Gordon Taylor predicted glass transition values is that they are generally understood to refer to the glass transition onset temperature. Where glass transitions occur over an extended temperature range, such as is the case with many POLYMERKETO systems, the Gordon Taylor predicted glass transition temperature may fall within the experimental glass transition temperature range, but deviate significantly from the glass transition onset temperature.

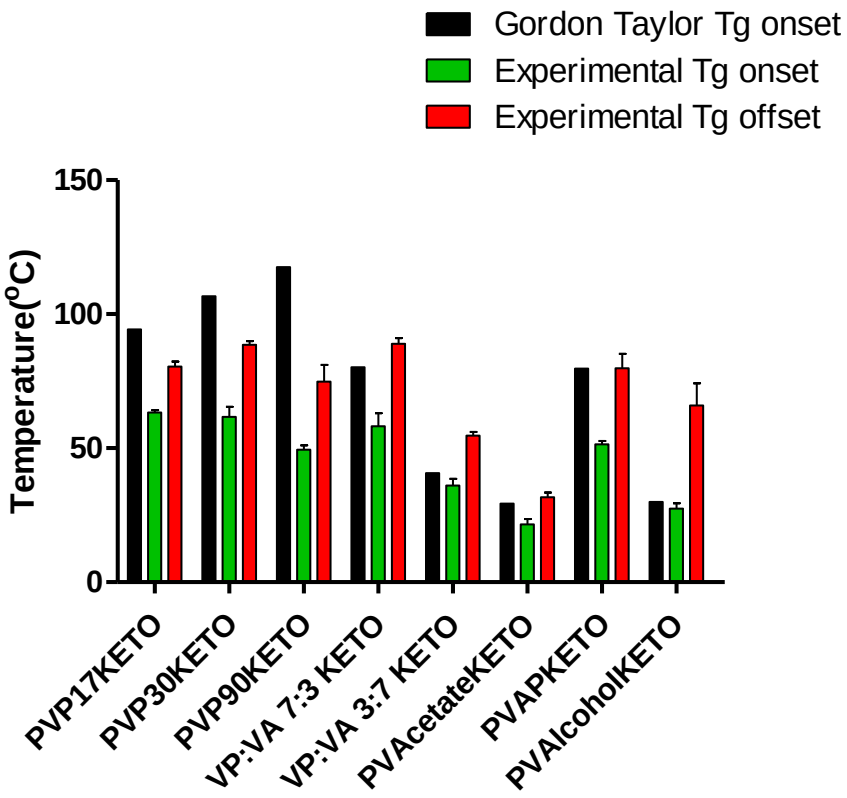

Figure 4.7: Experimental and predicted glass transition temperature values for POLYMERKETO systems with 20% w/w ketoprofen

4.2.2.2 pXRD analysis

The pXRD patterns of physical mixtures of crystalline ketoprofen and the studied polymers are shown in Figure 4.8a. The pXRD pattern of the PVP with the lowest molecular weight, PVP17, physically mixed with ketoprofen appears to have Bragg peaks which are greatly diminished relative to the equivalent higher molecular weight PVPs physical mixtures. This observation has been reported by other authors for ketoprofen and ibuprofen [235,236] . One explanation for this observation is that as the lower molecular weight PVPs have a higher number of terminal groups which are less sterically hindered and therefore more free to interact with the carboxylic acid group of ketoprofen resulting in a disturbance of the crystal packing [236]

The pXRD patterns shown in Figure 4.8 b) are the same systems post melt-quenching and cryo-milling. While all physical mixtures show Bragg peaks corresponding to crystalline ketoprofen, once melt-quenched all systems, except PVAPKETO and PVAlcoholKETO, are pXRD amorphous with no Bragg peaks visible.

For both PVAPKETO and PVAlcoholKETO the intensity of the Bragg peaks is reduced in the melt-quenched systems relative to the physical mixture, indicating some degree of amorphisation, but also that residual crystalline ketoprofen remains. Interestingly, one of the most intense ketoprofen peaks at 6.36^{o} is not present in these melt-quenched systems, which may be due to preferred orientation effects. As DSC showed no crystalline ketoprofen endotherm for the *in-situ* melt quenched systems (Section 4.2.2.1) it is somewhat surprising that crystalline ketoprofen peaks are visible using pXRD which is generally considered to be a less sensitive technique [211]. This may be explained by consideration that the DSC pan, where the glass transition measurements were taken, involves a much smaller sample size in a very controlled environment in comparison to the melt-quenched system, which was created using a hot-plate and liquid nitrogen. As the sample size was larger and the system was open to the environment there may have been a temperature gradient which did not allow ketoprofen to melt completely for these two systems.

Alternatively, the presence of residual crystalline ketoprofen in both systems may be due to rapid re-crystallisation of ketoprofen in the time between amorphisation via melt-quenching and recording of the pXRD pattern. Another explanation may be that ketoprofen may be soluble at this drug/polymer ratio (20% w/w ketoprofen) for both polymers at the elevated temperatures used in the DSC method and hence no crystalline endotherm is visible. The ketoprofen solubility limit may be lower for these polymers at the ambient temperatures used for pXRD.

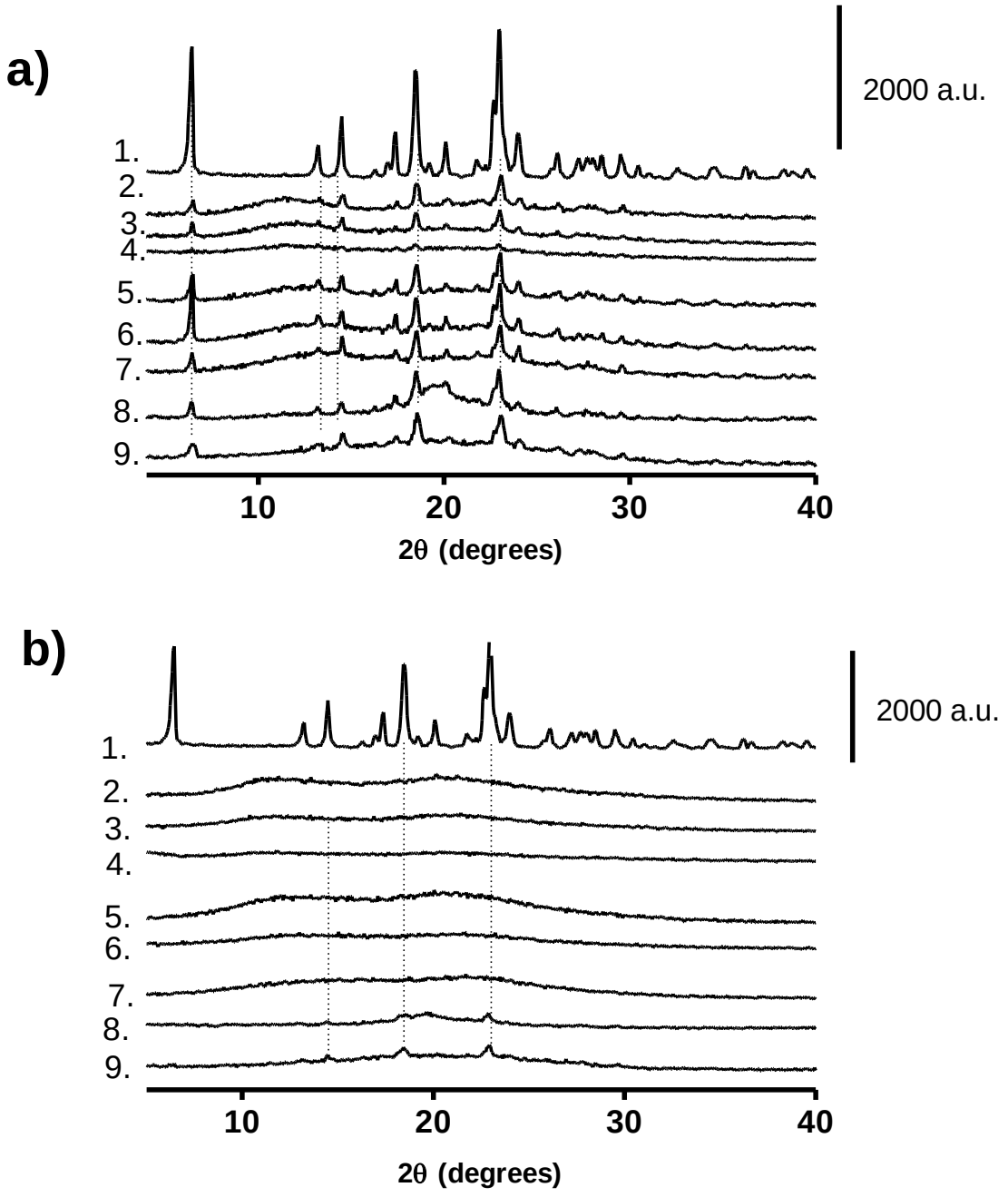

Figure 4.8: pXRD patterns of a) Physical mixtures of crystalline ketoprofen and polymers b) Melt-quenched and cryo-milled POLYMERKETO 1. Crystalline ketoprofen 2. PVP90KETO 3. PVP30KETO 4. PVP17KETO 5. VP:VA 7:3KETO 6. VP:VA 3:7KETO 7. PVAcetateKETO 8. PVAlcoholKETO 9. PVAPKETO

4.2.2.3 ATR-FTIR analysis

The intermolecular bonding between poly vinyl-based polymers and ketoprofen was investigated using ATR-FTIR. Intermolecular interactions or lack thereof are crucial in the understanding of the polymer mediated stabilisation of amorphous ketoprofen. It is known that the vinyl pyrrolidine functional group in PVP can hydrogen bond with the carboxylic acid carbonyl in ketoprofen, and that, in the PVPVA 6:4 co-polymer, the vinyl pyrrolidine functional group rather than the vinyl acetate group is preferentially involved in hydrogen bonding with the carboxylic acid carbonyl group of ketoprofen [11]. We aim to investigate if vinyl acetate, vinyl alcohol or vinyl phthalate functional groups can interact with the carbonyls of the carboxylic acid or the ketone of ketoprofen.

In crystalline ketoprofen, there are two carbonyl signals at 1694 cm^{-1} and 1653 cm^{-1}, corresponding to the dimer hydrogen bonded carbonyl group of the carboxylic acid and the carbonyl of the ketone respectively [11,237]. In amorphous ketoprofen the dimer carbonyl is slightly shifted to a higher wavenumber (blue shift) at 1705 cm^{-1} indicating that intermolecular hydrogen bonding is stronger in the crystalline state of ketoprofen than the amorphous state, as hydrogen bonding results in a lengthening of the carbonyl bond and lowers the frequency and hence wavenumber of the signal [238,239]. The ketone carbonyl at 1655 cm^{-1} in the amorphous ketoprofen sample is broader than that in the crystalline material indicating amorphisation [238]. Also notable in the amorphous spectra is the appearance of a shoulder at 1737 cm^{-1}. This amorphous ketoprofen shoulder has been assigned by other authors to the free acid (i.e. COOH) carbonyl of the carboxylic acid group, which is visible due to the presence of monomeric ketoprofen [11,238,240]. Monomeric ketoprofen has a higher wavenumber than dimeric ketoprofen as it is not stabilised through the same intermolecular hydrogen bonding network. Another observable difference between the crystalline and amorphous ketoprofen is noted in the fingerprint region. In crystalline ketoprofen there are 3 distinct peaks between 720 and 650 cm^{-1}, while in amorphous ketoprofen there are only 2 peaks visible in this region, which allows for this region to be used as an indicator of the physical state of ketoprofen [11].

As shown in Figures 4.9-4.11, PVP has one strong signal in the carbonyl region centred at 1653 cm^{-1} corresponding to the carbonyl of the vinyl pyrrolidone ring. This signal is present in all PVP polymers regardless of molecular weight. The physical mixtures (PM) of PVP17, PVP30 and PVP90 with 20% w/w ketoprofen appear to simply be an overlay of the IR spectra of each component, with the 3 peaks attributed to crystalline ketoprofen visible in the fingerprint region.

In contrast the melt-quenched (MQ) samples show 2 peaks in the fingerprint region indicating amorphisation of ketoprofen. The melt-quenched samples also show a red shift of the dimer carboxylic acid peak of ketoprofen causing it to overlap with the ketone of ketoprofen and the vinyl pyrrolidone peak, which indicates that amorphisation is associated with an increase in hydrogen bonding between ketoprofen and PVP. The amorphous ketoprofen monomeric shoulder is also present but is slightly shifted to lower wavenumbers at 1725 cm^{-1}, 1723 cm^{-1} and 1726 cm^{-1} for PVP17KETO PVP30KETO and PVP90KETO, respectively which is indicative of increased hydrogen bonding relative to ketoprofen in the amorphous state. It is clear therefore that melt-quenching PVP with 20% w/w ketoprofen results in an amorphous material which is characterised by increased hydrogen bonding relative to the physical mixture. These spectra are complementary to the mDSC results which showed that PVPKETO systems exhibited glass transition onset temperatures which deviated significantly from the Gordon-Taylor equation. It is clear from ATR-FTIR that hydrogen bonding is occurring between the ketoprofen carboxylic carbonyl and PVP. The ability of PVP to form hydrogen bonds with ketoprofen at the expense of stronger ketoprofen-ketoprofen hydrogen bonds explains the negative deviation of glass transition temperature from predicted values [233].

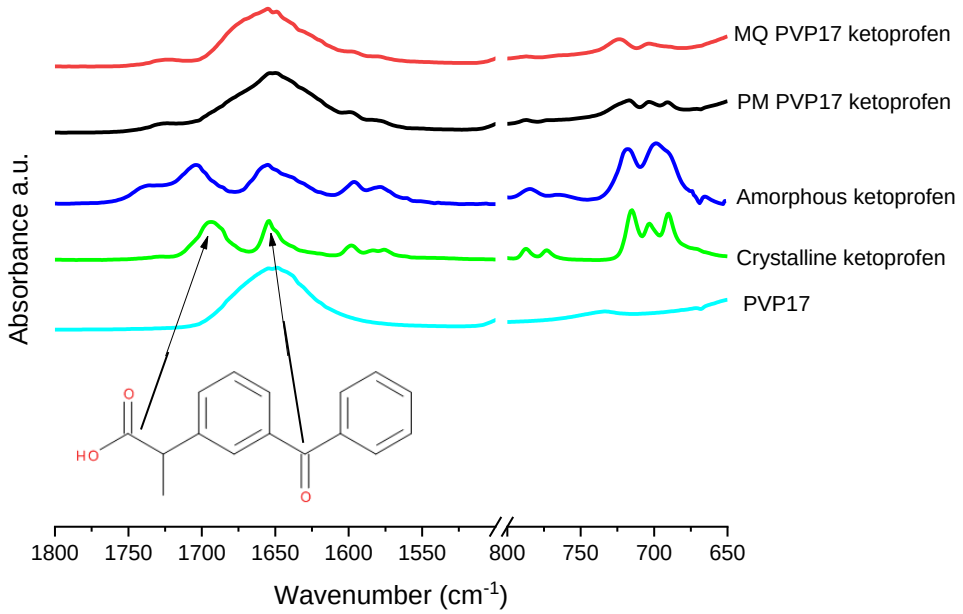

Figure 4.9: PVP17 and ketoprofen ATR-FTIR spectra. Melt-quenched (MQ) PVP17KETO and physical mixture (PM) PVP17KETO

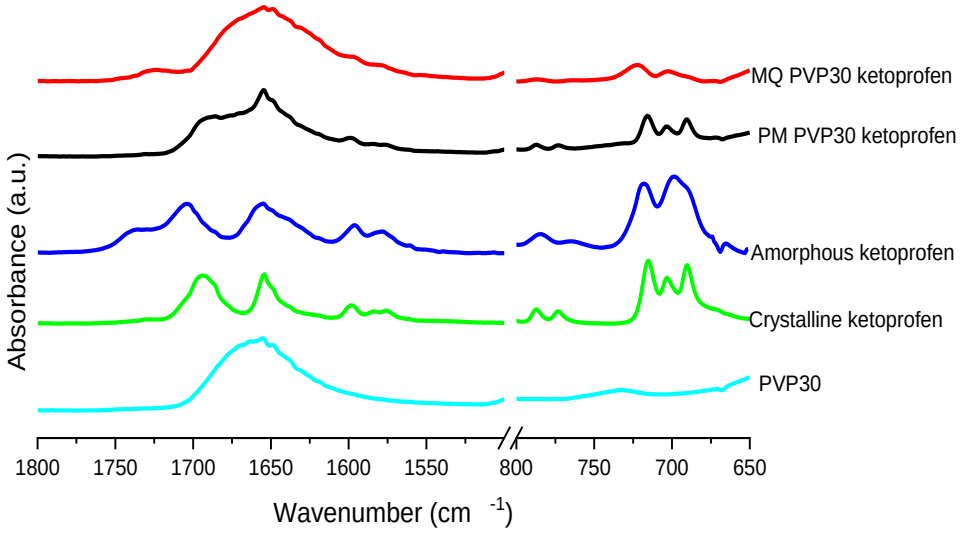

Figure 4.10: PVP30 and ketoprofen ATR-FTIR spectra. Melt-quenched (MQ) PVP30KETO and physical mixture (PM) PVP30KETO

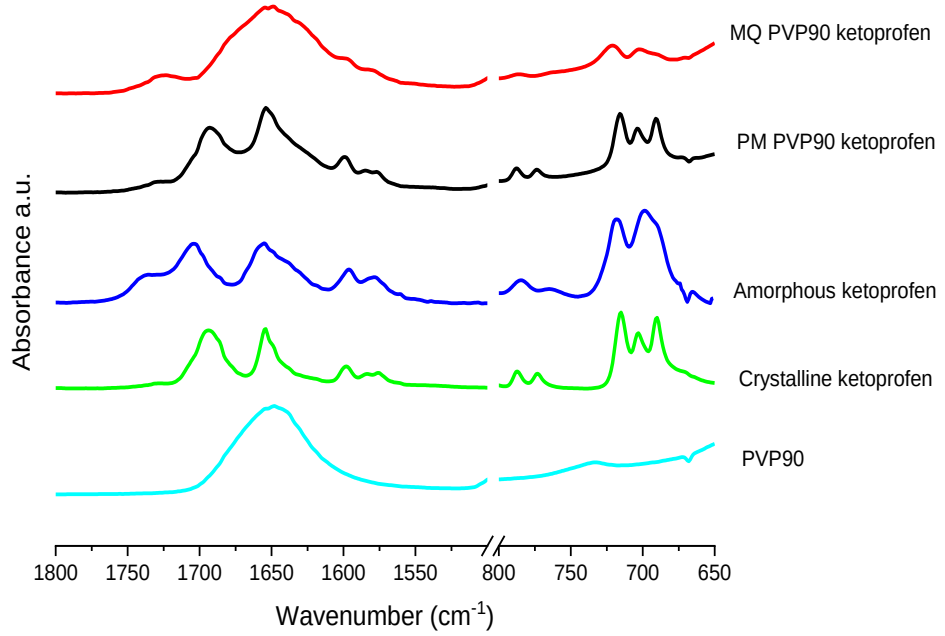

Figure 4.11: PVP90 and ketoprofen ATR-FTIR spectra. Melt-quenched (MQ) PVP90KETO and physical mixture (PM) PVP90KETO

As shown in Figure 4.12 VP:VA 7:3 has two carbonyl peaks apparent, a peak of low intensity at 1732 cm^{-1} corresponding to vinyl acetate and a peak of higher intensity at 1676 cm^{-1} corresponding to vinyl pyrrolidone. The relative intensity of these peaks is in accordance with the degree of substitution of each functional group on the polymer backbone. The physical mixture of polymer VP:VA 7:3 and 20% w/w ketoprofen shows two distinct peaks, one at 1735 cm^{-1} corresponding to the vinyl acetate group and one centred at 1671 cm^{-1} corresponding to the merging of the ketone of ketoprofen, dimer carbonyl of ketoprofen and vinyl pyrrolidone. In the melt-quenched sample, the fingerprint region shows two distinct peaks in the 650-720 cm^{-1} region indicating amorphisation, however there is no clear change in the carbonyl region. As three of the peaks of interest overlap it is challenging to interpret any subtle changes in this peak. It is clear however that the vinyl acetate signal remains unchanged, indicating that it is not involved in hydrogen bonding with ketoprofen.

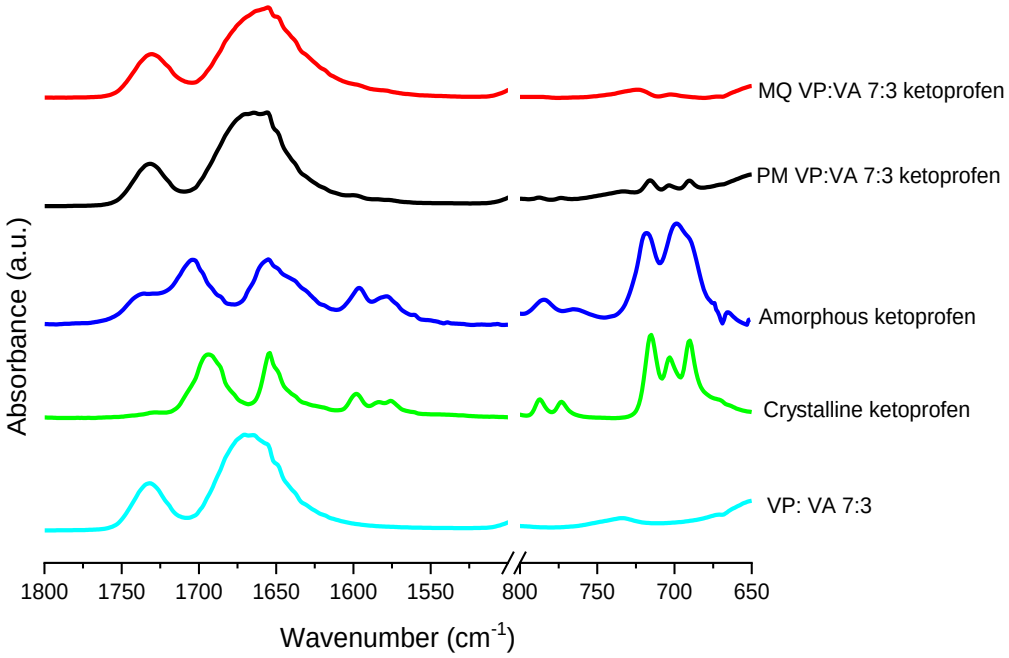

Figure 4.12: VP:VA 7:3 and ketoprofen ATR-FTIR spectra. Melt-quenched (MQ) VP:VA 7:3 KETO and physical mixture (PM) VP:VA 7:3 KETO

The VP:VA 3:7 co-polymer spectra in Figure 4.13 is similar to the VP:VA 7:3 co-polymer as there are two carbonyl peaks apparent, a peak at 1732 cm^{-1} corresponding to vinyl acetate and a peak of lower intensity at 1676 cm^{-1} corresponding to vinyl pyrrolidone. The physical mixture of VP: VA 3:7 polymer and 20% w/w ketoprofen spectra shows two distinct peaks, one at 1733 cm^{-1} corresponding to the vinyl acetate group and one centred at 1678 cm^{-1} corresponding to the merging of the dimer carbonyl of ketoprofen and vinyl pyrrolidone carbonyl. The ketone of ketoprofen is visible as a shoulder at 1657 cm^{-1}. In the melt-quenched sample, the fingerprint region shows two distinct peaks in the 650-720 cm^{-1} region indicating amorphisation. In the melt-quenched sample, the vinyl acetate region remains unchanged, while a broadening of the vinylpyrrolidone/ ketone carbonyl region is apparent. This is probably visible in this system and not

in the VP:VA 7:3 system as the vinyl pyrrolidone signal is less intense due to lower vinyl pyrrolidone content, allowing the broad amorphous ketone carbonyl signal to be observed.

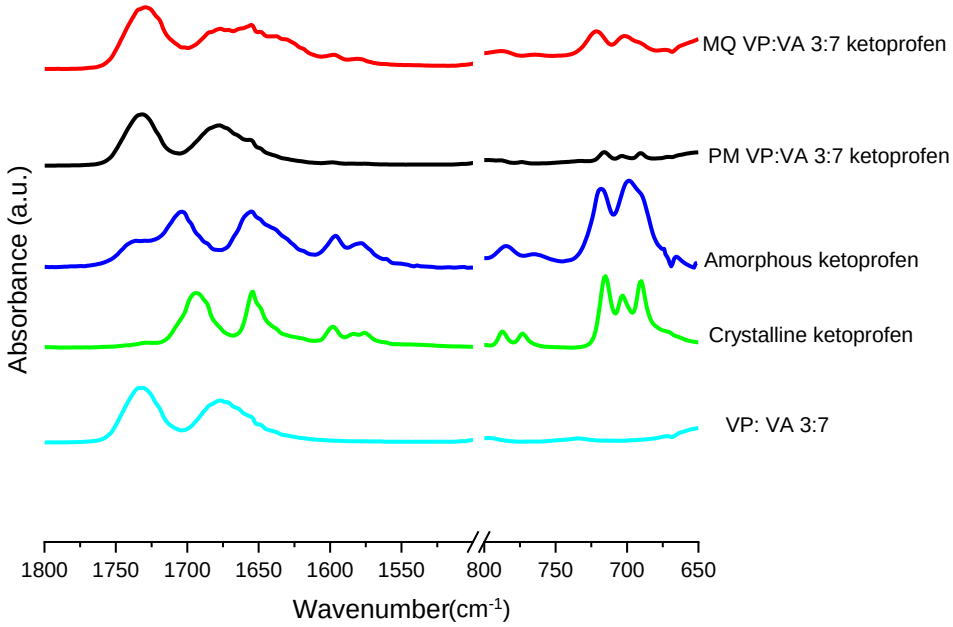

Figure 4.13: VP:VA 3:7 and ketoprofen ATR-FTIR spectra. Melt-quenched (MQ) VP:VA 3:7 KETO and physical mixture (PM) VP:VA 3:7KETO

As shown in Figure 4.14 PVAcetate has one strong signal in the carbonyl region at 1729 cm^{-1} corresponding to the carbonyl of the polyvinyl acetate group. The physical mixture of 80% w/w PVAcetate and 20% w/w ketoprofen appears to simply be an overlay of the spectra for crystalline ketoprofen and PVAcetate. Three carbonyl peaks are distinct in this region at 1730 cm^{-1}, 1697 cm^{-1} and 1656 cm^{-1} which are assigned to the vinyl acetate, dimer carboxylic acid and ketone carbonyls respectively. The physical mixture shows three peaks in the 720 to 650 cm^{-1} range indicating crystallinity. The melt-quenched sample shows two peaks in the same region indicating amorphisation. There are only two distinct carbonyl peaks in the melt quenched sample, one at 1658 cm^{-1} corresponding to the ketone group of ketoprofen and one at 1729 cm^{-1} which is a result of the merging of the vinyl acetate signal and the dimer amorphous ketoprofen signal.

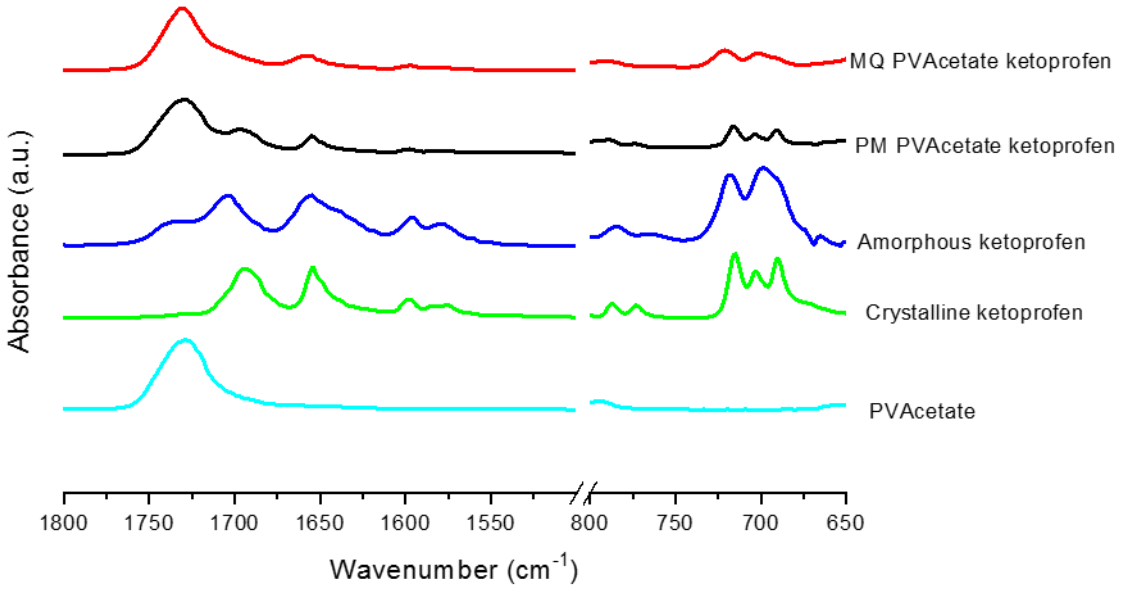

Figure 4.14: PVAcetate and ketoprofen ATR-FTIR spectra. Melt-quenched (MQ) PVAcetate KETO and physical mixture (PM) PVAcetate KETO

As shown in Figure 4.15, PVAlcohol has an alcohol signal at 3306 cm^{-1} as well as a carbonyl signal at 1723 cm^{-1} which is due to polyvinyl acetate present as an impurity. Polyvinyl acetate is present as it is the starting material which is hydrolysed in the manufacture of polyvinyl alcohol [141]. The spectra of the physcial mixture of PVAlcohol and 20% w/w ketoprofen appears to be a simple overlay of the spectra of the individual components. Interestingly, in the melt-quenched sample there is no change in the position of the alcohol signal relative to the physical mixture implying that this functional group is not involved in any intermolecular bonding with ketoprofen, which corresponds to DSC data. The melt-quenched sample shows a merging of carbonyl peaks between the dimer carbonyl of ketoprofen and the vinyl acetate carbonyl, similar to the PVAcetateKETO system, and the fingerprint region shows two peaks indicating that ketoprofen is present in the amorphous state.

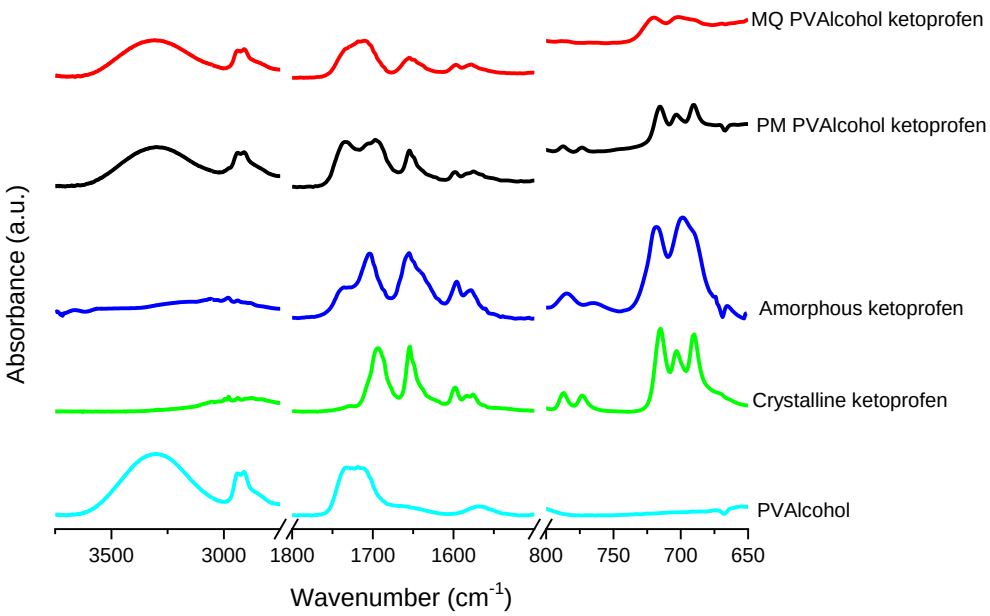

Figure 4.15: PVAlcohol and ketoprofen ATR-FTIR spectra. Melt-quenched (MQ) PVAlcohol KETO and physical mixture (PM) PVAlcohol KETO

As seen in Figure 4.16 PVAP has a broad carbonyl signal at 1705 cm^{-1} due to the merging of three carbonyls present in the structure of PVAP. Although there is an alcohol functional group present in the structure of PVAP there was no signal detected in the 3300 cm^{-1} region corresponding to this, indicating that the OH group may be involved in intramolecular bonding in PVAP. The spectra of the physical mixture of PVAP and crystalline ketoprofen appears to be an overlay of the individual components. In the melt quenched sample, the dimer carboxylic acid carbonyl of ketoprofen has merged with the carbonyls of PVAP and the characteristic three peaks centred around 700 cm^{-1} are absent, indicating that ketoprofen is present in the amorphous state.

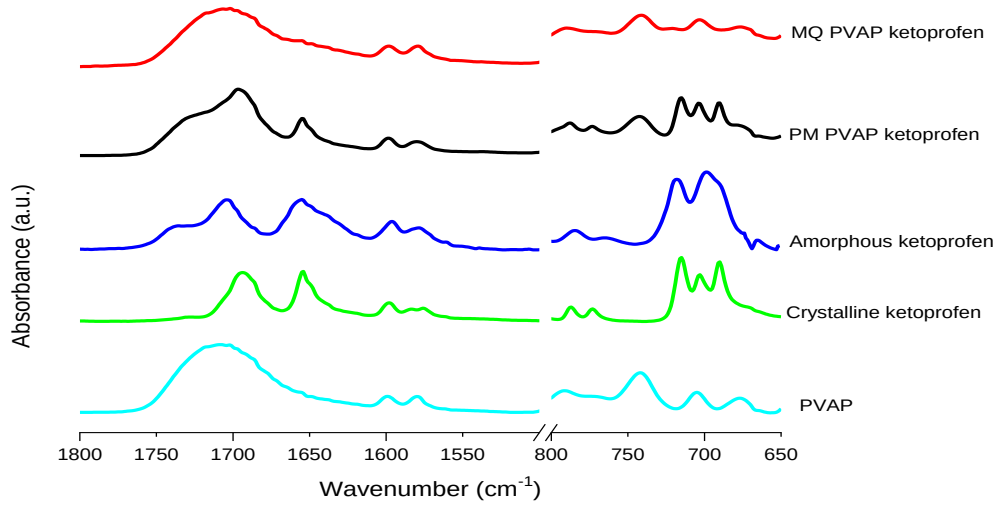

Figure 4.16: PVAP and ketoprofen ATR-FTIR spectra. Melt-quenched (MQ) PVAP KETO and physical mixture (PM) PVAP KETO

In conclusion, the ATR-FTIR analysis has shown that ketoprofen is ATR-FTIR amorphous for all of the systems studied. It also shows that by amorphising ketoprofen, the micro-environment of the carbonyl of the carboxylic acid functional group is altered, particularly with regard to its propensity to hydrogen bond. No shifts were observed with any vinyl acetate or vinyl alcohol groups indicating that these functional groups do not form hydrogen bonds with ketoprofen in the amorphous form. The only systems in which there was clear evidence of hydrogen bonding between ketoprofen and polymer were the PVPKETO systems which complements DSC findings. This is an interesting observation as the ability to hydrogen bond with a drug is generally considered to be a desirable attribute of a polymer as it can increase relaxation times of the drug in the amorphous state thereby prolonging amorphous state physical stability. In this instance, the ability of a polymer to hydrogen bond with the drug of interest has led to a lower glass transition temperature than expected, which would be predicted to result in poorer amorphous physical stability.

While PVAPKETO and PVAlcoholKETO had pXRD patterns with small peaks corresponding to small amounts of crystalline ketoprofen, crystalline ketoprofen was not observed in either DSC or ATR-FTIR analysis. As highlighted previously, one explanation for the DSC-amorphous nature of these POLYMERKETO systems may be that crystalline ketoprofen is soluble in these polymers at elevated temperatures, and therefore no melting endotherm event corresponding to the fusion temperature of the ketoprofen crystal is observed. As ATR-FTIR is a more sensitive technique than pXRD [211], it is therefore surprising that the melt-quenched cryo-milled PVAPKETO and PVAlcoholKETO systems are ATR-FTIR-amorphous. This observation may be due to some degree of amorphisation caused by the ATR-FTIR arm compressing the powdered sample against the crystal. Compression has been known to increase drug-polymer interaction and reduce drug crystallinity, as seen with PVPVA-naproxen systems [128].

4.2.3 Influence of polymer choice on water-induced phase transition

The relative humidity at which the relative humidity induced glass transition (RH_{Tg}) occurred, as well as the percentage of water uptake at the RH_{Tg}, were determined as described in Chapter 2 Section 2.2.3.7.1 and are shown in Figure 4.17. The RH_{Tg} is the relative humidity at which sufficient water has been adsorbed by the polymer for the glass transition to occur at the temperature of the analysis [112].

As PVAPKETO and PVAlcoholKETO are partially crystalline (pXRD) they were not deemed suitable for this analysis. Similarly, as this analysis was carried out at 25 ^{o}C , which is above the glass transition temperature of PVAcetateKETO, this system was not included in this analysis.

4.2.3.1 Influence of polymer molecular weight on water-induced phase transition

There was no statistically significant difference in the RH_{Tg} between PVP30KETO system and the other molecular weight PVP systems studied. A trend is apparent however, as shown in Figure 4.17a. As the molecular weight of PVP increases, the RH required for RH_{Tg} to occur increases. The mean RH_{Tg} (± standard error) for PVP17KETO, PVP30KETO and PVP90KETO were 49.61 ± 4.83 %, 51.44 ± 1.54 % and 58.71 ± 1.16 % respectively. This is likely due to the effect that increasing molecular weight has on increasing the thermal glass transition. As molecular weight increases, the thermal glass transition of the polymer increases (135 ^{o}C, 153 ^{o}C and 172 ^{o}C for PVP17,30 and 90 respectively- Figure 4.2) . The higher molecular weight PVP systems therefore require a higher RH to be reached before the amount of water adsorbed plasticizes the system to a a sufficent degree to enable a moisture induced glass transition to occur at 25 ^{o}C. This difference is small between the PVP17 and PVP30 systems while it is greater for the PVP90 system. As the molecular weights of these systems are 7,000-11,000, 54,000-55,000 and 1,000,000-1,500,000 g/mol respectively, this is logical. The higher molecular weight may mean that the water has more difficulty diffusing through the powder due to reduced molecular mobility caused by the high viscosity of the polymer.

As shown in Figure 4.17b, the percentage water uptake at the RH_{Tg} is higher for PVP90KETO compared to the lower molecular weight PVPKETO systems, which corresponds well with the afformentioned explanation of the relationship between RH_{Tg} values and molecular weight.

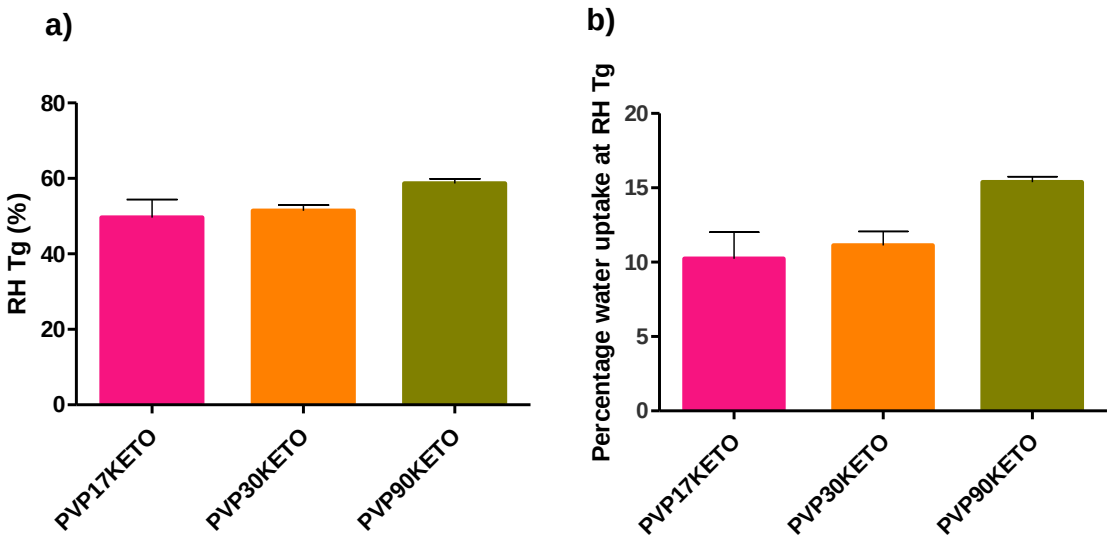

Figure 4.17: a) The relative humidity percentage at which a glass transition was induced for PVP-ketoprofen systems of differing molecular weights b) The mass percentage of water uptake for PVP-ketoprofen systems at the relative humidity induced glass transition for differing PVP molecular weights . Ketoprofen composition was 20% w/w for each system studied

4.2.3.2 Influence of polymer substitution ratio on water-induced phase transition

Similarly, a trend is apparent in the RH_{Tg} values of systems with different VP:VA ratios studied, as shown in Figure 4.18. As the ratio of VP: VA increases, the RH_{Tg} reduces. The RH_{Tg} values (± standard error) for VP:VA ratios of 10:0, 7:3 and 3:7 are 51.44 ± 1.54 %, 55.98 ± 0.88 % and 59.93 ± 1.84 % respectively. Increasing the vinyl acetate proportion in the system increases the hydrophobicity of the system and therefore higher RH is required for sufficient water to be adsorbed for phase transition to occur. In contrast to Figure 4.17 where higher RH_{Tg} systems had higher percentages of water uptake at RH_{Tg}, in Figure 4.18 higher RH_{Tg} systems had lower percentages of water uptake at RH_{Tg}. This is explained by consideration of the thermal glass transitions of these systems. The glass transition of polyvinyl acetate is 38 °C, and as the proportion of vinyl acetate increases the glass transition of the co-polymer reduces. The glass transitions of PVP30 (VP:VA 10:0), VP:VA 7:3 and VP:VA 3:7 are 153 °C, 114 °C and 58 °C respectively. Therefore the high vinyl acetate systems require less water to be sorbed for a water-induced phase transition to occur. In the case of the VP:VA 7:3 KETO sytem only 3.39% w/w water was required for RH_{Tg} to occur, but its hydrophobicity necessitated the RH to be nearly 60% before this amount of water could be sorbed. Where no vinyl acetate was present 11.13% w/w water was required for RH_{Tg} to occur but the hydrophilicity of the system meant that this quantity of water was sorbed by the time the system reached 51 % RH.

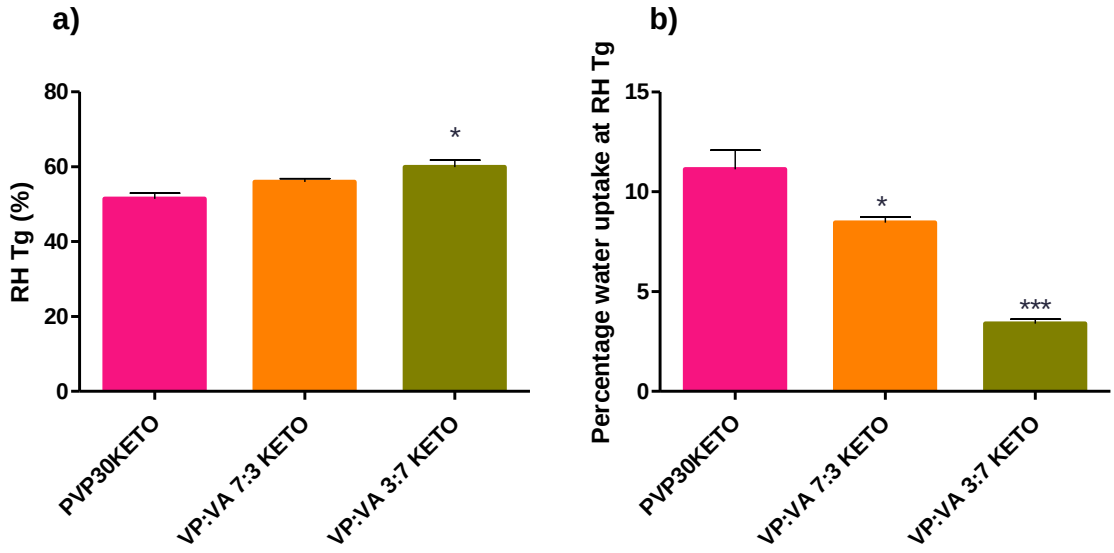

Figure 4.18: a) The relative humidity at which a glass transition was induced for polymer-ketoprofen systems of differing VP:VA substitution ratios b) The mass percentage of water uptake for polymer-ketoprofen systems at the relative humidity induced glass transition for differing VP:VA substitution ratios. Statistically significant difference ($p<0.05$) from PVP30KETO system denoted by *. Highly statistically significant difference ($p<0.001$) from PVP30KETO system denoted by *.**

As the data above refers to the RH_{Tg} at one relative humidity ramping rate (10 RH/ hour), it cannot be used to determine the critical relative humidity for these polymer-keto systems as this requires experiments at several relative humidity ramping rates to be performed. The critical relative humidity of a system is the humidity above which a glass transition will occur at a particular temperature given sufficient time to sorb moisture [112]. This can be used to prescribe storage conditions for the ASD. However it is clear from the data outlined above that higher polymer molecular weight and hence higher viscosity is protective against moisture induced phase transition, as is increasing the hydrophobic vinyl acetate component in the co-polymer.

4.2.4 Influence of polymer choice on dynamic solubility

The equilibrium solubility of ketoprofen in pH 1.20 at 37 ^{o}C was determined (as described in Chapter 2 Section 2.2.5.1) to be 0.157 ± 0.029 mg/mL at 24 hours. This value is close to another value reported in the literature of 0.130 mg/mL[241]. The dynamic solubility of the polymer-ketoprofen systems determined as described in Chapter 2 Section 2.2.5.2, are shown in Figure 4.19, where the dashed line represents the equilibrium solubility of crystalline ketoprofen.

As seen in Figure 4.19a all PVP-ketoprofen systems reach supersaturation relative to crystalline ketoprofen within two hours. The PVP90KETO system was slower to reach supersaturation than the lower molecular weight PVPKETO systems, which is likely due to the high viscosity of this polymer. The total degree of supersaturation is lower for PVP90KETO relative to the other two PVP polymers over two hours, although it is clear the degree of supersaturation is increasing with time. If the experiment had been conducted over a longer time frame, PVP90KETO may have attained the same degree of supersaturation as the lower molecular weight PVP systems, but this would not have been physiologically relevant. Interestingly PVP30KETO reached supersaturation faster than PVP17KETO which is a surprising result considering that the viscosity of PVP17 is lower than that of PVP30.

The ratio of vinyl pyrrolidone to vinyl acetate is clearly critical to the ability of ketoprofen ASDs to reach supersaturation as shown in Figure 4.19b. When this ratio reached 3:7 VP:VA or lower, the ASD was no longer able to reach supersaturation within two hours. This is due to the inherently low aqueous solubility of the vinylacetate functional group [141]. As shown in Figure 4.20, this relationship between vinylpyrrolidone composition and ketoprofen concentration after two hours is well described by a linear regression model, with an R^2 value of 0.96. No such relationship has been described in the literature previously, making this an interesting observation. A similar study, which examined the relationship between celecoxib supersaturation and PVPVA substitution ratio for celecoxib ASDs, found that while the vinyl pyrrolidone monomer was responsible for supersaturation, the vinyl acetate monomer was responsible for the prevention of recrystallisation during dissolution [242]. In the absence of API recrystallisation in the dissolution media, the degree of supersaturation appears to be dependent on the degree of vinyl pyrrolidone substitution.

The role that the polymer's substituent functional groups have on the degree of supersaturation achieved by ketoprofen is demonstrated in Figure 4.19c. While PVAlcoholKETO and PVAPKETO contained ketoprofen in a mixture of amorphous and crystalline states, these systems achieved supersaturation relative to the fully crystalline ketoprofen. This is in contrast to the PVAcetateKETO system, which although fully amorphous, did not achieve supersaturation of ketoprofen within 2

hours at pH 1.20. This work has highlighted that it is the aqueous solubility of the polymer, rather than the degree of amorphisation, which is critical to the ability of ketoprofen ASDs to achieve supersaturation.

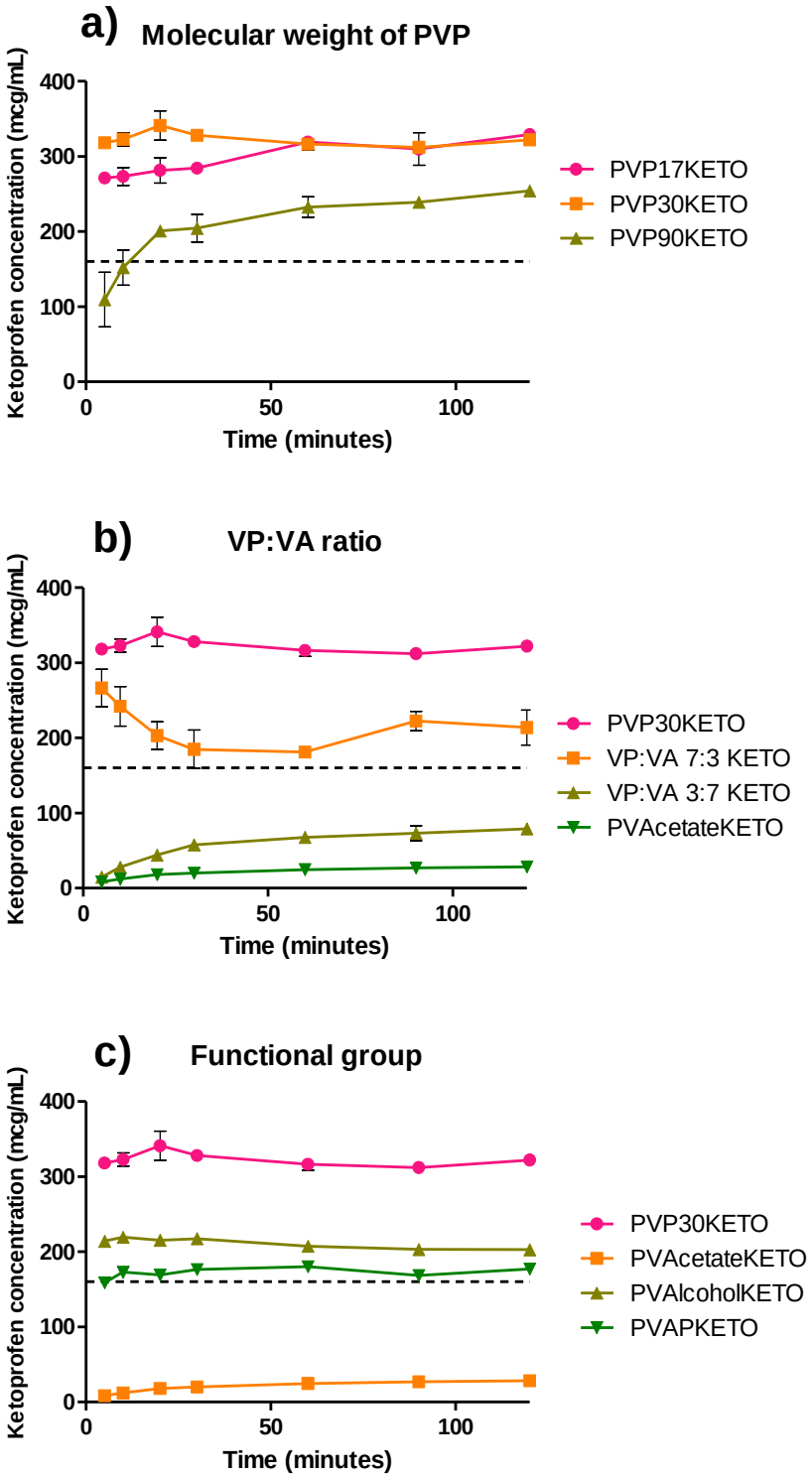

Figure 4.19: Dynamic solubility of POLYMERKETO systems at pH 1.2 and 37 °C over two hours. The dashed line represents the equilibrium solubility of crystalline ketoprofen

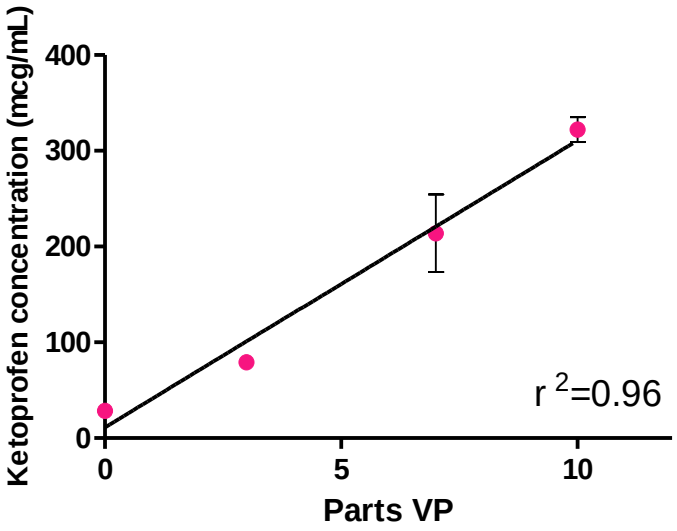

Figure 4.20: Dynamic solubility of vinyl pyrrolidone KETO systems at pH 1.2 at 2 hours versus parts vinyl pyrrolidone in the polymer

4.2.5 Influence of polymer choice on the stability of the glassy state

The pXRD patterns of POLYMERKETO systems placed in stability chambers maintained at 25 °C and a constant humidity of 0% RH or 75% RH over a period of 12 weeks are shown in Figure 4.21. The purple pattern in each graph is of a physical mixture of ketoprofen (20% w/w) and the polymer being tested. As can be seen in Figure 4.21, all PVPKETO systems remained amorphous regardless of polymer molecular weight or the humidity at which the system was stored. Similarly, the VP:VA co-polymer KETO and PVAcetateKETO systems remained amorphous within the time frame studied regardless of storage conditions. The PVAlcoholKETO system, which had some Bragg peaks corresponding to crystalline ketoprofen at the time of manufacture, appears to remain in a semi-crystalline state throughout the 12 weeks study without any significant change in peak intensity for samples stored at 0% RH and 75% RH. The PVAPKETO system, which had some small Bragg peaks corresponding to crystalline ketoprofen at the time of manufacture, displays peaks which are similar in intensity at 12 weeks in the sample stored at 0% RH and peaks which are slightly more intense at 12 weeks in the sample stored at 75% RH.

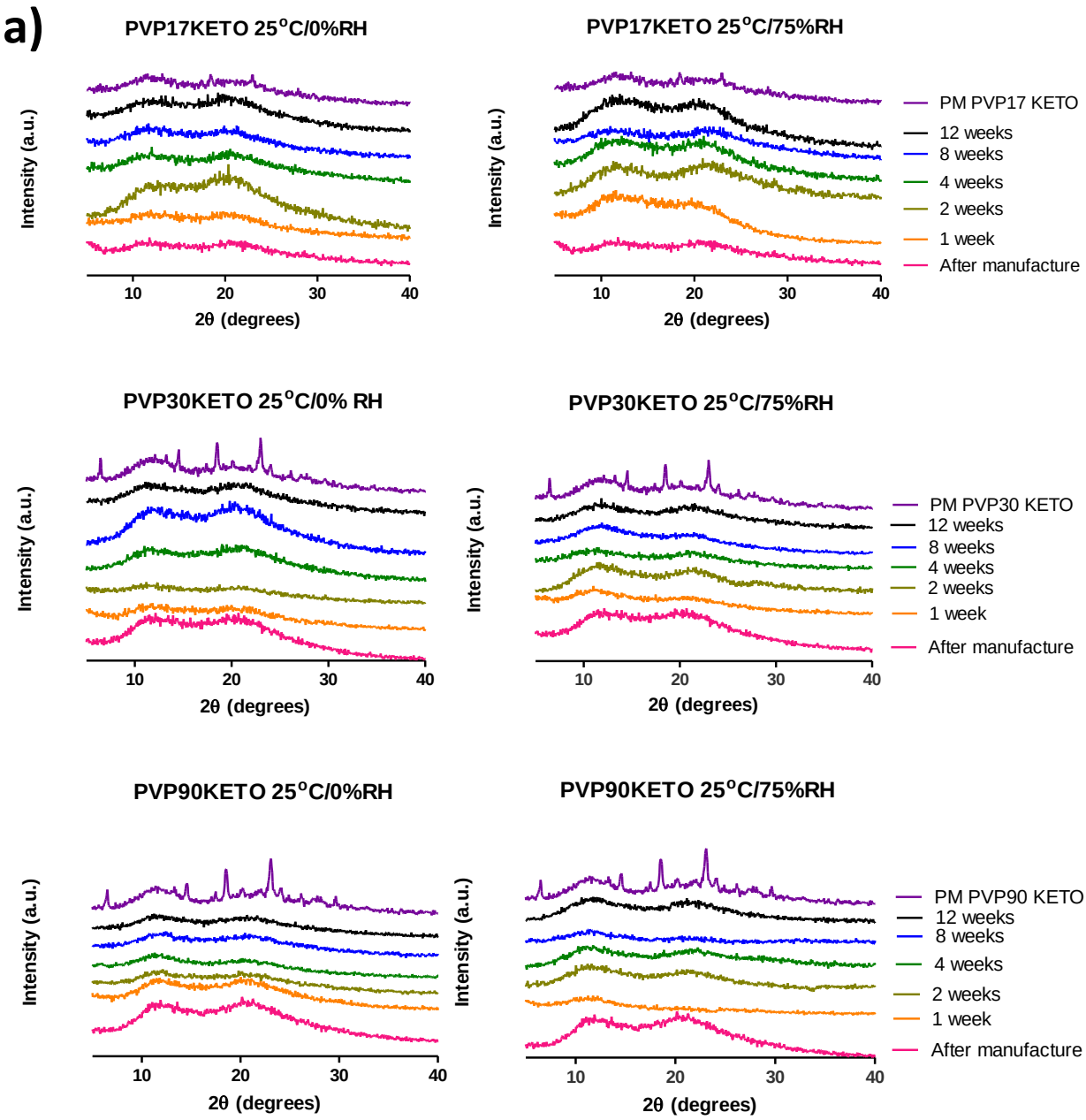

Figure 4.21 a) pXRD patterns of PVPKETO systems stored at 0% or 75% RH at 25 °C for 12 weeks

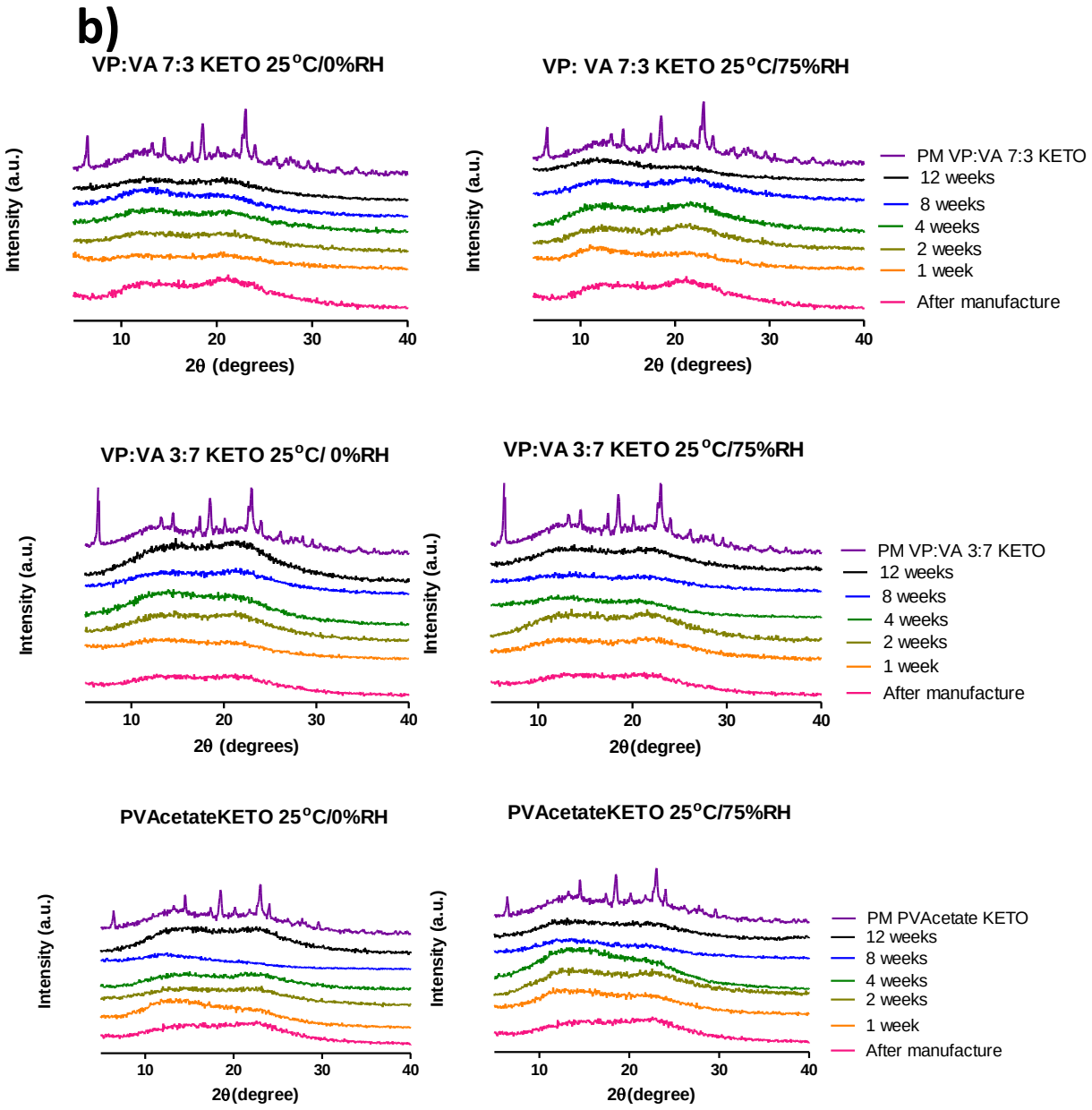

Figure 4.21 b) pXRD patterns of VP: VA 7:3 KETO, VP: VA 3:7 KETO and PVAcetateKETO systems stored at 0% or 75% RH at 25 °C for 12 weeks

c)

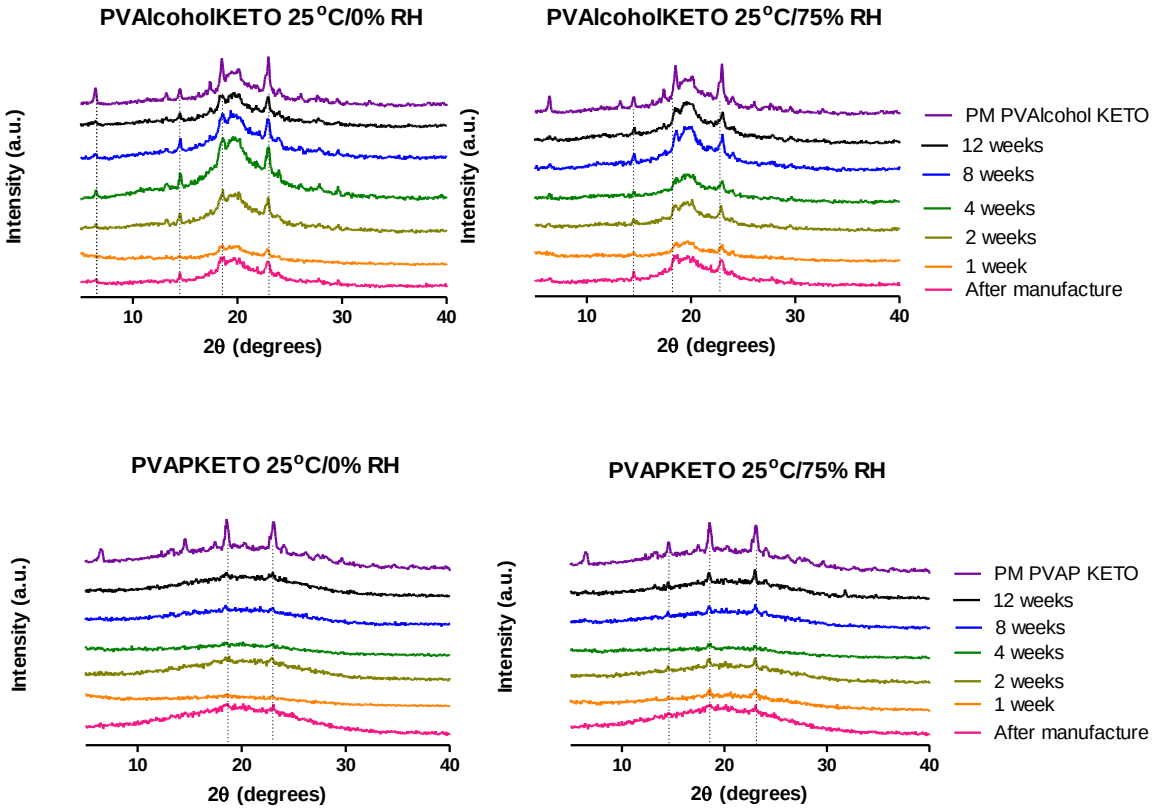

Figure 4.21 c) pXRD patterns of PVAPKETO and PVAlcoholKETO systems stored at 0% or 75% RH at 25 °C for 12 weeks

The glass transition onset temperatures and glass transition temperature widths of the same systems stored at 75% RH are shown in Figure 4.22. As can be seen in Figure 4.22a) the PVPKETO system which had the most significant glass transition onset temperature shift upon exposure to humidity was the PVP17KETO system. While the glass transition onset temperature of PVP17KETO, PVP30KETO and PVP90KETO were all similar after manufacture, it is apparent that after 12 weeks exposure to 75% RH the lower molecular weight PVP has a glass transition onset temperature which is more depressed, indicating increased water sorption relative to the other systems. Interestingly, the glass transition temperature widths, which may be considered a measure of the homogenity of the system [243], increased for all PVPKETO systems after 12 weeks exposure to moisture. This is likely due to the presence of moisture causing the system to become a ternary system of water, polymer and ketoprofen causing heterogeneity in the sample. There is no relationship apparent between the molecular weight of the polymer and the increase in glass transition temperature width over time

Figure 4.22b) shows the glass transition onset temperatures and glass transition temperature widths of the VP:VA KETO systems as well as the PVAcetateKETO and PVP30KETO systems. Directly after manufacture it is clear that the systems with higher vinyl pyrrolidone content have higher glass transition onset temperatures. After 12 weeks of storage at 75% RH, it is clear that the glass transition onset temperatures of the high vinyl actetate content samples (i.e. VP:VA 3:7 KETO and PVAcetateKETO) have not changed, while those with high vinyl pyrrolidone content (VP: VA 7:3 KETO AND PVP30KETO) have decreased. This is due to water sorption of the systems which depresses the glass transition temperature. Interestingly, the glass transition onset temperature of the PVP30KETO system and the VP:VA 3:7 KETO system were very similar after 12 weeks. The glass transition temperature width of the high vinyl pyrrolidone content systems also increased substantially over the 12 week time frame. The PVAlcohol and PVAP systems had no change in glass transition temperature over the time frame studied and a much smaller increase in glass transition temperature span relative to the other systems studied as shown in Figure 4.22 c).

a)

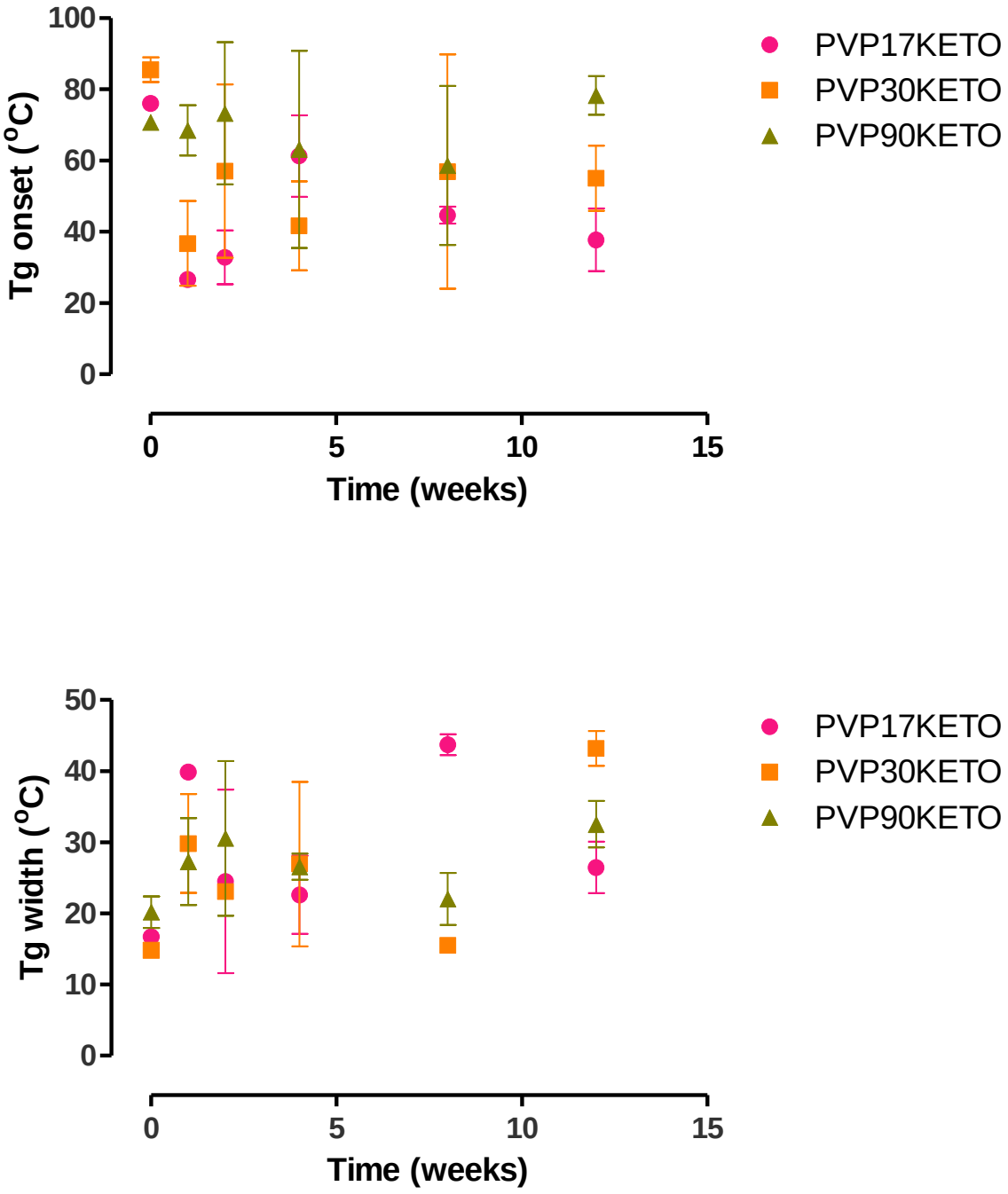

Figure 4.22 a) Glass transition onset temperatures and glass transition temperature widths of PVPKETO systems stored at 75% RH at 25 °C for 12 weeks

b)

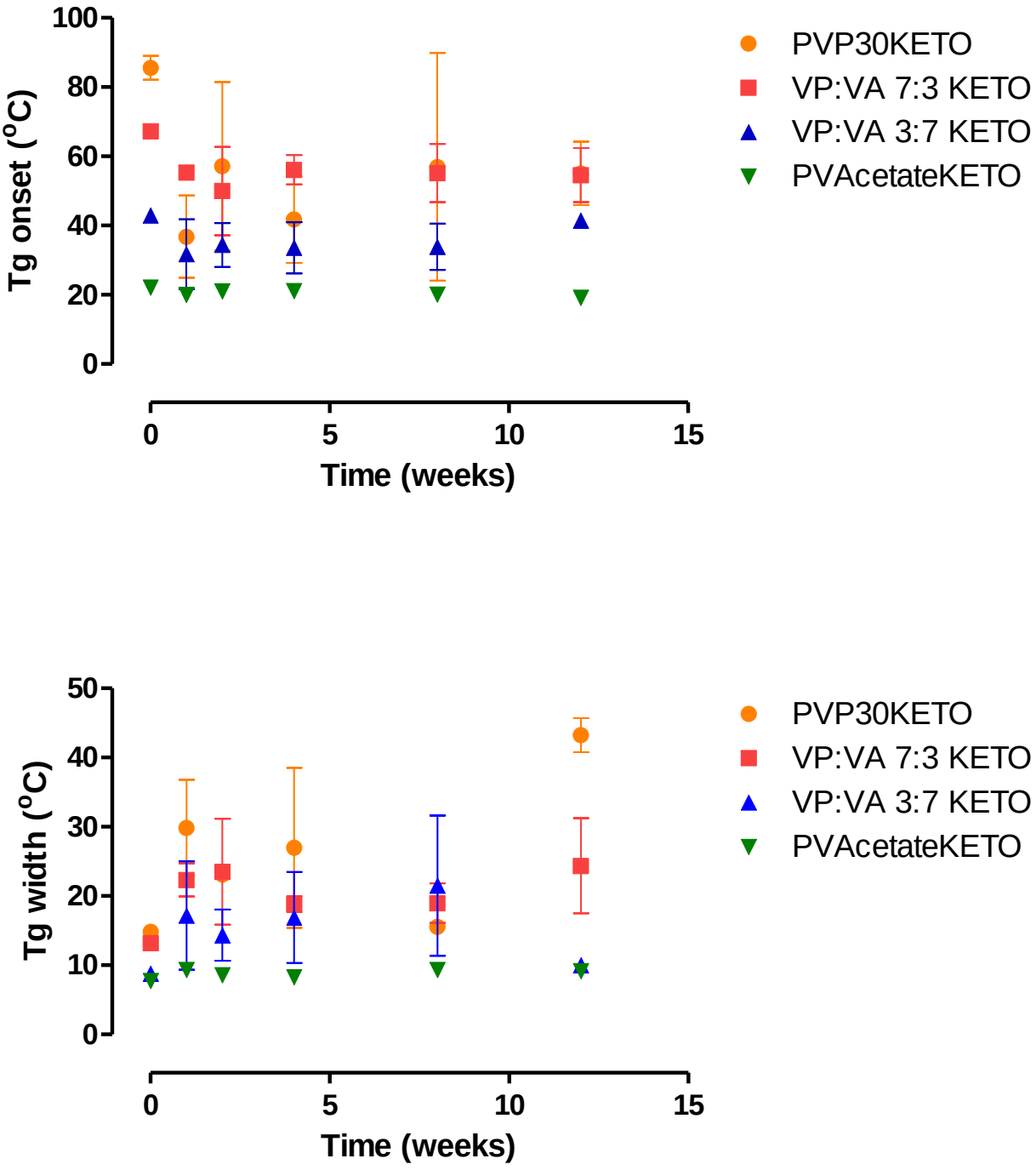

Figure 4.22 b) Glass transition onset temperatures and glass transition temperature widths of VP:VA KETO systems stored at 75% RH at 25 °C for 12 weeks

c)

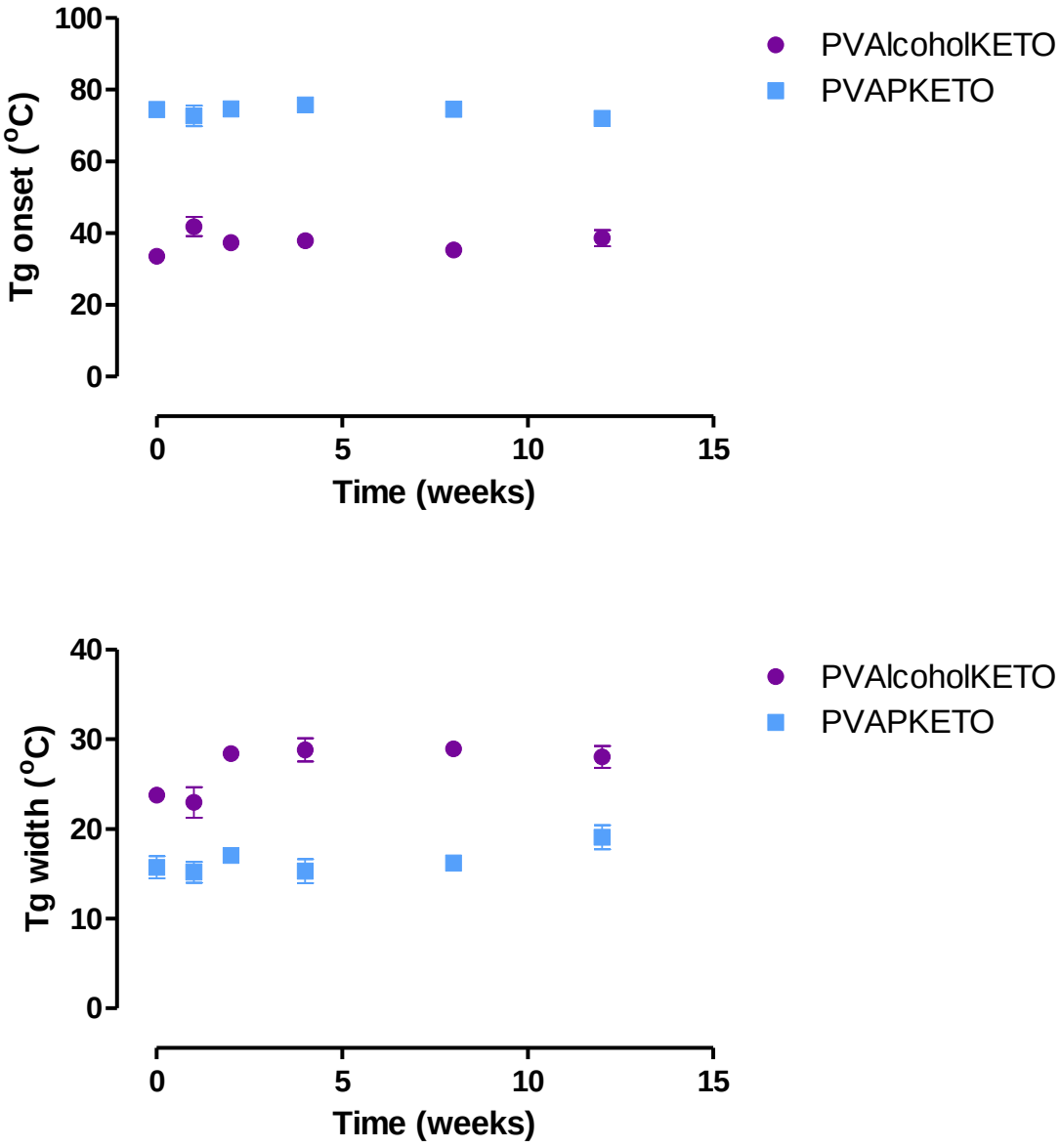

Figure 4.22 c) Glass transition onset temperatures and glass transition temperature widths of PVAlcoholKETO and PVAPKETO systems stored at 75% RH at 25 °C for 12 weeks

4.2.6 Influence of polymer choice on the processability of ASDs

4.2.6.1 Density and compressibility

The density and Carr's Compressibility Index (CCI) values for all melt quenched cryo-milled ketoprofen 20% w/w systems are shown in Table 4.4 and graphed, with significance levels indicated in Figure 4.23.

Table 4.4: Density and Carr's Compressibility Index values for melt-quenched cryo-milled polymer-ketoprofen systems. Mean values ± standard deviation

Polymer-ketoprofen system	True density (g/cm^3)	Bulk density (g/cm^3)	Tapped density (g/cm^3)	CCI
PVP90KETO	1.293 ± 0.001	0.244 ± 0.018	0.397 ± 0.033	38.50 ± 3.12
PVP30KETO	1.306 ± 0.002	0.237 ± 0.023	0.397 ± 0.063	40.00 ± 4.00
PVP17KETO	1.305 ± 0.002	0.267 ± 0.036	0.490 ± 0.039	45.50 ± 7.26
VP:VA 7:3 KETO	1.254 ± 0.004	0.212 ± 0.023	0.377 ± 0.032	43.71 ± 6.43
VP:VA 3:7 KETO	1.288 ± 0.001	0.264 ± 0.005	0.447 ± 0.021	40.67 ± 4.16
PVAcetateKETO	1.357 ± 0.001	0.112 ± 0.024	0.202 ± 0.019	45.00 ± 6.08
PVAlcoholKETO	1.396 ± 0.001	0.224 ± 0.005	0.439 ± 0.004	49.17 ± 1.44
PVAPKETO	1.461 ± 0.007	0.285 ± 0.019	0.589 ± 0.044	51.71 ± 0.40

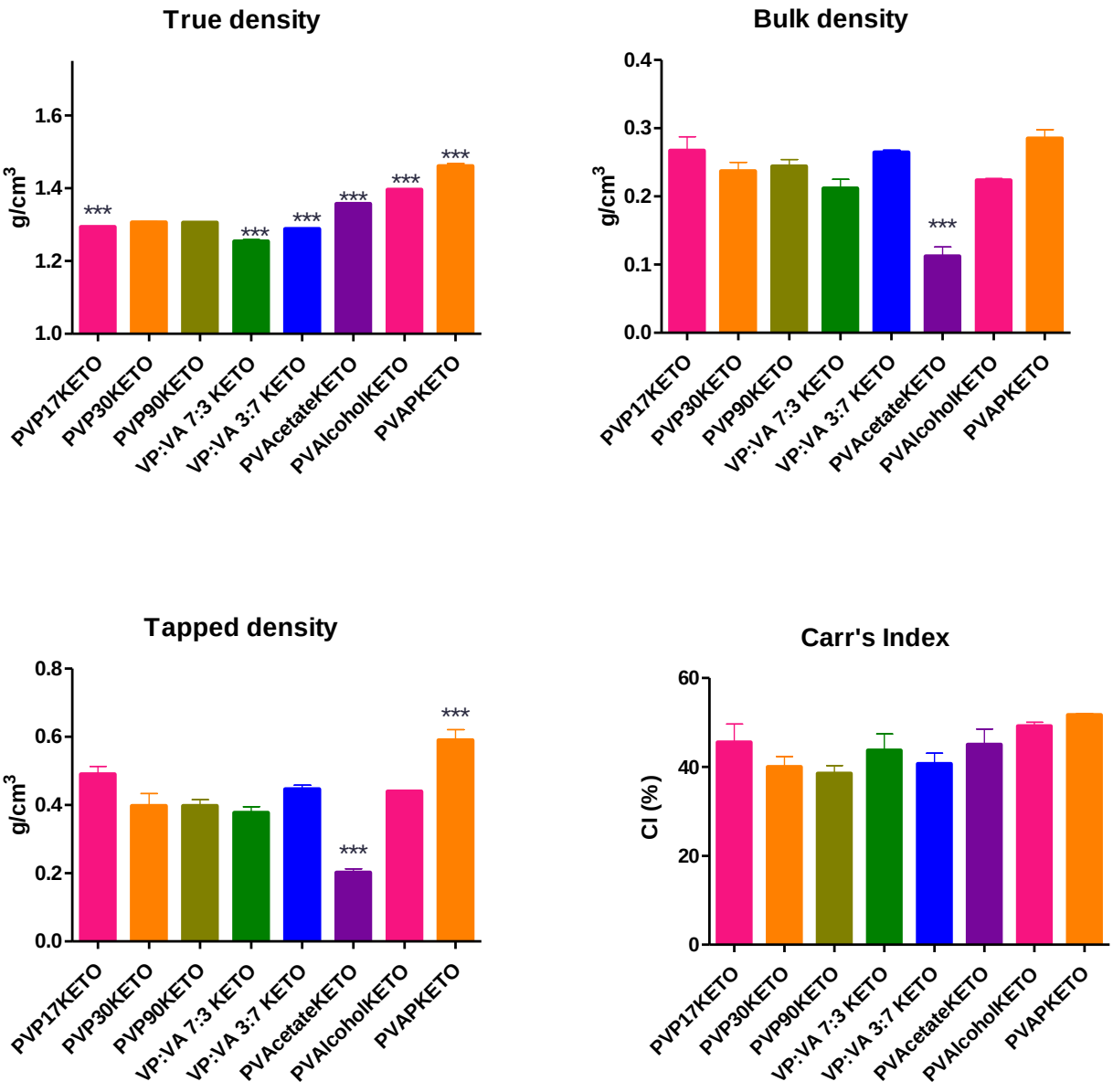

Figure 4.23: Density and Carr's Compressibility Index (CI) values for melt quenched cryo-milled polymer- ketoprofen systems. Highly statistically significant difference ($p<0.001$) from PVP30KETO system denoted by *.**

Regarding true density, it is interesting to note that the two highest values are for the semi-crystalline systems, PVAlcoholKETO and PVAPKETO. This is not unexpected as the crystallinity means that the material is more tightly packed and therefore denser [230]. However, when we examine the true density of these polymers (Table 4.2) it is clear that the polymers themselves have high density values. Although there is a statistically significant difference between PVP30KETO and PVP17KETO, there is no trend apparent in the true densities of PVPKETO systems of differing molecular weights. There does appear to be a trend towards increasing true density with increasing vinyl acetate ratio.

Relative to the PVP30KETO samples, only PVAcetateKETO showed a statistically significantly different bulk density value. This is likely because PVAcetateKETO is a supercooled liquid at room temperature (Tg=21 ^{o}C). It would be expected that a supercooled liquid would have a lower density than a substance in the amorphous/glassy state.

Relative to the PVP30KETO samples, only PVAcetateKETO and PVAPKETO had statistically significantly lower and higher tapped density values respectively. The lower tapped density for PVAcetateKETO probably stems from the fact that it is a supercooled liquid at room temperature as outlined above. As the PVAPKETO sample was partially crystalline, the higher density is logical as crystalline material is denser than amorphous material.

There is no statistically significant difference in the densities (bulk or tapped) of PVPKETO of different molecular weights or with polymer-ketoprofen systems with different VP:VA substitution ratios.

The differences observed in bulk/tapped density values did not translate into a difference in CCI values. Three of the samples (PVP30KETO, PVP90KETO and VP:VA 7:3) had CCI values of 36 which mean they would classified as powders exhibiting “very poor flow” in accordance with the British Pharmacopoeial Classification system [244]. The other samples all have CCI values > 37 meaning they are classified as exhibiting “very very poor flow”. None of these samples are ideal candidates for direct compression as they may struggle to flow from a hopper into a die. This suggests that granulation or the addition of a binder may be required for these samples to be compressed into tablets [122].

4.2.6.2 Tensile strength and ejection force

The tensile strength of tablets formed from the melt-quenched cryo-milled powders combined with MCC in a 1:1 w/w ratio, as well as the ejection force required to remove the tablet from the die, as

described in Chapter 2 Section 2.2.1.4.1, are shown in Figure 4.24. A physical mixture of polymer: ketoprofen: MCC 4:1:5 w/w/w was also tabletted for reference.

In general, the solid dispersion tablets have higher tensile strength and require less force for die-ejection than the physical mix, with some notable exceptions. The VP:VA 7:3 KETO and PVAPKETO solid dispersion tablets had very similar tensile strengths to their equivalent physical mixtures. The PVAcetateKETO solid dispersion tablets were weaker than their equivalent physical mixture. This may be explained by considering that the PVAcetateKETO system has a glass transition onset temperature (21 ^{o}C) very close to room temperature and therefore exists in the rubbery state at test conditions. This may mean that the mechanism by which the tablet deforms and breaks is different from the equivalent crystalline or amorphous state. This was observed experimentally as the PVAcetateKETO tablets were malleable and the force applied by the hardness testing machine resulted in tablet deformation rather than breakage, as was observed for all other systems. In addition to this, it was observed that the PVAcetateKETO system formed large rubbery clumps when allowed to equilibrate to room temperature, and as tensile strength is known to be inversely related to particle size [245], this result is not entirely unexpected.

The relationship between tensile strength and particle size may also explain how most of the POLYMERKETO solid dispersion system tablets were stronger than their equivalent physical mixture as they were milled as part of the method used to produce them. Another explanation for the solid dispersion tablet strength superiority may be that amorphous particles have been shown to have higher effective interparticulate contact area and stronger interparticulate bonding than crystalline particles, as has been shown to be the case for lactose [246]. This results in stronger compacts.

No trend was observed with regard to polymer molecular weight or substitution ratio and tablet tensile strength. However, the POLYMERKETO systems containing the vinyl pyrrolidone group (PVP17KETO, PVP30KETO, PVP90KETO, VP:VA 7:3 KETO, VP:VA 3:7 KETO) had higher tensile strengths than the systems which did not have this functional group. As PVP is also used as a binder excipient in formulations, and increasing the binder concentration is known to increase tablet hardness [122], the vinyl pyrrolidone moiety in solid dispersions has a dual functionality as a polymeric carrier but also as a binder.

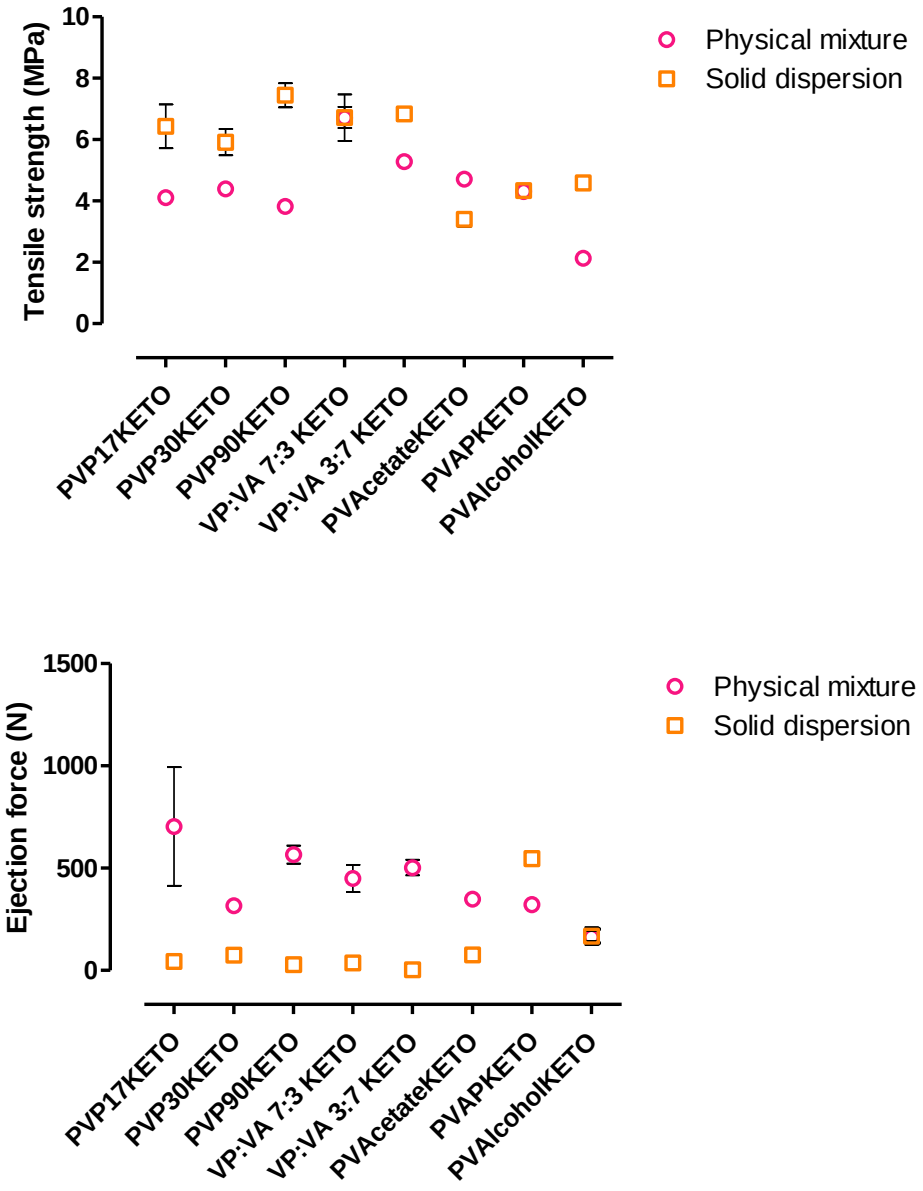

Figure 4.24: Tensile strength and ejection force of tablets formed from POLYMERKETO solid dispersion systems and equivalent physical mixtures

4.3 Conclusion:

This work has demonstrated that the choice of polymer when formulating a solid dispersion is critical to the material properties of the final product. Hydrogen bonding between the drug and polymer of choice is generally desirable due to the anticipated increase in glass transition temperature, beyond values predicted by the Gordon-Taylor equation (i.e. a positive deviation). However, where intra-molecular hydrogen bonding exists, such as the dimeric bond in ketoprofen, this positive deviation from the predicted glass transition temperature may not materialise due to a net loss in hydrogen bond strength in the system. A negative deviation from predicted glass transition temperature was observed between ketoprofen and vinyl pyrrolidone-vinyl acetate polymers, and the extent of this deviation was found to relate to the VP:VA ratio. The PVP30-ketoprofen system was characterised by a 45 ^{o}C negative deviation while the equivalent VP:VA 7:3 and 3:7 systems were characterised a 22 ^{o}C and 5 ^{o}C negative deviation respectively.

The hydrophilicity of the polymer rather than its ability to fully stabilise the drug in the amorphous state was found to be the predominant factor affecting the degree of supersaturation of ketoprofen in solution. For example, the polyvinyl alcohol-ketoprofen system achieved supersaturation over 2 hours while polyvinyl acetate-ketoprofen did not. This is particularly interesting as ketoprofen in the polyvinyl acetate system was fully amorphous, while ketoprofen in the polyvinyl alcohol system was partially crystalline.

This work has also demonstrated that, where possible, selection of a polymer with binder properties should be considered in order to maximise solid dispersion tablet strength and reduce the number of excipients required to tablet a formulation via direct compression. Polymers with a vinylpyrrolidone functional group appear to be more suitable for direct compression than those without as they produced tablets with higher tensile strengths (>5.9 MPa vs. <4.8).

Chapter 5: A comparison of spray dried and electrosprayed ASD particles

5.1. Introduction

Several amorphisation processes have been established to prepare ASDs of poorly soluble drugs. Such processes include spray drying, freeze-drying and hot melt extrusion [12]. Selection of a suitable amorphisation process must consider the API and polymer physicochemical properties such as the melt temperature, thermal degradation profile, glass transition temperature and solubility. Each method of ASD production has its own benefits and drawbacks and the selection of an inappropriate method may have a deleterious effect on ASD performance [12]. For example, thermolabile drugs such as ramipril, which degrades at its melt temperature, are not suitable candidates for hot melt extrusion without the use of a plasticiser [13]. Amorphisation by spray drying requires that the API of interest be dissolved at an appropriate concentration in a suitable solvent. By their very nature, APIs requiring amorphisation are poorly soluble in water, so spray drying generally necessitates the use of organic solvents to dissolve the compounds of interest. The use of organic solvents may be considered undesirable from both environmental and safety perspectives. The need for novel amorphisation methods is apparent and several groups have pioneered new techniques to generate ASDs, such as microwave methods [247,248], using friction and shear force [249] as well as amorphisation in situ [99]. Another pharmaceutical amorphisation technology which is gaining attention is the electrohydrodynamic route i.e. the production of amorphous particles through the application of an electrical current to a solution [14,85,250].

In electrohydrodynamic processes a solution is passed through a metal nozzle to which a strong electrical field is applied. When the electric potential between the nozzle and the collector is sufficiently high, fine droplets are formed at the capillary tip due to coulombic repulsion at the solution surface [14,15]. As the droplets travel from the needle tip to the collector, the solvent evaporates. The shape of the solution emerging from the nozzle is dependent on the interplay between the surface tension of the solvent and the electric stress induced at the nozzle orifice [251]. In electrospinning a stable jet of droplets is formed resulting in the production of fibres. By contrast in electrospraying there is no stable jet formation; the droplets form a Taylor cone and spherical particles are produced [14]. Electrospraying is most commonly known for its application in mass spectrometry, however its potential application in the pharmaceutical sector is an area of intensive research [252–254]. Although much of the research to date has been conducted at lab-scale, the potential applications of electrohydrodynamic processes in drug delivery have been demonstrated in the literature. A wide range of poorly water soluble APIs have been successfully formulated in the amorphous form via electrospraying, including indomethacin, ketoprofen, celecoxib and ritonavir [14]. Sustained-release electrosprayed amorphous solid dispersions of naproxen, doxorubicin and cisplatin have also been realised [252]. Due to the experimental scale at which

electrospraying has been conducted thus far, no ASD produced by electrospraying has reached the market thus far.

By contrast, spray drying has been used successfully to manufacture FDA approved ASDs since 1994. There are currently 10 FDA approved ASDs on the market which are amorphized through spray drying [2]. The spray drying process dates back to the 1870s [85] and is an established method of transforming a solution into a solid product. However, it was not until the late 1960s that the solubility enhancement of spray dried APIs was realised [72]. In the spray drying process, a solution is atomised and mixed with a drying gas before the solvent evaporates, allowing for the collection of dried particles which are generally in the low-micron size range [85]. The successful generation of an ASD via spray drying is dependent, not only on the inherent glass forming ability of the drug [4], but also on the solubility of the drug in the polymer [106], the drug polymer ratio used and the solvent system employed [85,255]

One potential advantage of the electrospraying process over spray drying is that it may enable the production of sub-micron particles with a very narrow particle size distribution [251]. The production of nano-amorphous material thus utilises two formulation techniques, disruption of the crystal lattice and particle size reduction. The enhancement in solubility due to nanonisation is explained through the Ostwald–Freundlich theory which describes the inverse relationship between particle size and solubility [55]. However, reducing particle size to the nano-region may result in unintended consequences for the physical stability of the amorphous state, as surface crystallisation is faster than bulk crystallisation [256]. The reduced particle size may also increase the hygroscopicity of the particles due to an increase in surface area and potential for water sorption.

The objective of this work is to compare the particle characteristics and dissolution performances of ASDs produced by the established spray drying method and the newer electrospraying approach. While both processes have been compared in detail in review articles [252,253] there are no head-to-head comparisons of powders produced by spray drying and electrospraying. Ketoprofen is used as a model API and PVP and its vinyl acetate co-polymer PVPVA64 are used as model polymers.

5.2 Results

5.2.1 Solution characterisation

The surface tension, viscosity and conductivity for the studied solutions at 25 °C, measured as described in Chapter 2 Section 2.2.2, are shown in Figure 5.1. The surface tensions for all systems studied were not significantly different (p=0.3) regardless of polymer type or ketoprofen loading.

The viscosity of the solutions increased with increasing polymer concentration and was higher for the solutions containing PVP relative to the solutions containing PVPVA, but this was not statistically significant (p=0.25). This slight difference in viscosity is not surprising as a study examining the melt viscosities of binary mixtures of indomethacin and either PVP or PVPVA found that the viscosity of the PVP/indomethacin mixture was significantly higher than of that of the PVPVA/indomethacin mixture [257].

Interestingly, the conductivity was dramatically different (p<0.001) for solutions containing the two structurally related polymers. The PVPVA containing solutions had very low electrical conductivity (<5 µS/cm) while the PVP containing solutions exhibited higher conductivity (>20 µS/cm), which increased with increasing PVP content, as has previously been observed [258]. This higher conductivity can be attributed to the high hygroscopicity of PVP relative to its vinyl acetate co-polymer [259,260]. This increase in electrical conductivity due to adsorbed moisture has previously been described for silica [261]. In electrohydrodynamic processes, as the electrical conductivity of a solution increases, the size of the particles produced decreases [14,262,263]. Therefore, it may be expected that particles produced by electrospraying from PVPVA-containing solutions will be larger than those produced using PVP-containing solutions.

As the material properties of particles produced by electrohydrodynamic processes are known to be a result of the interplay between surface tension, conductivity and solution viscosity and the only significant difference between the two sets of polymer solutions is the conductivity, it may be inferred that any difference in morphology may be attributed to this physicochemical difference.

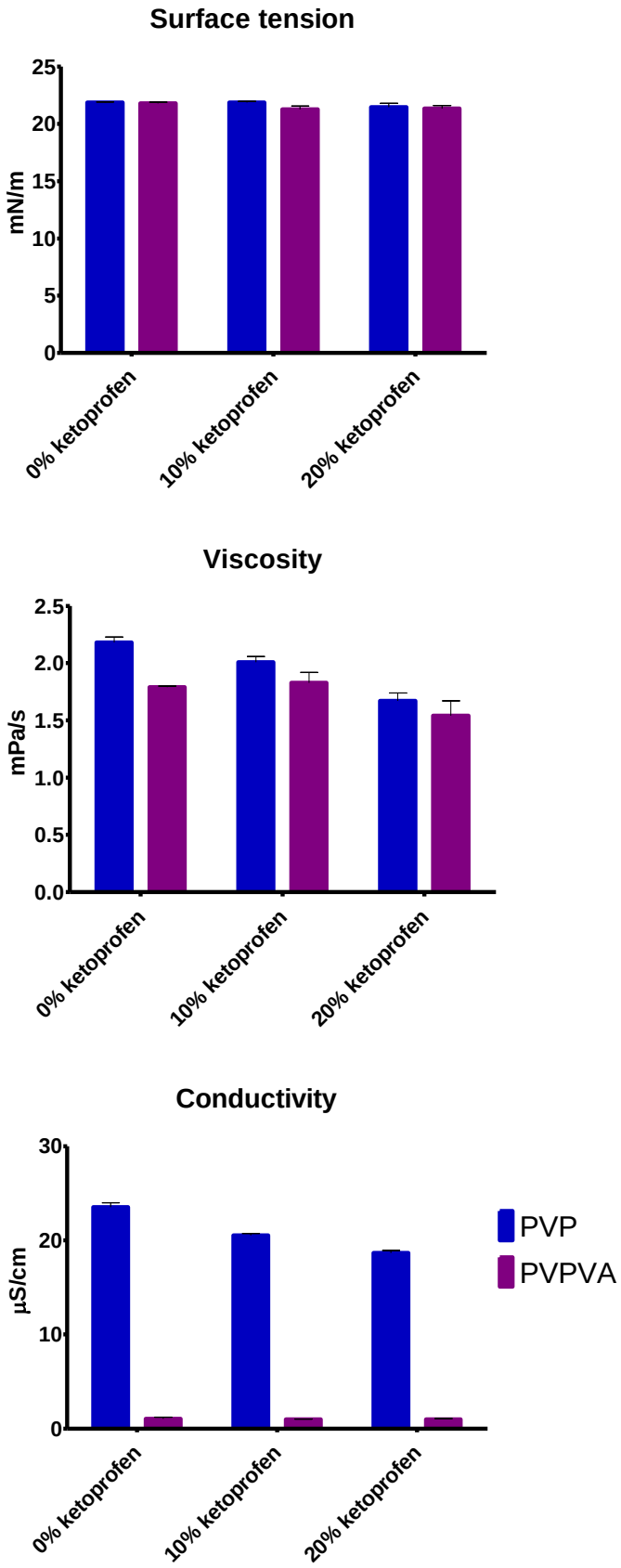

Figure 5.1: Surface tension, viscosity and conductivity of solutions subjected to spray drying and electrospraying

5.2.2 Particle morphology and size distribution analysis

5.2.2.1 Morphology of particles

Figure 5.2 shows SEM images of the particles produced by electrospraying and spray drying. Solutions containing no ketoprofen (i.e. polymer in ethanolic solutions), when spray dried, produced particles which displayed a "deflated balloon" morphology. This was observed for both PVP and PVPVA spray dried particles (Figure 5.2b and 5.2d). The appearance of this deflated balloon/shell morphology has previously been described for spray dried particles and can be explained through consideration of the dimensionless unit called the Peclet number. This parameter describes the relative speeds of the radial velocity of the receding droplet surface and the diffusional motion of the solute [264]. The Peclet number can be calculated using Equation 5.1

$$Pe_i = \frac{\mathrm{K}}{8D_i} \qquad \textbf{Equation 5.1}$$

In the above equation, K represents the evaporation rate of the solvent and D_i represents the diffusion coefficient of solute *i*. When the Peclet number is below 1 the diffusional motion is fast relative to the radial velocity of the droplet surface which means that there is an even distribution of solute precipitating at the surface of the particle and typically a solid sphere will form. In contrast, when the Peclet number is higher than 1, the surface of the droplet is evaporating more rapidly than the solute in the bulk of the droplet is diffusing to the surface. This results in the formation of voids and a shell morphology, which can collapse resulting in the observed deflated balloon effect [252,264]. Particles of the same composition produced by electrospraying were mostly spherical and without deformation (Figure 5.2a and 5.2c). The difference in morphology is evidence that the relative ratios between evaporation rate of solvent and diffusional motion of solute is different in spray drying and electrospraying. It may be that the lack of applied heat in electrospraying reduces the evaporation rate allowing the solute more time to diffuse through the droplet, resulting in a solid particle [252].

It is also clear that the two processes have produced particles with differing size ranges. While there are some fine particles in the sub-micron range produced by spray drying there are some larger particles spanning approximately 5 µm onto which finer particles have agglomerated. This is the case for both PVP and PVPVA. By contrast, the polymer particles produced by electrospraying are in the sub-micron range and in the case of PVP are relatively monodisperse and uniform in appearance. While the PVPVA particles produced by electrospraying are smaller than their spray dried counterpart, their morphology appears to be non-uniform with some spherical particles co-existing with oblong non-spherical particles.

When a binary mixture of either PVP or PVPVA and ketoprofen is spray dried the loss of the deflated balloon structure is apparent (Figure 5.2f, h, j, l). The morphology of these spray dried particles is spherical and there is no apparent difference in terms of shape or size between the two polymer systems or on increasing drug loading from 10% w/w to 20% w/w. This change in morphology to a solid sphere may be explained by considering that the solute being spray dried is now a binary system and therefore the diffusion co-efficient D_i will be different to that of a simple polymer solution in ethanol. As the spray drying parameters were consistent for all samples, it would not be anticipated that the evaporation rate changed significantly between the polymer and polymer-drug systems. Therefore, it may be inferred from this change in morphology that the diffusion co-efficient of ketoprofen and PVP or PVPVA mixtures in ethanol is higher than PVP or PVPVA in ethanol.

When the binary mixtures of PVP and ketoprofen were electrosprayed (Figure 5.2e, i), the same spherical morphology resulted as was observed for the polymer-only particles. The size and morphology of these PVP-ketoprofen particles appear monodisperse and uniform. By contrast, when binary mixtures of PVPVA and ketoprofen were electrosprayed (Figure 5.2 g, k) the morphology was a mixture of spheres and disk-shaped particles. Some "webbing" between the particles may also be observed. This may indicate that the jet produced at the nozzle orifice in the electrohydrodynamic process was alternating between stable and unstable modes, resulting in a mixture of electrospraying and electrospinning. The presence of electrosprayed beads co-existing with electrospun fibres has previously been described, and although having a hybrid morphology may have beneficial applications in terms of attaining a dual release profile, it is generally undesirable due to lack of particle uniformity [254]. The appearance of this hybrid morphology has previously been attributed to a low polymer concentration and the associated lower viscosity in the solution which is being processed, as well as a low net charge density which may be due to the conductivity of the solution [265]. Although the polymer concentration is the same for both PVP and PVPVA systems the viscosity of the PVPVA systems is slightly lower than the PVP systems as shown in Figure 5.1. The conductivity of the PVPVA system is significantly lower than in the PVP systems which is probably due to the higher moisture present in the PVP system. A combination of the lower viscosity and lower conductivity may explain the "bead on a string" morphology observed. Mechanistically speaking, the webbing observed in this study may be explained by the absence of polymer chain entanglements prior to the droplet reaching the Rayleigh limit. The Rayleigh limit is the maximum charge a droplet can hold before becoming unstable and precedes Coulombic fission, whereby smaller droplets are generated due to repulsive effects [266,267]. As the solvent evaporates from the droplet the charge concentration of the droplet increases [251]. As the PVP-ketoprofen systems are more conductive than the PVPVA-ketoprofen systems the charge concentration of

these droplets is higher, meaning that the Rayleigh limit is reached earlier for these droplets and therefore Coulombic fission occurs, resulting in spherical particles. Conversely, the lower conductivity of the PVPVA-ketoprofen systems may mean that the Rayleigh limit is reached at a later stage in the electrospraying process. The droplets therefore do not reduce in size as dramatically as the PVP particles, and at the time of reaching the Rayleigh limit the polymer in the droplet has not reached the polymer volume fraction at which a fully entangled network of polymer chain has formed [267]. This means that the droplet is deformed during the Coulombic fission process and webbing results.

The SEM analysis clearly shows that the morphology of the particles produced is dependent on the drug/polymer ratio, choice of polymer and the production method. Electrospraying produced particles that were largely monodisperse, while spray drying produced agglomerates of larger particles and finer particles. Electrosprayed material prepared using PVP was more uniform in size and morphology compared to material electrosprayed using the structurally related polymer, PVPVA. This may be attributed to the differences in hygroscopicity between the polymers, which in turn leads to a difference in the conductivity of the solutions and affects the interplay of forces in the electrohydrodynamic process. The electrosprayed formulation which was considered optimal was the PVP 20% w/w ketoprofen and approximately 35 mL of this solution was processed to facilitate further material characterisation and dissolution testing.

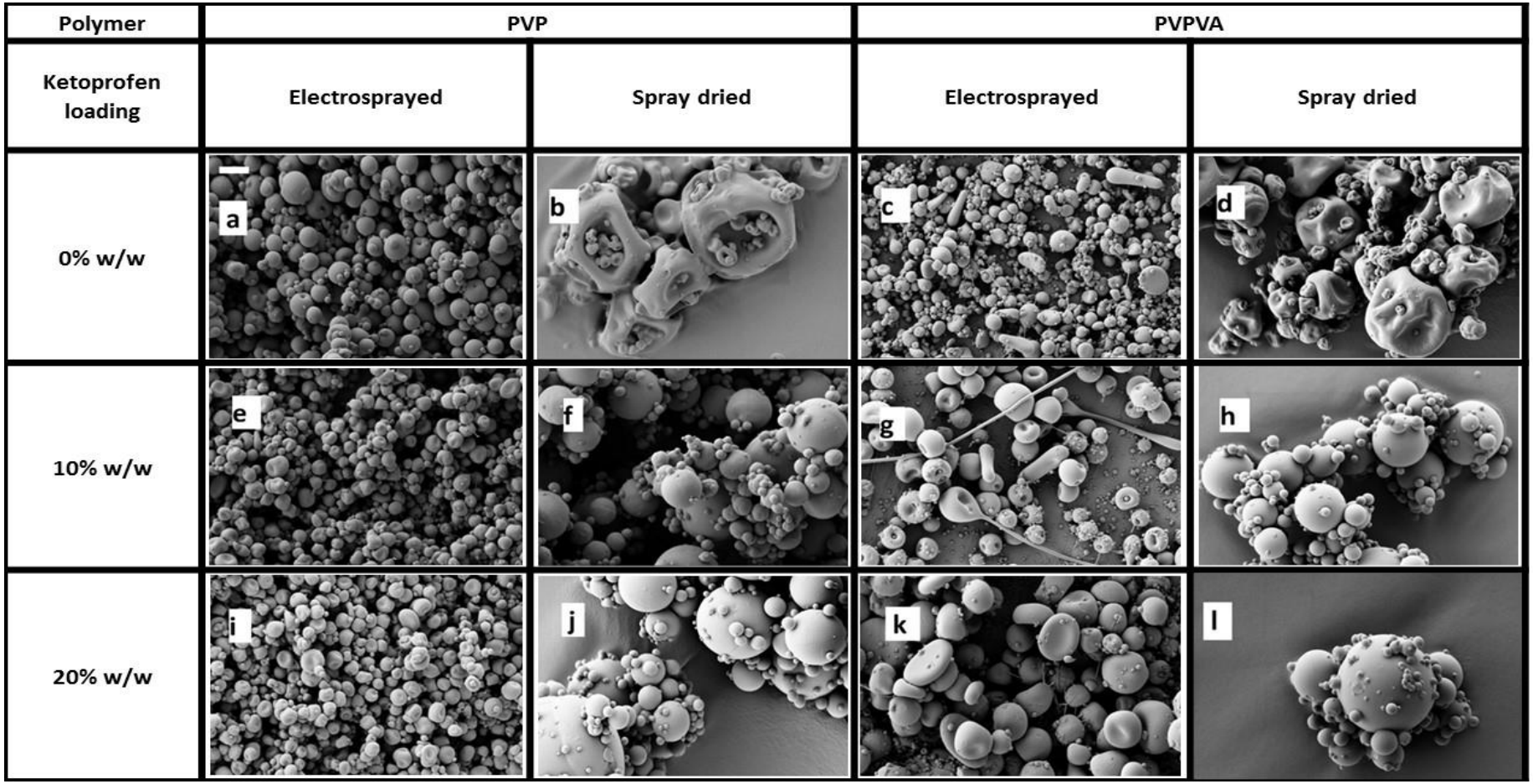

Figure 5.2: SEM images of particles produced using electrospraying and spray drying. The scale bar in image (a) represents 2 µm and is valid for all images.

5.2.2.2 Particle size analysis

Particle size analysis was carried out for particles produced using electrospraying and spray drying using SEM as described in Chapter 2 Section 2.2.3.9.1. The average diameters of the particles are shown in Table 5.1. In all systems, except the PVPVA 20% w/w ketoprofen system, the particles produced by electrospraying have smaller average diameters than those produced by electrospraying. The observed anomaly may be explained by considering the morphology of the particles produced by electrospraying PVPVA particles with 20% w/w ketoprofen loading (Figure 5.2c). These discus shaped particles may not be suitable for the particle sizing methodology which was employed, as this assumed a spherical shape.

There is less error associated with the average diameter values for the particles produced by electrospraying relative to those produced by spray drying, as the particles produced by the former process are more monodisperse than those produced by spray drying. This is reflected in the histograms representing size distributions of the dried particles in Figure 5.3 and Figure 5.4.

Table 5.1: Average diameter and standard error values for electrosprayed (ES) and spray dried (SD) polymer-ketoprofen systems.

Ketoprofen loading	PVP			PVPVA		
	SD (µm)	ES (µm)	p-value	SD (µm)	ES (µm)	p-value
0 % w/w	1.45 ± 0.09	0.89 ± 0.02	<0.0001	1.35 ± 0.09	0.68 ± 0.02	<0.0001
10% w/w	1.13 ± 0.06	0.79 ± 0.01	0.0742	1.08 ± 0.05	0.64 ± 0.03	<0.0001
20% w/w	1.11 ± 0.08	0.79 ± 0.02	0.2205	0.95 ± 0.06	1.12 ± 0.05	0.0225

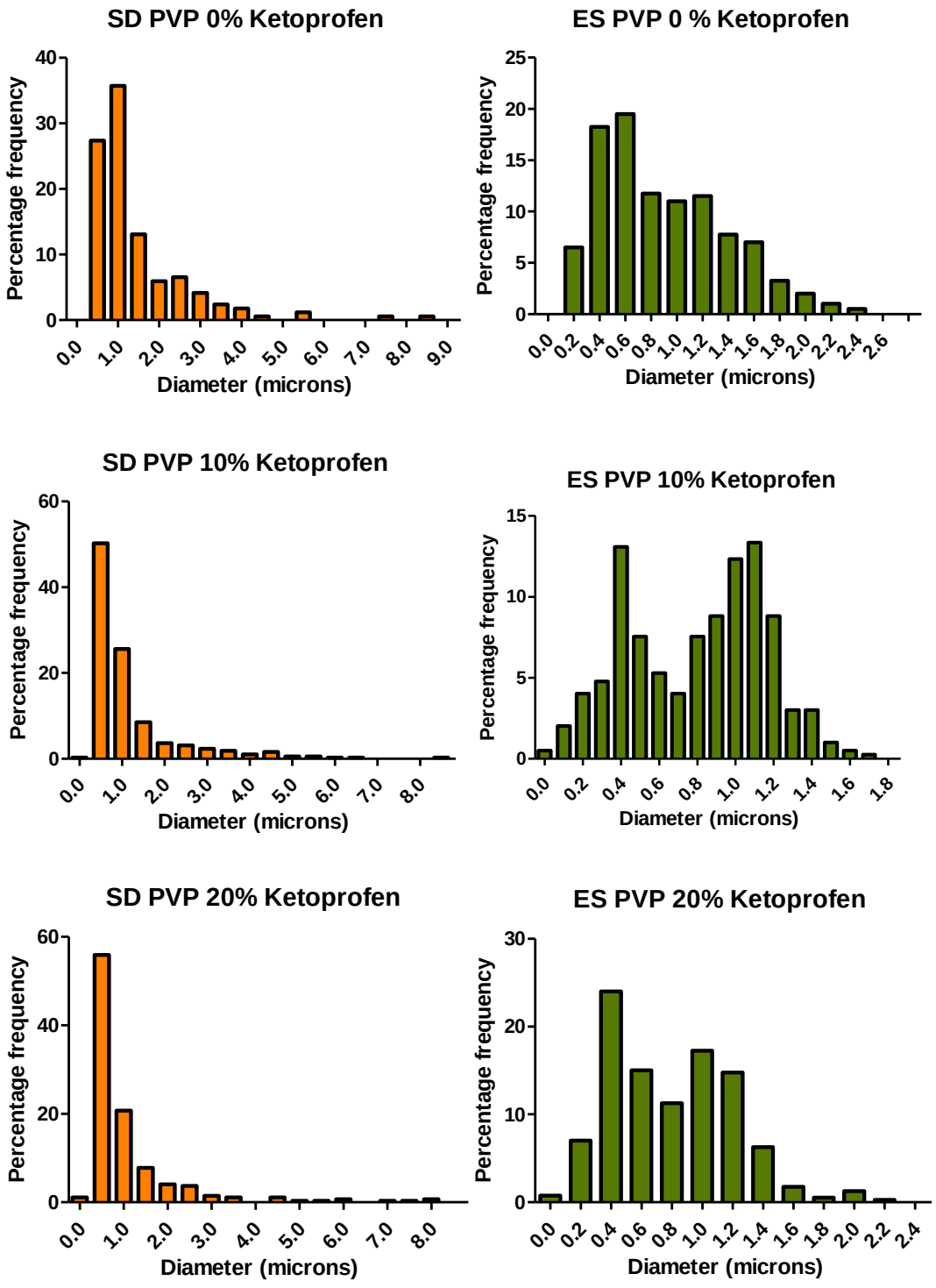

Figure 5.3: Particle size distribution for electrosprayed (ES) and spray dried (SD) PVP-ketoprofen systems

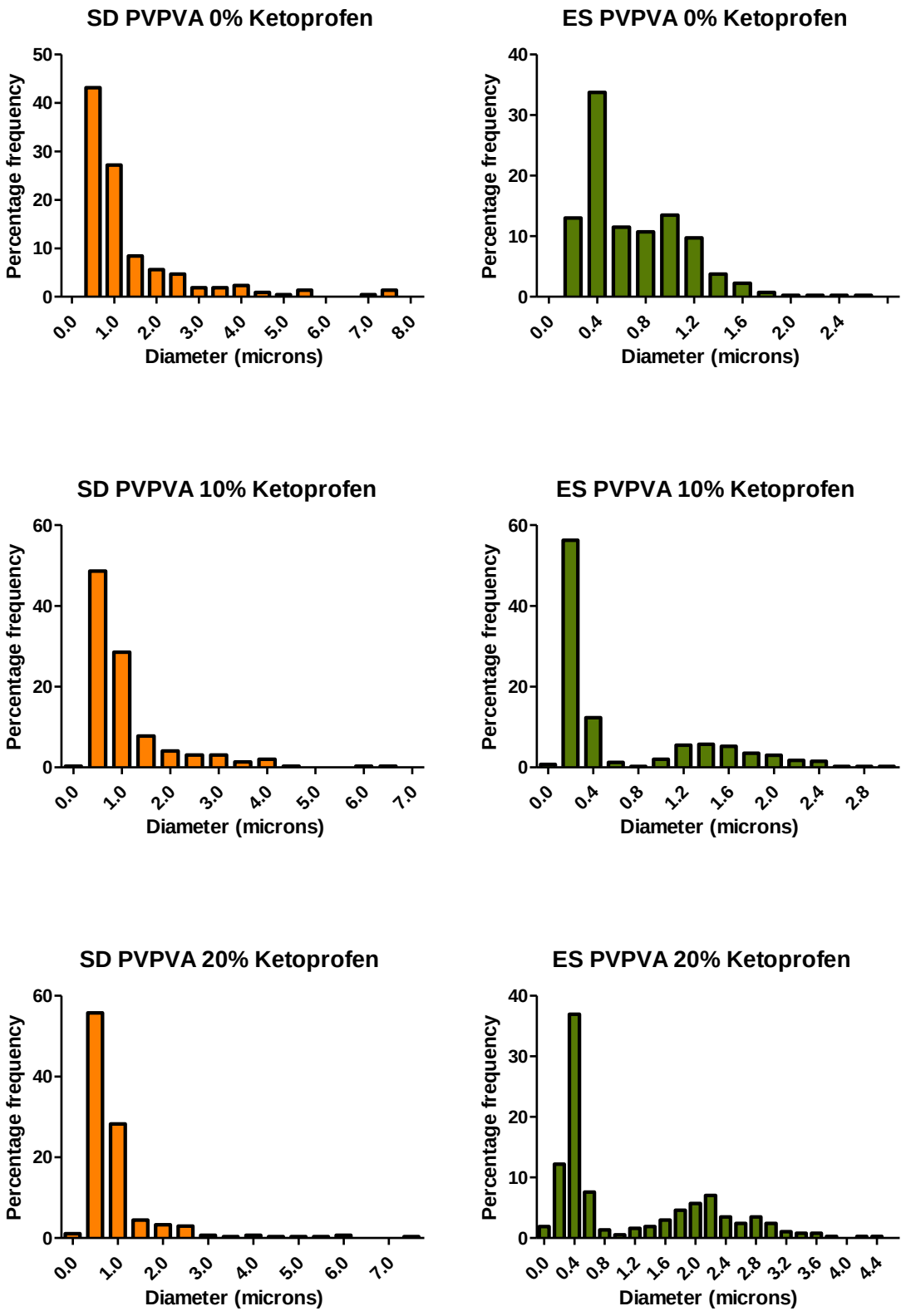

Figure 5.4: Particle size distribution for electrosprayed (ES) and spray dried (SD) PVPVA-ketoprofen systems

5.2.3 Solid state characterisation

5.2.3.1 Thermal analysis

Modulated differential scanning calorimetry traces for the particles produced by electrospraying and spray drying with PVP are shown in Figure 5.5. Traces i) iii) and v) are of PVP particles produced by spray drying containing no ketoprofen, 10% w/w ketoprofen and 20% w/w ketoprofen respectively. Traces ii) iv) and vi) are the equivalent particles produced by electrospraying. All traces show a single glass transition indicating ketoprofen and PVP miscibility, which has previously been demonstrated in the literature [235,237]. No traces show a melting endotherm, indicating the absence of crystalline ketoprofen. The glass transition onset temperatures for the electrosprayed and spray dried PVP-based particles containing 0% ketoprofen, 10% w/w ketoprofen and 20% w/w ketoprofen are 166 °C, 127 °C and 94 °C respectively. As ketoprofen loading increases the glass transition temperature reduces. This is because the glass transition temperature of ketoprofen is -6°C (Chapter 4 Figure 4.4) and as the mass fraction of this component increases, the glass transition of the amorphous solid dispersion reduces, in accordance with the Gordon-Taylor equation [94]. It is interesting to note that the glass transition onset temperatures are equivalent for particles produced by both processes. This is the first-time thermal profile equivalency has been demonstrated for ASDs produced by electrospraying and spray drying.

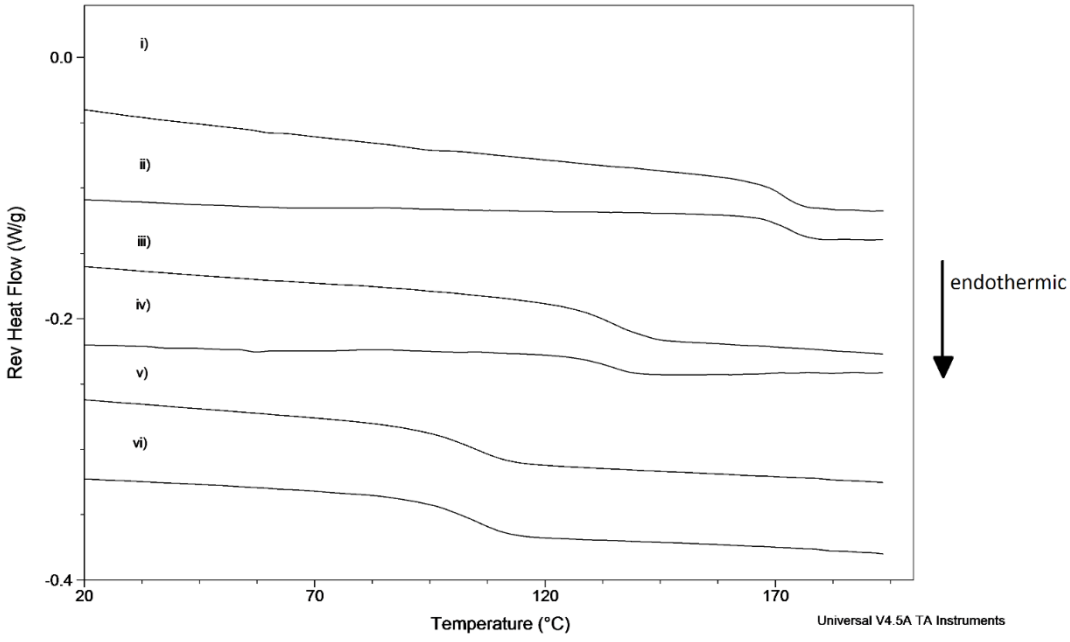

Figure 5.5: Second heating run (i.e. after heating and cooling) of modulated differential scanning calorimetry showing glass transitions i) spray dried PVP ii) electrosprayed PVP iii) spray dried PVP with 10% w/w ketoprofen iv) electrosprayed PVP with 10% w/w ketoprofen v) spray dried PVP with 20% w/w ketoprofen vi) electrosprayed PVP with 20% w/w ketoprofen

5.2.3.2 Thermogravimetric analysis

There was no statistically significant difference (p=0.75) in residual solvent/moisture levels between electrosprayed and spray dried PVP 20% w/w ketoprofen powder. The electrosprayed powder contained 5.31 (± 0.04) % moisture and the spray dried powder contained 5.52 (± 0.48) % moisture. Sample TGA traces are shown in Appendix m).

5.2.3.3 pXRD analysis

The pXRD patterns for the spray dried and electrosprayed PVP and PVPVA powders containing 20% w/w ketoprofen, crystalline ketoprofen and physical mixtures of PVP or PVPVA with 20% w/w crystalline ketoprofen are shown in Figure 5.6. All spray dried and electrosprayed powders show an amorphous halo pattern devoid of Bragg peaks indicating a lack of crystalline material in the powder. This is in contrast to crystalline ketoprofen which has Bragg peaks noticeable at 6 and 22.7 degrees 2θ which is apparent in the physical mixtures of polymer and crystalline ketoprofen (Figure 5.6 f and g). This demonstrates that both processes produced ketoprofen in the amorphous form.

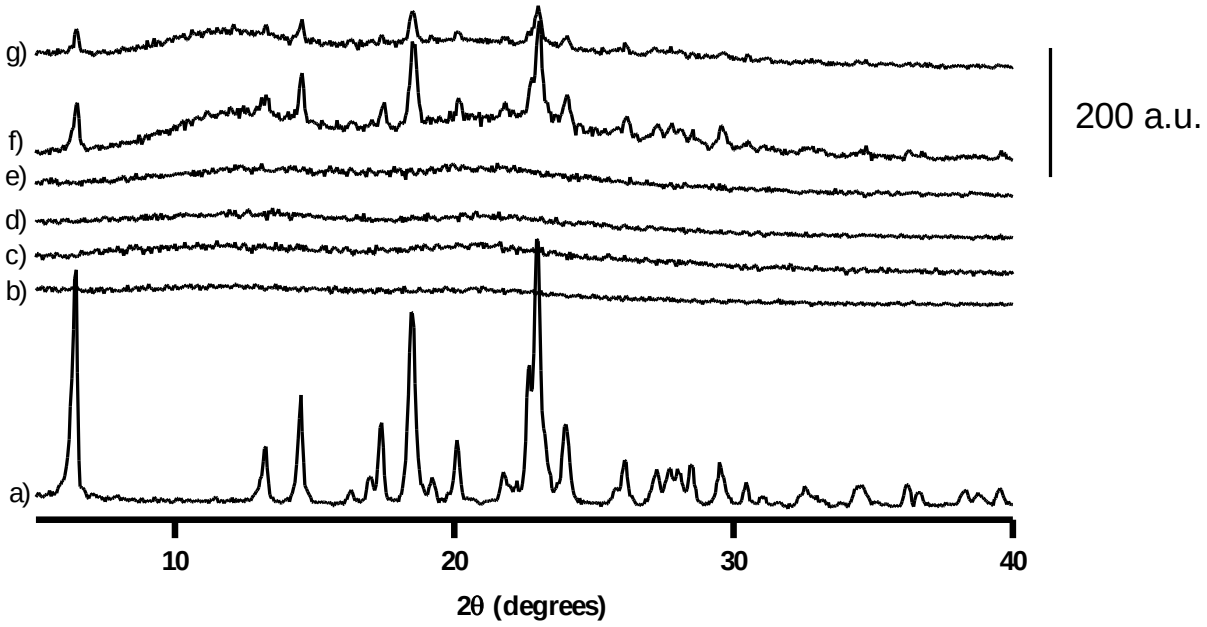

Figure 5.6 Powder X-ray diffraction patterns of: a) crystalline ketoprofen b) electrosprayed PVP 20% w/w ketoprofen c) spray dried PVP 20% w/w ketoprofen d) electrosprayed PVPVA 20% w/w ketoprofen e) spray dried PVPVA 20% w/w ketoprofen f) physical mixture of PVPVA and 20% w/w crystalline ketoprofen g) physical mixture of PVP and 20% w/w crystalline ketoprofen

5.2.3.4 ATR-FTIR analysis

The ATR-FTIR spectra for the spray dried and electrosprayed PVP containing 20% w/w ketoprofen as well as a physical mixture of PVP and crystalline ketoprofen at the same mass ratio is shown in Figure 5.7. It is clear from the spectra that the physical mixture differs in peak location and intensity at several positions from the amorphous solid dispersion. In the fingerprint region, crystalline ketoprofen exhibits a triplet peak centred around 700 cm^{-1}, while amorphous ketoprofen has a doublet peak in this region [11]. The ATR-FTIR spectra supports the pXRD and DSC data which shows that electrospraying and spray drying ketoprofen in combination with PVP results in an amorphous solid dispersion. Ketoprofen has two carbonyl groups, one is the carbonyl involved in the ketone functional group and the other in the carboxylic acid group. The wavenumber of the ketone carbonyl of ketoprofen is 1652 cm^{-1} which is present, and unchanged, in all spectra. This indicates the ketone of ketoprofen in not involved in any intermolecular interaction with the polymer, which is logical as it is in a sterically hindered position. The wavenumber of the dimer hydrogen bonded carboxylic acid carbonyl of ketoprofen is reported at 1690 cm^{-1} in the literature [237], but as this is very close to the peak of the pyrrolidone carbonyl (1681 cm^{-1}) there is often an overlap and distinguishing one peak from another may be challenging. In Figure 5.7, the mixture of PVP and crystalline ketoprofen shows the dimer hydrogen bonded carboxylic acid carbonyl of ketoprofen at 1690 cm^{-1}. Interestingly, the spray dried and electrosprayed samples lack this peak as it has merged with the peaks of the ketone of ketoprofen and the vinyl pyrrolidone peak which indicates increased hydrogen bonding [268]. The physical mixture of crystalline ketoprofen and PVP shows an additional peak at 1735 cm^{-1} which has been assigned by other authors to the free acid carbonyl of the carboxylic acid group, which is visible due to the presence of monomeric ketoprofen [11,237,238,240]. In the amorphous electrosprayed and spray dried material this free acid carbonyl is still visible but has shifted to a lower wavenumber at 1723 cm^{-1}, which again indicates hydrogen bonding between this functional group in ketoprofen and the polymer PVP. This data indicates that the intermolecular interaction between PVP and ketoprofen has not been affected by the amorphisation method chosen to produce the ketoprofen amorphous solid dispersion.

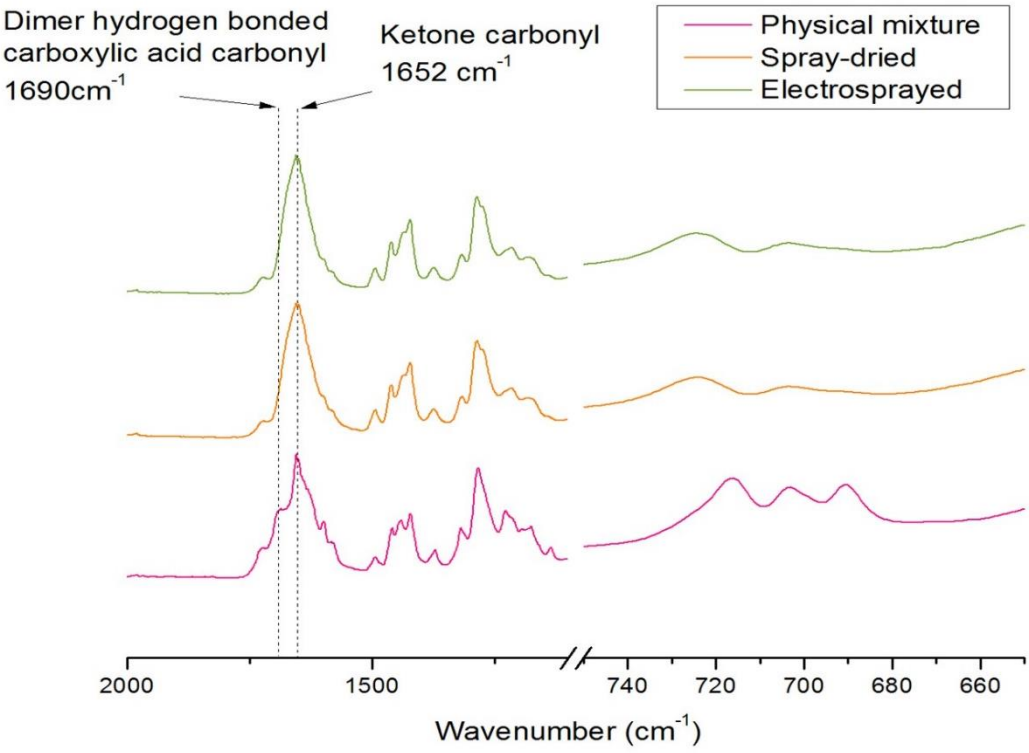

Figure 5.7: ATR-FTIR spectra for electrosprayed and spray dried amorphous solid dispersions of PVP and ketoprofen 20% w/w. A physical mixture of PVP and crystalline ketoprofen 20% w/w is included as a control.

5.2.3.5 Specific surface area analysis

The amorphous solid dispersion of ketoprofen produced by spray drying had a specific surface area of 1.97 (± 0.16) m^2/g, while the amorphous solid dispersion of ketoprofen produced by electrospraying had a specific surface area of 3.01 (± 0.12) m^2/g. This difference in specific surface area corresponds with the particle size results described in Section 5.2.2.2. Reduction in particle size is one strategy to increase the dissolution rate of poorly soluble drugs [254], in accordance with the Nernst-Brunner equation [38].

However, an increase in surface area may also be detrimental to the amorphous state stability of an ASD. It has previously been demonstrated that indomethacin crystallizes more rapidly in particles with a smaller particle size which has been explained by the surface mediated nucleation effect [256]. Similarly, felodipine has been shown to crystallise six times faster on the surface of the material relative to the bulk of the material [58,208]. This work has demonstrated for the first time that the specific surface area of an electrosprayed ASD is higher than the equivalent spray dried ASD.

5.2.4 Drug loading

The ketoprofen loadings for the PVP samples produced via spray drying and electrospraying which have theoretical ketoprofen contents of 20% w/w were 95.63 ± 1.81 % and 97.37 ± 1.56 %, respectively. The actual ketoprofen concentration was close to the theoretical concentration of ketoprofen, and there was no statistically significant difference in the ketoprofen loading between the ASDs prepared via spray drying and electrospraying as indicated by a p-value of 0.278.

5.2.5 Dissolution performance

The dissolution profiles of the amorphous solid dispersions of ketoprofen produced by spray drying and electrospraying containing 20% w/w ketoprofen at pH 1.2 in a flow through cell dissolution apparatus are shown in Figure 5.8. A physical mixture of PVP with 20% w/w crystalline ketoprofen raw material was included as a reference measurement. As can be seen, the dissolution rate and extent of dissolved ketoprofen material is higher for the spray dried and the electrosprayed ketoprofen relative to crystalline ketoprofen. However, there is no discernible difference in the dissolution rate between the spray dried and electrosprayed material. This may be because the ketoprofen release rate is very rapid from both amorphous systems, with more than 40% of the available ketoprofen dissolving within 5 minutes. With such rapid release rates, the sampling intervals chosen may not sufficiently demonstrate any difference. Additionally, the polydispersity of the spray dried material means that logically the very small particles observed in Figure 5.2j dissolve initially and as such there is no observed difference in the dissolution rate of the powder prepared by different methods. There is however a higher total release of ketoprofen from the electrosprayed material over the time-frame studied. The risk of crystallisation of the API during the dissolution test is low due to the stability of ketoprofen in the amorphous state [4] , as well as the fact that sink conditions were used. It is likely that the variation observed in the dissolution profile of the spray dried system stems from the polydispersity of particle size, which is not present in the electrosprayed system.

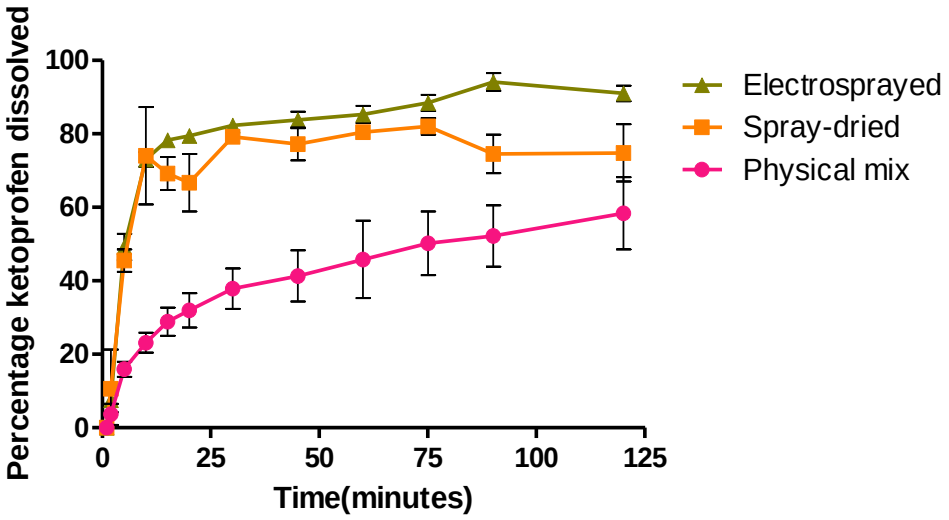

Figure 5.8: Dissolution profiles for electrosprayed and spray dried amorphous solid dispersions of PVP and ketoprofen 20% w/w at pH 1.2 (n=3)

5.2.6 Moisture diffusion studies and surface adsorption rates

The diffusion coefficient values of water vapour in the spray dried and electrosprayed PVP 20% w/w ketoprofen at various relative humidities are listed in Table 5.2. The physical state of all samples were checked via pXRD after exposure to high relative humidity in the DVS and were found to have maintained their amorphous state.

As can be seen from Table 5.2, the diffusion coefficient values, which are measures of the rate of moisture diffusion through the bulk of the powder, are not statistically significantly different ($p<0.05$) between the electrosprayed material and the equivalent spray dried material at all relative humidity conditions studied. Conversely, the rate of surface moisture adsorption shown in Figure 5.9 and Table 5.3 is significantly faster for the electrosprayed material compared to the spray dried material. As surface adsorption is typically much faster than bulk absorption [145], and the electrosprayed powder has a higher specific surface area than the equivalent spray dried powder, this result is not unexpected. As amorphous state instability is often driven by moisture-induced phase separation [111], this result highlights the importance of protecting amorphous solid dispersions from moisture during storage, particularly those that have a high specific surface area such as the electrosprayed material in this work.

Table 5.2: Water diffusion coefficient values for spray dried and electrosprayed PVP 20% w/w ketoprofen. Standard deviation values are in parenthesis

Relative humidity	Spray dried D (cm^2/s)	Electrosprayed D (cm^2/s)	p-value
20%	$5.87 \pm 1.16 \times 10^{-13}$	$4.96 \pm 0.49 \times 10^{-13}$	0.27
40%	$5.94 \pm 1.05 \times 10^{-13}$	$4.54 \pm 0.50 \times 10^{-13}$	0.11
60%	$4.16 \pm 0.92 \times 10^{-13}$	$2.96 \pm 0.27 \times 10^{-13}$	0.09
80%	$2.13 \pm 0.45 \times 10^{-13}$	$1.90 \pm 0.19 \times 10^{-13}$	0.45

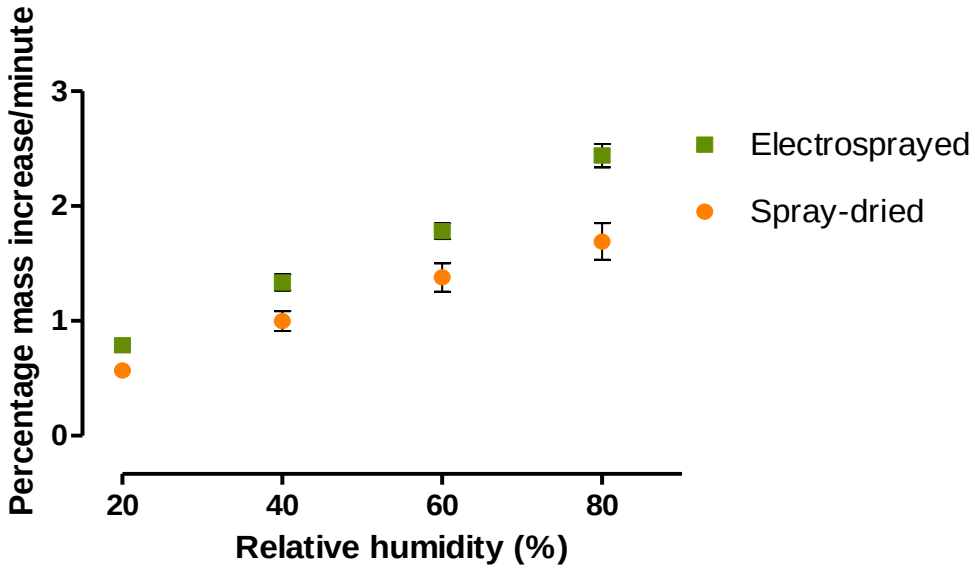

Figure 5.9: Surface moisture adsorption rates for electrosprayed and spray dried amorphous solid dispersions of PVP and ketoprofen 20% w/w at various relative humidities.

Table 5.3: Surface moisture adsorption rates with standard deviation for electrosprayed (ES) and spray dried (SD) amorphous solid dispersions of PVP and ketoprofen 20% w/w at various relative humidities.

Relative humidity	SD PVP 20% ketoprofen (% mass increase/minute)	ES PVP 20% ketoprofen (% mass increase/minute)	p-value
20%	0.57 ± 0.09	0.79 ± 0.06	0.02
40%	0.99 ± 0.15	1.33 ± 0.12	0.04
60%	1.38 ± 0.21	1.78 ± 0.11	0.04
80%	1.69 ± 0.28	2.44 ± 0.17	0.01

5.2.7 Density and compressibility

True density, bulk density, tapped density and Carr's Compressibility Index values for spray dried and electrosprayed PVP containing 20% w/w ketoprofen are shown in Table 5.4. The true density of the spray dried PVP containing 20% w/w ketoprofen was 1.25 (± 0.001) g/cm^3 and the true density of the equivalent electrosprayed PVP containing 20% w/w ketoprofen was 1.32 (± 0.009) g/cm^3. As true density is known to be inversely related to the degree of disorder present in a material [230], it may be inferred that the spray dried material is more "disordered" than the equivalent electrosprayed material. The bulk and tapped density of the two materials are also different. The Carr's Compressibility Index (CCI) is an indicator of powder flowability [244]. In the pharmaceutical industry the ability of a powder to flow freely is a desirable attribute to ensure a smooth flow of powder into direct compression dies allowing uniformity of content, weight and hardness. Interestingly the CCIs for the powders produced by the two different processes are dramatically different. The CCI value for the spray dried material is 16.67 (± 2.89), which means it would be classified as a powder exhibiting "fair" flow, while the CCI value for the equivalent electrosprayed material is 58.33 (± 2.89) meaning that it would be categorised as a "very very poor" flowing powder [244,269]. Electrospraying this amorphous solid dispersion resulted in smaller and narrower particle size distribution, and reduced flowability compared to the standard spray dried material. This inverse relationship between particle size and flowability has previously been described for pharmaceutical materials such as lactose, micro-crystalline cellulose and model APIs [270–272]. This poor flow is likely due to the adhesion of small particles leading to the formation of aggregates. This work has demonstrated that the flowability and hence processability of a spray dried amorphous solid dispersion is superior to an equivalent electrosprayed amorphous solid dispersion, which is caused by a difference in surface area and average particle size

Table 5.4: Density and Carr's Compressibility Index (CCI) for spray dried and electrosprayed PVP 20% w/w ketoprofen.

	True density (g/cm^3)	Bulk density (g/cm^3)	Tapped density (g/cm^3)	CCI
SD PVP with 20% w/w ketoprofen	1.25 ± 0.00	0.35 ± 0.04	0.42 ± 0.06	16.67 ± 2.89
ES PVP with 20% w/w ketoprofen	1.32 ± 0.01	0.16 ± 0.03	0.39 ± 0.08	58.33 ± 2.89

5.3 Conclusion

The need for novel methods of generating ASDs has led to intensive research into electrohydrodynamic processes, including electrospraying, for this purpose. A head-to-head comparison of powders produced using this newer method against the well-established spray drying method has not been performed until now.

The effect of solution parameters (such as viscosity) on the material properties of particles produced via spray drying is well explored. The same in-depth understanding of process parameters is not yet established in the electrospraying of ASDs. This work demonstrates that solution conductivity is a parameter critical to the morphology of particles produced via electrospraying, while it has no effect on particles produced via spray drying. As solution conductivity is clearly a critical quality attribute for successful electrospraying of a solution, attention should be paid to the interplay that drug and polymer choice, as well as loading, have on this parameter. PVP was found to confer higher conductivity to the solutions (> 20 μS/cm) in which it was dissolved compared to PVPVA (< 5 μS/cm). This is likely due to its higher hygroscopicity, and hence its sorbed moisture. Surface tension and viscosity were broadly similar across the various solutions tested.

The electrosprayed polymer-ketoprofen material was smaller in size (generally < 1 μm) and demonstrated a narrower particle size distribution compared to the equivalent spray dried material. Solid-state analysis revealed that both the spray dried and electrosprayed powders of PVP 20% w/w ketoprofen were amorphous and had very similar glass transitions (≈94 ^{o}C). Both powders dissolved rapidly at pH 1.2, with > 40% w/w of available ketoprofen dissolved withing 5 minutes. However, the electrosprayed powder exhibited a faster surface sorption of moisture than the equivalent spray dried powder.

While electrospraying may prove advantageous in the amorphisation of APIs unamenable to other methods (i.e. those which are thermally labile), if electrospraying is to be developed further as a standard amorphisation technique, the challenges posed by the sub-micron size of the particles it produces, such as poor flow and high hygroscopicity, must also be addressed.

Chapter 6.a: Photostability of ASDs of nifedipine

6.a.1 Introduction

The physical instability of the amorphous state and of amorphous solid dispersions has been well documented, as described in Chapter 1, Section 1.3. In contrast, the chemical stability of the amorphous state has not been investigated thoroughly. This is surprising, as the high free energy of the amorphous state, which is responsible for its rapid dissolution profile, would also be anticipated to lead to an increase in chemical reactivity relative to the crystalline state.

The literature to date relating to amorphous chemical stability has demonstrated that the amorphous form has a greater tendency to sorb moisture than the crystalline form [3]. This may allow chemical reactions involving water, such as hydrolysis, to proceed more readily in the amorphous state than in the crystalline state. However, even when the water content of the amorphous and crystalline forms of cephalosporin antibiotics are equivalent, the amorphous form exhibits a faster rate of chemical degradation [17,18]. This indicates that the presence of moisture alone does not explain the increased chemical degradation rate observed in the amorphous state. Amorphous state chemical degradation may proceed via different kinetic processes than the equivalent crystalline state, as has been observed for indomethacin [139].

Of interest in this chapter, is the process of photodegradation in the amorphous state. Photodegradation is a chemical reaction whereby a molecule is transformed as a result of exposure to light energy (photons). Photodegradation can occur in APIs, and photostability testing (i.e. testing the tendency of a material to photodegrade) is a requirement of most regulatory agencies [273]. If an API is liable to photodegradation, measures must be taken to minimise this process, so as to ensure therapeutic efficacy is maintained and to avoid the ingestion of potentially toxic photodegradant end products.

Solid-state photostability is known to be influenced by particle size [274], polymorphic form [275,276] and density [277,278]. Two studies have also shown that nifedipine, nimodipine [279] and an alpha adrenoreceptor blocker (MK-912) [280] show markedly faster photodecomposition in the amorphous state compared to their crystalline counterparts.

Formulation strategies which improve the photostability of various APIs have included complexation with cyclodextrins [281], nano-emulsions [282], surface coating [125,283] , incorporation into inorganic matrices [284] and cocrystal formation [285]. The purpose of this chapter is to investigate the effect of amorphous solid dispersion formulation on the photostability of an API using nifedipine as a model drug.

Nifedipine is a suitable model API as it readily converts to its nitrosophenylpyridine derivative (Impurity B) upon exposure to daylight, while exposure to UV light generates the

nitrophenylpyridine derivative (Impurity A) [158]. The molecular structures of nifedipine and its associated photodegradants are shown in Figure 6.a.1. The poor photostability of nifedipine relative to other dihydropyridine molecules has been attributed to the electronegativity of the o-nitro groups in the phenyl ring of nifedipine [286]. A study examining the mechanism of nifedipine photodegradation from solution showed that Impurity B is formed initially before a gradual oxidation to Impurity A [287]. As expected, photodegradation of nifedipine in the solid state was observed to be slower than from solution [287].

ASDs of nifedipine with various polymers generated via spray drying will be subjected to photostability testing. The degradation of nifedipine and simultaneous generation of nifedipine impurities will be monitored over time and formulation factors affecting photostability, if any, will be described.

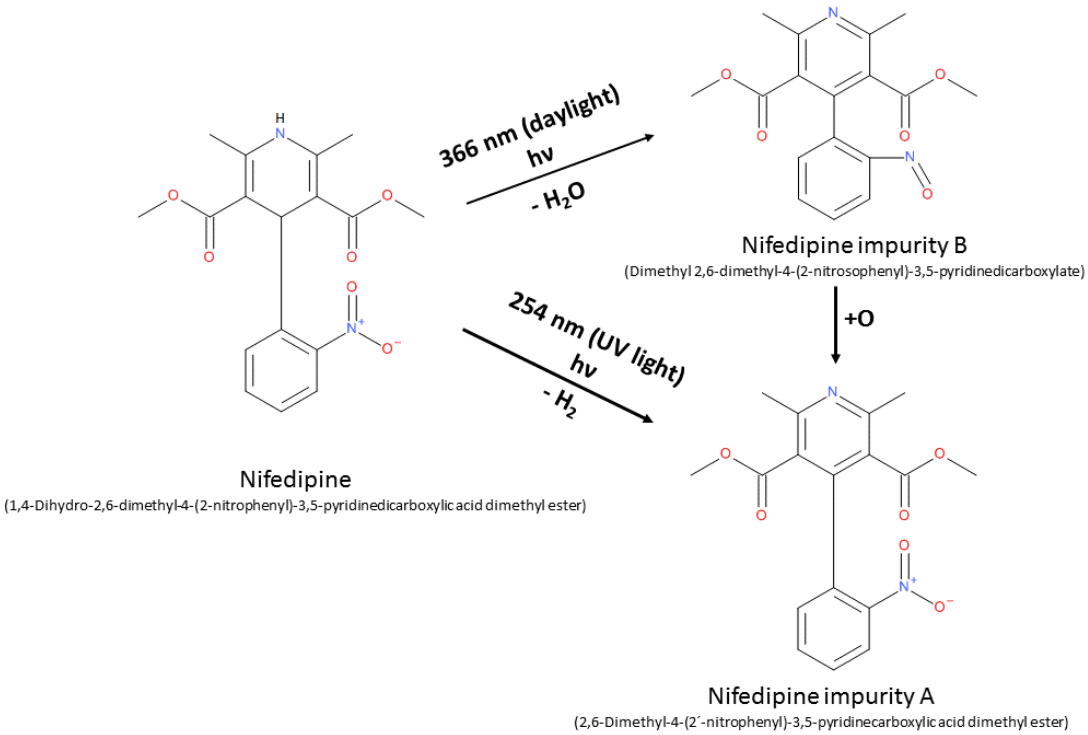

Figure 6.a.1: Molecular structures of nifedipine and associated photodegradant products

6.a.2 Results

6.a.2.1 Thermal analysis

The DSC thermograms of the polymers as received, along with a sample of nifedipine which had been melt-quenched *in situ* are shown in Figure 6.a.2 below.

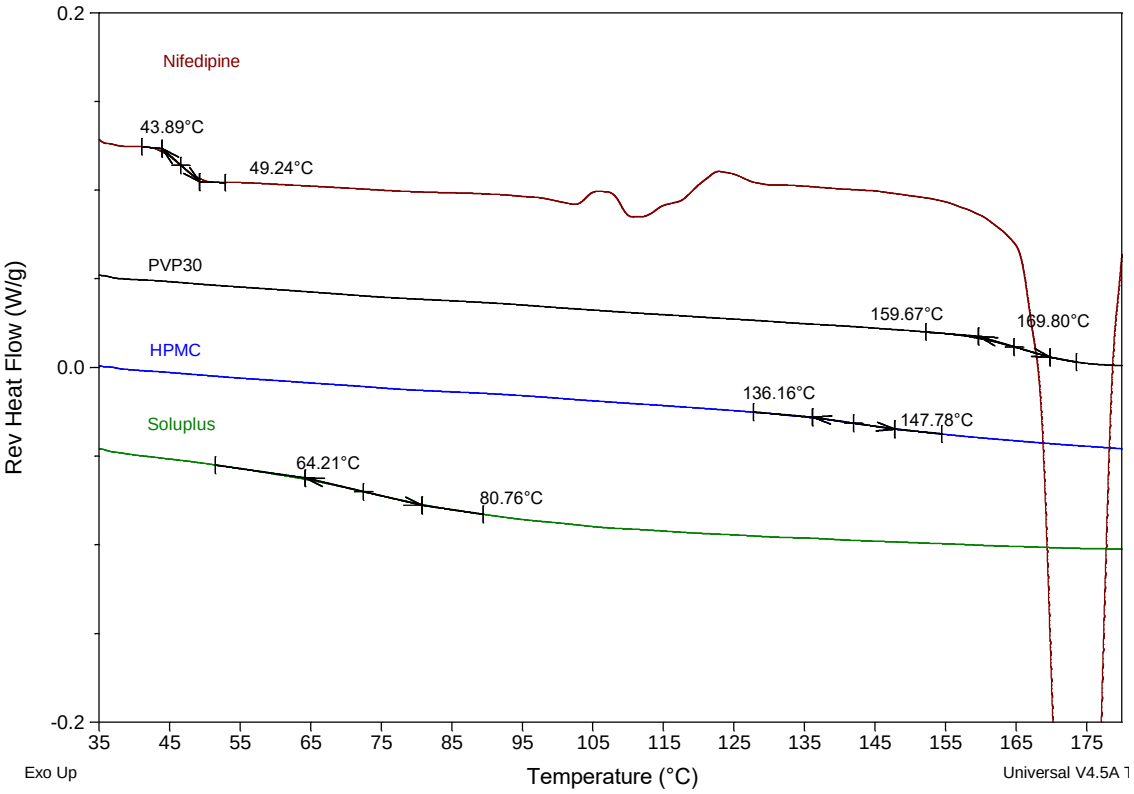

Figure 6.a.2: mDSC scans showing glass transition temperatures of polymers as received and an *in situ* melt-quenched sample of nifedipine

As expected, the DSC scans of the amorphous polymers show glass transitions and no melting endotherm. The sample of nifedipine which had been heated above its melt temperature and then cooled to 25 °C before being re-heated showed a glass transition at 44 °C, which agrees with literature values [125,288]. Some crystallisation (exotherm) is evident in the nifedipine sample before a melting endotherm, corresponding to the melting endotherm of the stable polymorph of nifedipine, is seen.

The DSC thermograms of the spray dried dispersions containing 30% w/w nifedipine are shown in Figure 6.a.3 below. While ASDs of PVP and Soluplus were DSC amorphous at 30% w/w nifedipine loading, the equivalent HPMC ASD was partially crystalline, as indicated by the presence of melting endotherms with onsets at 154 °C and 171 °C. The glass transition and thermal events observed for these binary systems are shown in Table 6.a.1. The presence of two melting endotherms indicates

that nifedipine is present as two distinct polymorphs, the most stable polymorph (Form 1- Tm 171 °C) and a metastable polymorph (Form 2- Tm 154 °C). Both of these melting points are depressed relative to those of their respective pure polymorphs (Tms of 173 °C and 161 °C respectively) [289], indicating that HPMC is partially miscible with nifedipine. The absence of a crystallisation exotherm indicates that the crystalline phases of the SD HPMC NIF 30% were present in the material prior to testing, and not caused by reheating in the DSC.

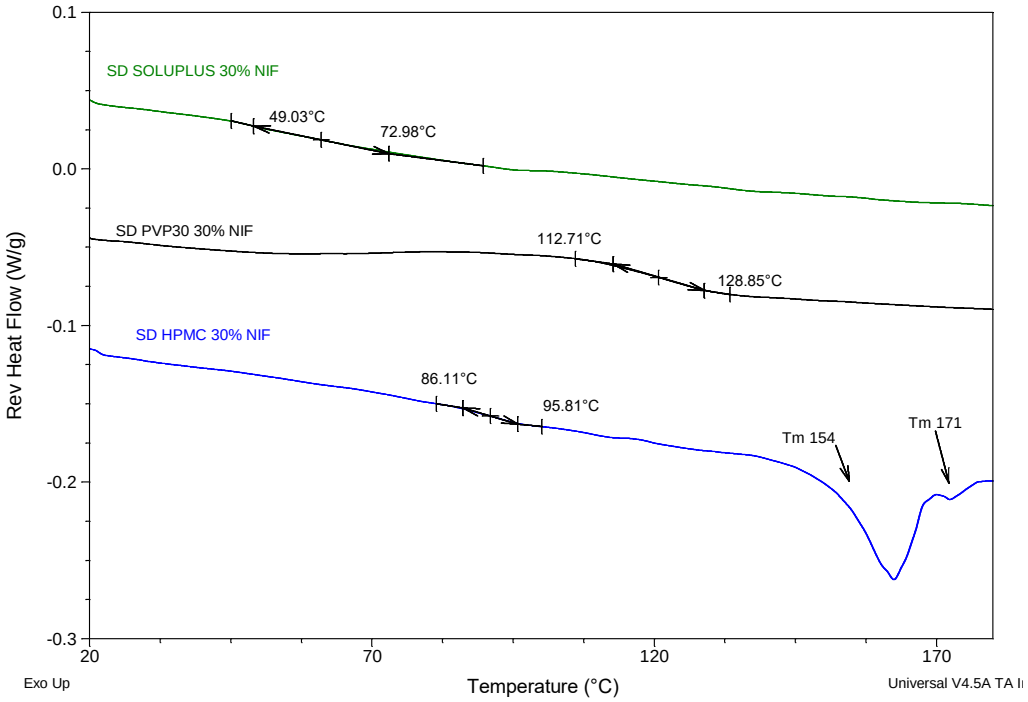

Figure 6.a.3 mDSC scans showing glass transition temperatures of spray dried polymers with nifedipine 30% w/w

The DSC scans of the spray dried dispersions containing 15% w/w nifedipine are shown in Figure 6.a.4. All six systems are amorphous as indicated by the presence of a glass transition temperature and the absence of an endothermic melting peak. The glass transition temperature onset, offset and width for all spray dried systems are detailed in Table 6.a.1. All systems with 15% w/w nifedipine loading have glass transitions which are higher than the equivalent 30% w/w nifedipine loading, in accordance with the Gordon-Taylor equation [94]. The spray dried HPMC 30% w/w nifedipine material was partially crystalline, while the equivalent 15% w/w nifedipine material was fully amorphous, indicating that the solubility limit of nifedipine in HPMC is greater than or equal to 15% w/w but less than 30% w/w

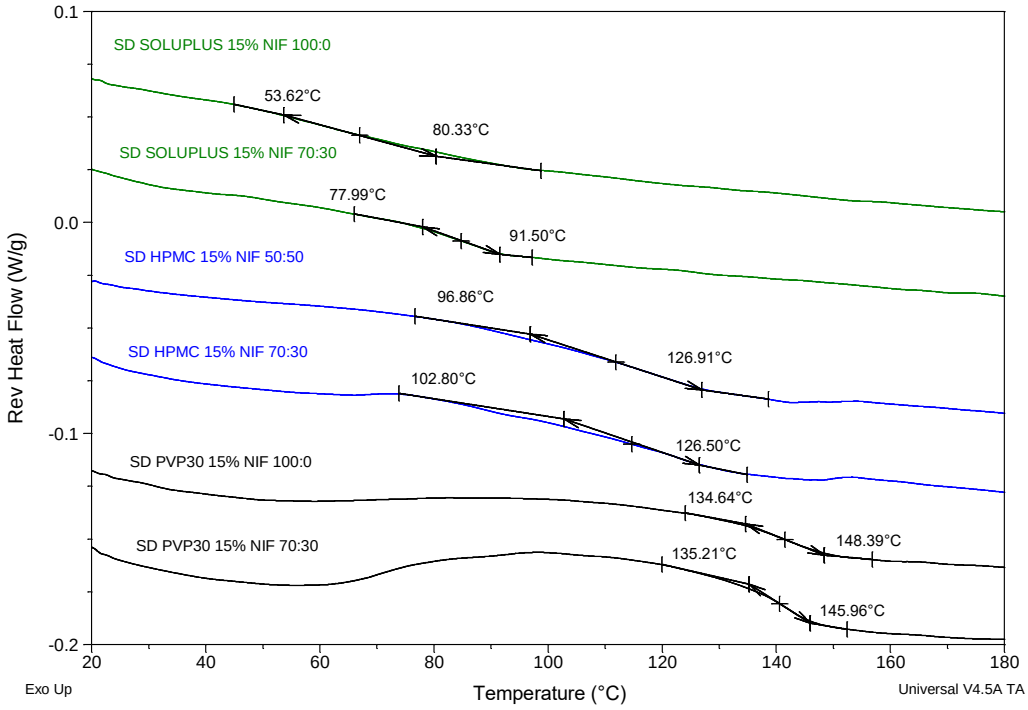

Figure 6.a.4:mDSC scans showing glass transition temperatures of spray dried polymers with nifedipine 15% w/w. Ratio refers to the ethanol:water ratio of the solvent system

The composition of the solvent from which the polymer-nifedipine system was spray dried appears to have negligible impact on the glass transition temperature for the PVP-nifedipine and HPMC-nifedipine systems but seems to have influenced the glass transition temperature of the Soluplus-nifedipine system (Table 6.a.1). Initially this was thought to be due to a difference in the residual solvent level (which may be due to polymer-solvent interaction strength) [290] or the hygroscopicity of the powders, as even low levels of solvents can significantly lower glass transition temperatures [85]. However solvent/moisture level as measured by TGA revealed no statistically significant difference in the residual solvent/ moisture level between the Soluplus-nifedipine systems which were spray dried from different solvent systems (Table 6.a.2). Sample raw data are shown in Appendix n.

Table 6.a.1: Glass transition onset (Tg onset) and offset (Tg offset) temperatures as well as glass transition temperature width (Tg width). Values are average values with standard deviation. Solvent system refers to the solvent composition (ethanol: water) from which the polymer-nifedipine system was spray dried

System	Solvent system	Tg onset (°C)	Tg offset (°C)	Tg width (°C)
SD Soluplus 30% NIF	100:0	51.45 ± 7.66	73.15 ± 4.66	21.70 ± 12.01
SD PVP30 30% NIF	100:0	112.83 ± 1.03	128.21 ± 1.35	15.37 ± 1.55
SD HPMC 30% NIF*	50:50	82.98 ± 2.67	95.15 ± 1.02	12.17 ± 2.22
SD Soluplus 15% NIF	100:0	53.54 ± 3.01	77.55 ± 4.59	24.01 ± 3.41
SD Soluplus 15% NIF	70:30	74.24 ± 0.28	90.12 ± 1.32	15.89 ± 1.59
SD PVP30 15% NIF	100:0	130.84 ± 1.43	148.61 ± 1.30	17.77 ± 2.13
SD PVP30 15% NIF	70:30	133.18 ± 3.60	146.51 ± 0.58	13.33 ± 0.25
SD HPMC 15% NIF	50:50	102.09 ± 8.01	126.57 ± 5.56	24.48 ± 6.61
SD HPMC 15% NIF	70:30	95.21 ± 11.37	128.17 ± 0.95	32.96 ± 12.29

* Partially crystalline sample

Table 6.a.2: Moisture/residual solvent levels of spray dried polymer-nifedipine systems with 15% w/w nifedipine loading. Results are expressed as the average of three replicates ± standard deviation. P-value refers to the pair of polymer-nifedipine systems in each row (i.e. HPMC-nifedipine 50:50 and 70:30 ethanol: water v/v)

Solvent system (Ethanol: water v/v)				
Polymer-nifedipine system	50:50	70:30	100:0	P-value
HPMC-nifedipine	1.56 (± 1.19) %	2.16 (± 1.64) %		0.93
PVP30-nifedipine		9.62 (± 4.03) %	8.84 (± 2.22) %	0.79
Soluplus-nifedipine		1.92 (± 0.84) %	1.02 (± 0.21) %	0.15

6.a.2.2 pXRD analysis

The powder X-ray diffraction patterns of the spray dried polymer-nifedipine systems are shown in Figure 6.a.5 below. A small Bragg peak is apparent in the SD HPMC 30% w/w nifedipine sample at 7.65 degrees 2θ (indicated by arrow). As thermal analysis showed crystalline material in the SD HPMC 30% w/w nifedipine sample, the pXRD pattern corresponds well to this.

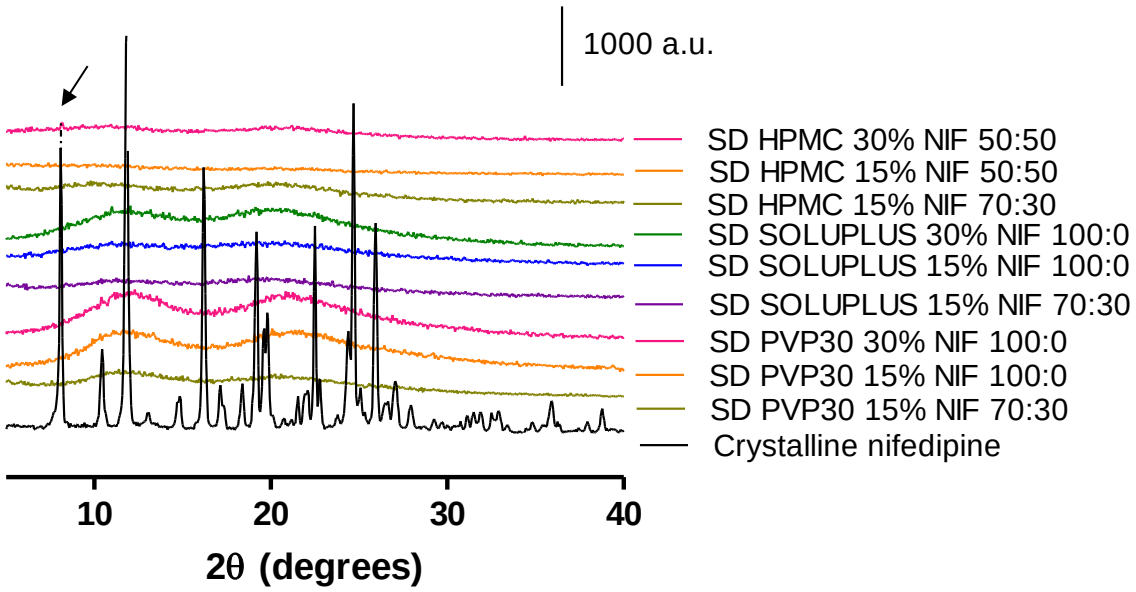

Figure 6.a.5: pXRD patterns of spray dried (SD) polymer- nifedipine systems with 30% and 15% w/w nifedipine loading, spray dried from solvent systems composed of different ratios of ethanol to water

6.a.2.3 Photostability analysis

As the purpose of this experiment was to determine the effect, if any, that polymer choice has on the photostability of ASDs of nifedipine, the systems with 15% w/w nifedipine underwent photostability testing and further characterisation. These fully X-ray and DSC amorphous systems were selected to avoid any confounding factors such as the crystallisation of nifedipine during photostability testing from a metastable polymorph state.

A secondary objective of this experiment was to determine the effect, if any, that solvent composition has on the photostability of spray dried polymer-nifedipine ASDs. To test this, the three polymer-nifedipine systems tested were each spray dried from two different solvent systems, resulting in a total of 6 spray dried systems which underwent photostability testing, as described in Chapter 2 Section 2.2.3.12. These were SD HPMC 15% NIF (70:30), SD HPMC 15% NIF (50:50), SD PVP30 15% NIF (100:0), SD PVP30 15% NIF (70:30), SD SOLUPLUS 15% NIF (100:0) and SD SOLUPLUS 15% NIF (70:30) where the ratio refers to the ethanol: water v/v ratio.

6.a.2.3.1 Influence of polymer choice on spray dried nifedipine ASD photostability

The photostability results for the systems spray dried from a solvent composition of 70:30 ethanol: water are shown in Figure 6.a.6 below.

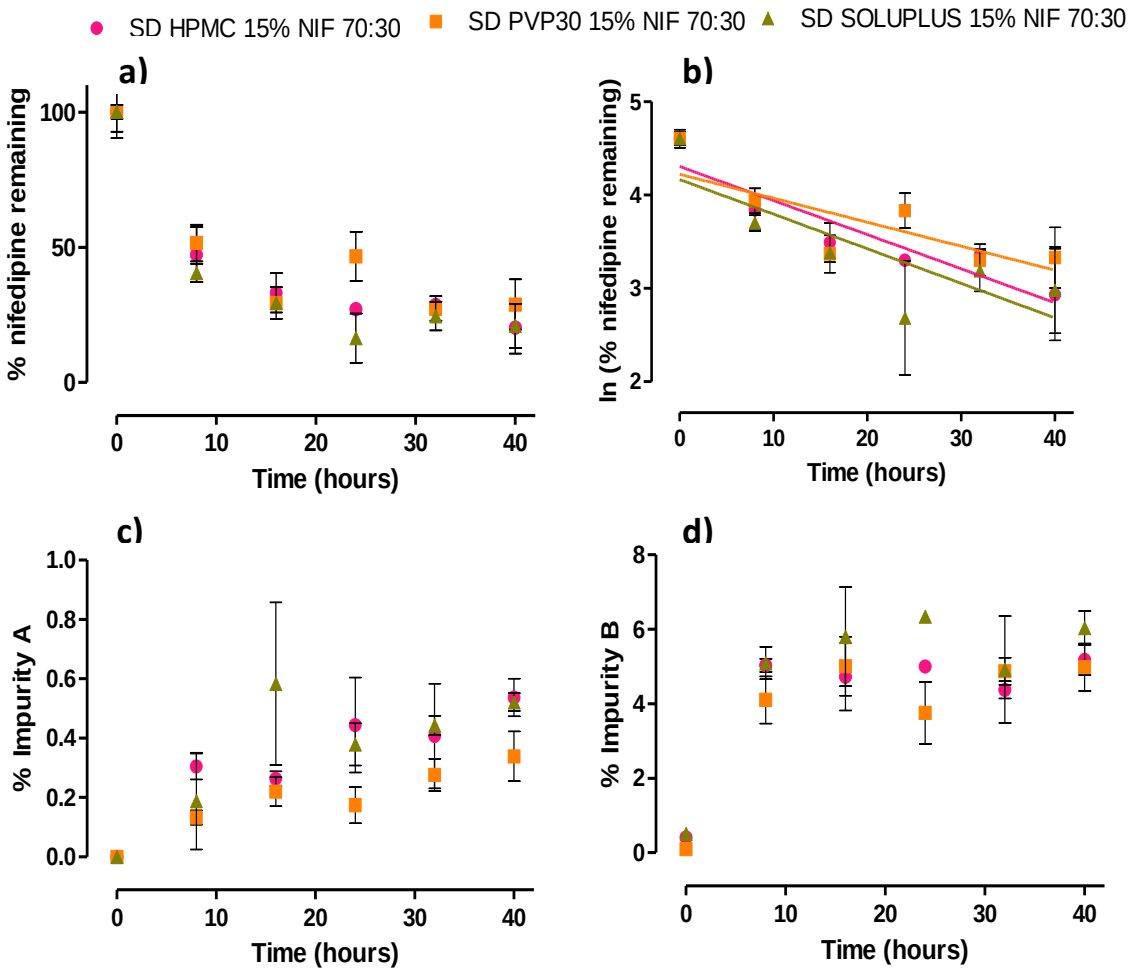

Figure 6.a.6: Nifedipine photodecomposition for spray dried ASDs with 15% w/w nifedipine spray dried from a solvent composition of 70:30 ethanol: water. a) Percentage nifedipine remaining over time b) Natural logarithm of percentage of nifedipine remaining over time. Solid lines represent the best linear fit of the data to first-order kinetics c) Percentage of Impurity A over time d) Percentage of Impurity B over time

As expected, the nifedipine content of the systems decreases after exposure to light for all systems. Photodecomposition is particularly rapid within the first 8 hours of exposure to light for all ASD systems. This rapid burst of photodecomposition has previously been attributed to the initial photodecomposition of all exposed nifedipine at the surface of particles [279]. As the concentration of nifedipine which is exposed to light reduces, the rate of photodecomposition reduces. The photodecomposition of nifedipine in the solid state (both crystalline and amorphous) has previously been described by first order kinetics, meaning that the rate of decomposition is dependent on the concentration of nifedipine available for reaction [274,279,281,286]. As the ASDs studied in this experiment are a mixture of amorphous nifedipine and amorphous polymer, the degradation rates were modelled for zero order, first order and second order kinetics, to determine which kinetic model fitted the decomposition process best. Graphical representations of the data fitted to this model is shown in Appendix o). The results of these fitted models are shown in Table 6.a.3 below.

Table 6.a.3: Photodecomposition rates (k) of ASDs with 15% w/w nifedipine spray dried using 70:30 ethanol: water using zero, first and second order rates

ASD system	Zero order		First order		Second order	
	k (% hr^{-1})	R^2	k (hr^{-1})	R^2	k ($\%^{-1}$ hr^{-1})	R^2
SD HPMC 15% NIF	1.67± 0.31	0.66	0.037 ± 0.005	0.75	0.0011 ± 0.0002	0.64
SD PVP30 15% NIF	1.31 ± 0.31	0.54	0.026 ± 0.006	0.55	0.0006 ± 0.0002	0.49
SD Soluplus 15% NIF	1.63 ± 0.34	0.59	0.037 ± 0.008	0.57	0.0011 ± 0.0004	0.30

As seen in Table 6.a.3 none of the kinetic models give particularly high R^2 values, but the first order model appears to give the best fit. There is only one report in the literature of the photodecomposition rate of amorphous nifedipine, which was determined to be 0.052 h^{-1} [279]. Direct comparison between the aforementioned study and this study is not possible as different photostability test conditions were used, and the particle size of the amorphous nifedipine is not specified. It is interesting however that the photodecomposition rates in the current study were determined to be lower than the rate reported in the literature for pure amorphous nifedipine. As the photodecomposition rate of nifedipine is described by first order-kinetics, lower concentrations of nifedipine (i.e. where nifedipine concentration is diluted by the presence of a polymer) will likely reduce the photodecomposition rate of nifedipine. It is therefore unclear whether it is the dilution effect or the stabilising effect of ASD polymers which may be responsible for any reduction in amorphous nifedipine photodecomposition rates.

Interestingly, the SD HPMC and SD Soluplus systems appear to exhibit similar decomposition rates, while the photodecomposition of the SD PVP30 system shows a slower, although statistically insignificantly different ($p>0.05$), photodecomposition rate. This trend corresponds well with the evolution of the photodecomposition impurity products as shown in Figure 6.a.6, with the SD PVP

system exhibiting lower levels of both impurities. The protective effect that the presence of PVP may have on the photodecomposition of APIs has previously been postulated to be due to its susceptibility to free radical attack because of the presence of abstractable hydrogens in the PVP molecule. This may mean that PVP acts as a free radical transfer agent, preventing the photodecomposition of an API [291].

The protective effect, if any, that a polymer in an ASD may have on the photodecomposition of nifedipine may also be due to the nature of the interaction between nifedipine and the polymer. It is conceivable that nifedipine molecules which are hydrogen bonded to a polymer may be less susceptible to photodecomposition, as intermolecular bonds would first have to be cleaved before the intramolecular rearrangements required for photodecomposition (shown in Figure 6.a.1) could occur. The literature has demonstrated that Soluplus does not form intermolecular bonds with nifedipine [292] while PVP readily forms hydrogen bonds with nifedipine [10]. This intermolecular interaction was deemed to be the reason that ASDs of PVP and nifedipine exhibited increased relaxation times and increased physical stability relative to equivalent ASDs of HPMCAS and PAA [10]. The current photostability study indicates that PVP-based ASDs may be more chemically stable than equivalent HPMC and Soluplus-based ASDs.

Interestingly, the R^2 value for the SD HPMC 15% NIF 70:30 system was higher than the other equivalent systems. A greater R^2 value for a first-order fit to the data suggests that the system is behaving like a nifedipine-only system, meaning that the nifedipine is either located at the surface of the particle or evenly distributed throughout the particle and not encapsulated to any great extent as this would protect nifedipine from exposure to light and delay photodegradation. This implies that there is a greater concentration of nifedipine at the surface of the SD HPMC 15% NIF 70:30 particles than the other systems, highlighting the importance that nifedipine encapsulation during the spray drying process has on photodecomposition.

6.a.2.3.2 Influence of solvent composition on spray dried nifedipine ASD photostability

In order to probe the effect that solvent composition may have on the photodecomposition of nifedipine in spray dried ASDs, the photodecomposition study was repeated for spray dried systems of the same polymer-nifedipine composition which were spray dried from a different ratio of ethanol: water. In an effort to deconvolute the dilution versus stabilisation effect that the amorphous polymers may be exerting, a physical mixture composed of the spray dried polymer and micronized crystalline nifedipine at the same mass ratio (15% w/w) nifedipine was included in the analysis. The photodecomposition rate of the micronized crystalline nifedipine was also determined. This should allow for the “dilution effect” that the polymers presence has on nifedipine photodecomposition rates to be examined. The degradation of nifedipine over time was fitted to

first order kinetics as shown in Figure 6.a.7 and the evolution of the nifedipine related impurities is shown in Figure 6.a.8. The photodecomposition rate for each system is detailed in Table 6.a.4 and graphed in Figure 6.a.9

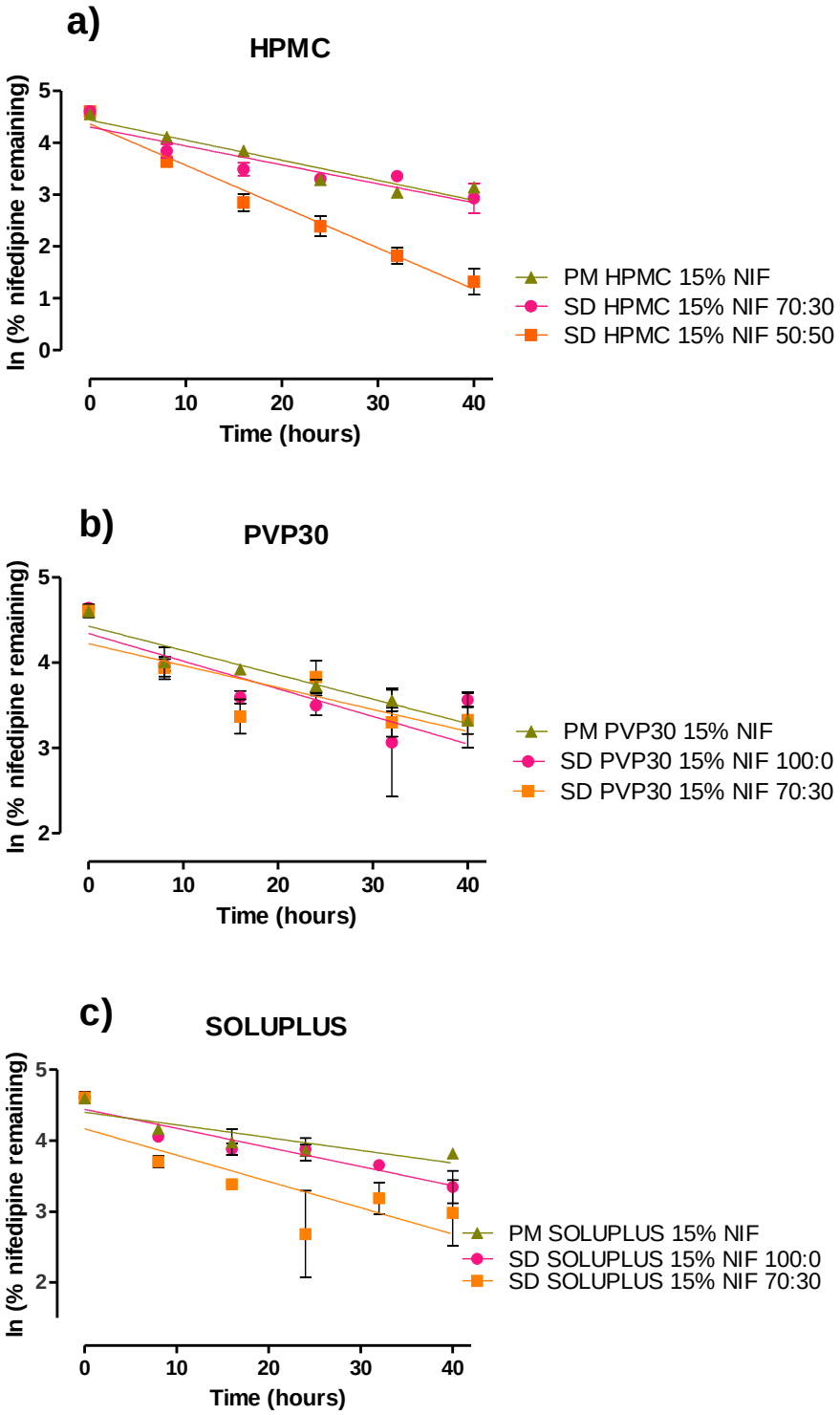

Figure 6.a.7: Natural logarithm of percentage of nifedipine remaining over time for polymer-nifedipine mixtures. PM = physical mixture SD = Spray dried. The ratio refers to ratio of ethanol to water in the solution which was spray dried. Solid lines represent the best linear fit of the data to first-order kinetics

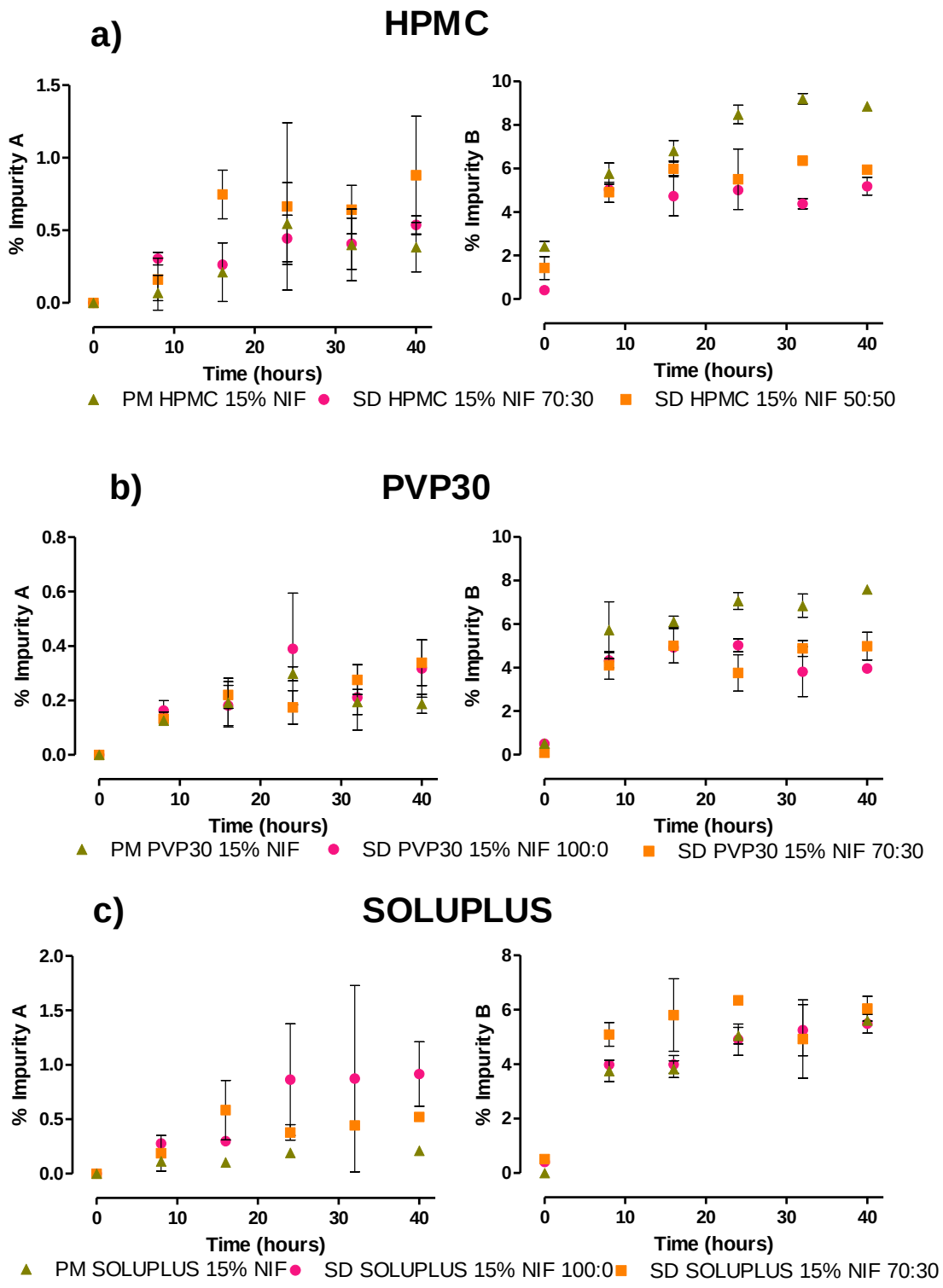

Figure 6.a.8: Photodecomposition related impurities concentration over time for polymer-nifedipine mixtures. PM = physical mixture SD = Spray dried. The ratio refers to ratio of ethanol to water in the solution which was spray dried.

Table 6.a.4: First-order photodecomposition rates (k) of nifedipine-polymer systems with 15% w/w nifedipine. PM = physical mixture SD = Spray dried. The ratio refers to ratio of ethanol to water in the solution which was spray dried. * System contains crystalline nifedipine

System	k (hr^{-1})	R^2
SD HPMC 15% NIF 50:50	0.0796 ± 0.0051	0.94
SD HPMC 15% NIF 70:30	0.0365 ± 0.0054	0.75
*PM HPMC 15% NIF	0.0387 ± 0.0032	0.90
SD PVP30 15% NIF 100:0	0.0324 ± 0.0068	0.60
SD PVP30 15% NIF 70:30	0.0257 ± 0.0060	0.55
*PM PVP30 15% NIF	0.0285 ± 0.0026	0.88
SD Soluplus 15% NIF 100:0	0.0269 ± 0.0029	0.84
SD Soluplus 15% NIF 70:30	0.0371 ± 0.0081	0.57
*PM Soluplus 15% NIF	0.0179 ± 0.0032	0.71
Crystalline nifedipine	0.0469 ± 0.0081	0.83

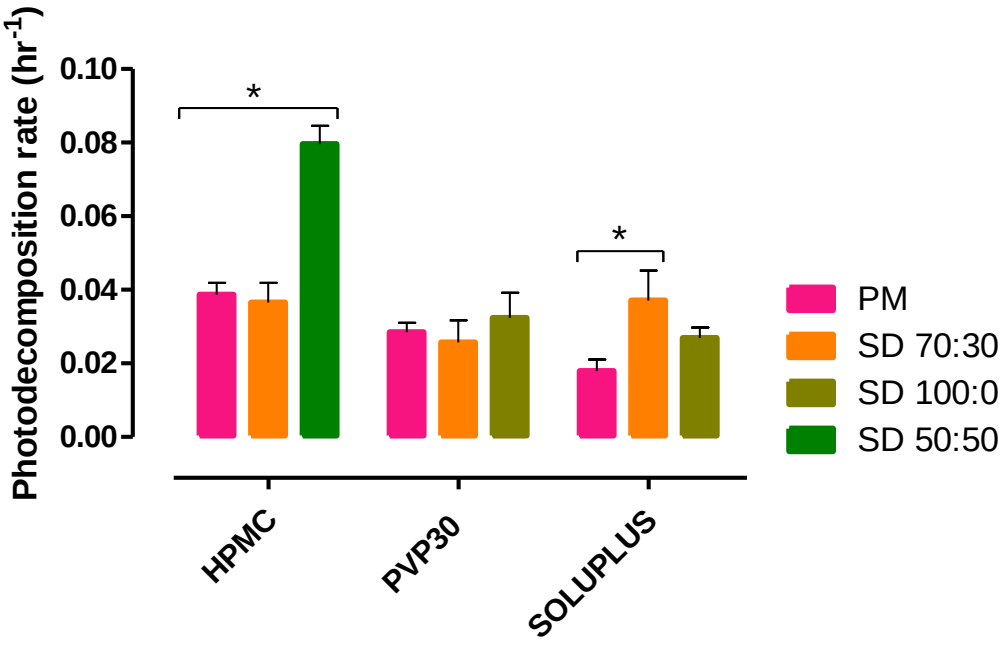

Figure 6.a.9: First-order photodecomposition rates (k) of nifedipine-polymer systems with 15% w/w nifedipine. PM = physical mixture SD = Spray dried. The ratio refers to ratio of ethanol to water in the solution which was spray dried. * refers to a statistically significant difference ($p<0.05$)

As shown in Figure 6.a.7, the rate of nifedipine photodecomposition in SD HPMC 15% NIF and SD Soluplus 15% NIF systems appears to be influenced by the composition of the solution from which the polymer-nifedipine system was spray dried. For both of these polymers, the systems which were spray dried from solutions containing a higher content of water (SD HPMC 15% NIF 50:50 and

SD Soluplus 15% NIF 70:30) exhibited poorer photostability than the systems which were spray dried from solutions containing less water (SD HPMC 15% NIF 70:30) or no water (SD Soluplus 15% NIF 100:0). The same effect was not seen in the spray dried nifedipine PVP systems, where the solvent composition of the solution which was spray dried appeared to have little impact on the rate of photodecomposition of nifedipine and there was no statistically significant difference in the photodecomposition rates for all three PVP based systems.

Interestingly, the system which was spray dried from the solution containing the highest proportion of water (SD HPMC 15% NIF 50:50) demonstrated the fastest photodecomposition rate (k=0.0796 hr^{-1}). This rate was twice as fast as any other rate determined for the other nifedipine-polymer systems (Table 6.a.4). As nifedipine photodecomposition follows first order kinetics, the greater the concentration of nifedipine available, the faster the rate of photodecomposition will be [279]. This implies that the SD HPMC 15% NIF 50:50 system has a greater nifedipine concentration at the surface of its particles than the other systems. This is supported by the high R^2 value that the SD HPMC 15% NIF 50:50 exhibited when fitted to first order kinetics (R^2 = 0.94). These results highlight the critical role that solvent composition has on the photodecomposition of spray dried nifedipine-polymer particles, presumably due to the influence that solvent composition has on particle formation [293]. As the spray dyer inlet temperature was higher for the systems containing water than for those which did not contain water (105 ^oC versus 78 ^oC), this may also have contributed to the surface enrichment of nifedipine, as has been demonstrated previously for the structurally related molecule nimodipine [294]. However, inlet temperature alone does not explain the observed differences, as both of the HPMC-nifedipine systems were spray dried using an inlet temperature of 105 ^oC. The association between residual solvent or moisture levels and the photostability of the spray dried systems was also examined by measuring moisture/ solvent levels using TGA. While PVP-nifedipine systems contained more moisture than the equivalent HPMC-nifedipine and Soluplus-nifedipine systems (≈ 9% w/w vs. ≈ 2% w/w), there was no statistically significant differences between each pair of polymer-nifedipine systems spray dried from different solvent systems (Table 6.a.2). This highlights that moisture/ residual solvent levels were not a factor which contribute to the observed differences in photostability.

Attempts were made to quantify the amount of nifedipine at the surface of the spray dried HPMC particles using X-ray photon spectroscopy (XPS), but unfortunately these attempts were unsuccessful due to limit of detection issues. Further work is clearly needed to determine the molecular composition of the surface of these spray dried particles, but the role of solvent composition is clearly critical to spray dried amorphous nifedipine photodecomposition rate.

The photodecomposition rate of micronized crystalline nifedipine was determined to be 0.0469 ± 0.0081 hr^{-1}. The same micronized crystalline nifedipine physically mixed with polymers in a 15% to

85% nifedipine to polymer ratio was determined to exhibit photodecomposition rates of 0.0387 ± 0.0032, 0.0285 ± 0.0026 and 0.0179 ± 0.0032 hr^{-1} for HPMC, PVP30 and Soluplus systems respectively. This demonstrates that by diluting crystalline nifedipine with polymers, its photodecomposition rate is reduced substantially. The difference in photodecomposition rates between the physical mixtures of polymers and crystalline nifedipine may be due to differing susceptibility to free radical attack. PVP and Soluplus contain amide groups in their molecular structure, while HPMC does not. A structure activity relationship study of caffeic acid amide and ester analogues and their free radical scavenging ability found that the presence of an amide functional group increased the free radical scavenging activity of the molecule [295]. This may explain why HPMC has the fastest photodecomposition rate in a physical mixture with nifedipine, while PVP and Soluplus exhibit slower photodecomposition rates.

Regarding the impurity profiles, as shown in Figure 6.a.8, the SD HPMC 15% NIF 50:50 system shows higher Impurity A and Impurity B levels than the equivalent SD HPMC 15% NIF 70:30 system. This is logical, as the photodecomposition rate of the SD HPMC 15% NIF 50:50 system was higher than the photodecomposition rate of the SD HPMC 15% NIF 70:30 system.

Interestingly, the PM HPMC 15% NIF and PM PVP30 15% NIF systems had higher Impurity B levels than their spray dried counterparts, even though their overall photodecomposition rates were similar to, if not slower than, their spray dried counterparts (Figure 6.a.9). The same was not true for the Impurity A levels of the same systems, which were similar to the spray dried systems. As the presence of Impurity A is known to result from the oxidation of Impurity B [287], it would be anticipated that as Impurity B levels increase, Impurity A levels increase, but this is not the case in this instance. This indicates that the degradation pathways for the spray dried and physical mixture systems may be different.

In the SD Soluplus systems, the system spray dried from a solvent containing water (SD Soluplus 15% NIF 70:30) exhibited higher Impurity B levels at early time points compared to the equivalent system spray dried from ethanol alone (SD Soluplus 15% NIF 100:0). This corresponds well to the nifedipine photodegradation rates for these systems. For ASDs of nifedipine containing Soluplus and HPMC it appears that the Impurity B levels are higher in systems which were spray dried from solvents containing water. Interestingly the PM Soluplus system shows similar Impurity B and lower Impurity A levels than the equivalent spray dried systems.

6.a.2.4 Specific surface area analysis

The specific surface area of the polymer-nifedipine systems which had been spray dried using a 70:30 ethanol: water solvent system was determined as described in Chapter 2 Section 2.2.3.5. The specific surface area of the SD HPMC 15% NIF 50:50 and the SD Soluplus 15% NIF 100:0 systems

were also determined as these systems appeared to show different photodecomposition rates compared to their SD 70:30 counterparts (Figure 6.a.7). The results are shown in Figure 6.a.10 below. There was no statistically significant ($p<0.05$) difference in the specific surface area values of the systems spray dried from a 70:30 ethanol: water solvent system. This indicates that polymer choice had no impact on the surface area of the spray dried nifedipine ASDs. Interestingly, there was no statistically significant difference in the specific surface areas of the SD HPMC systems spray dried from differing ethanol: water ratios. The SD Soluplus systems, spray dried from different solvent systems also had statistically insignificant differences in specific surface area values. As these systems show markedly different photodecomposition rates (Table 6.a.3), but the specific surface area values are very similar, this adds to the aforementioned theory that there is a difference in the distribution of nifedipine at the surface of the particles rather than a difference in their surface area.

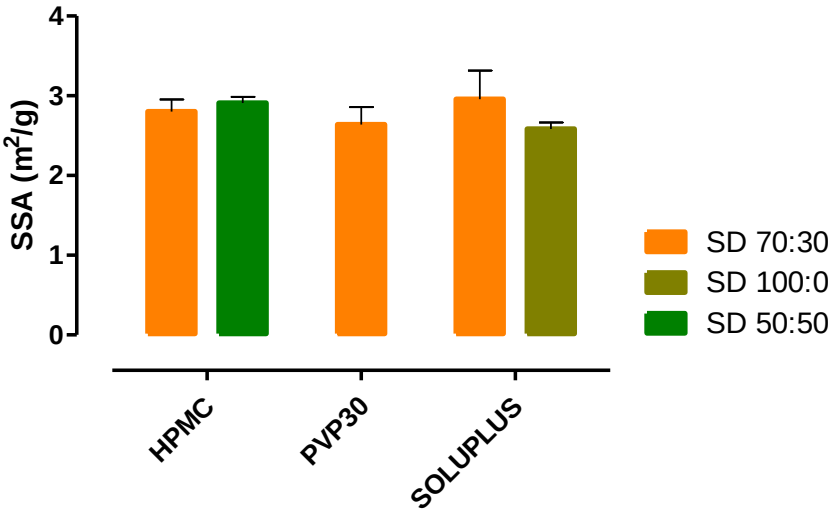

Figure 6.a.10: Specific surface area of spray dried polymer-nifedipine systems with 15% w/w nifedipine. The ratio refers to the ratio of ethanol to water in the solution from which the particles were spray dried

6.a.2.5 Particle size analysis

The particle size of the polymer-nifedipine systems were measured as described in Chapter 2 Section 2.2.3.9.2 and are detailed in Figure 6.a.11.

Table 6.a.5: Particle size distribution of polymer-nifedipine systems (15% nifedipine w/w) which were subjected to photostability testing

System	Nifedipine state	Solvent system	D_{10} (µm)	D_{50} (µm)	D_{90} (µm)
SD HPMC NIF	Amorphous	50:50	2.63 ± 0.17	9.48 ± 0.45	22.43 ± 1.97
SD HPMC NIF	Amorphous	70:30	1.84 ± 0.02	5.29 ± 0.12	13.00 ± 0.44
PM HPMC NIF	Crystalline	N/A	2.39 ± 0.02	7.12 ± 0.02	20.73 ± 0.21
SD PVP30 NIF	Amorphous	100:0	1.09 ± 0.18	3.55 ± 0.44	7.57 ± 1.13
SD PVP30 NIF	Amorphous	70:30	1.37 ± 0.03	4.24 ± 0.13	9.55 ± 0.25
PM PVP30 NIF	Crystalline	N/A	1.37 ± 0.01	3.99 ± 0.06	12.70 ± 1.05
SD Soluplus NIF	Amorphous	100:0	0.97 ± 0.02	3.41 ± 0.03	6.97 ± 0.06
SD Soluplus NIF	Amorphous	70:30	3.79 ± 0.36	19.57 ± 6.20	731.33 ± 255.76
PM Soluplus NIF	Crystalline	N/A	1.69 ± 0.03	4.67 ± 0.09	12.50 ± 0.70

Interestingly, the SD HPMC 15% NIF 70:30 and the SD PVP30 15% NIF 70:30 systems had very similar particle size distributions, while the SD SOLUPLUS 15% NIF 70:30 system had much larger D10 and D90 values. This may be due to the presence of agglomerates in the SD SOLUPLUS 15% NIF 70:30 system which were not dispersed into individual particles during the particle sizing.

Interestingly, the SD HPMC 15% NIF system which was spray dried from 50:50 ethanol: water had higher D10, D50 and D90 values compared to the SD HPMC 15% NIF system which was spray dried from 70:30 ethanol: water. This is surprising, as the SD HPMC 15% NIF 50:50 system demonstrated a more rapid nifedipine photodecomposition compared to SD HPMC 15% NIF 70:30 in spite of a larger particle size, which is usually associated with a lower photodecomposition rate [274]. This points towards other factors, such as the surface distribution of nifedipine, as the driving force for nifedipine photodecomposition in ASDs.

6.a.2.6 Particle morphology analysis

The particle morphology of all spray dried nifedipine-polymer 15% NIF w/w systems were captured using scanning electron microscopy as described in Chapter 2 Section 2.2.3.8 and are shown in Figure 6.a.11 below.

Comparing the particle morphology of the three polymer nifedipine systems spray dried from a 70:30 ethanol: water solvent system the Soluplus and HPMC-based systems appear to have some

crumpled particles mixed with spherical particles while the equivalent PVP system, appears to have a smoother surface. The addition of water into the solvent system appeared to have a smoothing effect on the surface morphology of the PVP system as the 100:0 system displays some dimpling compared to the 70:30 system where this effect is not apparent. This is in contrast to the Soluplus and HPMC systems where the dimpling/crumpling effect is maintained, if not increased, on the addition/increase of water to the spray drying solvent system.

The differing morphologies of spray dried particles has previously been explained by Peclet number theory [264]. This parameter describes the relative speeds of the radial velocity of the receding droplet surface and the diffusional motion of the solute, as described in Chapter 5 Section 5.2.2.1. When the Peclet number is below 1 the diffusional motion is fast relative to the radial velocity of the droplet surface which means that there is an even distribution of solute precipitating at the surface of the particle and typically a solid sphere will form. In contrast, when the Peclet number is higher than 1, the surface of the droplet is evaporating more rapidly than the solute in the bulk of the droplet is diffusing to the surface. This results in dimpling and surface enrichment of the particle [264]. It is proposed that the SD HPMC 15% NIF 50:50 system has a Peclet number greater than the other systems and therefore has a higher degree of nifedipine enrichment at the surface of the particle. This is supported by the excellent fit (R^2=0.94) of this system's photodecomposition profile to the first-order kinetics that nifedipine particles are known to exhibit [274].

As the solvent systems containing water were processed via spray drying using an inlet temperature of 105 ^{o}C compared to an inlet temperature of 78 ^{o}C for the ethanol only systems, the evaporation rates of these systems were likely different. The ratio of ethanol to water in the spray dried systems will also affect the diffusion of the solutes through the droplets as they dry. It is clear that Peclet number theory plays a role in the morphology and hence the photodecomposition rates of spray dried ASDs of nifedipine. Further work is needed to tease out the various contributing factors to the highly dimpled (and presumably nifedipine enriched) surface observed in the SD HPMC 15% NIF 50:50 sample which exhibited a faster nifedipine photodecomposition rate compared to equivalent samples prepared from different solvent systems or different polymers.

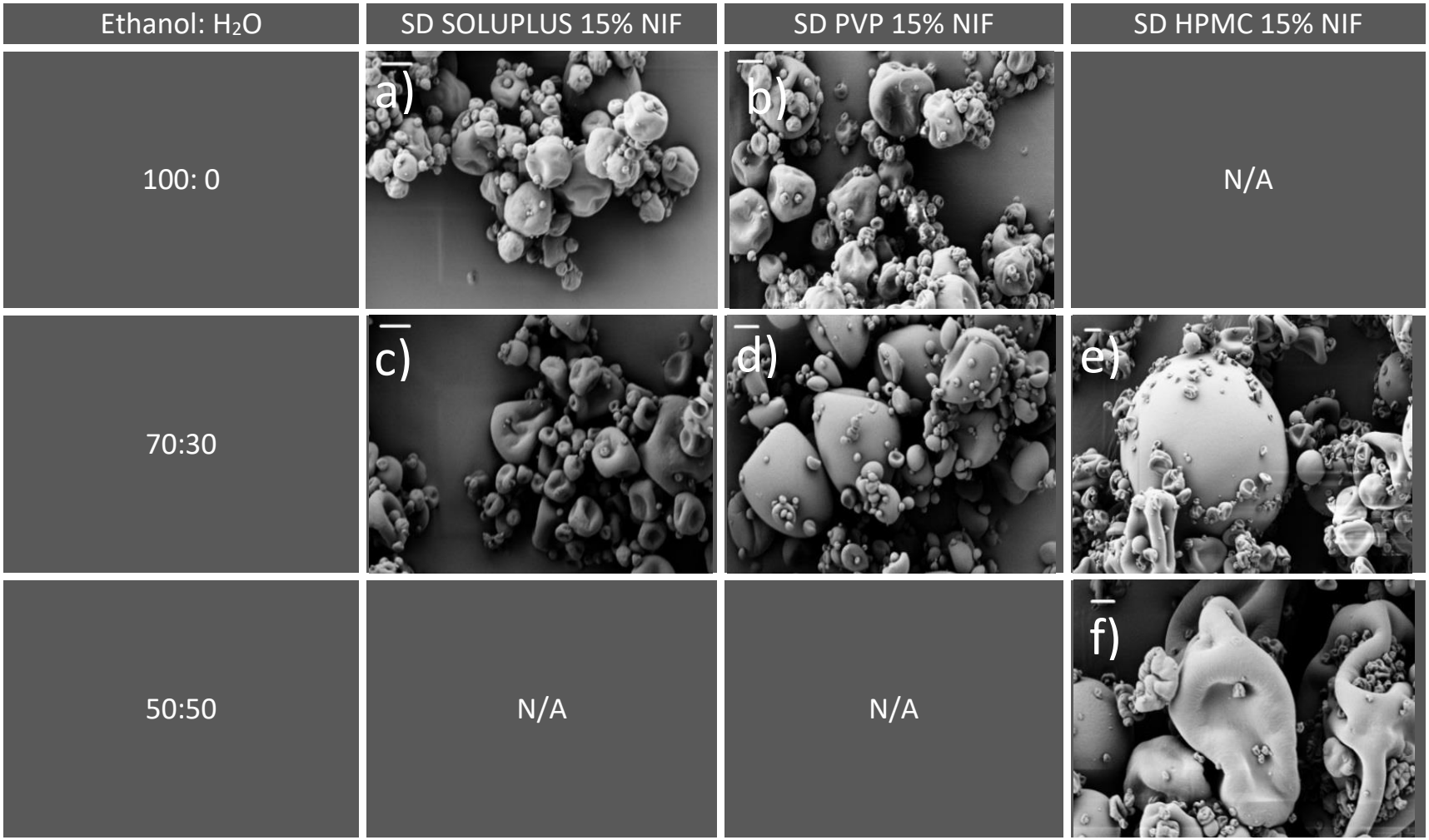

Figure 6.a.11: SEM images of spray dried nifedipine-polymer particles (15% w/w drug loading), spray dried from different solvent systems. The scale bar in the upper left corner of each image represents 2 µm.

6.a.3 Conclusion

This study has demonstrated that spray dried ASDs of nifedipine demonstrate markedly different photostabilities depending on the solvent system and/or drying temperature which was used to during spray drying.

Crystalline nifedipine which was simply mixed with different polymers demonstrated different photodegradation rates which is attributed to differential abilities of the polymers to inhibit free radical transfer.

When spray dried using the same solvent system, the PVP-nifedipine powder exhibited a slower (although statistically insignificantly different) photodegradation rate and lower photodegradant related impurity levels than equivalent HPMC and Soluplus systems, which may be due to intermolecular interactions. In contrast to studies of crystalline nifedipine, where particle size (and therefore specific surface area) is the biggest determinant of photodegradation rate, in ASDs of nifedipine the polymer choice and the morphology of the particle formed during the spray drying process appears to have the biggest influence on photodegradation rate. This is assumed to be due to the surface enrichment of nifedipine, but further work is needed to demonstrate this experimentally.

Chapter 6.b: Design and characterisation of an ASD of nifedipine for the treatment of autonomic dysreflexia

6.b.1 Introduction

Nifedipine is a calcium channel blocker used clinically in the management of hypertension. Generally nifedipine is formulated as an extended release preparation due to its short half-life of 8 hours [296,297]. Nifedipine is also licensed for the treatment of the circulatory disorder, Raynaud's syndrome, and immediate release preparations are available for this indication [158] . The immediate release formulations of nifedipine are also used for the treatment of autonomic dysreflexia, which is an unlicensed indication [298].

Autonomic dysreflexia (AD) is a life threatening hypertensive crisis that people with spinal cord injuries are at risk of developing [299] . AD is most prevalent in people with injuries above the T6 level. Estimates of the prevalence of AD in people with injuries above the T6 level range from 48% to 90%, highlighting the pervasiveness of this disease [300]. An episode of AD is commonly triggered by noxious stimuli below the injury level, such as bladder distention or colonic irritation [298]. This irritation results in a substantial unopposed sympathetic nervous system discharge causing symptoms such as sweating, headache and a profound rise in blood pressure. While non-pharmacological interventions such as emptying a catheter or loosening any tight clothing may resolve the condition, in extreme AD pharmacological therapy is indicated [298].

In the pharmacological management of AD, the "bite and swallow" method is commonly advised. This involves the patient, healthcare professional or caregiver crushing/rupturing a 10 mg nifedipine soft gelatine capsule before the patient swallows the capsule and the liquid nifedipine content. Although the content of the liquid capsule may be released in the mouth of the patient using this technique, nifedipine absorption is minimal via the sublingual or buccal route [301,302] . It is therefore the intestinal absorption of nifedipine which is critical to its therapeutic effect [303] and a sublingual formulation would not be appropriate for the treatment of AD.

The "bite and swallow" administration of nifedipine in the treatment of AD has been associated with serious adverse effects such as hypotension [304,305]. These adverse effects may, in part, be attributed to an erratic drug release profile which is anticipated from the rupturing of a liquid capsule [306], but experimental evidence of this is lacking.

The administration of nifedipine in AD is an unlicensed use, even without splitting open the liquid capsule, which represents a modification of the medicine. Medicines modification, such as splitting, often voids the license of a medicine which can have significant liability implications for healthcare professionals in the event of an adverse event [307]. The "bite and swallow" administration of nifedipine in the treatment of AD therefore represents an unlicensed modification to a medicine

being used for an unlicensed therapeutic indication. The need for an alternative formulation from both patient safety and healthcare professional liability perspectives is apparent.

This work aims to design a rapidly dissolving ASD of nifedipine for the treatment of AD, and to compare this to the release of nifedipine from a ruptured liquid capsule, which is the current standard of care. Four polymers (HPMC, PVP30, PVP17 and Soluplus) were selected for this purpose, and their solid state properties and dissolution profiles were compared to the current standard of care.

6.b.2 Results

6.b.2.1 pXRD analysis

The powder X-ray diffraction patterns for the spray dried polymer-nifedipine powders used in this study prior to and after tabletting (as described in Chapter 2 Section 2.2.1.4.2) are shown in Figure 6.b.1 below. The spray dried powders were all X-ray amorphous after spray drying, as expected from Chapter 6.a. of this chapter. After these powders were mixed with MCC and tabletted, a Bragg peak (located at approximately 25 degrees 2θ) is evident in all four of the nifedipine-polymer systems. This peak originates from MCC as evidenced by its diffractogram and is due to its semi-crystalline nature. No Bragg peak corresponding to crystalline nifedipine is evident in the powders post-tabletting, indicating that pressure-induced crystallisation is not a concern for these systems using the selected tabletting parameters.

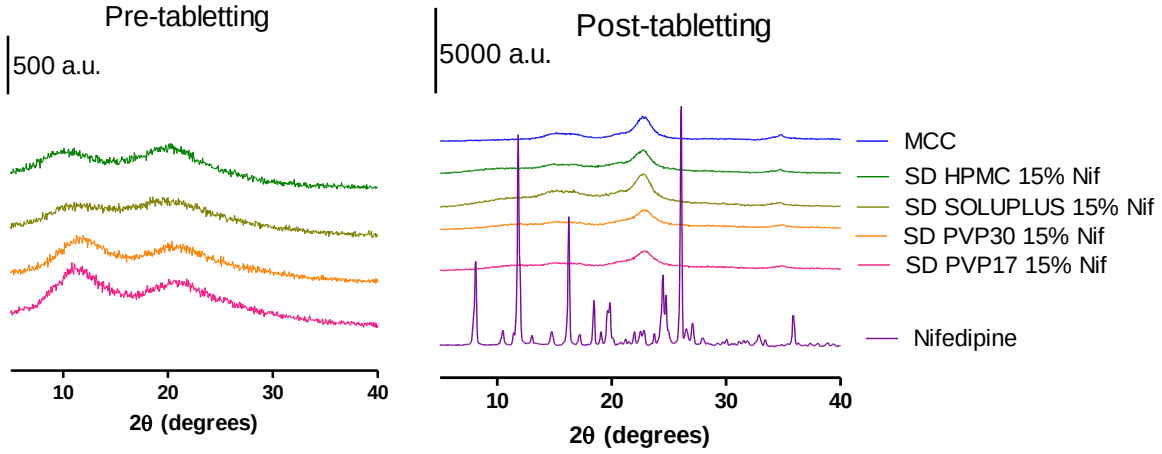

Figure 6.b.1: pXRD patterns of spray dried nifedipine-polymer systems with 15% w/w nifedipine pre and post tabletting. The pXRD patterns of crystalline nifedipine and MCC are shown for reference.

6.b.2.2 Nifedipine equilibrium solubility determination

Nifedipine's equilibrium solubility at 37 °C in aqueous media at pH 1.2 was determined as described in Chapter 2 Section 2.2.5.3. This value was determined to be 9.34 (± 2.70) µg/mL at 24 hours and 9.36 (± 1.12) µg/mL at 96 hours. This is similar to an equilibrium solubility value of nifedipine in 0.01M HCl at 37 °C reported in the literature of 10.91 ± 2.27 µg/mL [308]. As the dose of nifedipine used in the treatment of AD is 10 mg and the standard paddle apparatus uses a media volume of 900 mL, if the entirety of the nifedipine dose were to dissolve, this would represent a supersaturated state (11.11 µg/mL), meaning that standard test conditions are far from sink conditions. With this is mind, the traditional paddle method as well as a modified bi-phasic media

paddle method, which should be more representative of *in vivo* sink conditions, was used to test the tablets.

6.b.2.3 Dissolution testing

6.b.2.3.1 Traditional paddle method

The release of nifedipine from Adalat® capsules which had been cut open as described in Chapter 2 Section 2.2.4.3.1 and tested using the traditional paddle method is shown in Figure 6.b.2 below.

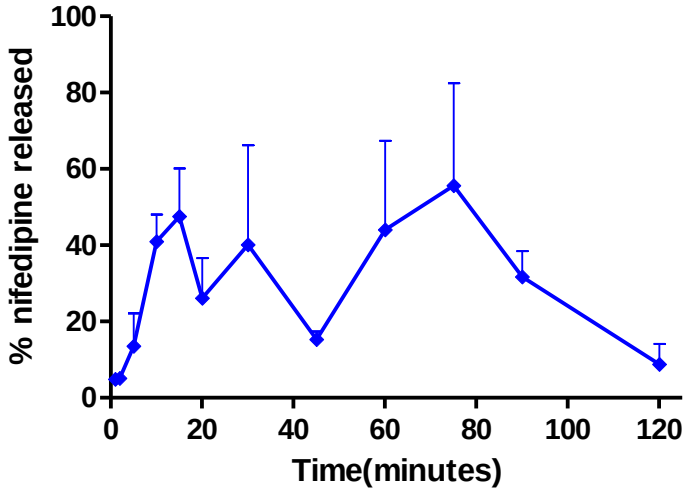

Figure 6.b.2: Nifedipine release from Adalat® capsules using the traditional paddle method at pH 1.2. n=3

The release of nifedipine from the split Adalat® capsules was initially rapid, as 48% of the available nifedipine was released within 15 minutes of the capsule being added to the dissolution vessel. However, the measured nifedipine release was erratic at later time points and reduced to only 8% at two hours. One explanation for this observation may be that an emulsion is formed *in situ* in the paddle apparatus. As peppermint oil is listed as an excipient in Bayer's literature pertaining to Adalat® [309], it is feasible that as nifedipine is released from the Adalat® capsule, the force of the paddle's rotation allows an emulsion to form. The log P of nifedipine is 2.5 [310] , meaning that nifedipine exhibits greater solubility in lipophilic media (such as peppermint oil) than in aqueous media. This implies that if an emulsion is formed, the nifedipine released from the Adalat® capsule will preferentially reside in the peppermint oil phase rather than the aqueous phase. This may account for the erratic release profile which was measured as seen in Figure 6.b.2, as sampling was occurring from a heterogenous system. This observation of inconsistent nifedipine release from lipid filled capsules has previously been described in the literature [157].

As shown in Figure 6.b.3, the release of nifedipine from the PVP17 tablets and PVP30 tablets was faster and greater than for the HPMC and Soluplus tablets. The Soluplus tablets exhibited no release of nifedipine over the two hours studied, which is surprising, as Soluplus is an amorphous polymer designed to improve the solubility of poorly soluble compounds. However, on examining the literature, this observation has been made previously for Soluplus-containing systems [13]. This was attributed to the fact that one of the constituent monomers of the co-polymer Soluplus, polyvinyl caprolactam, is insoluble in aqueous solutions above 35 °C. This can cause gelation at the surface of the tablet [311], which can inhibit API release. As the test conditions were carried out at 37 °C it is feasible that this is what caused complete inhibition of nifedipine release. This theory is supported by the fact that the Soluplus tablets showed smooth, uneroded gelled surfaces after recovery from the dissolution bath and a previous study in the literature which showed poor nifedipine dissolution form nifedipine-Soluplus co-precipitates [312].

The HPMC tablet shows gradual release of nifedipine, which is unsuited to use in AD. The slow release of nifedipine from HPMC tablets is also likely due to gelation. HPMC, when used as a polymer in ASD tablets is known to form a gelling matrix upon exposure to water [122]. The release of nifedipine from the ASD tablets is more consistent than for the Adalat® capsules. The initial release of nifedipine from the PVP17 and PVP30 tablets is similar to the Adalat® capsule and as these results were promising, these tablets were also tested using the modified paddle dissolution method, to better model *in vivo* dissolution.

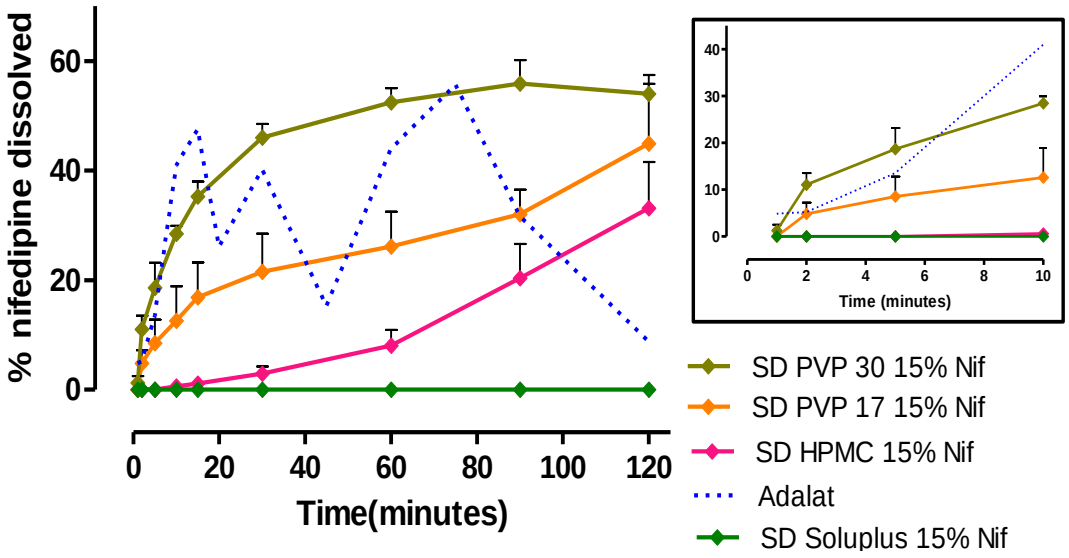

Figure 6.b.3: Nifedipine release profiles from ASD tablets using traditional paddle method. Inlay shows the first 15 minutes. The dashed blue line represents nifedipine release from Adalat® capsules

The solid fractions remaining in the dissolution vessels after 2 hours were extracted and dried, as described in Chapter 2 Section 2.2.4.3.1. Their pXRD patterns are shown in Figure 6.b.4 below.

As shown in Figure 6.b.4.a, the Bragg peaks present in the solid fractions of the ASD formulations correspond to those of MCC. In contrast, there are small Bragg peaks present in the post-dissolution solid fraction of the Adalat capsule which corresponds to the Bragg peaks present in crystalline nifedipine. This implies that nifedipine crystallised from the liquid capsule Adalat formulation during the dissolution process and explains the gradual reduction in nifedipine concentration for this formulation, particularly after 75 minutes (Figure 6.b.4.b). This was not observed for the solid fractions of the ASD formulations, which is likely due to the inhibitory effect that the selected polymers have on nifedipine crystallisation [80].

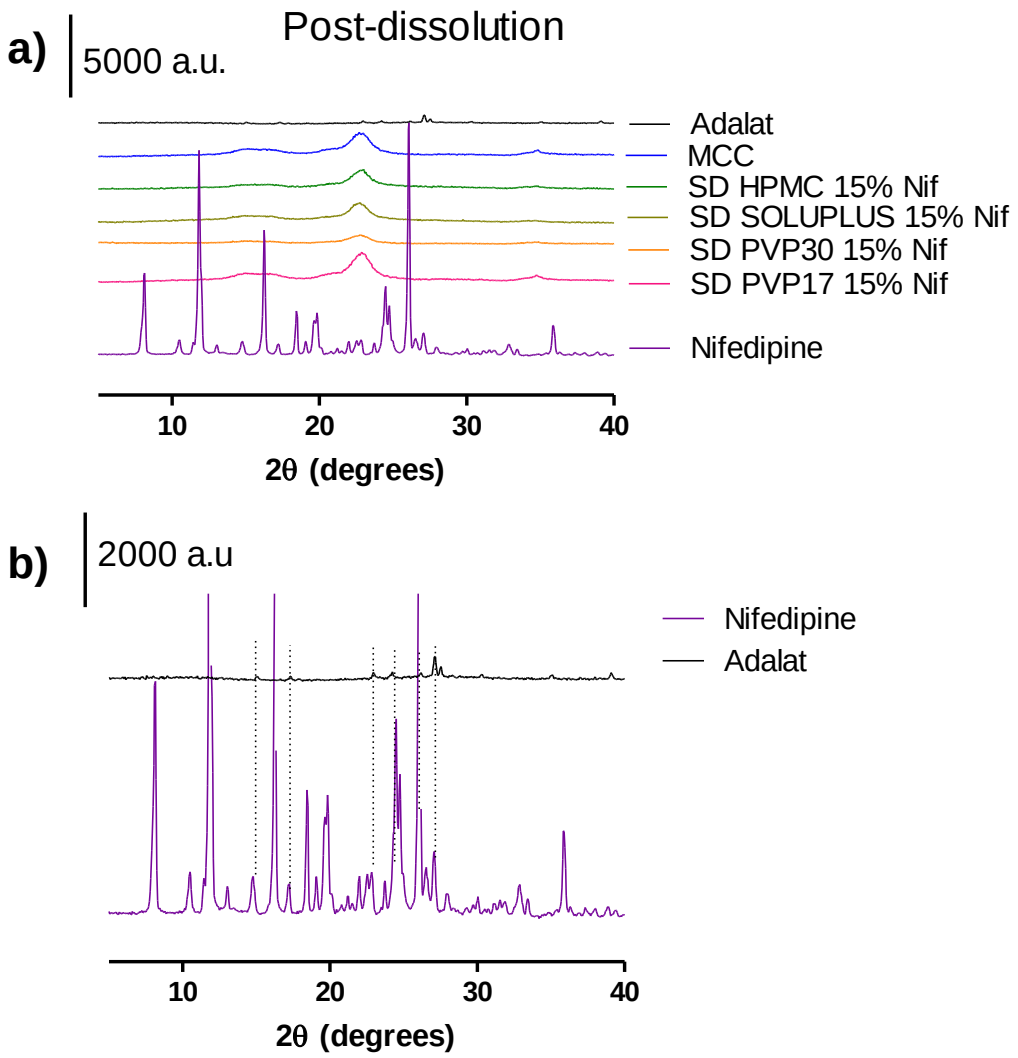

Figure 6.b.4: a) pXRD patterns of the post-dissolution solid fractions of Adalat® and ASD formulations. MCC and nifedipine pXRD patterns included for reference b) pXRD patterns of the post-dissolution solid fraction of Adalat highlighting the Bragg peaks which correspond to crystalline nifedipine

6.b.2.3.2 Biphasic media paddle method

The Adalat® capsules, PVP17 and PVP30 tablets were tested using the modified paddle method as outlined in Chapter 2 Section 2.2.4.3.2 and results are shown in Figure 6.b.5. This method was used as it should provide a better model of nifedipine dissolution and absorption *in vivo*. Octanol models the gastrointestinal mucosa, and partition into octanol represents the "absorption" of nifedipine [157]. As seen in Figure 6.b.5, the nifedipine dissolution/ release from the tablets and capsules respectively, was quite similar for the three systems. All three systems exhibited rapid release in the aqueous phase, with 40% or more of the available nifedipine being liberated within 15 minutes, however the dissolution of nifedipine from the ASD formulations is faster than the release from the Adalat capsule with 22% and 26% of the available nifedipine dissolved within 2 minutes for the PVP30 and PVP17 tablets respectively, while no nifedipine release was detected in the same time period for the Adalat capsules.

The nifedipine concentration reduces over time in the aqueous phase as it migrates into the octanol phase, mimicking nifedipine absorption *in vivo*. The nifedipine concentration in the octanol phase is highest for the PVP17 tablet at early time points and is similar for the PVP30 and Adalat formulations. This result indicates that the ASD preparations of nifedipine had release profiles similar to and, in the case of PVP17, marginally faster than the current standard of care in the treatment of AD. The PVP17-nifedipine system may have faster migration into the octanol phase than the equivalent PVP30 system due to the polymer's lower molecular weight and associated lower viscosity.

This result is promising and indicates that an ASD formulation is an appropriate alternative to the current unlicensed practice of splitting open Adalat capsules. It also demonstrates that the use of a biphasic media may be an appropriate adaptation to standard dissolution testing where therapeutic dosing results in non-sink conditions, particularly where hydrophobic excipients, such as oils are included in the formulation.

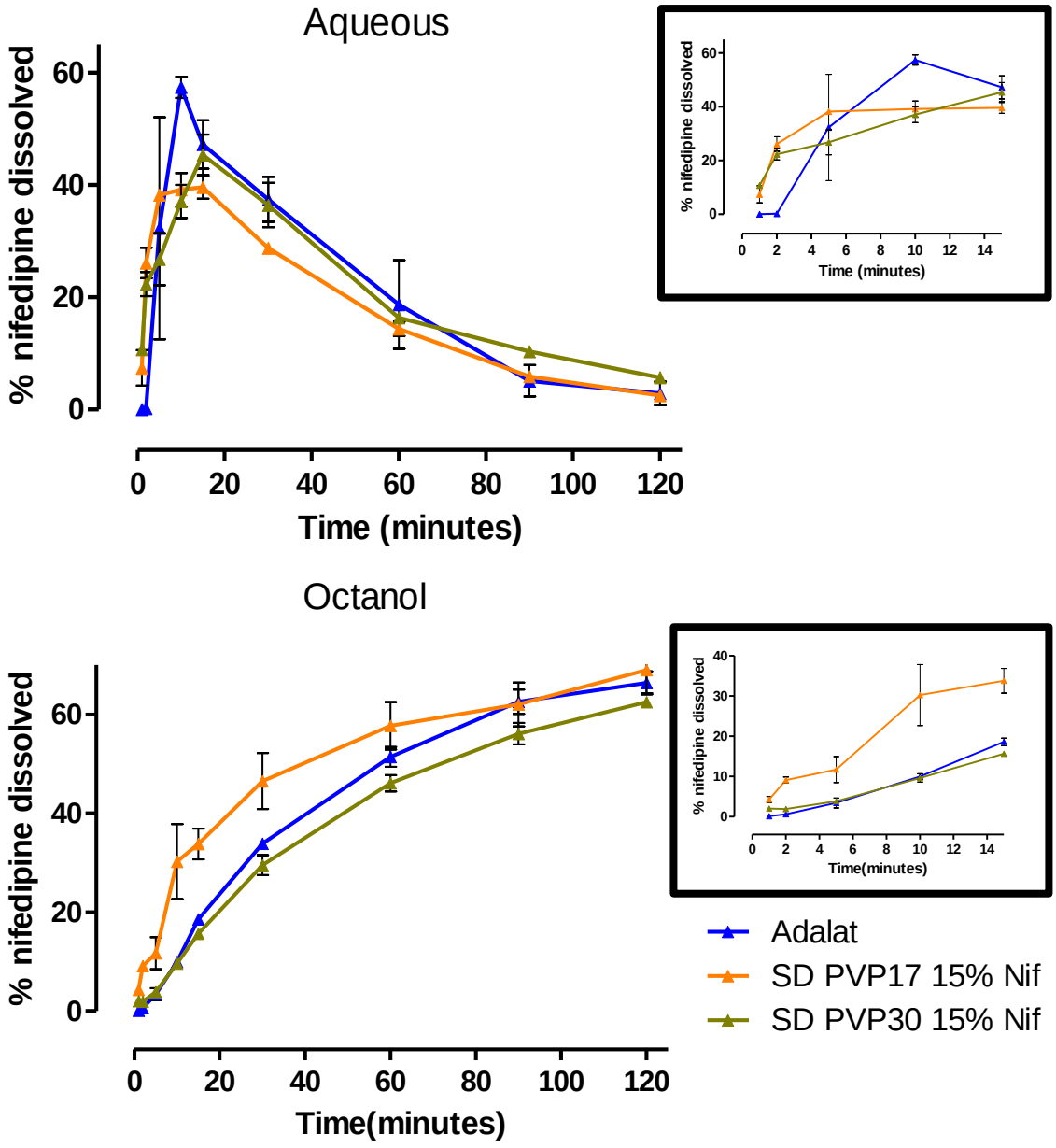

Figure 6.b.5: Nifedipine dissolution profile for Adalat® capsules and PVP17 and PVP30 ASD tablets in aqueous and octanol phases using modified paddle method. Inlays show first 15 minutes.

6.b.3. Conclusion

This preliminary study has shown that an ASD formulation is a viable alternative to the current standard treatment for AD. The current practice of splitting open a liquid capsule of nifedipine can lead to an erratic release profile and modelling such a practice is challenging using traditional dissolution methods due to the presence of lipophilic excipients. A biphasic medium, which includes a lipophilic component such as octanol, can model the *in vivo* absorption of nifedipine under non-sink aqueous conditions and provided a more appropriate model in this case.

Four polymers (HPMC, Soluplus, PVP17 and PVP30) were tested for their suitability for nifedipine ASD development for the treatment of AD. The highly water-soluble polymer PVP was found to facilitate rapid dissolution of nifedipine from an ASD tablet, in contrast to Soluplus and HPMC, the use of which resulted in the release of nifedipine being hindered due to gelling. The lower molecular weight PVP polymer was found to partition into the octanol phase more rapidly than its higher molecular weight counterpart, underlining the importance of polymer physicochemical properties in ASD development.

While further work is needed in the development of an ASD nifedipine formulation for the treatment of AD, this study has highlighted the potential utility of ASD formulations in medical emergencies.

Chapter 7: General discussion and conclusions

7.1 General discussion and conclusions

As outlined in the origin and scope section, the aim of this thesis was to explore various factors which affect the stability and performance of ASDs. A wide variety of such factors have been identified from the literature and expanded upon in this thesis.

While attempts were made to determine if any difference exists in the glass forming ability or glass stability of a racemic mixture compared to enantiopure ibuprofen, as indicated in Chapter 3, results did not provide a conclusive answer to the question posed. From examining the literature [5,6,183] the expectation would be that S IBU may be more stable in the glassy/amorphous state compared to R,S IBU. Experimentally, while S IBU appeared to have a greater tendency towards crystallisation from the supercooled state during non-isothermal crystallisation studies than R,S IBU, there were inconsistent findings across replicates. In contrast, enthalpy relaxation studies showed that R,S IBU appeared to relax faster in the amorphous state compared to S IBU, but there was a high degree of error associated with these results. BDS provided insight into the molecular mobility of R,S IBU and S IBU. The apparent crystallisation of polymorphic form II of R,S IBU during BDS testing was captured for the first time as a result of the work undertaken in this thesis. Only one secondary process was observed in amorphous R,S IBU while two secondary processes were observed for S IBU, although one of these may relate to a degradant product. This is in contrast to more detailed studies from the literature which have demonstrated that S IBU and R,S IBU both possess four relaxation processes [149,190]. This points towards a thermodynamic, rather than kinetic driving force governing any difference in the crystallisation tendencies of R,S IBU or S IBU from the amorphous state. This thesis has highlighted that thermal methods alone are probably not appropriate for determining the glass forming ability and stability differences of so called "good glass formers" [4] , such as ibuprofen, as the tendency towards crystallisation is low and therefore extremely low cooling rates may be required to allow for any difference in crystallisation between the racemic mixture and the enantiopure form of an API to become apparent. While further work is clearly needed, it is evident that the chirality of an API is a factor which may affect the glass forming ability and/or stability of the glassy state and formulators should consider this during the development of an ASD.

The concept that chiral recognition may exist in an ASD formed from a chiral API and a chiral polymer, such as the cellulose based polymers, is certainly an interesting topic. If chiral recognition exists in ASDs, this may be another factor that can affect the physical stability of ASDs. The mechanism by which chiral discrimination occurs was postulated to stem from opposing enantiomers of the API possessing different strengths of intermolecular interaction with the

polymer, however this was demonstrated experimentally in only one study [7]. Although chiral recognition is generally understood to refer to two opposing enantiomers, in the context of ASD development, it would be highly unlikely from a clinical perspective, for two opposing enantiomers of the same API to be under consideration for formulation development. A more probable situation which could be envisaged would be a racemic switch from a racemic mixture to a single active enantiomer of an API. No studies have examined the impact that a racemic switch may have on the stability of an ASD. The work carried out in this thesis represents only the third reported study to examine chiral recognition in an ASD, and the first study, to our knowledge, that has examined the impact that a racemic switch may have on ASD stability.

Cryo-milling IBU with four different cellulose polymers did not result in complete amorphisation of IBU for any of the systems studied. The melting points of the crystalline IBU which remained in the mixture was more significantly depressed for the HPMC and the HPMCAS systems compared to the HPC and HPMCP systems. The melting point of the R IBU HPMCAS was significantly more depressed (7 ^{o}C) than for the S IBU HPMCAS system, while the S IBU HPMC system contained significantly less (approximately 20% less) crystalline IBU than the R IBU HPMC system. These findings are interesting and point towards chiral recognition existing in these systems. The significant difference in melting point depression provides evidence of differing degrees of miscibility between cryo-milled HPMCAS R IBU and cryo-milled HPMCAS S IBU [102]. The difference in proportion of crystalline material between cryo-milled HPMC S IBU and cryo-milled HPMC R IBU indicates that there is a difference in the ability of HPMC to facilitate amorphisation depending on the enantiomer of IBU with which it is cryo-milled. This theory was supported further by spherulite growth studies, which demonstrated that the growth rate of S IBU spherulites in the presence of 5% HPMC was significantly lower than for the equivalent R IBU spherulites. Interestingly, these observations do not correlate well with the ATR-FTIR spectra findings, which showed that there were different ratios of monomeric to dimeric IBU in the cryo-milled R IBU HPMCP and S IBU HPMCP systems, but that these ratios were very similar for the cryo-milled R IBU and S IBU HPMC and HPMCAS systems. This indicates that differences in hydrogen bonding between R IBU and cellulose polymers and S IBU and cellulose polymers do not predict differences in miscibility or ability to facilitate amorphisation. These stereoselective phenomena must, therefore, be due to differences in the strength of other forms of intermolecular interaction between IBU and the cellulose polymers, such as Van der Waals interactions.

As part of the work carried out in this thesis, the role that the manufacturing method plays in chiral recognition was also examined. A system which appeared to show chiral recognition when

produced via cryo-milling (IBU-HPMC), was also produced via spray drying. In the literature, the term "chiral recognition" generally refers to two substances which are in solution. As the spray drying studies undertaken start with a system in solution, it was thought that, due to the more intimate mixing of substances that this allows, any stereoselective effect may be enhanced. In fact, what was observed was that the spray dried R IBU HPMC and the spray dried S IBU HPMC systems were both completely pXRD amorphous, in contrast to their cryo-milled equivalents, for which S IBU HPMC was less crystalline than R IBU HPMC. The spray dried R,S IBU HPMC was also less crystalline than its equivalent cryo-milled system, but some crystalline IBU remained, as evidenced via pXRD and DSC. One explanation for the attenuation of the stereoselective effect when R IBU HPMC and S IBU HPMC were spray dried is that, by solubilising the two components, more intimate molecular mixing of HPMC and IBU occurred than when these systems were cryo-milled. This mixing at the molecular level allowed IBU to be stabilised in the amorphous form in contrast to the cryo-milled system [126]. ATR- FTIR spectra demonstrated that although both spray dried S IBU HPMC and spray dried R IBU HPMC were amorphous, there were clear differences between the hydrogen bonding profile of the carbonyl in the IBU molecule when spray dried with HPMC depending on which enantiomer of IBU was used. This finding indicates that although spray drying resulted in a loss of stereoselective facilitation of amorphisation, it did result in a stereoselective intermolecular interaction between IBU and HPMC. Regarding spray dried R,S IBU HPMC it is interesting to note that at the same weight ratio, the racemic compound was partially crystalline in contrast to both of its single enantiomer counterparts. This observation may stem from differences in the thermodynamic properties of their crystalline states.

The objective of the second experimental chapter was to examine how polymer selection affects a wide variety of ASD properties. The glass transition temperatures of ASDs which were prepared using a PVP of higher molecular weight were observed to deviate the most from Gordon-Taylor predicted Tg values due to the viscosity of the polymer limiting the diffusion of ketoprofen through the polymeric matrix. The ASDs with high VA content demonstrated glass transition temperatures which were closest to the Gordon-Taylor predicted values, which is due to their low propensity to form hydrogen bonds with ketoprofen, allowing the stronger dimeric ketoprofen hydrogen bonds to remain intact.

The effect that relative humidity had on the ASDs was explored using the concept of RH_{Tg} i.e. the relative humidity at which the amorphous material is plasticised by the presence of moisture to the extent that it converts to a supercooled liquid. A trend between the RH_{Tg} and molecular weight of the PVP-based ASDs was apparent, as the higher the molecular weight of the PVP, the higher was

the RH_{Tg} value. This is likely due to the high viscosity of the higher molecular weight systems which limited the diffusion of the water. Similarly, a trend between the RH_{Tg} and the ratio of VP:VA in the ASD was also apparent. The systems with higher VA content had higher RH_{Tg} values, while the systems with higher VP content had lower RH_{Tg} values. This trend is due to the hydrophobicity of the VA moiety, which is protective against moisture sorption and associated plasticisation. To our knowledge, this is the first study which has examined the role of polymer weight or substitution ratio on RH_{Tg}. The RH_{Tg} measurements correlated well with the glass transition temperature depression which was observed for the ASDs after 12 weeks of exposure to 75% RH. Low molecular weight PVP systems exhibited the highest degree of plasticisation, while high molecular weight PVP systems exhibited the lowest degree of plasticisation. Similarly, the ASDs with high VP content exhibited plasticisation after storage at 75% RH while the high VA content systems did not show plasticisation.

The effect that polymer selection has on supersaturation was also examined. Interestingly, the hydrophobic nature of the polymeric component of the ASD, rather than complete amorphisation, was found to be critical to the extent of ketoprofen supersaturation which was achieved. Although the PVAcetateKETO system was completely pXRD amorphous, its hydrophobicity meant that supersaturation of ketoprofen was not achieved within 2 hours. This experiment has highlighted that the aqueous solubility of the polymer, a factor which is often overlooked, has a critical role in determining ASD supersaturation.

The role that polymer selection has on the processability of ASDs is an area of research which has not been investigated thoroughly [122]. While no trend was observed between polymer molecular weight or substitution ratio and the compressibility of the ASD powder, the systems which contained VP demonstrated higher tensile strength than the systems which did not contain this functional group. This points towards the dual functionality, as a binder and an amorphous stabiliser, that VP-containing polymers possess in ASD systems. The advantages and disadvantages associated with different poly-vinyl polymer properties, as demonstrated in Chapter 4, are summarised in Table 7.1 below.. While the PVP polymers have proven to be very popular in ASD development, their desirable high glass transition temperature may be offset during storage due their propensity to sorb moisture. Identifying the optimal VP:VA ratio will help to ensure that achieving excellent aqueous solubility does not jeopardise the solid-state stability of the amorphous state. It is clear from the studies presented in this thesis that the optimal VP:VA ratio lies somewhere between 3:7 and 7:3. While the PVPVA polymer which is commonly used in ASD systems has a VP:VA ratio (6:4) which falls in between these ratios, it would be interesting to

examine the effect that 4:6 and 5:5 VP:VA systems have on ASD properties to identify if the commercially used polymer could be improved upon.

Table 7.1:Summary of the effects of poly-vinyl polymer properties on ASD performance

Poly-vinyl polymer property	Effect on ASD performance
High Mw	• Higher glass transition temperature • More resistant to water induced phase transition • Slower to reach supersaturation
High VP content	• Higher glass transition temperature • More prone to water induced phase transition • Higher degree of supersaturation • Higher propensity to hydrogen bond with API • Any VP content associated with higher tablet tensile strength
High VA content	• Lower glass transition temperature • Less prone to water induced phase transition • Lower degree of supersaturation • Lower propensity to hydrogen bond with API

Chapter 5 examined the effect that ASD manufacturing method has on the material properties of ASD powders. The more traditional spray drying ASD manufacturing method was compared to the more novel electrospraying process. As both processes necessitate solubilising the API and the polymer prior to processing, the interaction between solution properties and manufacturing process on particle properties could also be evaluated. The electrosprayed particles exhibited a more monodisperse particle size distribution compared to the equivalent spray dried particles. The electrosprayed particles were also, generally, smaller than the spray dried particles as they were devoid of large agglomerates. It was interesting to note that the ketoprofen-polymer solutions which had lower conductivity values (PVPVA-KETO), exhibited webbing between particles, which is likely due to the electrospraying jet alternating between stable and unstable modes.

The solid-state characteristics of the spray dried and the electrosprayed ASD were very similar as the glass transition temperature, ketoprofen loading, ATR-FTIR spectra and the pXRD pattern were all comparable. The dissolution profiles of both ASD systems were also very similar, and both ASDs dissolved faster than the equivalent physical mixture. The smaller particle size of the electrosprayed ASD was associated with a faster rate of surface adsorption of water and poorer flow. While the need for novel ASD manufacturing methods is clear, in this instance electrospraying did not provide any benefit to ASD performance and actually produced ASD material which was sub-optimal with respect to processability, compared to the traditional spray drying process, which is associated with

a much higher throughput rate. Therefore, at lab scale, spray drying is a more efficient process for producing ASDs of ketoprofen with desirable material properties for downstream processing.

Chapter 6 focussed on the chemical stability, specifically the photostability of amorphous nifedipine. This was of interest as the chemical stability of the amorphous state is often overlooked.. While the photostability of amorphous nifedipine has previously been demonstrated to be poorer than the photostability of crystalline nifedipine [279], no work thus far has examined whether the generation of an ASD may improve the photostability of amorphous nifedipine. All spray dried ASD systems exhibited lower amorphous nifedipine photodecomposition rates than the amorphous nifedipine photodecomposition rate which was reported in the literature [279]. When the systems were spray dried from the same solvent system, the PVP30-nifedipine system had a slightly lower photodecomposition rate than the equivalent Soluplus-nifedipine and HPMC-nifedipine systems. This was attributed to a combination of PVP's ability to hydrogen bond to nifedipine and the presence of the vinyl-pyrrolidone functional group.

The photodecomposition rates of the spray dried HPMC-nifedipine and Soluplus-nifedipine systems increased when they were spray dried using a higher proportion of water in the solvent system. This observation is thought to be due to the influence that the change in solvent composition had on the distribution of nifedipine at the surface of the particles. Some evidence for this is seen in the SEM images which demonstrate significant crumpling of the spray dried particles originating from a high-water content solvent system. It was highlighted that the surface enrichment of amorphous nifedipine is a critical factor governing its photostability when formulated as an ASD. This is contrast to crystalline nifedipine where particle size, and therefore specific surface area are the critical material attributes governing nifedipine photostability. This work also highlights that the chemical stability of the amorphous state, which is often overlooked, should be assessed prior to the development of an ASD.

The final objective of this thesis was to apply the knowledge gained through undertaking this body of work, to an area of unmet clinical need. This aim has been fulfilled, in part, through the development of an immediate release ASD formulation of nifedipine for the treatment of autonomic dysreflexia. Soluplus and HPMC were found to be inappropriate polymer choices for this purpose due their negligible and slow release of nifedipine respectively. By contrast, PVP17 and PVP30 demonstrated rapid dissolution of nifedipine, which was comparable to the nifedipine release observed from the current practice of splitting open a liquid capsule of nifedipine which represents an unlicensed modification of a medicine. These formulations clearly warrant further

development as current practice puts patients and the healthcare professionals advocating such practices at unacceptable risk.

Overall this thesis has demonstrated that a multitude of factors affect the stability and performance of ASDs of poorly soluble APIs.

7.2 Main findings

- There is evidence of chiral recognition between IBU and the cellulose polymers, particularly with HPMC and HPMCAS. S IBU appears to be more stable in the amorphous state when combined with HPMC compared to R IBU.
- Solid dispersions of HPMC and IBU produced via spray drying exhibit higher amorphous content compared to equivalent material prepared via cryo-milling. This is attributed to the greater extent of molecular mixing which occurs in solution-mediated processes.
- In the event of a racemic switch from a spray dried IBU HPMC ASD to the active enantiomer S IBU HPMC, at 60% IBU loading, amorphous IBU content would increase and the dissolution rate of the system would also increase.
- ASDs of ketoprofen and various poly-vinyl polymers were found to exhibit different characteristics depending on the molecular weight and the substitution ratio of the co-polymer.
- RH_{Tg} values were found to correlate well with the extent of plasticisation which was observed upon exposure of ketoprofen ASDs to high relative humidity.
- The extent of supersaturation achieved by the ketoprofen-polymer systems was found to depend largely on the aqueous solubility of the polymer, rather than the complete amorphisation of ketoprofen.
- Electrospraying was determined to produce ASD material which was comparable with ASD material produced via spray drying in terms of dissolution performance. However, the smaller particle size associated with the electrosprayed material resulted in a faster surface adsorption rate of moisture compared to the spray dried material, as well as poorer compressibility.
- By formulating nifedipine as an ASD, the photostability of amorphous nifedipine was improved.
- The photostability of amorphous nifedipine in ASDs was found to be poorer for two of the systems which were spray dried from a solvent system containing a higher proportion of water. This was attributed to the effect that the solvent composition has on particle formation, and surface enrichment of nifedipine.

- PVP polymers were found to be suitable for the development of an immediate release of an ASD formulation of nifedipine for the treatment of autonomic dysreflexia.

7.3 Future work

- Repeat the glass forming ability and glass stability experiments using a chiral "poor glass former" [4] API. It would be interesting to use a panel of such APIs, including racemic conglomerates and racemic compounds with varying ratios in the heats of fusion/melting points between the racemic mixture and the enantiopure API. This could enable further insight into the influence of thermodynamic properties on the amorphous stability of chiral APIs.

- Investigate if chiral discrimination is also seen when R IBU and S IBU are spray dried with HPMCAS, as this polymer showed significant stereoselectivity with regard to melting point depression of cryo-milled crystalline ibuprofen.

- As solution conductivity is a critical factor in the electrospraying process, it would be interesting to investigate how the drug loading of an API-polymer salt forming system influences solution conductivity and thus the morphology of the electrosprayed particles.

- Investigate the surface composition of spray dried ASDs of nifedipine using spray dried systems with a higher nifedipine concentration via X-ray photoelectron spectroscopy (XPS) to overcome limit of detection issues.

- Repeat the photostability studies using differing ethanol:water solvent ratios to determine if there is a trend between reduced photostability and increased water content.

- Develop the PVP17 Nifedipine ASD formulation further by testing downstream properties such as flow, tensile strength and friability. It would also be interesting to carry out a permeability assay, such as a parallel artificial membrane permeability assay (PAMPA) using the liquid content of a split Adalat® capsule and a PVP-nifedipine ASD.

References

1. Lipinski CA. Poor aqueous solubility – an industry wide problem in drug discovery. *Am Pharm Rev*. 2002;5(November):82-85.

2. Jermain S V., Brough C, Williams RO. Amorphous solid dispersions and nanocrystal technologies for poorly water-soluble drug delivery – An update. *Int J Pharm*. 2018;535(1-2):379-392. doi:10.1016/j.ijpharm.2017.10.051

3. Hancock BC, Zografi G. Characteristics and significance of the amorphous state in pharmaceutical systems. *J Pharm Sci*. 1997;86(1):1-12. doi:10.1021/js9601896

4. Baird JA, Van Eerdenbrugh B, Taylor LS. A classification system to assess the crystallization tendency of organic molecules from undercooled melts. *J Pharm Sci*. 2010;99(9):3787-3806. doi:10.1002/jps.22197

5. Viel Q, Delbreilh L, Coquerel G, Petit S, Dargent E. Molecular mobility of an amorphous chiral pharmaceutical compound: Impact of chirality and chemical purity. *J Phys Chem B*. 2017;121(32):7729-7740. doi:10.1021/acs.jpcb.7b05667

6. Atawa B, Couvrat N, Coquerel G, Dargent E, Saiter A. Impact of chirality on the glass forming ability and the crystallization from the amorphous state of 5-ethyl-5-methylhydantoin, a chiral poor glass former. *Int J Pharm*. 2018;540(1-2):11-21. doi:10.1016/j.ijpharm.2018.01.050

7. Sato T, Taylor LS. Chiral discrimination by a cellulose polymer: differential crystallization inhibition of enantiomers in amorphous dispersions. *CrystEngComm*. 2015;17(27):5046-5053. doi:10.1039/C5CE00810G

8. Miyazaki T, Aso Y, Yoshioka S, Kawanishi T. Differences in crystallization rate of nitrendipine enantiomers in amorphous solid dispersions with HPMC and HPMCP. *Int J Pharm*. 2011;407(1-2):111-118. doi:10.1016/j.ijpharm.2011.01.035

9. Rumondor ACF, Taylor LS. Effect of polymer hygroscopicity on the phase behavior of amorphous solid dispersions in the presence of moisture. *Mol Pharm*. 2010;7(2):477-490. doi:10.1021/mp9002283

10. Kothari K, Ragoonanan V, Suryanarayanan R. The role of drug-polymer hydrogen bonding interactions on the molecular mobility and physical stability of nifedipine solid dispersions. *Mol Pharm*. 2015;12(1):162-170. doi:10.1021/mp5005146

11. Chan SY, Chung YY, Cheah XZ, Tan EYL, Quah J. The characterization and dissolution performances of spray dried solid dispersion of ketoprofen in hydrophilic carriers. *Asian J Pharm Sci*. 2015;10(5):372-385. doi:10.1016/j.ajps.2015.04.003

12. Agrawal AM, Dudhedia MS, Patel AD, Raikes MS. Characterization and performance assessment of solid dispersions prepared by hot melt extrusion and spray drying process. *Int J Pharm*. 2013;457(1):71-81. doi:10.1016/j.ijpharm.2013.08.081

13. Kelleher JF, Gilvary GC, Madi AM, Jones DS, Li S, Tian Y, Almajaan A, Senta-Loys Z, Andrews GP, Healy AM. A comparative study between hot-melt extrusion and spray-drying for the manufacture of anti-hypertension compatible monolithic fixed-dose combination products. *Int J Pharm*. 2018;545(1-2):183-196. doi:10.1016/j.ijpharm.2018.05.008

14. Smeets A, Clasen C, Van den Mooter G. Electrospraying of polymer solutions: Study of formulation and process parameters. *Eur J Pharm Biopharm*. 2017;119:114-124. doi:10.1016/j.ejpb.2017.06.010

15. Kawakami K, Zhang S, Chauhan RS, Ishizuka N, Yamamoto M, Masaoka Y, Kataoka M, Yamashita S, Sakuma S. Preparation of fenofibrate solid dispersion using electrospray deposition and improvement in oral absorption by instantaneous post-heating of the formulation. *Int J Pharm*. 2013;450(1-2):123-128. doi:10.1016/j.ijpharm.2013.04.006

16. Yu D-G, Williams GR, Yang J-HJ-M, Wang X, Yang J-HJ-M, Li X-Y. Solid lipid nanoparticles self-assembled from electrosprayed polymer-based microparticles. *J Mater Chem*. 2011;21(40):15957. doi:10.1039/c1jm12720a

17. Pikal MJ, Lukes AL, Lang JE, Gaines K. Quantitative crystallinity determinations for β-lactam antibiotics by solution calorimetry: Correlations with stability. *J Pharm Sci*. 1978;67(6):767-773. doi:10.1002/jps.2600670609

18. Pikal MJ, Lukes AL, Lang JE. Thermal decomposition of amorphous β-lactam antibacterials. *J Pharm Sci*. 1977;66(9):1312-1316. doi:10.1002/jps.2600660927

19. Balant LP. Is there a need for more precise definitions of bioavailability? - Conclusions of a Consensus Workshop, Munich, September 9, 1989; under the patronage of the F.I.P. *Eur J Clin Pharmacol*. 1991;40(2):123-126. doi:10.1007/BF00280064

20. Kelly J, McGarry K, O'Malley K, O'Brien E. Bioavailability of labetalol increases with age. *Br J Clin Pharmacol*. 1982;14(2):304-305. doi:10.1111/j.1365-2125.1982.tb01983.x

21. Lindholm A, Welsh M, Alton C, Kahan BD. Demographic factors influencing cyclosporine

pharmacokinetic parameters in patients with uremia: Racial differences in bioavailability. *Clin Pharmacol Ther*. 1992;52(4):359-371. doi:10.1038/clpt.1992.156

22. Martinez MN, Amidon GL. A mechanistic approach to understanding the factors affecting drug absorption: a review of fundamentals. *J Clin Pharmacol*. 2002;42(6):620-643. http://www.ncbi.nlm.nih.gov/pubmed/12043951.

23. Lill J, Bauer LA, Horn JR, Hansten PD. Cyclosporine–drug interactions and the influence of patient age. *Am J Heal Pharm*. 2000;57(17):1579-1584. doi:10.1093/ajhp/57.17.1579

24. Veber DF, Johnson SR, Cheng HY, Smith BR, Ward KW, Kopple KD. Molecular properties that influence the oral bioavailability of drug candidates. *J Med Chem*. 2002;45(12):2615-2623. doi:10.1021/jm020017n

25. Amidon GL, Lennernäs H, Shah VP, Crison JR. A theoretical basis for a biopharmaceutic drug classification: The correlation of in vitro drug product dissolution and in vivo bioavailability. *Pharm Res*. 1995;12(3):413-420.

26. Food and Drug Administration. *Waiver of In Vivo Bioavailability and Bioequivalence Studies for Immediate-Release Solid Oral Dosage Forms Based on a Biopharmaceutics Classification System Guidance for Industry*.; 2017. https://www.fda.gov/media/70963/download.

27. Yazdanian M, Briggs K, Jankovsky C, Hawi A. The “high solubility” definition of the current FDA guidance on biopharmaceutical classification system may be too strict for acidic drugs. *Pharm Res*. 2004;21(2):293-299. doi:10.1023/B:PHAM.0000016242.48642.71

28. Butler JM, Dressman JB. The developability classification system: application of biopharmaceutics concepts to formulation development. *J Pharm Sci*. 2010;99(12):4940-4954. doi:10.1002/jps.22217

29. Lipinski CA, Lombardo F, Dominy BW, Feeney PJ. Experimental and computational approaches to estimate solubility and permeability in drug discovery and development settings. *Adv Drug Deliv Rev*. 2012;64(SUPPL.):4-17. doi:10.1016/j.addr.2012.09.019

30. Lipinski CA. Drug-like properties and the causes of poor solubility and poor permeability. *J Pharmacol Toxicol Methods*. 2000;44(1):235-249. doi:10.1016/S1056-8719(00)00107-6

31. Lipp R. The innovator pipeline: Bioavailability challenges and advanced oral drug delivery opportunities. *Am Pharm Rev*. 2013;16(3):14-16. https://www.americanpharmaceuticalreview.com/Featured-Articles/135982-The-Innovator-Pipeline-Bioavailability-Challenges-and-Advanced-Oral-Drug-Delivery-

Opportunities/.

32. DiMasi JA, Grabowski HG, Hansen RW. Innovation in the pharmaceutical industry: New estimates of R&D costs. *J Health Econ*. 2016;47:20-33. doi:10.1016/j.jhealeco.2016.01.012

33. Bhattachar SN, Deschenes LA, Wesley JA. Solubility: it's not just for physical chemists. *Drug Discov Today*. 2006;11(21-22):1012-1018. doi:10.1016/j.drudis.2006.09.002

34. Bevernage J, Brouwers J, Annaert P, Augustijns P. Drug precipitation-permeation interplay: Supersaturation in an absorptive environment. *Eur J Pharm Biopharm*. 2012;82(2):424-428. doi:10.1016/j.ejpb.2012.07.009

35. Ku MS, Dulin W. A biopharmaceutical classification-based right-first-time formulation approach to reduce human pharmacokinetic variability and project cycle time from first-in-human to clinical proof-of-concept. *Pharm Dev Technol*. 2012;17(3):285-302. doi:10.3109/10837450.2010.535826

36. Noyes AA, Whitney WR. The rate of solution of solid substances in their own solutions. *J Am Chem Soc*. 1897;19(12):930-934. doi:10.1021/ja02086a003

37. Nernst W, E. Brunner. Reaktionsgeschwindigkeit in heterogenen systemen. *Zeitschrift für Phys Chemie*. 1904;47(1):56–102. doi:10.1515/zpch-1904-4705

38. Dokoumetzidis A, Macheras P. A century of dissolution research: From Noyes and Whitney to the Biopharmaceutics Classification System. *Int J Pharm*. 2006;321(1-2):1-11. doi:10.1016/j.ijpharm.2006.07.011

39. Aulton ME, Taylor KMG. Scientific principles of dosage form and design. In: Aulton ME, Taylor KMG, eds. *Aulton's Pharmaceutics- The Design and Manufacture of Medicines*. 4th ed. Edinburgh: Churchill Livingston; 2013:24.

40. Pouton CW. Formulation of poorly water-soluble drugs for oral administration: Physicochemical and physiological issues and the lipid formulation classification system. *Eur J Pharm Sci*. 2006;29(3-4 SPEC. ISS.):278-287. doi:10.1016/j.ejps.2006.04.016

41. Kawabata Y, Wada K, Nakatani M, Yamada S, Onoue S. Formulation design for poorly water-soluble drugs based on biopharmaceutics classification system: Basic approaches and practical applications. *Int J Pharm*. 2011;420(1):1-10. doi:10.1016/j.ijpharm.2011.08.032

42. Stephenson GA, Aburub A, Woods TA. Physical stability of salts of weak bases in the solid-

state. *J Pharm Sci*. 2011;100(5):1607-1617. doi:10.1002/jps.22405

43. Berge S, Bighley L, Monkhouse D. Pharmaceutical Salts. *J Pharm Sci*. 1977;66(1):1-19.

44. Childs SL, Stahly GP, Park A. The salt-cocrystal continuum: The influence of crystal structure on ionization state. *Mol Pharm*. 2007;4(3):323-338. doi:10.1021/mp0601345

45. Rodriguez-Aller M, Guillarme D, Veuthey JL, Gurny R, Pouton CW, Fahr A, Liu X, Gibaldi M, Feldman S. Strategies for formulating and delivering poorly water-soluble drugs. *J Drug Deliv Sci Technol*. 2015;30(10):342-351. doi:10.1016/j.jddst.2015.05.009

46. Rautio J, Kumpulainen H, Heimbach T, Oliyai R, Oh D, Järvinen T, Savolainen J. Prodrugs: Design and clinical applications. *Nat Rev Drug Discov*. 2008;7(3):255-270. doi:10.1038/nrd2468

47. Sanches BMA, Ferreira EI. Is prodrug design an approach to increase water solubility? *Int J Pharm*. 2019;568(May):118498. doi:10.1016/j.ijpharm.2019.118498

48. Stella VJ, Nti-Addae KW. Prodrug strategies to overcome poor water solubility. *Adv Drug Deliv Rev*. 2007;59(7):677-694. doi:10.1016/j.addr.2007.05.013

49. Schultheiss N, Newman A. Pharmaceutical cocrystals and their physicochemical properties. *Cryst Growth Des*. 2009;9(6):2950-2967. doi:10.1021/cg900129f

50. Thakuria R, Delori A, Jones W, Lipert MP, Roy L, Rodríguez-Hornedo N. Pharmaceutical cocrystals and poorly soluble drugs. *Int J Pharm*. 2013;453(1):101-125. doi:10.1016/j.ijpharm.2012.10.043

51. Qiao N, Li M, Schlindwein W, Malek N, Davies A, Trappitt G. Pharmaceutical cocrystals: An overview. *Int J Pharm*. 2011;419(1-2):1-11. doi:10.1016/j.ijpharm.2011.07.037

52. Greenhalgh DJ, Williams AC, Timmins P, York P. Solubility parameters as predictors of miscibility in solid dispersions. *J Pharm Sci*. 1999;88(11):1182-1190. doi:10.1021/js9900856

53. Szejtli J. Utilization of cyclodextrins in industrial products and processes. *J Mater Chem*. 1997;7(4):575-587. doi:10.1039/a605235e

54. Gould S, Scott RC. 2-Hydroxypropyl-β-cyclodextrin (HP-β-CD): A toxicology review. *Food Chem Toxicol*. 2005;43(10):1451-1459. doi:10.1016/j.fct.2005.03.007

55. Serrano DR, Gallagher KH, Healy AM. Emerging nanonisation technologies: tailoring crystalline versus amorphous nanomaterials. *Curr Top Med Chem*. 2015;22(15):2327-2340.

56. Muller RH, Keck CM. Challenges and solutions for the delivery of biotech drugs - A review of drug nanocrystal technology and lipid nanoparticles. *J Biotechnol*. 2004;113(1-3):151-170. doi:10.1016/j.jbiotec.2004.06.007

57. Onoue S, Yamada S, Chan HK. Nanodrugs: Pharmacokinetics and safety. *Int J Nanomedicine*. 2014;9(1):1025-1037. doi:10.2147/IJN.S38378

58. Healy AM, Worku ZA, Kumar D, Madi AM. Pharmaceutical solvates, hydrates and amorphous forms: A special emphasis on cocrystals. *Adv Drug Deliv Rev*. 2017;117:25-46. doi:10.1016/j.addr.2017.03.002

59. Rodríguez-Spong B, Price CP, Jayasankar A, Matzger AJ, Rodríguez-Hornedo N. General principles of pharmaceutical solid polymorphism: A supramolecular perspective. *Adv Drug Deliv Rev*. 2004;56(3):241-274. doi:10.1016/j.addr.2003.10.005

60. Guzmán HR, Tawa M, Zhang Z, Ratanabanangkoon P, Shaw P, Gardner CR, Chen H, Moreau J, Almarsson Ö, Remenar JF. Combined use of crystalline salt forms and precipitation inhibitors to improve oral absorption of celecoxib from solid oral formulations. *J Pharm Sci*. 2007;96(10):2686-2702. doi:10.1002/jps.20906

61. Bauer J, Spanton S, Henry R, Quick J, Dziki W, Porter W, Morris J. Ritonavir: An extraordinary example of conformational polymorphism. *Pharm Res*. 2001;18(6):859-866. doi:10.1023/A:1011052932607

62. Haleblian J, McCrone W. Pharmaceutical applications of polymorphism. *J Pharm Sci*. 1969;58(8):911-929. doi:10.1002/jps.2600580802

63. Singhal D, Curatolo W. Drug polymorphism and dosage form design: A practical perspective. *Adv Drug Deliv Rev*. 2004;56(3):335-347. doi:10.1016/j.addr.2003.10.008

64. Aguiar AJ, Krc J, Kinkel AW, Samyn JC. Effect of polymorphism on the absorption of chloramphenicol from chloramphenicol palmitate. *J Pharm Sci*. 1967;56(7):847-853. doi:10.1002/jps.2600560712

65. Khalil SA, Moustafa MA, Ebian AR, Motawi MM. GI absorption of two crystal forms of sulfameter in man. *J Pharm Sci*. 1972;61(10):1615-1617. doi:10.1002/jps.2600611015

66. Armando JA, Joyce EZ. Dissolution behaviour of polymorphs of chloramphenicol palmitate and mefenamic Acid. *J Pharm Sci*. 1969;58(8):983-987.

67. Brittain HG, Grant DJW. Effects of polymorphism and solid-state solvation on solubility and

dissolution rate. In: Brittain HG, ed. *Polymorphism in Pharmaceutical Solids*. 2nd ed. New York: Informa Healthcare USA; 2009:436-473.

68. Llinàs A, Goodman JM. Polymorph control: past, present and future. *Drug Discov Today*. 2008;13(5-6):198-210. doi:10.1016/j.drudis.2007.11.006

69. Hancock BC, Parks M. What is the true solubility advantage for amorphous pharmaceuticals? *Pharm Res*. 2000;17(4):397-404. doi:10.1023/A:1007516718048

70. Miller JM, Beig A, Carr RA, Spence JK, Dahan A. A win-win solution in oral delivery of lipophilic drugs: Supersaturation via amorphous solid dispersions increases apparent solubility without sacrifice of intestinal membrane permeability. *Mol Pharm*. 2012;9(7):2009-2016. doi:10.1021/mp300104s

71. Beig A, Miller JM, Lindley D, Carr RA, Zocharski P, Agbaria R, Dahan A. Head-to-head comparison of different solubility-enabling formulations of etoposide and their consequent solubility-permeability interplay. *J Pharm Sci*. 2015;104(9):2941-2947. doi:10.1002/jps.24496

72. Chiou WL, Riegelman S. Pharmaceutical applications of solid dispersion systems. *J Pharm Sci*. 1971;60(9):1281-1302. doi:10.1002/jps.2600600902

73. Laitinen R, Priemel PA, Surwase S, Graeser K, Strachan CJ, Grohganz H, Rades T. Theoretical considerations in developing amorphous solid dispersions. In: Shah NH, Sandhu HK, Soon Choi D, Chokshi H, Malick AW, eds. *Amorphous Solid Dispersions: Theory and Practice*. 1st ed. New York: Springer; 2014:35-91.

74. Van Den Mooter G. The use of amorphous solid dispersions: A formulation strategy to overcome poor solubility and dissolution rate. *Drug Discov Today Technol*. 2012;9(2):e79-e85. doi:10.1016/j.ddtec.2011.10.002

75. McCarthy CA, Ahern RJ, Dontireddy R, Ryan KB, Crean AM. Mesoporous silica formulation strategies for drug dissolution enhancement: a review. *Expert Opin Drug Deliv*. 2016;13(1):93-108. doi:10.1517/17425247.2016.1100165

76. Dengale SJ, Grohganz H, Rades T, Löbmann K. Recent advances in co-amorphous drug formulations. *Adv Drug Deliv Rev*. 2016;100(2016):116-125. doi:10.1016/j.addr.2015.12.009

77. Jensen KT, Larsen FH, Cornett C, Löbmann K, Grohganz H, Rades T. Formation mechanism of coamorphous drug-amino acid mixtures. *Mol Pharm*. 2015;12(7):2484-2492.

doi:10.1021/acs.molpharmaceut.5b00295

78. Kasten G, Löbmann K, Grohganz H, Rades T. Co-former selection for co-amorphous drug-amino acid formulations. *Int J Pharm*. 2019;557(November 2018):366-373. doi:10.1016/j.ijpharm.2018.12.036

79. Alonzo DE, Zhang GGZ, Zhou D, Gao Y, Taylor LS. Understanding the behavior of amorphous pharmaceutical systems during dissolution. *Pharm Res*. 2010;27(4):608-618. doi:10.1007/s11095-009-0021-1

80. Raina SA, Alonzo DE, Zhang GGZ, Gao Y, Taylor LS. Impact of polymers on the crystallization and phase transition kinetics of amorphous nifedipine during dissolution in aqueous media. *Mol Pharm*. 2014;11(10):3565-3576. doi:10.1021/mp500333v

81. Shi N-Q, Jin Y, Zhang Y, Che X-X, Xiao X, Cui G-H, Chen Y-Z, Feng B, Li Z-Q, Qi X-R. The influence of cellulosic polymer's variables on dissolution/solubility of amorphous felodipine and crystallization inhibition from a supersaturated state. *AAPS PharmSciTech*. 2019;20(1):1-14. doi:10.1208/s12249-018-1266-y

82. Brouwers J, Brewster ME, Augustijns P. Supersaturating drug delivery systems: the answer to solubility-limited oral bioavailability? *J Pharm Sci*. 2009;98(8):2549-2572. doi:10.1002/jps.21650

83. Graeser KA, Patterson JE, Zeitler JA, Gordon KC, Rades T. Correlating thermodynamic and kinetic parameters with amorphous stability. *Eur J Pharm Sci*. 2009;37(3-4):492-498. doi:10.1016/j.ejps.2009.04.005

84. Mahlin D, Bergström CASS. Early drug development predictions of glass-forming ability and physical stability of drugs. *Eur J Pharm Sci*. 2013;49(2):323-332. doi:10.1016/j.ejps.2013.03.016

85. Paudel A, Worku ZA, Meeus J, Guns S, Van Den Mooter G. Manufacturing of solid dispersions of poorly water soluble drugs by spray drying: Formulation and process considerations. *Int J Pharm*. 2013;453(1):253-284. doi:10.1016/j.ijpharm.2012.07.015

86. Van Eerdenbrugh B, Baird JA, Taylor LS. Crystallization tendency of active pharmaceutical ingredients following rapid solvent evaporation — classification and comparison with crystallization tendency from undercooled melts. *J Pharm Sci*. 2010;99(9):3826-3838. doi:10.1002/jps.22214

87. Bellantone RA. Fundamentals of amorphous systems: thermodynamic aspects. In: Shah N,

Sandhu H, Soon Choi D, Chokshi H, Malick AW, eds. *Amorphous Solid Dispersions: Theory and Practice*. 1st ed. New York: Springer; 2014:5-6.

88. Rams-Baron M, Wojnarowska Z, Grzybowska K, Dulski M, Knapik J, Jurkiewicz K, Smolka W, Sawicki W, Ratuszna A, Paluch M. Toward a better understanding of the physical stability of amorphous anti-inflammatory agents: The roles of molecular mobility and molecular interaction patterns. *Mol Pharm*. 2015;12(10):3628-3638. doi:10.1021/acs.molpharmaceut.5b00351

89. Hancock BC, Shamblin SL, Zografi G. Molecular mobility of amorphous pharmaceutical solids below their glass transition temperatures. *Pharm Res*. 1995;12(6):799-806. doi:https://doi.org/10.1023/A:1016292416526

90. Beaman RG. Relation between (apparent) second-order transition temperature and melting point. *J Polym Sci*. 1952;9(5):470-472. doi:10.1002/pol.1952.120090510

91. Kauzmann W. The nature of the glassy state and the behavior of liquids at low temperatures. *Chem Rev*. 1948;43(2):219-256. doi:10.1021/cr60135a002

92. Kissi EO, Grohganz H, Löbmann K, Ruggiero MT, Zeitler JA, Rades T. Glass-transition temperature of the β-relaxation as the major predictive parameter for recrystallization of neat amorphous drugs. *J Phys Chem B*. 2018;122(10):2803-2808. doi:10.1021/acs.jpcb.7b10105

93. Baghel S, Cathcart H, O'Reilly NJ. Polymeric amorphous solid dispersions: a review of amorphization, crystallization, stabilization, solid-state characterization, and aqueous solubilization of biopharmaceutical classification system class II drugs. *J Pharm Sci*. 2016;105(9):2527-2544. doi:10.1016/j.xphs.2015.10.008

94. Gordon M, Taylor JS. Ideal copolymers and the second-order transitions of synthetic rubbers. I. noncrystalline copolymers. *J Appl Chem*. 1952;2(9):493-500. doi:10.5254/1.3539818

95. Wu JX, Yang M, Berg F Van Den, Pajander J, Rades T, Rantanen J. Influence of solvent evaporation rate and formulation factors on solid dispersion physical stability. *Eur J Pharm Sci*. 2011;44(5):610-620. doi:10.1016/j.ejps.2011.10.008

96. Hilton JE, Summers MP. The effect of wetting agents on the dissolution of indomethacin solid dispersion systems. *Int J Pharm*. 1986;31(1-2):157-164. doi:10.1016/0378-5173(86)90226-7

97. Broman E, Khoo C, Taylor LS. A comparison of alternative polymer excipients and processing methods for making solid dispersions of a poorly water soluble drug. *Int J Pharm*. 2001;222(1):139-151. doi:10.1016/S0378-5173(01)00709-8

98. Li B, Konecke S, Harich K, Wegiel L, Taylor LS, Edgar KJ. Solid dispersion of quercetin in cellulose derivative matrices influences both solubility and stability. *Carbohydr Polym*. 2013;92(2):2033-2040. doi:10.1016/j.carbpol.2012.11.073

99. Priemel PA, Laitinen R, Grohganz H, Rades T, Strachan CJ. In situ amorphisation of indomethacin with Eudragit® E during dissolution. *Eur J Pharm Biopharm*. 2013;85(3 PART B):1259-1265. doi:10.1016/j.ejpb.2013.09.010

100. Doreth M, Löbmann K, Grohganz H, Holm R, Lopez de Diego H, Rades T, Priemel PA. Glass solution formation in water - In situ amorphization of naproxen and ibuprofen with Eudragit®E PO. *J Drug Deliv Sci Technol*. 2016;34:32-40. doi:10.1016/j.jddst.2016.02.003

101. Qian F, Huang J, Hussain MA. Drug–polymer solubility and miscibility: stability consideration and practical challenges in amorphous solid dispersion development. *J Pharm Sci*. 2010;99(7):2941-2947. doi:10.1002/jps.22074

102. Marsac PJ, Li T, Taylor LS. Estimation of drug-polymer miscibility and solubility in amorphous solid dispersions using experimentally determined interaction parameters. *Pharm Res*. 2009;26(1):139-151. doi:10.1007/s11095-008-9721-1

103. Flory PJ. Thermodynamics of high polymer solutions. *J Chem Phys*. 1942;10(1):51-61. doi:10.1063/1.1723621

104. Huggins ML. Thermodynamic properties of solutions of long-chain compounds. *Ann N Y Acad Sci*. 1942;43(1):1-32. doi:10.1111/j.1749-6632.1942.tb47940.x

105. Thakral S, Thakral NK. Prediction of drug-polymer miscibility through the use of solubility parameter based flory-huggins interaction parameter and the experimental validation: PEG as model polymer. *J Pharm Sci*. 2013;102(7):2254-2263. doi:10.1002/jps.23583

106. Knopp MM, Tajber L, Tian Y, Olesen NE, Jones DS, Kozyra A, Löbmann K, Paluch K, Brennan CM, Holm R, Healy AM, Andrews GP, et al. Comparative study of different methods for the prediction of drug-polymer solubility. *Mol Pharm*. 2015;12(9):3408-3419. doi:10.1021/acs.molpharmaceut.5b00423

107. Van Krevelen DW, Te Nijenhuis K. Cohesive Properties and Solubility. In: Van Krevelen DW, ed. *Properties of Polymers*. Vol i. 4th ed. Amsterdam: Elsevier B.V; 2009:189-227.

doi:10.1016/B978-0-08-054819-7.00007-8

108. Newman A, Engers D, Bates S, Ivanisevic I, Kelly RC, Zografi G. Characterization of amorphous API:Polymer mixtures using X-ray powder diffraction. *J Pharm Sci*. 2008;97(11):4840-4856. doi:10.1002/jps.21352

109. Aso Y, Yoshioka S, Miyazaki T, Kawanishi T, Tanaka K, Kitamura S, Takakura A, Hayashi T, Muranushi N. Miscibility of nifedipine and hydrophilic polymers as measured by 1H-NMR spin–lattice relaxation. *Chem Pharm Bull (Tokyo)*. 2007;55(8):1227-1231. doi:10.1248/cpb.55.1227

110. Marsac PJ, Rumondor ACF, Nivens DE, Kestur US, Stanciu L, Taylor LS. Effect of temperature and moisture on the miscibility of amorphous dispersions of felodipine and poly(vinyl pyrrolidone). *J Pharm Sci*. 2010;99(1):169-185. doi:10.1002/jps.21809

111. Luebbert C, Sadowski G. Moisture-induced phase separation and recrystallization in amorphous solid dispersions. *Int J Pharm*. 2017;532(1):635-646. doi:10.1016/j.ijpharm.2017.08.121

112. Burnett DJ, Thielmann F, Booth J. Determining the critical relative humidity for moisture-induced phase transitions. *Int J Pharm*. 2004;287(1-2):123-133. doi:10.1016/j.ijpharm.2004.09.009

113. Theil F, Anantharaman S, Kyerematen SO, Van Lishaut H, Dreis-Kühne SH, Rosenberg J, Mägerlein M, Woehrle GH. Frozen in time: kinetically stabilized amorphous solid dispersions of nifedipine stable after a quarter century of storage. *Mol Pharm*. 2017;14(1):183-192. doi:10.1021/acs.molpharmaceut.6b00783

114. Vasanthavada M, Tong WQ, Joshi Y, Kislalioglu MS. Phase behavior of amorphous molecular dispersions II: Role of hydrogen bonding in solid solubility and phase separation kinetics. *Pharm Res*. 2005;22(3):440-448. doi:10.1007/s11095-004-1882-y

115. Al-Obaidi H, Buckton G. Evaluation of griseofulvin binary and ternary solid dispersions with HPMCAS. *AAPS PharmSciTech*. 2009;10(4):1172-1177. doi:10.1208/s12249-009-9319-x

116. Al-Obaidi H, Ke P, Brocchini S, Buckton G. Characterization and stability of ternary solid dispersions with PVP and PHPMA. *Int J Pharm*. 2011;419(1-2):20-27. doi:10.1016/j.ijpharm.2011.06.052

117. Prasad D, Chauhan H, Atef E. Amorphous stabilization and dissolution enhancement of amorphous ternary solid dispersions: Combination of polymers showing drug-polymer

interaction for synergistic effects. *J Pharm Sci*. 2014;103(11):3511-3523. doi:10.1002/jps.24137

118. Noolkar SB, Jadhav NR, Bhende SA, Killedar SG. Solid-state characterization and dissolution properties of meloxicam–moringa coagulant–PVP ternary solid dispersions. *AAPS PharmSciTech*. 2013;14(2):569-577. doi:10.1208/s12249-013-9941-5

119. Hanada M, Jermain S V., Williams RO. Enhanced dissolution of a porous carrier–containing ternary amorphous solid dispersion system prepared by a hot melt method. *J Pharm Sci*. 2018;107(1):362-371. doi:10.1016/j.xphs.2017.09.025

120. Mura P, Moyano JR, González-Rodríguez ML, Rabasco-Alvaréz AM, Cirri M, Maestrelli F. Characterization and dissolution properties of ketoprofen in binary and ternary solid dispersions with polyethylene glycol and surfactants. *Drug Dev Ind Pharm*. 2005;31(4-5):425-434. doi:10.1080/03639040500214621

121. Bhugra C, Pikal MJ. Role of thermodynamic, molecular, and kinetic factors in crystallization from the amorphous state. *J Pharm Sci*. 2008;97(4):1329-1349. doi:10.1002/jps.21138

122. Démuth B, Nagy ZK, Balogh A, Vigh T, Marosi G, Verreck G, Van Assche I, Brewster ME. Downstream processing of polymer-based amorphous solid dispersions to generate tablet formulations. *Int J Pharm*. 2015;486(1-2):268-286. doi:10.1016/j.ijpharm.2015.03.053

123. Leane MM, Sinclair W, Qian F, Haddadin R, Brown A, Tobyn M, Dennis AB. Formulation and process design for a solid dosage form containing a spray-dried amorphous dispersion of ibipinabant. *Pharm Dev Technol*. 2013;18(2):359-366. doi:10.3109/10837450.2011.619544

124. Kestur US, Ivanesivic I, Alonzo DE, Taylor LS. Influence of particle size on the crystallization kinetics of amorphous felodipine powders. *Powder Technol*. 2013;236:197-204. doi:10.1016/j.powtec.2012.02.010

125. Zhu L, Wong L, Yu L. Surface-enhanced crystallization of amorphous nifedipine. *Mol Pharm*. 2008;5(6):921-926. doi:10.1021/mp8000638

126. Caron V, Tajber L, Corrigan OI, Healy AM. A comparison of spray drying and milling in the production of amorphous dispersions of sulfathiazole/polyvinylpyrrolidone and sulfadimidine/ polyvinylpyrrolidone. *Mol Pharm*. 2011;8(2):532-542. doi:10.1021/mp1003674

127. Worku ZA, Paudel A, Van Den Mooter G. Can compression induce demixing in amorphous solid dispersions? A case study of naproxen-PVP K25. *Eur J Pharm Biopharm*.

2012;81(1):207-213. doi:10.1016/j.ejpb.2012.01.007

128. Worku ZA, Aarts J, Van Den Mooter G. Influence of compression forces on the structural stability of naproxen/PVP-VA 64 solid dispersions. *Mol Pharm*. 2014;11(4):1102-1108. doi:10.1021/mp5001313

129. Sandhu H, Shah N, Chokshi H, Malick AW. Overview of amorphous solid dispersion technologies. In: Shah NH, Sandhu HK, Soon Choi D, Chokshi H, Malick AW, eds. *Amorphous Solid Dispersions: Theory and Practice*. 1st ed. New York: Springer; 2014:91-122.

130. Tian Y, Booth J, Meehan E, Jones DS, Li S, Andrews GP. Construction of drug-polymer thermodynamic phase diagrams using flory-huggins interaction theory: Identifying the relevance of temperature and drug weight fraction to phase separation within solid dispersions. *Mol Pharm*. 2013;10(1):236-248. doi:10.1021/mp300386v

131. Hancock BC, Zografi G. The relationship between the glass transition temperature and the water content of amorphous pharmaceutical solids. *Pharm Res*. 1994;11(4):471-477.

132. Van den Mooter G, Wuyts M, Blaton N, Busson R, Grobet P, Augustijns P, Kinget R. Physical stabilisation of amorphous ketoconazole in solid dispersions with polyvinylpyrrolidone K25. *Eur J Pharm Sci*. 2000;12(3):261-269. doi:10.1016/S0928-0987(00)00173-1

133. Grzybowska K, Paluch M, Grzybowski A, Wojnarowska Z, Hawelek L, Kolodziejczyk K, Ngai KL. Molecular dynamics and physical stability of amorphous anti-inflammatory drug: celecoxib. *J Phys Chem B*. 2010;114(40):12792-12801. doi:10.1021/jp1040212

134. Chmiel K, Knapik-Kowalczuk J, Jurkiewicz K, Sawicki W, Jachowicz R, Paluch M. A new method to identify physically stable concentration of amorphous solid dispersions (I): case of flutamide + Kollidon VA64. *Mol Pharm*. 2017;14(10):3370-3380. doi:10.1021/acs.molpharmaceut.7b00382

135. Knapik J, Wojnarowska Z, Grzybowska K, Tajber L, Mesallati H, Paluch KJ, Paluch M. Molecular dynamics and physical stability of amorphous nimesulide drug and its binary drug-polymer systems. *Mol Pharm*. 2016;13(6):1937-1946. doi:10.1021/acs.molpharmaceut.6b00115

136. Craig DQM, Royall PG, Kett VL, Hopton ML. The relevance of the amorphous state to pharmaceutical dosage forms: Glassy drugs and freeze dried systems. *Int J Pharm*. 1999;179(2):179-207. doi:10.1016/S0378-5173(98)00338-X

137. Oberholtzer ER, Brenner GS. Cefoxitin sodium: Solution and solid-state chemical stability studies. *J Pharm Sci*. 1979;68(7):863-866. doi:10.1002/jps.2600680720

138. Strickley RG, Anderson BD. Solid-state stability of human insulin I. mechanism and the effect of water on the kinetics of degradation in lyophiles from pH 2–5 solution. *Pharm Res*. 1996;13(8):1142-1153. doi:10.1023/A:1016043715791

139. Carstensen JT, Morris T. Chemical stability of indomethacin in the solid amorphous and molten states. *J Pharm Sci*. 1993;82(6):657-659. doi:10.1002/jps.2600820622

140. Shah N, Iyer RM, Mair HJ, Choi DS, Tian H, Diodone R, Fähnrich K, Pabst-Ravot A, Tang K, Scheubel E, Grippo JF, Moreira SA, et al. Improved human bioavailability of vemurafenib, a practically insoluble drug, using an amorphous polymer-stabilized solid dispersion prepared by a solvent-controlled coprecipitation process. *J Pharm Sci*. 2013;102(3):967-981. doi:10.1002/jps.23425

141. Rowe RC, Sheskey PJ, Quinn ME. *Handbook of Pharmaceutical Excipients*. 6th ed. Washington, D.C.: Pharmaceutical Press; 2009. doi:10.1007/978-1-908517-43-2

142. Williams G, Watts DC. Non-symmetrical dielectric relaxation behaviour arising from a simple empirical decay function. *Trans Faraday Soc*. 1970;66(1):80-85. http://www.rsc.org/Publishing/Journals/TF/article.asp?doi=TF9706600080.

143. Haque MK, Kawai K, Suzuki T. Glass transition and enthalpy relaxation of amorphous lactose glass. *Carbohydr Res*. 2006;341(11):1884-1889. doi:10.1016/j.carres.2006.04.040

144. Healy AM, McDonald BF, Tajber L, Corrigan OI. Characterisation of excipient-free nanoporous microparticles (NPMPs) of bendroflumethiazide. *Eur J Pharm Biopharm*. 2008;69(3):1182-1186. doi:10.1016/j.ejpb.2008.04.020

145. Burnett DJ, Thielmann F. *Calculation of Diffusion Constants in a Pharmaceutical Powder Using DVS - Application Note 30*. https://www.surfacemeasurementsystems.com/downloads/dvs-application-notes/.

146. Burnett DJ, Garcia AR, Thielmann F. Measuring moisture sorption and diffusion kinetics on proton exchange membranes using a gravimetric vapor sorption apparatus. *J Power Sources*. 2006;160:426-430. doi:10.1016/j.jpowsour.2005.12.096

147. Barham AS, Tewes F, Healy AM. Moisture diffusion and permeability characteristics of hydroxypropylmethylcellulose and hard gelatin capsules. *Int J Pharm*. 2015;478(2):796-803. doi:10.1016/j.ijpharm.2014.12.029

148. Kremer F, Schönhals A. Analysis of dielectric spectra – model functions. In: Kremer F, Schönhals A, eds. *Broadband Dielectric Spectroscopy*. Berlin, Heidelberg: Springer Berlin Heidelberg; 2003:61-63. doi:10.1007/978-3-642-56120-7

149. Brás AR, Noronha JP, Antunes AMM, Cardoso MM, Schönhals A, Affouard F, Dionísio M, Correia NT. Molecular motions in amorphous ibuprofen as studied by broadband dielectric spectroscopy. *J Phys Chem B*. 2008;112(35):11087-11099. doi:10.1021/jp8040428

150. Fulcher GS. Analysis of recent measurements of the viscosity of glasses. *J Am Ceram Soc*. 1925;8(6):339-355. doi:10.1111/j.1151-2916.1925.tb16731.x

151. Tammann G, Hesse W. Die Abhängigkeit der Viscosistat von der Temperatur bei unterkühlten Flüssigkeiten'. *Allg Chemie*. 1926;156:245-257.

152. Böhmer R, Ngai KL, Angell CA, Plazek DJ. Nonexponential relaxations in strong and fragile glass formers. *J Chem Phys*. 1993;99(5):4201-4209. doi:10.1063/1.466117

153. Greenspan L. Humidity fixed points of binary saturated aqueous solutions. *J Res Natl Bur Stand Sect A Phys Chem*. 1977;81A(1):89. doi:10.6028/jres.081A.011

154. Dudognon E, Correia NT, Danède F, Descamps M. Solid-solid transformation in racemic ibuprofen. *Pharm Res*. 2013;30(1):81-89. doi:10.1007/s11095-012-0851-0

155. Zhang Y, Huo M, Zhou J, Zou A, Li W, Yao C, Xie S. DDSolver: An add-in program for modeling and comparison of drug dissolution profiles. *AAPS J*. 2010;12(3):263-271. doi:10.1208/s12248-010-9185-1

156. British Pharmacopeia. Appendix XII B. Dissolution. In: *British Pharmacopeia*. ; 2019.

157. Pillay V, Fassihi R. A new method for dissolution studies of lipid-filled capsules employing nifedipine as a model drug. *Pharm Res*. 1999;16(2):333-337. doi:10.1023/A:1011959914706

158. British Pharmacopeia. Nifedipine monograph. British Pharmacopeia. https://www.pharmacopoeia.com/bp-2019/monographs/?date=2019-07-01. Published 2019. Accessed August 4, 2019.

159. Devarakonda B, Hill RA, De Villiers MM. The effect of PAMAM dendrimer generation size and surface functional group on the aqueous solubility of nifedipine. *Int J Pharm*. 2004;284(1-2):133-140. doi:10.1016/j.ijpharm.2004.07.006

160. Caner H, Groner E, Levy L, Agranat I. Trends in the development of chiral drugs. *Drug*

Discov Today. 2004;9(3):105-110. doi:10.1016/S1359-6446(03)02904-0

161. Lorenz H, Perlberg A, Sapoundjiev D, Elsner MP, Seidel-Morgenstern A. Crystallization of enantiomers. *Chem Eng Process Process Intensif*. 2006;45(10):863-873. doi:10.1016/j.cep.2005.11.013

162. Cahn RS, Ingold C, Prelog V. Specification of molecular chirality. *Angew Chemie Int Ed English*. 1966;5(4):385-415. doi:10.1002/anie.196603851

163. Fraga LR, Diamond AJ, Vargesson N. Thalidomide and Birth Defects. In: *ELS*. Chichester, UK: John Wiley & Sons, Ltd; 2016:1-11. doi:10.1002/9780470015902.a0026052

164. Eriksson T, Bjorkman S, Roth B, Hoglund P. Intravenous formulations of the enantiomers of thalidomide: pharmacokinetic and initial pharmacodynamic characterization in man. *J Pharm Pharmacol*. 2000;52(7):807-817. doi:10.1211/0022357001774660

165. Singh Sekhon B. Exploiting the power of stereochemistry in drugs: an overview of racemic and enantiopure drugs. *J Mod Med Chem*. 2013;1:10-36. doi:10.12970/2308-8044.2013.01.01.2

166. Adams SS, Bresloff P, Mason CG. Pharmacological differences between the optical isomers of ibuprofen: evidence for metabolic inversion of the (-)-isomer. *J Pharm Pharmacol*. 1976;28(3):256-257. doi:10.1111/j.2042-7158.1976.tb04144.x

167. H. Brooks W, C. Guida W, G. Daniel K. The significance of chirality in drug design and development. *Curr Top Med Chem*. 2011;11(7):760-770. doi:10.2174/156802611795165098

168. Erb S. Single-enantiomer drugs poised for further market growth. *Pharm Technol*. 2006;30:s14-s18.

169. Miller CP, Ullrich JW. A consideration of the patentability of enantiomers in the pharmaceutical industry in the United States. *Chirality*. 2008;20(6):762-770. doi:10.1002/chir.20520

170. Calcaterra A, D'Acquarica I. The market of chiral drugs: Chiral switches versus de novo enantiomerically pure compounds. *J Pharm Biomed Anal*. 2018;147:323-340. doi:10.1016/j.jpba.2017.07.008

171. Bhushan R, Martens J. Resolution of Enatiomers of Ibuprofen by Liquid Chromatogarphy: A Review. *BiomedChromatogr*. 1998;12(November 1997):309-316.

172. Srisanga S, Ter Horst JH. Racemic compound, conglomerate, or solid solution: Phase diagram screening of chiral compounds. *Cryst Growth Des*. 2010;10(4):1808-1812. doi:10.1021/cg901483v

173. Mitchell AG. Racemic drugs: racemic mixture, racemic compound, or pseudoracemate? *J Pharm Pharm Sci*. 1998;1(1):8-12.

174. Dwivedi SK, Sattari S, Jamali F, Mitchell AG. Ibuprofen racemate and enantiomers: Phase diagram, solubility and thermodynamic studies. *Int J Pharm*. 1992;87(1-3):95-104. doi:10.1016/0378-5173(92)90232-Q

175. Otero-De-La-Roza A, Hein JE, Johnson ER. Reevaluating the stability and prevalence of conglomerates: implications for preferential crystallization. *Cryst Growth Des*. 2016;16(10):6055-6059. doi:10.1021/acs.cgd.6b01088

176. Gallis HE, Van Miltenburg JC, Oonk HAJ. Polymorphism of mixtures of enantiomers: A thermodynamic study of mixtures of D- and L-limonene. *Phys Chem Chem Phys*. 2000;2(24):5619-5623. doi:10.1039/b005603k

177. Viel Q, Brandel C, Cartigny Y, Eusebio ME, Canotilho J, Dupray V, Dargent E, Coquerel G, Petit S. Crystallization from the amorphous state of a pharmaceutical compound: Impact of chirality and chemical purity. *Cryst Growth Des*. 2017;17(1):337-346. doi:10.1021/acs.cgd.6b01566

178. Kim TH, Shibata T, Kojima S, Shin DM, Hwang YH, Ko JH. Comparison of thermal and elastic properties of glassy racemic and enantiomorphic ibuprofen studied by Brillouin light scattering and modulated differential scanning calorimetry. *Curr Appl Phys*. 2014;14(7):965-969. doi:10.1016/j.cap.2014.05.001

179. Snatzke G. Enantiomers, Racemates, and Resolutions. *Berichte der Bunsengesellschaft für Phys Chemie*. 1982;86(11):1087-1087. doi:10.1002/bbpc.198200035

180. Gavezzotti A, Rizzato S. Are racemic crystals favored over homochiral crystals by higher stability or by kinetics? Insights from comparative studies of crystalline stereoisomers. *J Org Chem*. 2014;79(11):4809-4816. doi:10.1021/jo500528k

181. Wallach O. Zur Kenntniss der Terpene und der ätherischen Oele. *Justus Liebig's Ann der Chemie*. 1895;286(1):90-118. doi:10.1002/jlac.18952860105

182. Brock CP, Schweizer WB, Dunitz JD. On the validity of Wallach's rule: on the density and stability of racemic crystals compared with their chiral counterparts. *J Am Chem Soc*.

1991;113(26):9811-9820. doi:10.1021/ja00026a015

183. Adrjanowicz K, Kaminski K, Paluch M, Niss K. Crystallization behavior and relaxation dynamics of supercooled S-ketoprofen and the racemic mixture along an isochrone. *Cryst Growth Des*. 2015;15(7):3257-3263. doi:10.1021/acs.cgd.5b00373

184. Fox MA, Whitesell JK. *Organic Chemistry*. 3rd ed. Jones and Bartlett Publishers; 2004. http://physicalscience.jbpub.com/orgo/interactive_glossary_showterm.cfm?term=Chiral recognition.

185. Booth TD, Wahnon D, Wainer IW. Is chiral recognition a three-point process? *Chirality*. 1997;9(2):96-98. doi:10.1002/(SICI)1520-636X(1997)9:2<96::AID-CHIR2>3.0.CO;2-E

186. Davankov VA. The nature of chiral recognition: Is it a three-point interaction? *Chirality*. 1997;9(2):99-102. doi:10.1002/(SICI)1520-636X(1997)9:2<99::AID-CHIR3>3.0.CO;2-B

187. Saylor Academy. Chp 24 Organic compounds. General Chemistry: Principles, Patterns, and Applications v. 1.0. https://saylordotorg.github.io/text_general-chemistry-principles-patterns-and-applications-v1.0/s28-organic-compounds.html. Published 2012. Accessed August 26, 2019.

188. Berthod A. Chiral recognition mechanisms. *Anal Chem*. 2006;78(7):2093-2099. doi:10.1021/ac0693823

189. Rekharsky M, Inoue Y. Chiral recognition thermodynamics of β-cyclodextrin: The thermodynamic origin of enantioselectivity and the enthalpy-entropy compensation effect. *J Am Chem Soc*. 2000;122(18):4418-4435. doi:10.1021/ja9921118

190. Shin DM, Hwang YH, Ko JH, Kojima S. Relaxation behaviors of enantiomorphic S-ibuprofen as revealed by dielectric and photon correlation spectroscopies. *Curr Appl Phys*. 2015;15(9):958-963. doi:10.1016/j.cap.2015.05.012

191. Baird JA, Santiago-Quinonez D, Rinaldi C, Taylor LS. Role of viscosity in influencing the glass-forming ability of organic molecules from the undercooled melt state. *Pharm Res*. 2012;29(1):271-284. doi:10.1007/s11095-011-0540-4

192. Lu ZP, Tan H, Ng SC, Li Y. The correlation between reduced glass transition temperature and glass forming ability of bulk metallic glasses. *Scr Mater*. 2000;42(7):667-673. doi:10.1016/S1359-6462(99)00417-0

193. Turnbull D. Under what conditions can a glass be formed? *Contemp Phys*. 1969;10(5):473-

488. doi:10.1080/00107516908204405

194. Zhou D, Zhang GGZ, Law D, Grant DJW, Schmitt EA. Physical stability of amorphous pharmaceuticals: Importance of configurational thermodynamic quantities and molecular mobility. *J Pharm Sci*. 2002;91(8):1863-1872. doi:10.1002/jps.10169

195. Kawakami K, Ida Y. Direct observation of the enthalpy relaxation and the recovery processes of maltose-based amorphous formulation by isothermal microcalorimetry. *Pharm Res*. 2003;20(9):1430-1436. http://www.ncbi.nlm.nih.gov/pubmed/14567638.

196. Hancock BC, Shamblin SL. Molecular mobility of amorphous pharmaceuticals determined using differential scanning calorimetry. *Thermochim Acta*. 2001;380(2):95-107. doi:10.1016/S0040-6031(01)00663-3

197. Graeser KA, Patterson JE, Zeitler JA, Rades T. The role of configurational entropy in amorphous systems. *Pharmaceutics*. 2010;2(2):224-244. doi:10.3390/pharmaceutics2020224

198. Kawai K, Hagiwara T, Takai R, Suzuki T. Comparative investigation by two analytical approaches of enthalpy relaxation for glassy glucose, sucrose, maltose, and trehalose. *Pharm Res*. 2005;22(3):490-495. doi:10.1007/s11095-004-1887-6

199. Adrjanowicz K, Kaminski K, Wojnarowska Z, Dulski M, Hawelek L, Pawlus S, Paluch M, Sawicki W. Dielectric relaxation and crystallization kinetics of ibuprofen at ambient and elevated pressure. *J Phys Chem B*. 2010;114(19):6579-6593. doi:10.1021/jp910009b

200. Dudognon E, Danède F, Descamps M, Correia NT. Evidence for a new crystalline phase of racemic ibuprofen. *Pharm Res*. 2008;25(12):2853-2858. doi:10.1007/s11095-008-9655-7

201. Grzybowska K, Capaccioli S, Paluch M. Recent developments in the experimental investigations of relaxations in pharmaceuticals by dielectric techniques at ambient and elevated pressure. *Adv Drug Deliv Rev*. 2016;100:158-182. doi:10.1016/j.addr.2015.12.008

202. Angell C. Relaxation in liquids, polymers and plastic crystals — strong/fragile patterns and problems. *J Non Cryst Solids*. 1991;131-133:13-31. doi:10.1016/0022-3093(91)90266-9

203. King MD, Buchanan WD, Korter TM. Understanding the terahertz spectra of crystalline pharmaceuticals: terahertz spectroscopy and solid-state density functional theory study of (S)-(+)-ibuprofen and (RS)-ibuprofen. *J Pharm Sci*. 2011;100(3):1116-1129. doi:10.1002/jps.22339

204. Taylor LS, Zografi G. Spectroscopic characterization of interactions between PVP and indomethacin in amorphous molecular dispersions. *Pharm Res*. 1997;14(12):1691-1698. doi:https://doi.org/10.1023/A:1012167410376

205. De Brabander C, Van Den Mooter G, Vervaet C, Remon JP. Characterization of ibuprofen as a nontraditional plasticizer of ethyl cellulose. *J Pharm Sci*. 2002;91(7):1678-1685. doi:10.1002/jps.10159

206. Yashima E, Okamoto Y. Chiral discrimination on polysaccharides derivatives. *Bull Chem Soc Jpn*. 1995;68(12):3289-3307. doi:10.1246/bcsj.68.3289

207. Grinberg N. Mechanistic aspects of chiral discrimination on modified cellulose. *Anal Chem*. 1997;69(12):1999-2007. doi:10.1021/ac961241l

208. Kestur US, Taylor LS. Role of polymer chemistry in influencing crystal growth rates from amorphous felodipine. *CrystEngComm*. 2010;12(8):2390. doi:10.1039/c001905d

209. Iervolino M, Cappello B, Raghavan SL, Hadgraft J. Penetration enhancement of ibuprofen from supersaturated solutions through human skin. *Int J Pharm*. 2001;212(1):131-141. doi:10.1016/S0378-5173(00)00603-7

210. Pirkle WH, Pochapsky TC. Considerations of chiral recognition relevant to the liquid chromatographic separation of enantiomers. *Chem Rev*. 1989;89(2):347-362. doi:10.1021/cr00092a006

211. Shah B, Kakumanu VK, Bansal AK. Analytical techniques for quantification of amorphous/crystalline phases in pharmaceutical solids. *J Pharm Sci*. 2006;95(8):1641-1665. doi:10.1002/jps.20644

212. Nguyen LA, He H, Pham-Huy C. Chiral drugs: an overview. *Int J Biomed Sci*. 2006;2(2):85-100.

213. Huang Y, Dai W-G. Fundamental aspects of solid dispersion technology for poorly soluble drugs. *Acta Pharm Sin B*. 2014;4(1):18-25. doi:10.1016/j.apsb.2013.11.001

214. Savin DA, Larson AM, Lodge TP. Effect of composition on the width of the calorimetric glass transition in polymer-solvent and solvent-solvent mixtures. *J Polym Sci Part B Polym Phys*. 2004;42(7):1155-1163. doi:10.1002/polb.10776

215. Angell CA. Liquid fragility and the glass transition in water and aqueous solutions. *Chem Rev*. 2002;102(8):2627-2650. doi:10.1021/cr000689q

216. Lehto VP, Tenho M, Vähä-Heikkilä K, Harjunen P, Päällysaho M, Välisaari J, Niemelä P, Järvinen K. The comparison of seven different methods to quantify the amorphous content of spray dried lactose. *Powder Technol*. 2006;167(2):85-93. doi:10.1016/j.powtec.2006.05.019

217. Food and Drug Administration. *Guidance for Industry: Immediate Release Solid Oral Dosage Forms – Scale-up and Postapproval Changes: Chemistry, Manufacturing, and Controls; in Vitro Dissolution Testing, and in Vivo Bioequivalance Documentation*. Rockville; 1995. https://www.fda.gov/media/70949/download.

218. Food and Drug Administration. *Guidance for Industry Dissolution Testing of Immediate Release Solid Oral Dosage Forms*. Rockville; 1997. https://www.fda.gov/media/70936/download.

219. Matsumoto T, Zografi G. Physical properties of solid molecular dispersions of indomethacin with poly(vinylpyrrolidone) and poly (vinylpyrrolidone-co-vinyl-acetate) in relation to indomethacin crystallization. *Pharm Res*. 1999;16(11):1722-1728.

220. Mohammed NN, Majumdar S, Singh A, Deng W, Murthy NS, Pinto E, Tewari D, Durig T, Repka MA. Klucel™ EF and ELF polymers for immediate-release oral dosage forms prepared by melt extrusion technology. *AAPS PharmSciTech*. 2012;13(4):1158-1169. doi:10.1208/s12249-012-9834-z

221. Knopp MM, Olesen NE, Holm P, Langguth P, Holm R, Rades T. Influence of polymer molecular weight on drug-polymer solubility: A comparison between experimentally determined solubility in PVP and prediction derived from solubility in monomer. *J Pharm Sci*. 2015;104(9):2905-2912. doi:10.1002/jps.24410

222. Rask MB, Knopp MM, Olesen NE, Holm R, Rades T. Influence of PVP/VA copolymer composition on drug-polymer solubility. *Eur J Pharm Sci*. 2016;85:10-17. doi:10.1016/j.ejps.2016.01.026

223. Fox TG, Flory PJ. Second-order transition temperatures and related properties of polystyrene. I. Influence of molecular weight. *J Appl Phys*. 1950;21(6):581-591. doi:10.1063/1.1699711

224. Porter SC, Ridgway K. An evaluation of the properties of enteric coating polymers: measurement of glass transition temperature. *J Pharm Pharmacol*. 1983;35(6):341-344. doi:10.1111/j.2042-7158.1983.tb02953.x

225. Dinunzio JC, Miller DA, Yang W, McGinity JW, Williams RO. Enhancing polymers for improved bioavailability of itraconazole. *Mol Pharm*. 2008;5(6):968-980. doi:10.1016/j.ejps.2008.02.007.(16)

226. Bai Q, Zhang G, Xu B, Feng X, Jiang H, Li H. Thermal and water dual-responsive shape memory poly(vinyl alcohol)/Al2O3 nanocomposite. *RSC Adv*. 2015;5(111):91213-91217. doi:10.1039/c5ra17103b

227. Koosha M, Mirzadeh H, Shokrgozar MA, Farokhi M. Nanoclay-reinforced electrospun chitosan/PVA nanocomposite nanofibers for biomedical applications. *RSC Adv*. 2015;5(14):10479-10487. doi:10.1039/c4ra13972k

228. Pal K, Banthia A, Majumdar D. Preparation and characterization of polyvinyl alcohol-gelatin hydrogel membranes for biomedical applications. *AAPS PharmSciTech*. 2007;8(1):21.

229. Saleki-Gerhardt A, Ahlneck C, Zografi G. Assessment of disorder in crystalline solids. *Int J Pharm*. 1994;101(3):237-247. doi:10.1016/0378-5173(94)90219-4

230. Hancock BC, Carlson GT, Ladipo DD, Langdon BA, Mullarney MP. Comparison of the mechanical properties of the crystalline and amorphous forms of a drug substance. *Int J Pharm*. 2002;241(1):73-85. doi:10.1016/S0378-5173(02)00133-3

231. Yuan X, Xiang TX, Anderson BD, Munson EJ. Hydrogen bonding interactions in amorphous indomethacin and its amorphous solid dispersions with poly(vinylpyrrolidone) and poly(vinylpyrrolidone-co-vinyl acetate) studied using 13C solid-state NMR. *Mol Pharm*. 2015;12(12):4518-4528. doi:10.1021/acs.molpharmaceut.5b00705

232. Sathigari SK, Radhakrishnan VK, Davis VA, Parsons DL, Babu RJ. Amorphous-state characterization of efavirenz-polymer hot-melt extrusion systems for dissolution enhancement. *J Pharm Sci*. 2012;101(9):3456-3464. doi:10.1002/jps.23125

233. Taylor LS, Zografi G. Sugar-polymer hydrogen bond interactions in lyophilized amorphous mixtures. *J Pharm Sci*. 1998;87(12):1615-1621.

234. Rumondor ACF, Marsac PJ, Stanford LA, Taylor LS. Phase behavior of poly(vinylpyrrolidone) containing amorphous solid dispersions in the presence of moisture. *Mol Pharm*. 2009;6(5):1492-1505. doi:10.1021/mp900050c

235. Di Martino P, Joiris E, Gobetto R, Masic A, Palmieri GF, Martelli S. Ketoprofen-poly(vinylpyrrolidone) physical interaction. *J Cryst Growth*. 2004;265(1-2):302-308. doi:10.1016/j.jcrysgro.2004.02.023

236. Sekizaki H, Danjo K, Eguchi H, Yonezawa Y, Sunada H, Otsuka A. Solid-state interaction of ibuprofen with polyvinylpyrrolidone. *Chem Pharm Bull (Tokyo)*. 1995;43(6):988-993.

237. Rumondor ACF, Marsac PJ, Stanford LA, Taylor LS. Phase behavior of poly (vinylpyrrolidone) containing amorphous solid dispersions in the presence of moisture. *Mol Pharm*. 2009;86(1):47-60. doi:10.1021/mp900050c

238. Gupta MK, Vanwert A, Bogner RH. Formation of physically stable amorphous drugs by milling with neusilin. *J Pharm Sci*. 2003;92(3):536-551. doi:10.1002/jps.10308

239. Pavia DL, Lampman GM, Kriz GS. *Introduction to Spectroscopy*. 5th ed. Stamford: Cengage Learning; 2015.

240. Rumondor ACF, Konno H, Marsac PJ, Taylor LS. Analysis of the moisture sorption behavior of amorphous drug-polymer blends. *J Appl Polym Sci*. 2010;117(2):1055-1063. doi:10.1002/app.31803

241. Granero GE, Ramachandran C, Amidon GL. Rapid in vivo dissolution of ketoprofen: Implications on the biopharmaceutics classification system. *Pharmazie*. 2006;61(8):673-676.

242. Knopp MM, Nguyen JH, Mu H, Langguth P, Rades T, Holm R. Influence of Copolymer Composition on In Vitro and In Vivo Performance of Celecoxib-PVP/VA Amorphous Solid Dispersions. *AAPS J*. 2016;18(2):416-423. doi:10.1208/s12248-016-9865-6

243. Qian F, Huang J, Zhu Q, Haddadin R, Gawel J, Garmise R, Hussain M. Is a distinctive single Tg a reliable indicator for the homogeneity of amorphous solid dispersion? *Int J Pharm*. 2010;395(1-2):232-235. doi:10.1016/j.ijpharm.2010.05.033

244. British Pharmacopeia. Appendix XVII N. Powder Flow. British Pharmacopeia. https://www.pharmacopoeia.com/bp-2019/appendices/appendix-17/appendix-xvii-n--powder-flow1.html?date=2019-01-01&text=carr. Published 2019.

245. McKenna A, McCafferty DF. Effect of particle size on the compaction mechanism and tensile strength of tablets. *J Pharm Pharmacol*. 1982;34(6):347-351. doi:10.1111/j.2042-7158.1982.tb04727.x

246. Sebhatu T, Alderborn G. Relationships between the effective interparticulate contact area and the tensile strength of tablets of amorphous and crystalline lactose of varying particle size. *Eur J Pharm Sci*. 1999;8(4):235-242. doi:10.1016/S0928-0987(99)00025-1

247. Doreth M, Hussein MA, Priemel PA, Grohganz H, Holm R, Lopez de Diego H, Rades T, Löbmann K. Amorphization within the tablet: Using microwave irradiation to form a glass solution in situ. *Int J Pharm*. 2017;519(1-2):343-351. doi:10.1016/j.ijpharm.2017.01.035

248. Moneghini M, Bellich B, Baxa P, Princivalle F. Microwave generated solid dispersions containing Ibuprofen. *Int J Pharm*. 2008;361(1-2):125-130. doi:10.1016/j.ijpharm.2008.05.026

249. Ellenberger DJ, Miller DA, Williams RO. Expanding the application and formulation space of amorphous solid dispersions with KinetiSol®: a review. *AAPS PharmSciTech*. 2018;19(5):1933-1956. doi:10.1208/s12249-018-1007-2

250. Bock N, Woodruff MA, Hutmacher DW, Dargaville TR. Electrospraying, a reproducible method for production of polymeric microspheres for biomedical applications. *Polymers (Basel)*. 2011;3(1):131-149. doi:10.3390/polym3010131

251. Xie J, Jiang J, Davoodi P, Srinivasan MP, Wang CH. Electrohydrodynamic atomization: A two-decade effort to produce and process micro-/nanoparticulate materials. *Chem Eng Sci*. 2015;125:32-57. doi:10.1016/j.ces.2014.08.061

252. Bohr A, Boetker J, Rades T, Rantanen J, Yang M, Bøtker J. Application of spray-drying and electrospraying/electospinning for poorly watersoluble drugs: A particle engineering approach. *Curr Pharm Des*. 2014;20(3):325-348. doi:10.2174/13816128113199990399

253. Peltonen L, Valo H, Kolakovic R, Laaksonen T, Hirvonen J. Electrospraying, spray drying and related techniques for production and formulation of drug nanoparticles. *Expert Opin Drug Deliv*. 2010;7(6):705-719. doi:10.1517/17425241003716802

254. Yu DG, Li JJ, Williams GR, Zhao M, Bhat PP, Pasquali M, McKinley GH, Basaran OA. Electrospun amorphous solid dispersions of poorly water-soluble drugs: A review. *J Control Release*. 2018;292(August 2015):91-110. doi:10.1016/j.jconrel.2018.08.016

255. Ansari MT, Sunderland VB. Solid dispersions of dihydroartemisinin in polyvinylpyrrolidone. *Arch Pharm Res*. 2008;31(3):390-398. doi:10.1007/s12272-001-1169-6

256. Crowley KJ, Zografi G. The effect of low concentrations of molecularly dispersed poly (vinylpyrrolidone) on indomethacin crystallization from the amorphous state. 2003;20(9).

257. Chokshi RJ, Sandhu HK, Iyer RM, Shah NH, Malick AW, Zia H. Characterization of physico-mechanical properties of indomethacin and polymers to assess their suitability for hot-melt extrusion processs as a means to manufacture solid dispersion/solution. *J Pharm Sci*.

2005;94(11):2463-2474. doi:10.1002/jps.20385

258. Rasekh M, Karavasili C, Soong YL, Bouropoulos N, Morris M, Armitage D, Li X, Fatouros DG, Ahmad Z. Electrospun PVP-indomethacin constituents for transdermal dressings and drug delivery devices. *Int J Pharm*. 2014;473(1-2):95-104. doi:10.1016/j.ijpharm.2014.06.059

259. Weuts I, Kempen D, Decorte A, Verreck G, Peeters J, Brewster M, Van Den Mooter G. Physical stability of the amorphous state of loperamide and two fragment molecules in solid dispersions with the polymers PVP-K30 and PVP-VA64. *Eur J Pharm Sci*. 2005;25(2-3):313-320. doi:10.1016/j.ejps.2005.03.012

260. Taylor LS, Langkilde FW, Zografi G. Fourier transform Raman spectroscopic study of the interaction of water vapor with amorphous polymers. *J Pharm Sci*. 2001;90(7):888-901. doi:10.1002/jps.1041

261. Parks GA, Anderson JH. The electrical conductivity of silica gel in the presence of adsorbed water. *J Phys Chem*. 1968;177(3):3662-3668. doi:10.1021/j100856a051

262. Samprasit W, Akkaramongkolporn P, Ngawhirunpat T, Rojanarata T, Kaomongkolgit R, Opanasopit P. Fast releasing oral electrospun PVP/CD nanofiber mats of taste-masked meloxicam. *Int J Pharm*. 2015;487(1-2):213-222. doi:10.1016/j.ijpharm.2015.04.044

263. Xu Y, Hanna MA. Electrospray encapsulation of water-soluble protein with polylactide. Effects of formulations on morphology, encapsulation efficiency and release profile of particles. *Int J Pharm*. 2006;320(1-2):30-36. doi:10.1016/j.ijpharm.2006.03.046

264. Vehring R. Pharmaceutical particle engineering via spray drying. *Pharm Res*. 2008;25(5):999-1022. doi:10.1007/s11095-007-9475-1

265. Fong H, Chun I, Reneker DH. Beaded nanofibers formed during electrospinning. *Polymer (Guildf)*. 1999;40(16):4585-4592. doi:10.1016/S0032-3861(99)00068-3

266. Rayleigh, Lord. On the equilibrium of liquid conducting masses charged with electricity. *Philos Mag Ser 5*. 1882. doi:10.1080/14786448208628425

267. Almería B, Deng W, Fahmy TM, Gomez A. Controlling the morphology of electrospray-generated PLGA microparticles for drug delivery. *J Colloid Interface Sci*. 2010;343(1):125-133. doi:10.1016/j.jcis.2009.10.002

268. Joseph J, Jemmis ED. Red-, blue-, or no-shift in hydrogen bonds: A unified explanation. *J Am Chem Soc*. 2007;129(15):4620-4632. doi:10.1021/ja067545z

269. Shah RB, Tawakkul MA, Khan MA. Comparative evaluation of flow for pharmaceutical powders and granules. *AAPS PharmSciTech*. 2008;9(1):250-258. doi:10.1208/s12249-008-9046-8

270. Guenette E, Barrett A, Kraus D, Brody R, Harding L, Magee G. Understanding the effect of lactose particle size on the properties of DPI formulations using experimental design. *Int J Pharm*. 2009;380(1-2):80-88. doi:10.1016/j.ijpharm.2009.07.002

271. Gamble JF, Chiu WS, Tobyn M. Investigation into the impact of sub-populations of agglomerates on the particle size distribution and flow properties of conventional microcrystalline cellulose grades. *Pharm Dev Technol*. 2011;16(5):542-548. doi:10.3109/10837450.2010.495395

272. Sandler N, Wilson D. Prediction of granule packing and flow behavior based on particle size and shape analysis. *J Pharm Sci*. 2010;99(2):958-968. doi:10.1002/jps.21884

273. Baertschi SW, Alsante KM, Tønnesen HH. A critical assessment of the ICH guideline on photostability testing of new drug substances and products (Q1B): recommendation for revision. *J Pharm Sci*. 2010;99(7):2934-2940. doi:10.1002/jps.22076

274. Teraoka R, Otsuka M, Matsuda Y. Evaluation of photostability of solid-state dimethyl 1,4-dihydro-2,6-dimethyl-4-(2-nitro-phenyl)-3,5-pyridinedicarboxylate by using Fourier-transformed reflection-absorption infrared spectroscopy. *Int J Pharm*. 1999;184(1):35-43. doi:10.1016/S0378-5173(99)00089-7

275. Matsuda Y, Akazawa R, Teraoka R, Otsuka M. Pharmaceutical evaluation of carbamazepine modifications: comparative study for photostability of carbamazepine polymorphs by using fourier-transformed reflection-absorption infrared spectroscopy and colorimetric measurement. *J Pharm Pharmacol*. 1994;46(3):162-167. doi:10.1111/j.2042-7158.1994.tb03770.x

276. Teraoka R, Otsuka M, Matsuda Y. Evaluation of photostability of solid-state nicardipine hydrochloride polymorphs by using Fourier-transformed reflection-absorption infrared spectroscopy - Effect of grinding on the photostability of crystal form. *Int J Pharm*. 2004;286(1-2):1-8. doi:10.1016/j.ijpharm.2004.07.026

277. Royal JS, Torkelson JM. Physical aging effects on molecular-scale polymer relaxations monitored with mobility-sensitive fluorescent molecules. *Macromolecules*. 1993;26(20):5331-5335. doi:10.1021/ma00072a009

278. Qiu Y, Antony LW, De Pablo JJ, Ediger MD. Photostability can be significantly modulated by molecular packing in glasses. *J Am Chem Soc*. 2016;138(35):11282-11289. doi:10.1021/jacs.6b06372

279. Grooff D, Francis F, De Villiers MM, Ferg E. Photostability of crystalline versus amorphous nifedipine and nimodipine. *J Pharm Sci*. 2013;102(6):1883-1894. doi:10.1002/jps.23533

280. Qin X, Frech P. Liquid chromatography / mass spectrometry (LC / MS) identification of photooxidative degradates of crystalline and amorphous MK-912. *Structure*. 2001;90(7):833-844.

281. Bayomi MA, Abanumay KA, Al-Angary AA. Effect of inclusion complexation with cyclodextrins on photostability of nifedipine in solid state. *Int J Pharm*. 2002;243(1-2):107-117. doi:10.1016/S0378-5173(02)00263-6

282. Lai F, Pireddu R, Corrias F, Fadda AM, Valenti D, Pini E, Sinico C. Nanosuspension improves tretinoin photostability and delivery to the skin. *Int J Pharm*. 2013;458(1):104-109. doi:10.1016/j.ijpharm.2013.10.007

283. Ramadan A, El-Massik M, El-Khordagui L, Daabis N, Hammouda Y. Surface treatment: A potential approach for enhancement of solid-state photostability. *Int J Pharm*. 2006;307(2):141-149. doi:10.1016/j.ijpharm.2005.09.030

284. Ambrogi V, Nocchetti M, Latterini L. Promethazine-montmorillonite inclusion complex to enhance drug photostability. *Langmuir*. 2014;30(48):14612-14620. doi:10.1021/la5033898

285. Geng N, Chen JM, Li ZJ, Jiang L, Lu TB. Approach of cocrystallization to improve the solubility and photostability of tranilast. *Cryst Growth Des*. 2013;13(8):3546-3553. doi:10.1021/cg400518w

286. Kawabe Y, Nakamura H, Hino E, Suzuki S. Photochemical stabilities of some dihydropyridine calcium-channel blockers in powdered pharmaceutical tablets. *J Pharm Biomed Anal*. 2008;47(3):618-624. doi:10.1016/j.jpba.2008.01.042

287. Sadana GS, Ghogare AB. Mechanistic studies on photolytic degradation of nifedipine by use of 1H-NMR and 13C-NMR spectroscopy. *Int J Pharm*. 1991;70(1-2):195-199. doi:10.1016/0378-5173(91)90181-M

288. Madejczyk O, Kaminska E, Tarnacka M, Dulski M, Jurkiewicz K, Kaminski K, Paluch M. Studying the crystallization of various polymorphic forms of nifedipine from binary mixtures with the use of different experimental techniques. *Mol Pharm*. 2017;14(6):2116-

2125. doi:10.1021/acs.molpharmaceut.7b00228

289. Vippagunta SR, Maul KA, Tallavajhala S, Grant DJW. Solid-state characterization of nifedipine solid dispersions. *Int J Pharm*. 2002;236(1-2):111-123. doi:10.1016/S0378-5173(02)00019-4

290. Bain DF, Munday DL, Smith A. Solvent influence on spray-dried biodegradable microspheres. *J Microencapsul*. 1999;16(4):453-474. doi:10.1080/026520499288915

291. Tønnesen HH. Formulation and stability testing of photolabile drugs. *Int J Pharm*. 2001;225(1-2):1-14. doi:10.1016/S0378-5173(01)00746-3

292. Soulairol I, Tarlier N, Bataille B, Cacciaguerra T, Sharkawi T. Spray-dried solid dispersions of nifedipine and vinylcaprolactam/vinylacetate/PEG6000for compacted oral formulations. *Int J Pharm*. 2015;481(1-2):140-147. doi:10.1016/j.ijpharm.2015.01.012

293. Vehring R, Foss WR, Lechuga-Ballesteros D. Particle formation in spray drying. *J Aerosol Sci*. 2007;38(7):728-746. doi:10.1016/j.jaerosci.2007.04.005

294. Chen Z, Yang K, Huang C, Zhu A, Yu L, Qian F. Surface enrichment and depletion of the active ingredient in spray dried amorphous solid dispersions. *Pharm Res*. 2018;35(2). doi:10.1007/s11095-018-2345-1

295. Son S, Lewis BA. Free radical scavenging and antioxidative activity of caffeic acid amide and ester analogues: Structure-activity relationship. *J Agric Food Chem*. 2002;50(3):468-472. doi:10.1021/jf010830b

296. Castañeda-Hernández G, Hoyo-Vadillo C, Palma-Aguirre JA, Flores-Murrieta FJ. Pharmacokinetics of oral nifedipine in different populations. *J Clin Pharmacol*. 1993;33(2):140-145. doi:10.1002/j.1552-4604.1993.tb03934.x

297. Raemsch KD, Sommer J. Pharmacokinetics and metabolism of nifedipine. *Hypertension*. 1983;5(4_pt_2). doi:10.1161/01.HYP.5.4_Pt_2.II18

298. National Rehabilitation Hospital. *Policy and Procedure for the Management of Autonomic Dysreflexia Table of Contents*. Dun Laoghaire; 2015.

299. Krassioukov A, Warburton DE, Teasell R, Eng JJ. A systematic review of the management of autonomic dysreflexia after spinal cord injury. *Spinal Cord Inj Rehabil Evid*. 2010;3.0(3):1-33. _http://www.scireproject.com/book/export/htm. doi:10.1016/j.apmr.2008.10.017.A

300. Myers J, Lee M, Kiratli J. Cardiovascular disease in spinal cord injury: An overview of

prevalence, risk, evaluation, and management. *Am J Phys Med Rehabil*. 2007;86(2):142-152. doi:10.1097/PHM.0b013e31802f0247

301. Van Harten J, Danhof M, Burggraaf K, Van Brummelen P, Breimer DD. Negligible sublingual absorption of nifedipine. *Lancet*. 1987;330(8572):1363-1365. doi:10.1016/S0140-6736(87)91258-X

302. Grossman E. Should a moratorium be placed on sublingual nifedipine capsules given for hypertensive emergencies and pseudoemergencies? *JAMA J Am Med Assoc*. 1996;276(16):1328. doi:10.1001/jama.1996.03540160050032

303. Grundy JS, Foster RT. The nifedipine gastrointestinal therapeutic system (GITS). *Clin Pharmacokinet*. 1996;30(1):28-51. doi:10.2165/00003088-199630010-00003

304. Varon J, Marik PE. Clinical review: The management of hypertensive crises. *Crit Care*. 2003;7(5):374-384. doi:10.1186/cc2351

305. Angeli P, Chiesa M, Caregaro L, Merkel C, Sacerdoti D, Rondana M, Gatta A. Comparison of sublingual captopril and nifedipine in immediate treatment of hypertensive emergencies. *Arch Intern Med*. 1991;151(8):678-682. doi:10.1001/archinte.1992.00400200147032

306. Cilurzo F, Minghetti P, Casiraghi A, Montanari L. Characterization of nifedipine solid dispersions. *Int J Pharm*. 2002;242(777157964):313-317. doi:10.1080/03639040701498759

307. Mc Gillicuddy A, Crean AM, Kelly M, Sahm L. Oral medicine modification for older adults: A qualitative study of nurses. *BMJ Open*. 2017;7(12):1-11. doi:10.1136/bmjopen-2017-018151

308. Nader AM, Quinney SK, Fadda HM, Foster DR. Effect of gastric fluid volume on the in vitro dissolution and in vivoa absorption of BCS Class II drugs: a case study with nifedipine. *AAPS J*. 2016;18(4):981-988. doi:10.1208/s12248-016-9918-x

309. Bayer AG. *Adalat 10mg Soft Capsules Patient Information Leaflet*.; 2018. http://www.mhra.gov.uk/home/groups/spcpil/documents/spcpil/con1542950198838.pdf.

310. Kim JY, Kim S, Papp M, Park K, Pinal R. Hydrotropic solubilization of poorly water-soluble drugs. *J Pharm Sci*. 2010;99(9):3953-3965. doi:10.1002/jps.22241

311. Hugouvieux V, Axelos MAV, Kolb M. Micelle formation, gelation and phase separation of amphiphilic multiblock copolymers. *Soft Matter*. 2011;7(6):2580-2591. doi:10.1039/c0sm01018a

312. Cavallari C, Ternullo S, Tarterini F, Fini A. Release problems for nifedipine in the presence of Soluplus. *J Pharm Pharm*. 2016;3(2):1-13. doi:10.15436/2377-1313.16.020

Appendix

a) Sample ibuprofen HPLC trace

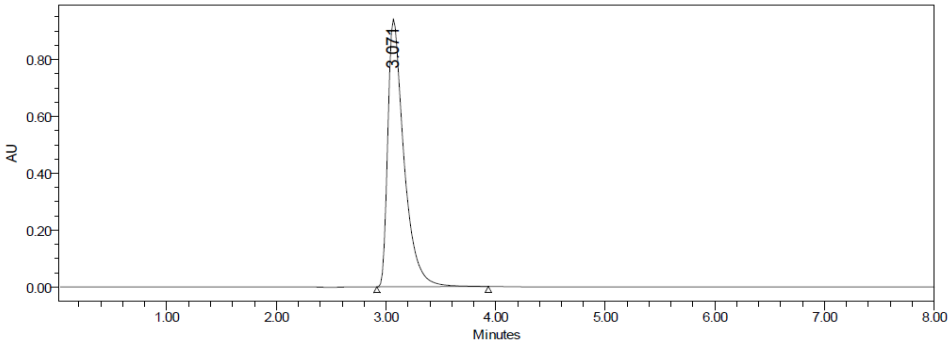

b) Sample ketoprofen HPLC trace

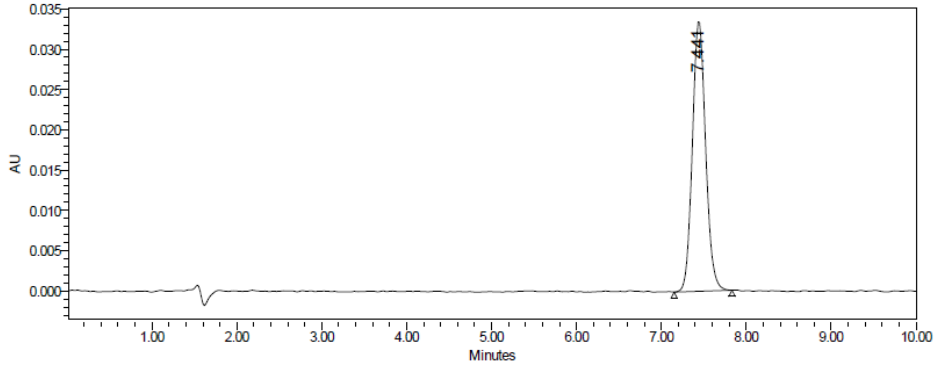

c) Sample nifedipine photostability indicating method trace

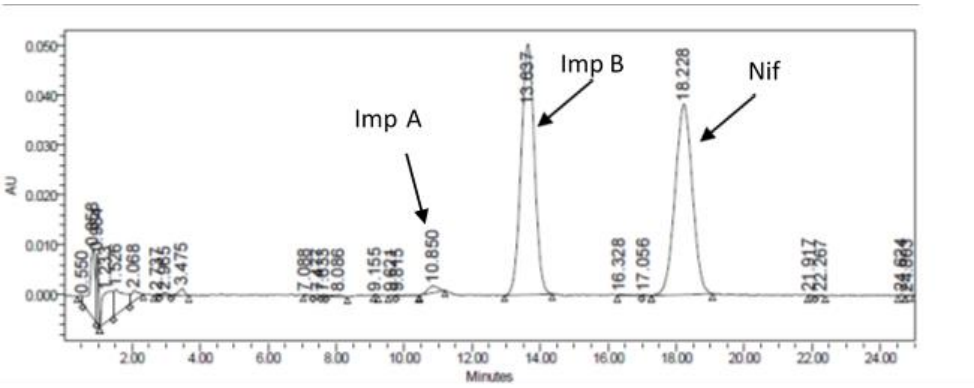

d) Sample nifedipine biphasic dissolution medium method trace

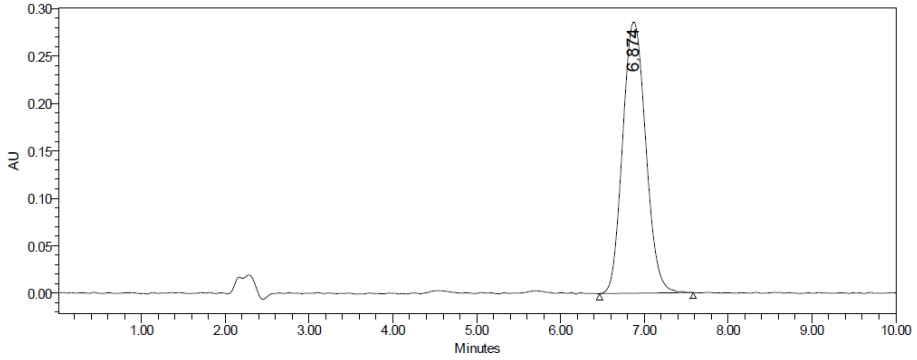

e) Sample R,S IBU HPLC calibration curve

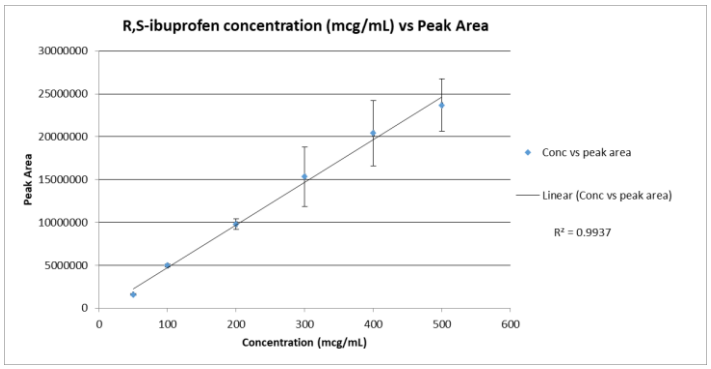

f) Sample S IBU HPLC calibration curve

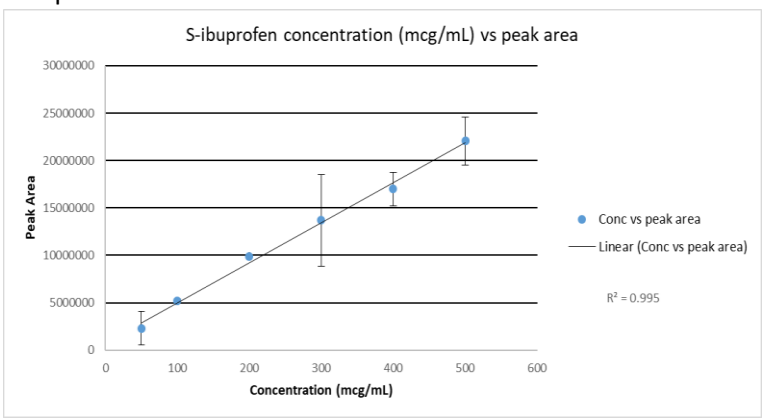

g) Sample KETO HPLC calibration curve

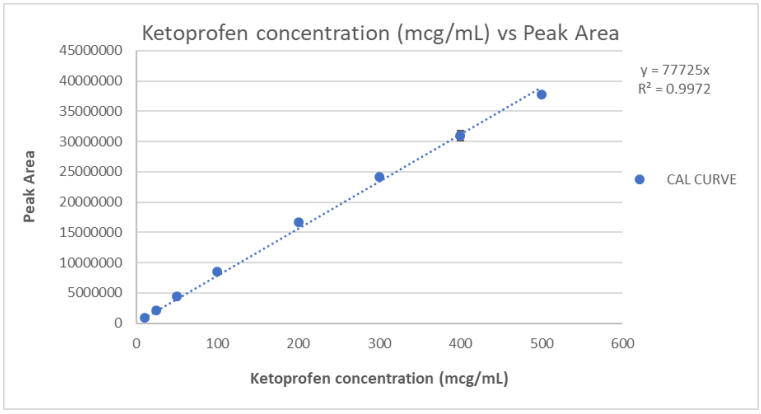

h) Sample nifedipine photostability indicating HPLC calibration curve

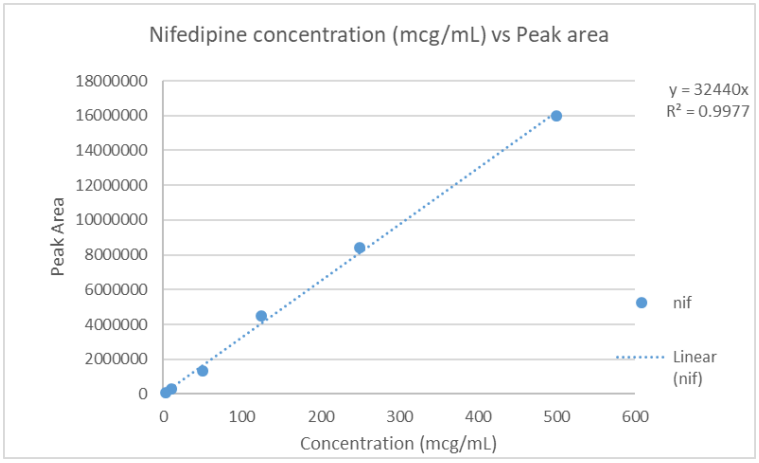

i) Sample nifedipine impurity A HPLC calibration curve

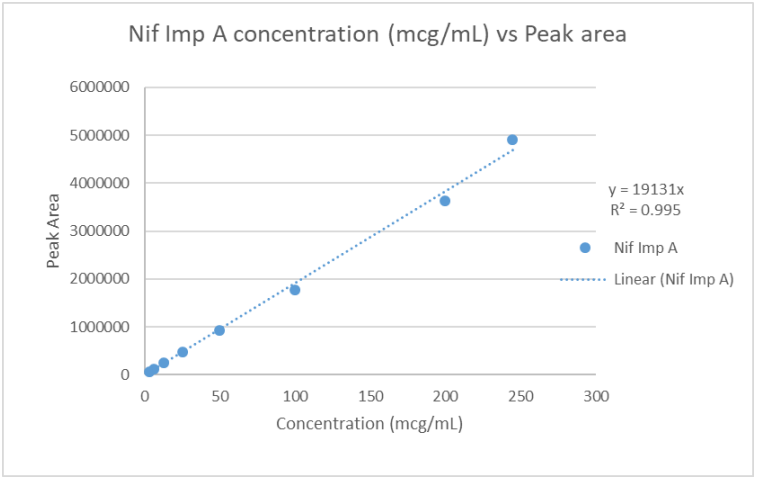

j) Sample nifedipine Impurity B HPLC calibration curve

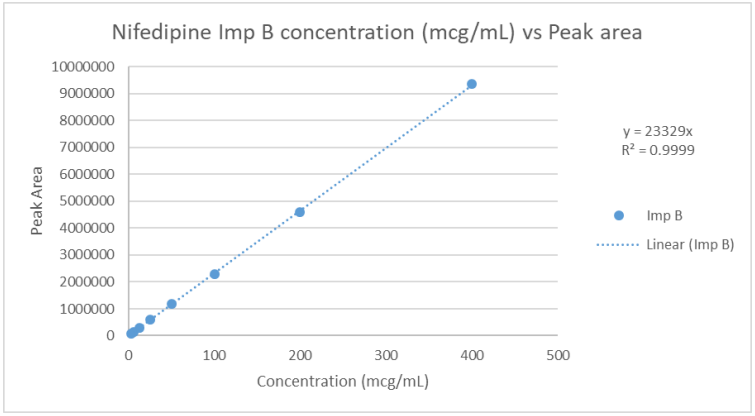

k) Sample nifedipine biphasic media method HPLC calibration curve

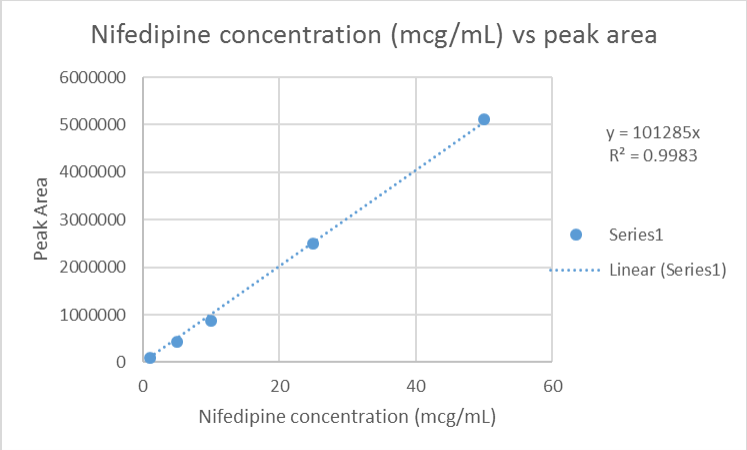

l) Sample DSC data relating to Table 3.1 and 3.2

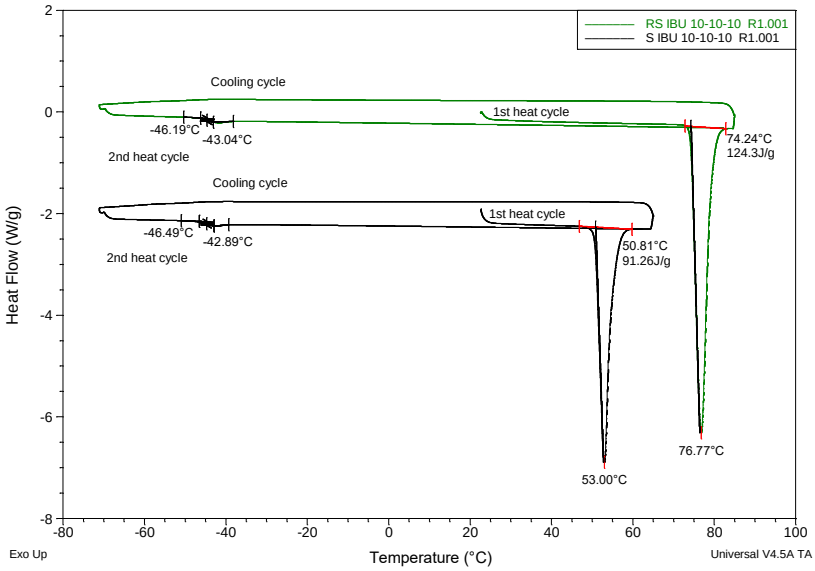

m) Sample TGA data relating to section 5.2.3.2

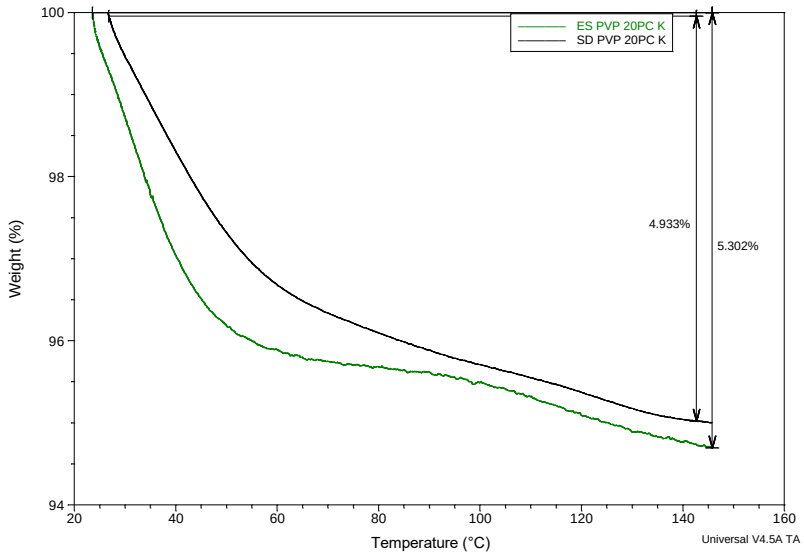

n) Sample TGA data relating to Table 6.a.2

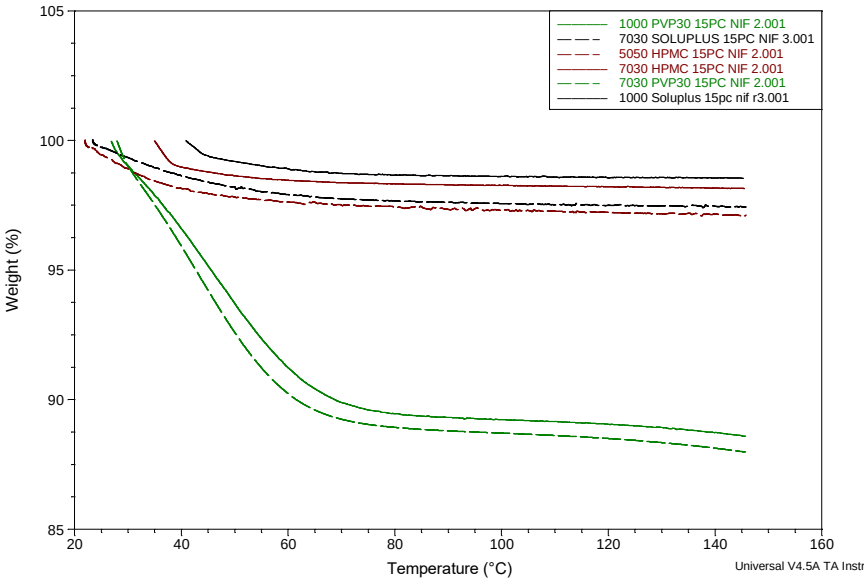

o)

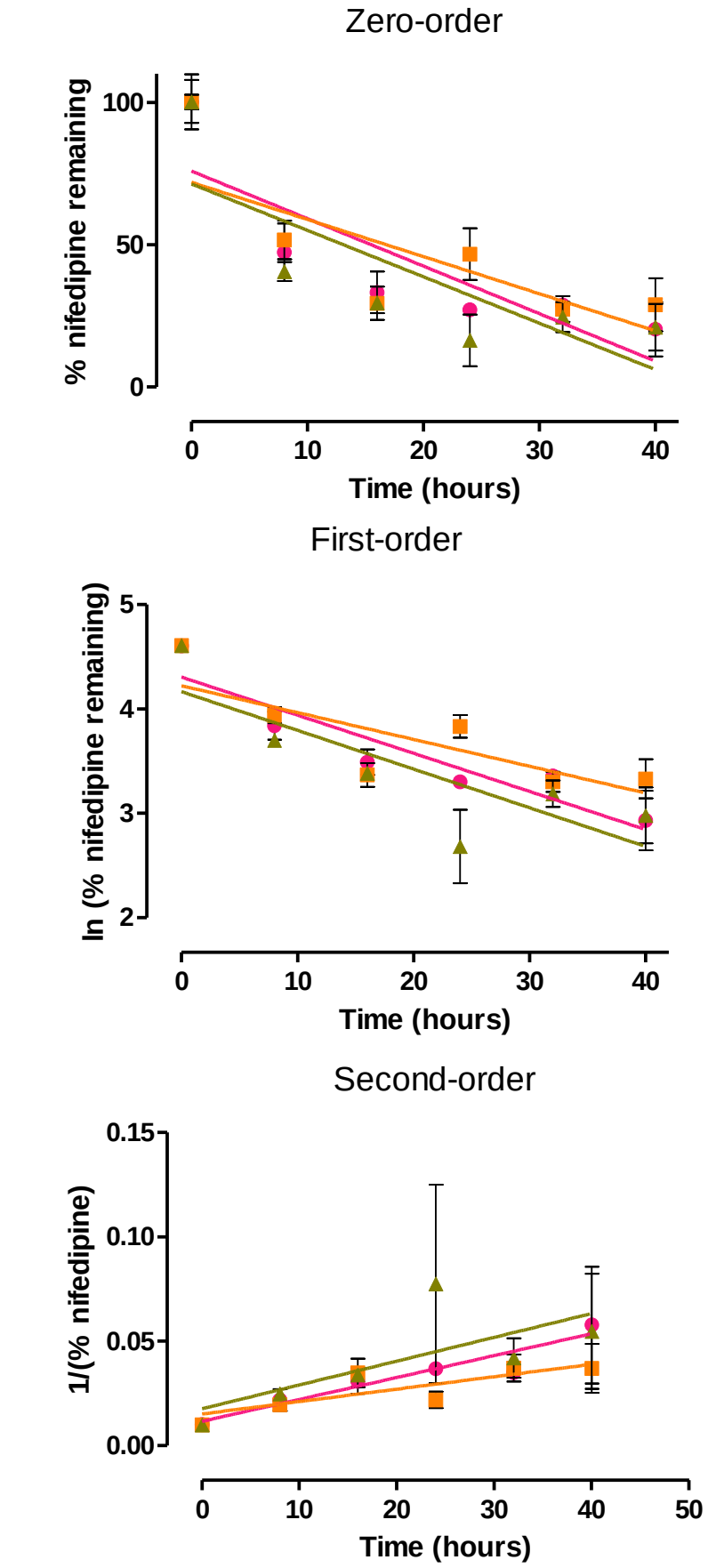
Zero-order
% nifedipine remaining
100
50
0
0
10
20
30
40
Time (hours)
First-order
ln (% nifedipine remaining)
5
4
3
2
0
10
20
30
40
Time (hours)
Second-order
1/(% nifedipine)
0.15
0.10
0.05
0.00
0
10
20
30
40
50
Time (hours)
SD HPMC 15% NIF 70:30
SD PVP30 15% NIF 70:30
SD SOLUPLUS 15% NIF 70:30